TECHNIQUES FOR TAILORING

SONAR TRANSDUCER RESPONSES

by

Geoffrey A. Steel B.Sc

Submitted for the Degree of

Doctor of Philosophy

Department of Electronic and Electrical Engineering,

University of Birmingham.

October 1986.

SYNOPSIS

This work is concerned with the design of sonar transducers operating in the frequency range 100 kHz to 1 MHz. The transducer frequency responses are predicted using a one-dimensional transmission line analysis. Differences between predicted and measured results are shown to be caused by intermodal coupling between planar and thickness modes of vibration.

Conventional transducer designs achieve wide bandwidth using quarter-wave matching layers. In this work the piezoelectric-tunable transducer is investigated as a possible alternative. This structure consists of a pair of ceramics, one of which is driven by a voltage source and the other has a passive electrical load. It is shown that the resonant frequency is variable over more than one octave but the instantaneous bandwidth is only around 10% of the centre frequency. The same transducer can be controlled actively by applying voltages to both ceramics. In this case transducer characteristics are determined by the relative amplitude and phase of the two voltage sources, which can be chosen to give the same results as with passive control.

Data is often required for the velocity and attenuation of sound in the materials being used. For this purpose several measuring techniques are described, all of which use a solid buffer rod in place of the more common water tank measurements.

Acknowledgements

This research was funded by an industrial studentship arranged between S.E.R.C. and Marconi Underwater Systems Limited. I am employed by M.U.S.L at Croxley Green, where the transducer design team is run by Mr C.Pearcy. His valuable advice and encouragement have maintained my interest in acoustics both before and during my postgraduate studies. I am grateful to my supervisors, Dr B.V.Smith and Dr B.K.Gazey, for their guidance, without which the work would not be possible. I also wish to thank Mr J.Nibblett for valuable help with mechanical problems and Mr J.Dunn whose practical experience is always at hand.

CONTENTS

LIST OF SYMBOLS

Symbols Common to all Chapters

ρ = density
c = speed of sound
f = frequency
k = wavenumber ($=\omega/c$)
l = thickness
λ = wavelength

η = efficiency
γ = propagation constant
a = absorption
h_{33} = piezoelectric constant
ε = permittivity
ω = angular frequency

Z_F = impedance on front of ceramic ($=R_F+jX_F$)
Z_B = " " back " " ($=R_B+jX_B$)
Z_T = terminating impedance ($=R_T+jX_T$)
Z_C = ceramic impedance

f_o = resonant frequency
g_o = conductance at resonance
Q = magnification factor ($=f_o$/bandwidth)

Symbols for Chapter 2

ρ_c = density of ceramic
c_c = speed of sound in ceramic
Z_m = matching layer impedance

Symbols for Chapter 3

Z_o = characteristic impedance of transmission line
x = length of transmission line

Symbols for Chapter 4

	Impedance	Thickness	Wavenumber	Velocity	Absorption
Perspex	Z_P	l_P	k_P	c_P	a_P
Sample	Z_S	l_S	k_S	c_S	a_S
Bond	Z_b	l_b	k_b	-	-

$|R|$ = modulus of reflection coefficient
ϕ = phase " " "
ϕ_t = phase shift on transmission from rod to sample
ψ = electrical phase shift
Pr = received pressure
P_t = transmitted pressure
Λ = maximum/minimum ratio in interference pattern

F = impedance ratio: $\dfrac{Z_b^2 + Z_P Z_S}{Z_b(Z_P + Z_S)}$

Symbols for Chapter 5

Z_{PL} = impedance of passive electrical load ($=R_{PL}+jX_{PL}$)
l_o = drive ceramic thickness
l_1 = control ceramic thickness

Symbols for Chapter 6

	Drive ceramic	Control ceramic	Coupling layer
Voltage	E_o	E_1	-
Capacitance	C_o	C_1	-
Impedance	Z_c	Z_c	Z_m
Thickness	l_o	l_1	l_m
Wavenumber	k_o	k_1	k_m

Z_S = impedance to be synthesised
γ_m = coupling layer propagation constant ($=a_m+jk_m$)
ϕ = phase of control voltage relative to drive voltage

F_o = Thevenin equivalent source for drive ceramic
Z_o = " " impedance " " "
F_1 = " " source for control ceramic
Z_1 = " " impedance " " "

$\nu + j\sigma$ = impedance ratio ($=F_1/F_o$)
$Z_{Po}, Z_{Qo}, Z_{P1}, Z_{Q1}$: mechanical impedances, see section 6.2

CHAPTER 1

Introduction

Useful sonar frequencies extend from infrasonic signals of a few Hertz up to ultrasonic signals of several MHz. The choice of operating frequency for a particular sonar depends largely on range and resolution requirements. At high frequencies the wavelength is small so high resolution can be achieved, but sound absorption and thermal background noise both increase with frequency and limit the operating range. Therefore long range sonars always use low frequencies which give comparatively poor resolution.

Infrasonic frequencies are often produced by high power non-reversible sources such as explosives. The rest of the frequency range can be covered by transducers with linear and reversible properties. Early transducer designs were based on piezoelectric crystals, such as quartz and Rochelle salt, which have simple geometrical shapes and are only suitable for a limited number of applications. It is now more common to use electrostrictive ceramics, such as barium titanate and lead zirconate titanate (PZT), which can be manufactured in any required shape. Transducers can also be constructed using magnetostrictive materials although these are only suitable for operation up to 200 kHz.

Most sonar systems require transducers to be easily manufactured and have reliable properties which are stable over the expected operating life. An important mechanical design consideration is the ability to withstand the high hydrostatic pressure experienced in deep water operation. High power transducers must also withstand

large temperature variations and prolonged temperature cycling.

Sophisticated signal processing techniques are often used to improve range resolution and signal-to-noise ratio. These techniques depend on the use of short acoustic pulses or swept frequency signals, both of which require very wide bandwidth transducers and therefore present considerable design problems.

For good signal-to-noise ratio it is important to have high power handling capability on transmission, along with high efficiency to ensure minimum heating effect and best use of available power. On reception high sensitivity is important and for wide bandwidth systems a flat non-resonant frequency response is often required.

At low frequencies transducers are small compared with the wavelength of sound in water. Simple designs include ceramic spheres and cylinders encapsulated in rubber for protection. More complicated designs are usually based on the Langevin sandwich transducer. This is a layered structure composed of a piezoelectric ceramic disc bonded to metal head and tail masses which are chosen to produce the required resonant frequency and bandwidth. Sandwich transducers can only be used at frequencies up to about 100 kHz. Beyond this frequency the assumption of small diameter in wavelengths, on which the design depends, becomes invalid, and there is an additional problem that sufficiently thin acoustic bonds between the components are hard to produce.

The present investigation is concerned with the design of high frequency transducers operating between 100 kHz and 1 MHz. In this frequency range wide band reception can be achieved using polyvinylidene fluoride (PVDF) membranes or thin ceramic plates

operated below resonance. These are relatively simple structures. Therefore this work concentrates mainly on the transmission of sound, which presents greater design problems. At frequencies above 200 kHz ceramic plates vibrating in thickness mode can be used. These have large diameters in wavelengths and therefore produce very narrow beams. More complicated transducers have backing and matching layers to improve bandwidth and impulse response. The design of these layers is widely discussed in the literature and Chapter 2 gives a review of published information.

The assumption of large diameter in wavelengths allows a simple one-dimensional analysis of transducers using an equivalent circuit. This was originally developed by Mason (1) and is described in Chapter 2. Computer programs have been developed for application of this analysis to various layered structures. The analysis only represents thickness mode vibrations of the ceramic but in practice planar modes are always present as well. Fundamental planar resonances occur at frequencies which are too low to be of interest but higher overtones may couple with the thickness resonance. This causes differences between predicted and measured results. Therefore when using Mason's model it is important to be aware of the limitations of a one-dimensional analysis. The purpose of Chapter 3 is to provide a detailed comparison between predicted and measured performance of simple transducers so that program limitations can be studied and taken into account when designing more complicated structures.

Conventional techniques for high frequency transducer design begin with a ceramic of fixed resonant frequency and control its bandwidth using adjacent passive layers. An alternative design has

recently been suggested (31) in which two (or more) ceramic layers are included. One ceramic is driven by a voltage source while the other has a passive electrical load, usually an inductor or capacitor. This structure is called a piezoelectric-tunable transducer and has the interesting property of variable resonant frequency. A detailed investigation of its behavior is presented in Chapter 5 using both computer simulation and practical results.

Replacing the passive electrical load by a voltage source allows active control of the piezoelectric-tunable transducer. The relative amplitude and phase of the two voltage sources determine the transducer characteristics. Equations derived in Chapter 6 allow a number of responses to be generated, including variable resonant frequency, and these are studied using the necessary control electronics.

The computer simulation involved in this work requires accurate data for sound velocity and absorption in each material. Such data is not readily available, especially for composite materials, so a rapid, convenient technique is required for measuring acoustic properties. A common measuring technique involves immersion of the sample in water, or other low-loss fluid, but solid buffer-rod measurements have also been described (9,28,29) and these have the advantage of simplified experimental set up. In Chapter 4 theoretical aspects of the buffer rod technique used by Pelmore (29) are described. Two further methods are then developed which allow greater accuracy using the same apparatus. These methods are convenient for general use in the design and construction of high frequency sonar transducers.

CHAPTER 2

A Review of Published Information

2.1 Equivalent Circuits

In order to investigate the performance of electroacoustic transducers it is essential to have a theoretical model of their behaviour. This model is required to represent the transfer of electrical to acoustical energy and vice-versa. Sonar transducers are always connected to electrical circuits, both for transmitting and receiving, so it is convenient to use an equivalent electrical circuit to predict their behavior. The shape and mode of vibration of the piezoelectric material define the equivalent circuit components and in 1948 Mason (1) showed that a ceramic plate vibrating in thickness mode could be represented by the circuit of figure 2a(i). The circuit has two mechanical ports, corresponding to the two ceramic faces, and one electrical port. Transfer between electrical and acoustical energy is indicated by an ideal transformer whose turns ratio has units of Newtons/Volt.

Force and particle velocity are represented by their electrical equivalents of voltage and current respectively. The ratio of force/velocity is mechanical impedance which has units of Kg/s and for plane waves is equal to ρc*Area (1). The product ρc is the ratio of pressure/velocity, or characteristic acoustic impedance of the material, and has units of Rayls ($Kgm^{-2}s^{-1}$). The front and back faces of the ceramic are loaded with mechanical impedances Z_F and Z_B which in general are complex and frequency dependent. Therefore if Z_F and Z_B

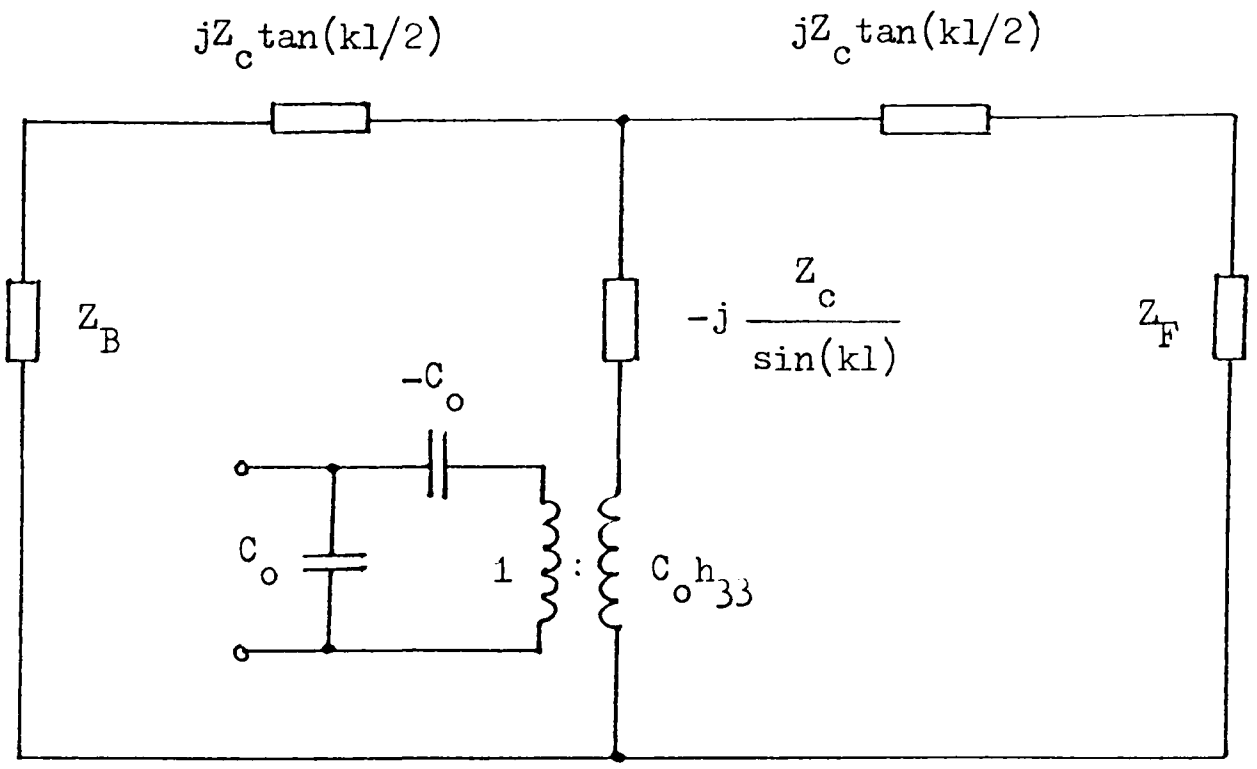

(i) Mason's equivalent circuit.

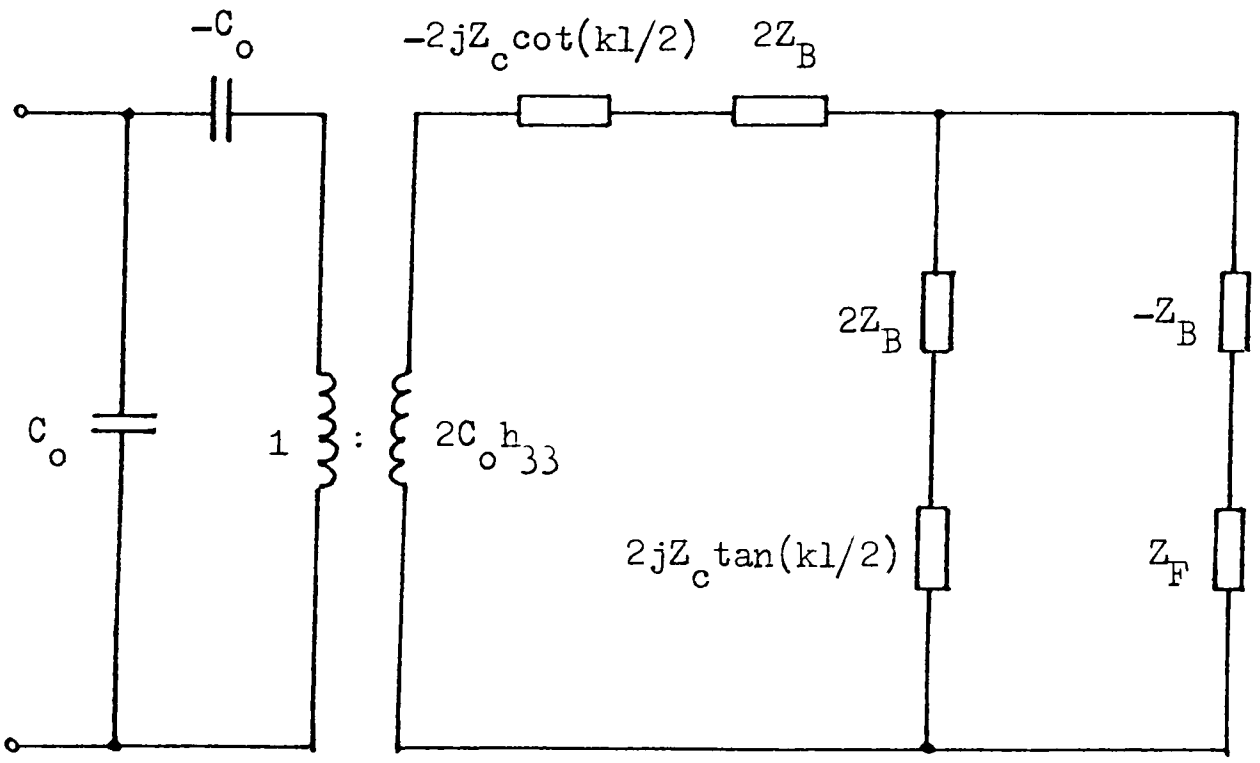

(ii) Transformed circuit due to Kossoff.

Figure 2a Equivalent circuits for a piezoelectric ceramic vibrating in thickness mode.

can be found this equivalent circuit provides a means of analysing the transducer performance.

The trigonometrical components of Mason's equivalent circuit are a transmission line representation of the ceramic. In practice the terms tan(kl/2) and 1/sin(kl) are sometimes inconvenient as they can simultaneously become infinite. To overcome this problem Kossoff (2) showed that the circuit of figure 2a(i) can be transformed into the more convenient form of figure 2a(ii).

Mason's equivalent circuit applies for all frequencies, however considerable simplification is possible for certain operating conditions. In particular near the half-wave resonant frequency Mason's model can be approximated (2) by the much simpler lumped element circuit of figure 2b. A similar circuit can be derived for the resonance of a quarter-wave piezoelectric plate with rigid backing (3).

In 1970 Krimholtz, Leedom and Matthaei (4) developed an alternative equivalent circuit for a piezoelectric ceramic vibrating in thickness mode. The so called KLM model is shown in figure 2c and represents the ceramic as a length of transmission line. Again the transfer between electrical and mechanical energy is indicated by a transformer but in this model the turns ratio is frequency dependent. The main advantage of the KLM model is that it contains a single coupling point at the centre of the transducer and some authors (5,6,33,39) have found this more useful than Mason's model, particularly for transient response analysis.

Several disadvantages of electrical equivalent circuits are outlined by Hayward (7), who has shown that a greater understanding of electromechanical interaction can be obtained by a systems feedback

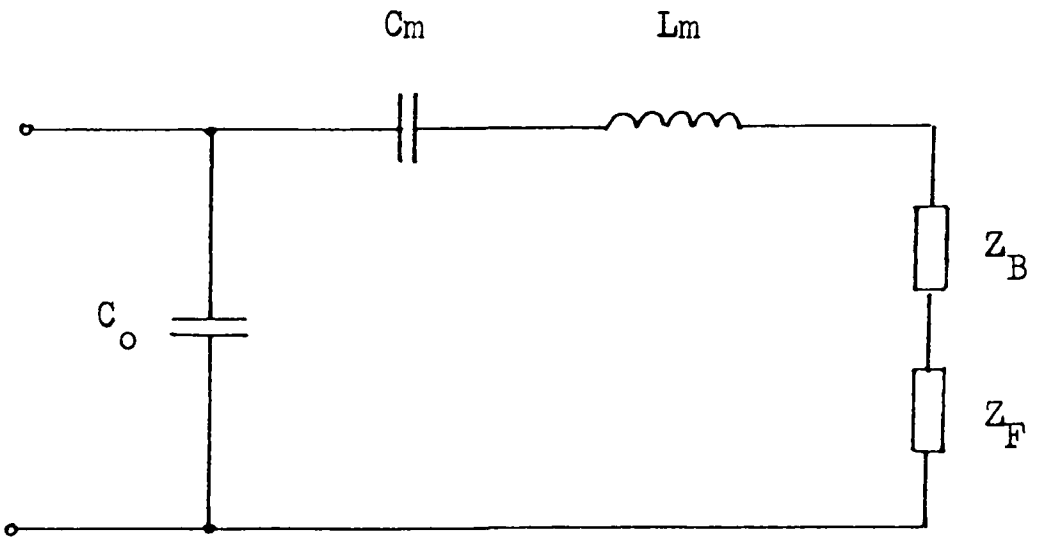

Figure 2b Simplified circuit for a piezoelectric ceramic near the half-wavelength resonant frequency.

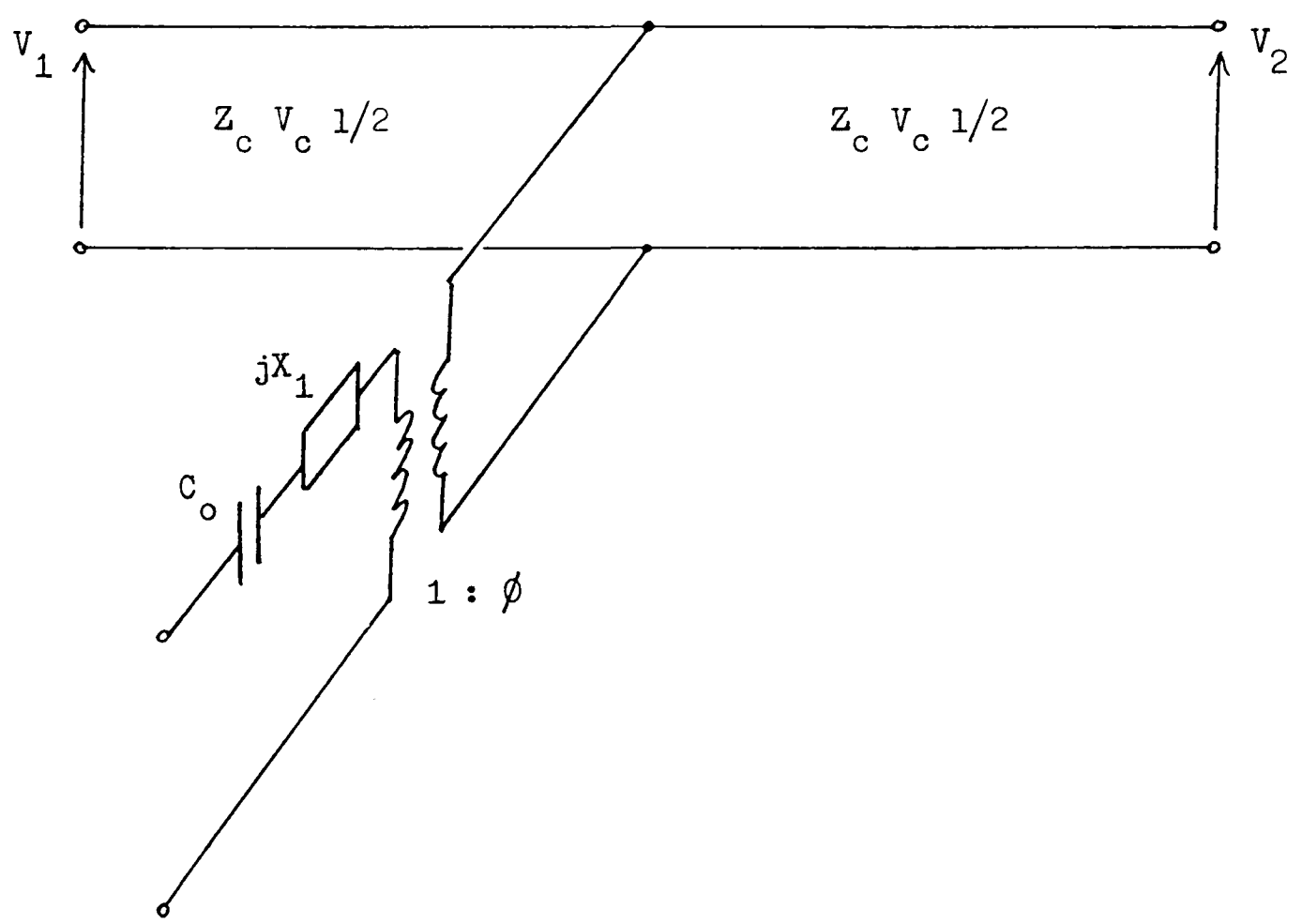

Figure 2c KLM model for a thickness expander plate.

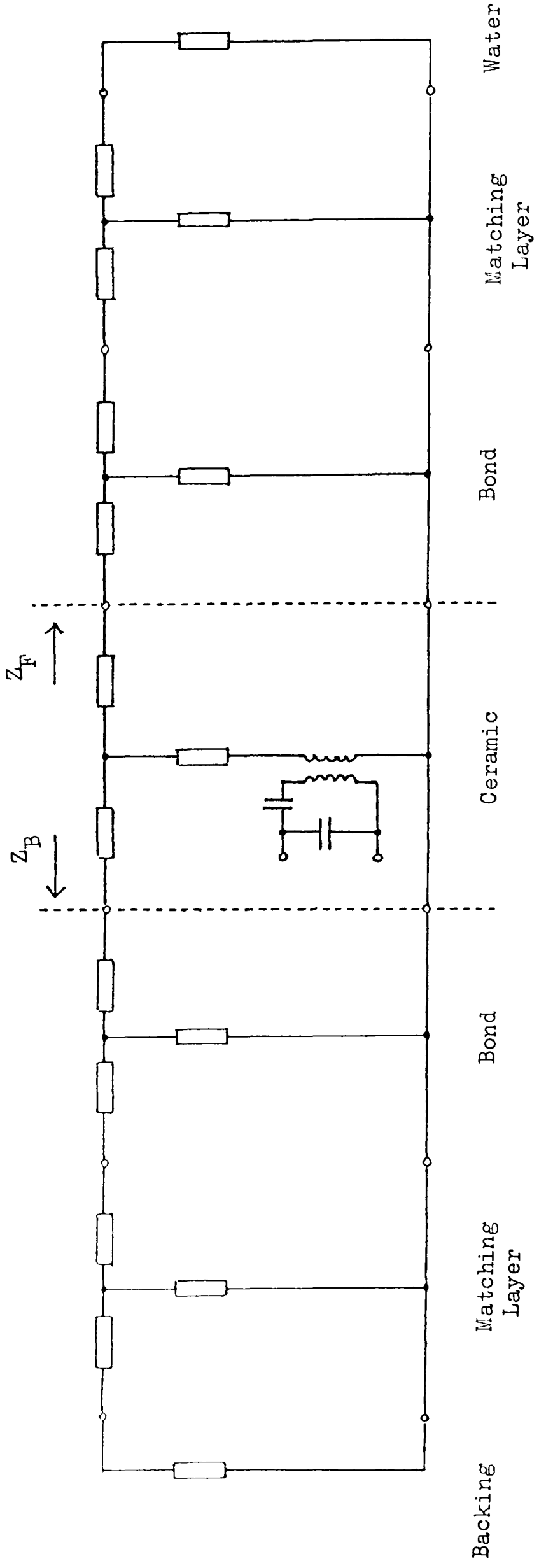

Figure 2d Transducer structure represented as a series of transmission line sections. Any number of sections can be added according to the required number of layers.

approach. He has derived two models, for transmission and reception, which are suitable for computer analysis and show close agreement with measured results. In a recent paper Hayward and Jackson (40) have extended these ideas to develop a lattice model for piezoelectric material. The ceramic is represented as a general three port linear system which can be used in the analysis of multilayer transducers. Again close agreement is reported between predicted and measured results.

2.2 Mechanical Transmission Line Representation

Both faces of the ceramic are loaded by one or more layers of material. Typically these layers will include metals, plastics, matching layers and also bonds between them. For the purpose of the present investigation it is convenient to represent these layers by a mechanical transmission line as shown in figure 2d. The impedances on the ceramic faces can then be found by transmission line analysis (9,10), details of which are given in chapter 3.

All the circuits discussed so far are based on a one-dimensional model of the transducer structure. It is assumed that the lateral dimensions of the ceramic are large in wavelengths so that planar resonances can be ignored. In practice this assumption is often not valid, and predicted results differ from measured performance because of intermodal coupling. Such effects have been studied in detail by Koymen (10).

2.3 Common Designs for High Frequency Sonar Transducers

The requirements for wide bandwidth and high efficiency have been the subject of many theoretical studies. In sonar transducers these are difficult to achieve simultaneosly. Figure 2b shows that near resonance the impedances Z_F and Z_B, on the front and back faces of the ceramic respectively, can be considered in series. The Q factor is approximately given by (11):

$$Q = \frac{\pi Z_c}{2(Z_F+Z_B)} \qquad \text{Equation 2.1}$$

where Z_c is the mechanical impedance of the ceramic, i.e. $\rho_c c_c$*Area. High efficiency can be achieved using an air backed ceramic radiating into water through a thin protective layer. However the impedance of ceramic is always large compared with that of water e.g. $\rho_c c_c \cong 34.5$ Mrayls for PZT-4 (12). Substitution into the above formula indicates a very high value of Q=36 for the simple air backed design, giving the problems of narrow bandwidth and therefore poor impulse response. (Equation 2.1 is derived from an approximate analysis which ignores the negative capacitance shown in figure 2a. A more detailed analysis predicts Q=28 for the air backed case). The Q can be lowered by increasing Z_B, but this causes greater power loss in the backing because Z_F and Z_B are in series. Therefore this gives lower efficiency and demonstrates the general problem of trade-off between bandwidth and efficiency.

The use of quarter-wave matching layers offers an alternative solution to the problem of narrow bandwidth. An air backed

ceramic matched to the water load by a quarter-wave plate retains the advantage of high efficiency but can be made to have a bandwidth of over 30% (3). Smith and Gazey (13) have shown that a transducer of this kind can be analysed as a half section constant-K filter, giving an optimum matching layer impedance $Z_m=(2Z_c Z_T^2)^{1/3}$ where Z_T is the terminating impedance. The circuit can be made into a full section filter by addition of a parallel inductor (14). This changes the optimum matching layer impedance to $Z_m=(Z_c Z_T^2)^{1/3}$ and gives a further increase in bandwidth without loss of efficiency.

A further increase in bandwidth is possible using two or more quarter-wave matching layers (5,15). Goll and Auld (15) have shown that a relative bandwidth of 70% can be produced using a pair of matching layers composed of quartz and lucite. There is a further advantage that these materials have more reliable properties than epoxy/metal composites used in single matching layer designs (3,6,16).

For transducers operating at depth the simple air backed design is unsuitable because of its inability to withstand high hydrostatic pressure. The usual solution is to support the ceramic on a highly absorbing backing of low impedance. A commonly used material is epoxy loaded with pulverised fly-ash (PFA) which gives an efficiency typically in the range of 40% to 60% (3). A more efficient low impedance backing, which includes two quarter-wave matching layers, has been described by Koymen (10,17).

In high resolution sonars the ability to produce very short pulses may be of greater importance than efficiency. Short pulses are also required for non-destructive testing and medical applications. Very wide bandwidth transducers of low efficiency can be constructed

with backing materials of the same impedance as ceramic. They are used to transmit very short pulses by excitation with impulses or step functions. Epoxy loaded with tungsten powder is often used as a backing but Bainton and Silk (16) have reported considerable difficulty in achieving the correct impedance with this material. An alternative approach is to use a ceramic backing but this has the problem of low attenuation. Several other high impedance backing materials are described by Sayers and Tait (18) and a useful summary is given by Low and Jones (19).

Even if the correct impedance is available, Low (20) and Silk (6) have shown that for good transient response an extremely thin bond (less than $\lambda/200$) is required between ceramic and backing. This is hard to achieve in practice. For some wide bandwidth applications it is possible to match the ceramic to a backing of lower impedance using a quarter-wave plate, but Silk (6) has shown that such designs are not suitable for the production of very short pulses.

It is possible to transmit broadband signals by modifying the electrical driving waveform in a predetermined way which is specific to the particular transducer. This technique is described as precompensation. An example is given by Augustine and Andersen (8) who show that a lossless equalization network can be inserted between the voltage source and the transducer. By this method any transducer can be matched to a specified source resistance giving maximally flat power gain. At low frequencies Holly (42) has shown that Weiner filter theory can be applied to precompensation. A digital filter is used to shape the voltage waveform according to time domain data measured for the transducer. Successful application of this technique is reported

for a transducer operating in the frequency range 7 - 37 kHz.

Finally it is worth noting that several wide bandwidth, high frequency transducers have been designed using polyvinylidene fluoride (PVDF or PVF_2). This piezoelectric polymer is most suitable for hydrophones (21) but Bainton et al (22) have shown that it can be used as a low efficiency transmitter. A layer of PVDF bonded directly to a silicon wafer can form the gate of an MOS field-effect transistor as described by Swartz and Plummer (23). This device is suitable both for transmitting and receiving and appears to have great potential for operation at frequencies above 1MHz.

CHAPTER 3

Computer Simulation of Transducer Performance and Comparison with Practical Results

3.1 Transmission Line Analysis

The equations used in transmission line analysis are described in detail by Connor (24) and a useful summary of their application to acoustics is given by Bobber (25).

Figure 3a shows a transmission line of characteristic impedance Z_o and length x terminated by an impedance Z_T. The input impedance of this transmission line is:

$$Zin = Z_o \left[\frac{Z_T \cosh(\gamma x) + Z_o \sinh(\gamma x)}{Z_o \cosh(\gamma x) + Z_T \sinh(\gamma x)} \right] \qquad \text{Equation 3.1}$$

In this equation γ is the propagation coefficient and is defined as $\gamma = a + jk$ where a is the absorption coefficient in nepers/m and k is the wavenumber.

The characteristic mechanical impedance of an absorbing medium is complex (2,25) and approximately given by:

$$Z = R + jX = \rho c[1 + ja/k] \qquad \text{Equation 3.2}$$

Most materials have such low absorption that their reactance can be ignored. However for general use in computer programs imaginary parts should be included so that $Z_o = R_o + jX_o$ and $Z_T = R_T + jX_T$.

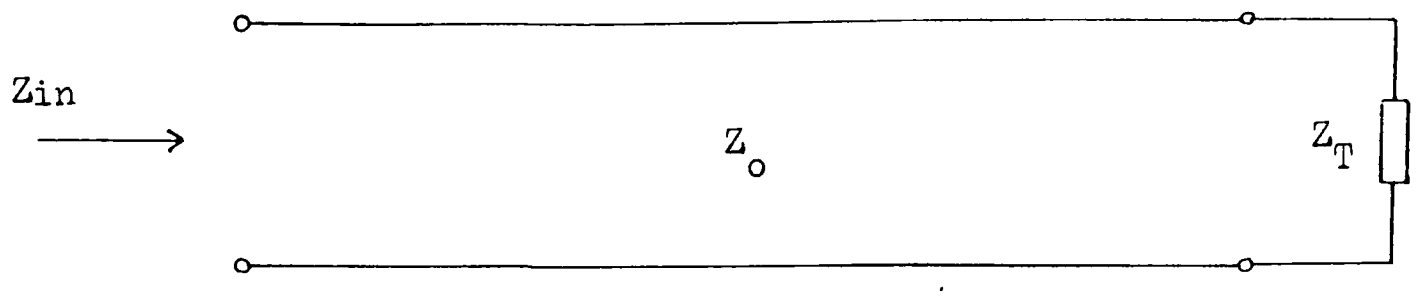

(i) Electrical transmission line

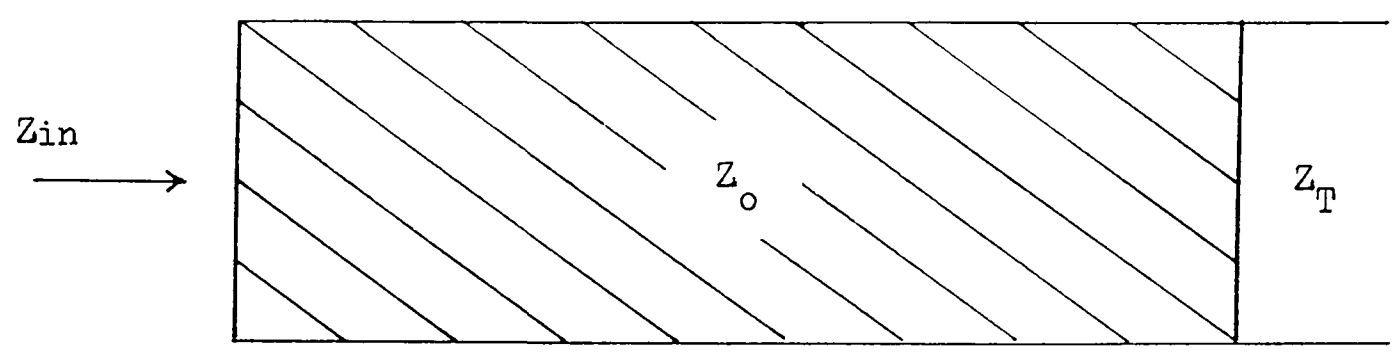

(ii) Mechanical transmission line

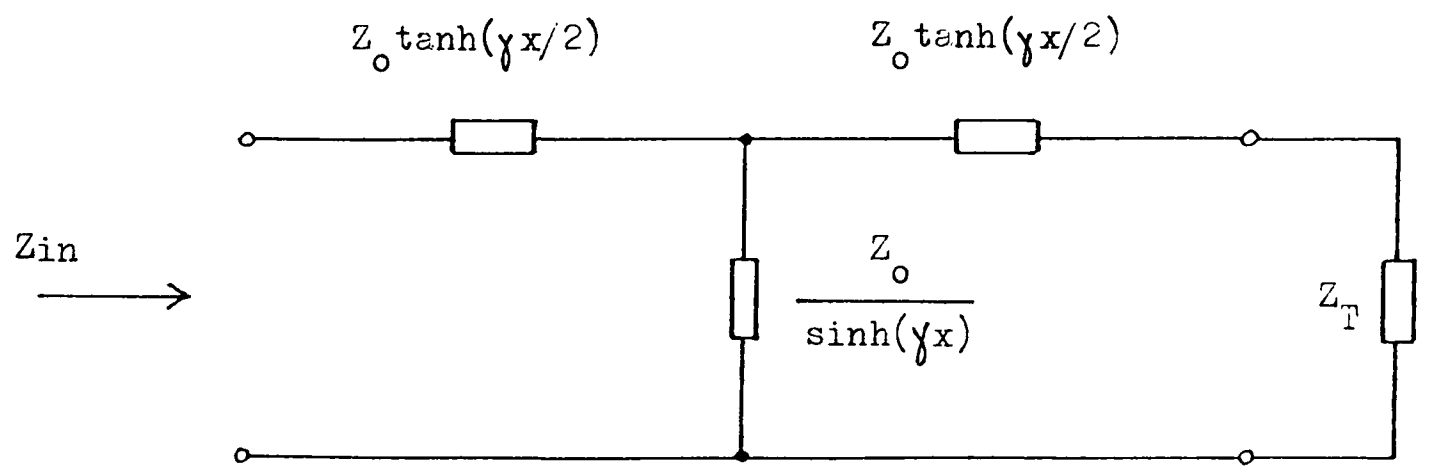

(iii) The equivalent circuit for both.

Figure 3a Electrical and mechanical transmission lines.

3.2 Description of the Computer Program

The complete equivalent circuit of a multilayer transducer was shown in figure 2d. Analysis of this circuit can give the pressure and particle velocity at any interface and also the admittance seen at the electrical terminals. For experimental purposes it is most convenient to work in terms of admittance as this allows theoretical predictions to be compared directly with easily measured results.

An interactive FORTRAN program called PASSIVE_LOAD was written to find the admittance of any transducer structure of the kind shown in figure 2d. The program has five sections and works as follows:

1. Density, speed of sound and absorption of a number of materials are read from data files.

2. A description of the transducer is entered. This defines the number of layers, thickness and composition of each layer, cross-sectional area and frequency range of interest.

3. Impedances on the front and back faces of the ceramic are calculated at suitable frequency intervals. This is done using equation 3.1 for each layer, starting at the ends of the structure and working towards the ceramic.

4. The circuit of figure 2a is used to calculate conductance (G) and susceptance (B) at each frequency.

5. Results are shown either as linear plots of G and B against frequency, or as a circle diagram which is a plot of B against G (11,27).

3.3 Comparison of Predicted and Measured Results

In order to investigate the validity of computer predictions two transducers, TB1 and TB2, were designed for operation at 500 kHz. Admittance measurements were taken at each stage of construction so that loading effects could be monitored.

TB1 was designed as a wide bandwidth transducer of low efficiency and is shown in figure 3b. The backing is Stycast 1264 epoxy resin loaded with iron filings to give a high impedance. The active element is a 4mm thick, 25mm square PZT-4 ceramic supplied by Vernitron. It is glued to the backing with quick-set Araldite. A thin layer of Stycast 1264 protects the front of the ceramic. It was evacuated while in liquid form to remove air bubbles then machined to the desired thickness after setting. The whole structure is mounted in a 50mm diameter Tufnol tube.

TB2 was designed for higher efficiency narrow bandwidth operation. The backing has a low impedance and is composed of Stycast 1264 loaded with pulverised fly-ash. The rest of the design is the same as TB1 and details are given in figure 3c.

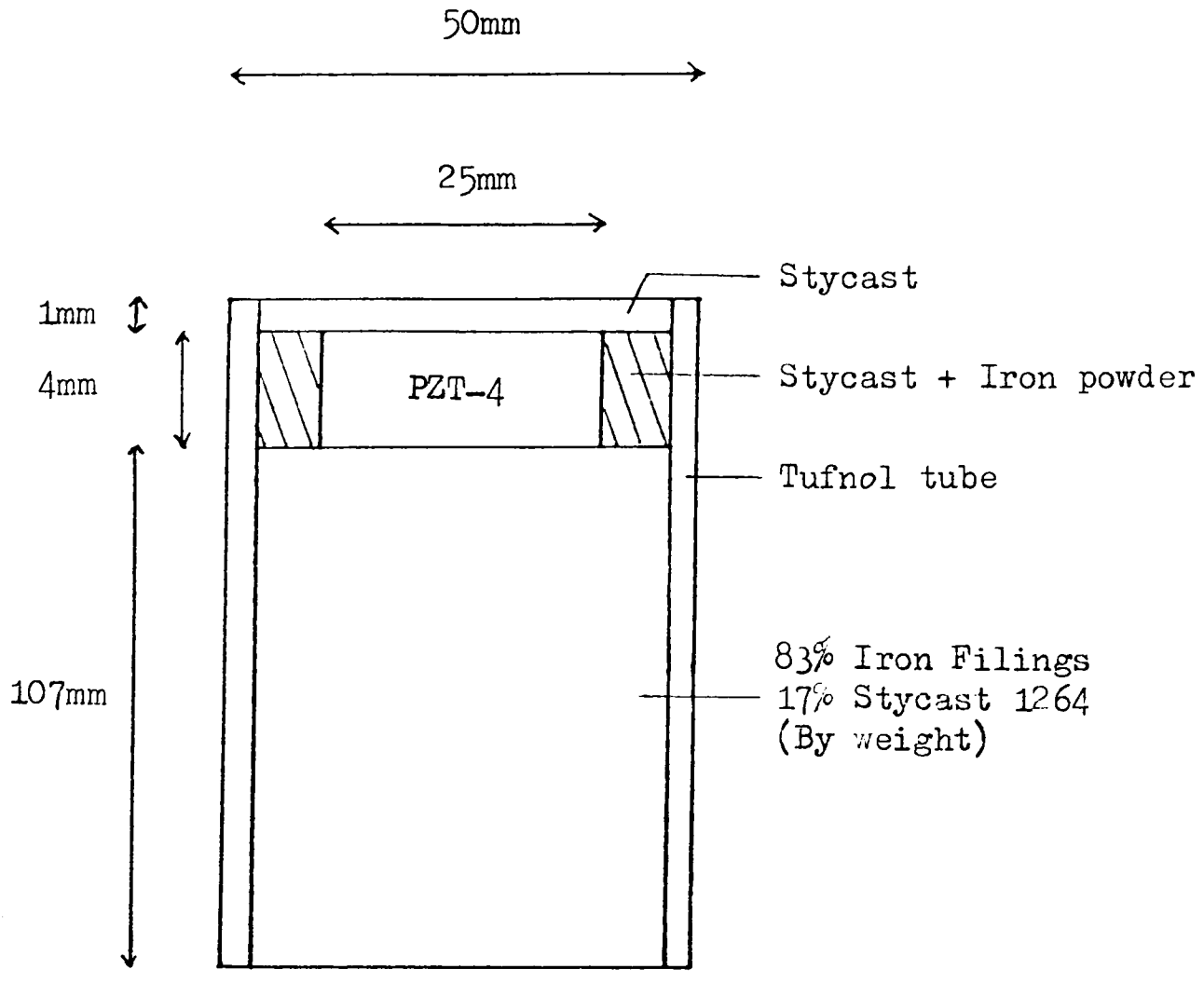

Figure 3b Cross section of TB1.

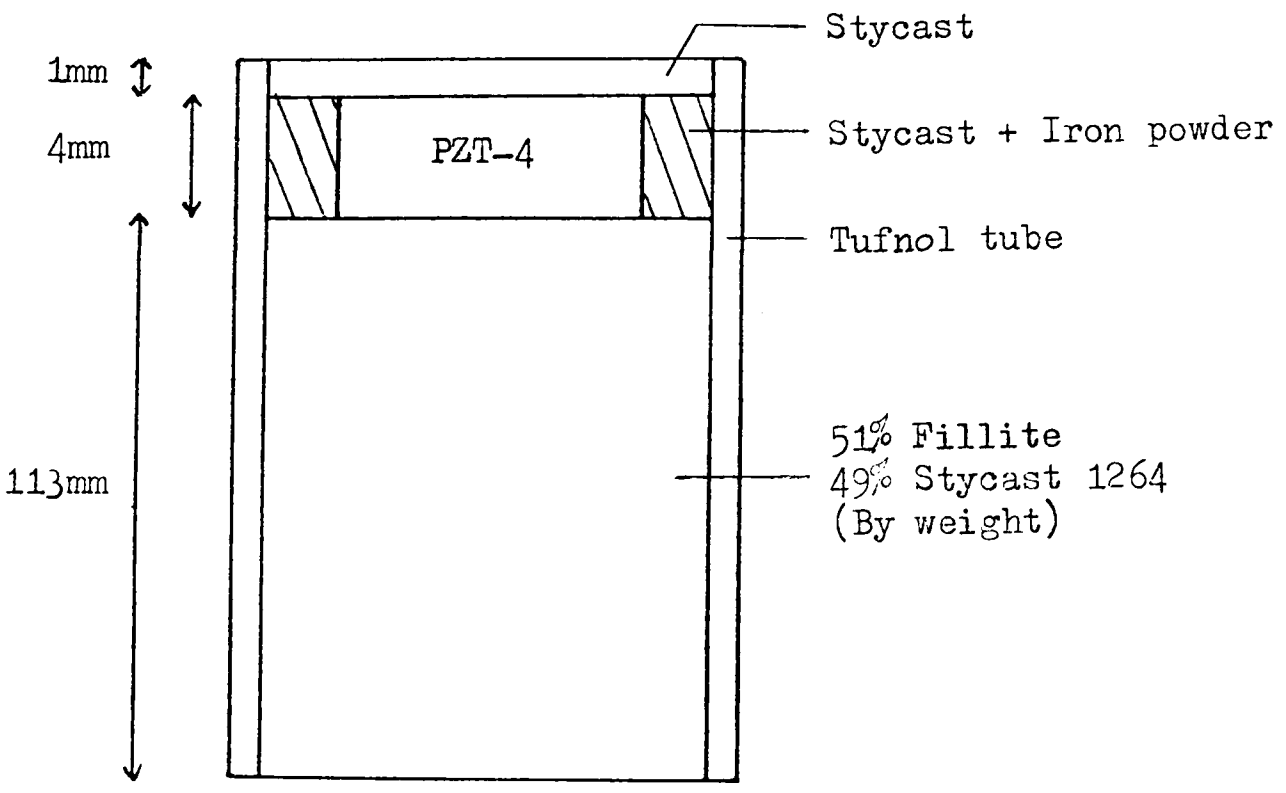

Figure 3c Cross section of TB2.

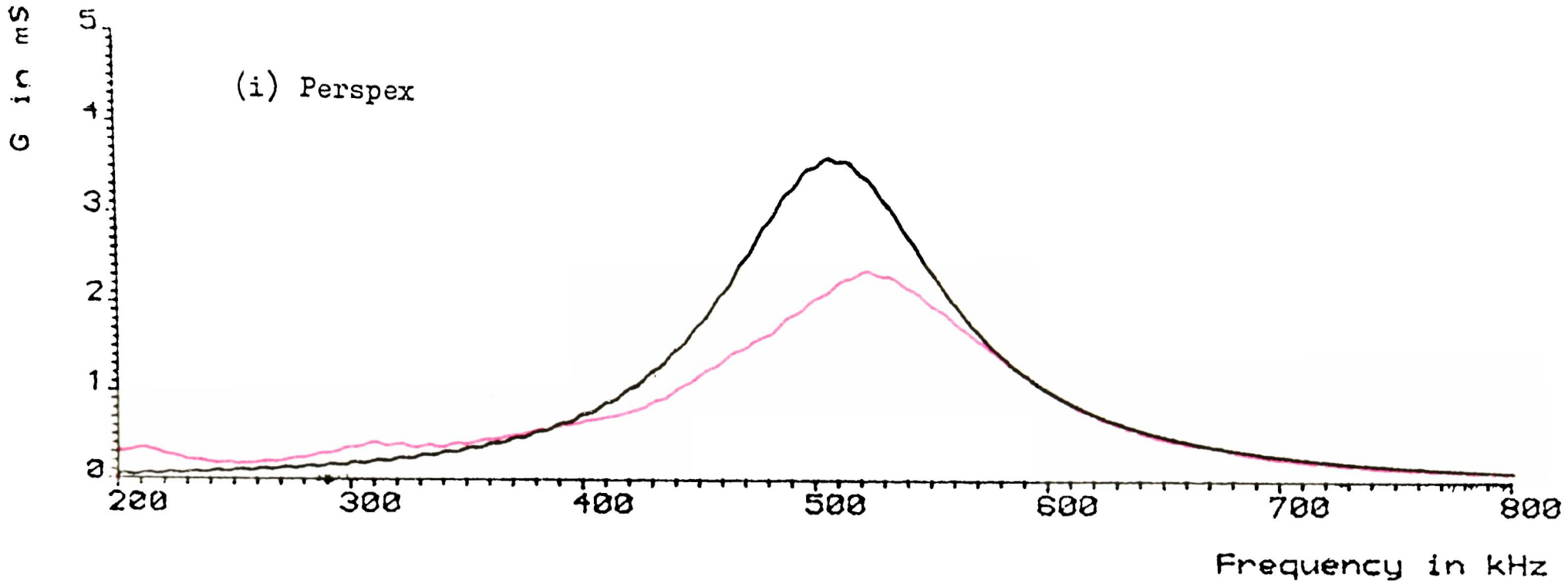

Figure 3d

Predicted and measured conductance for TB1 with perspex and air loads.

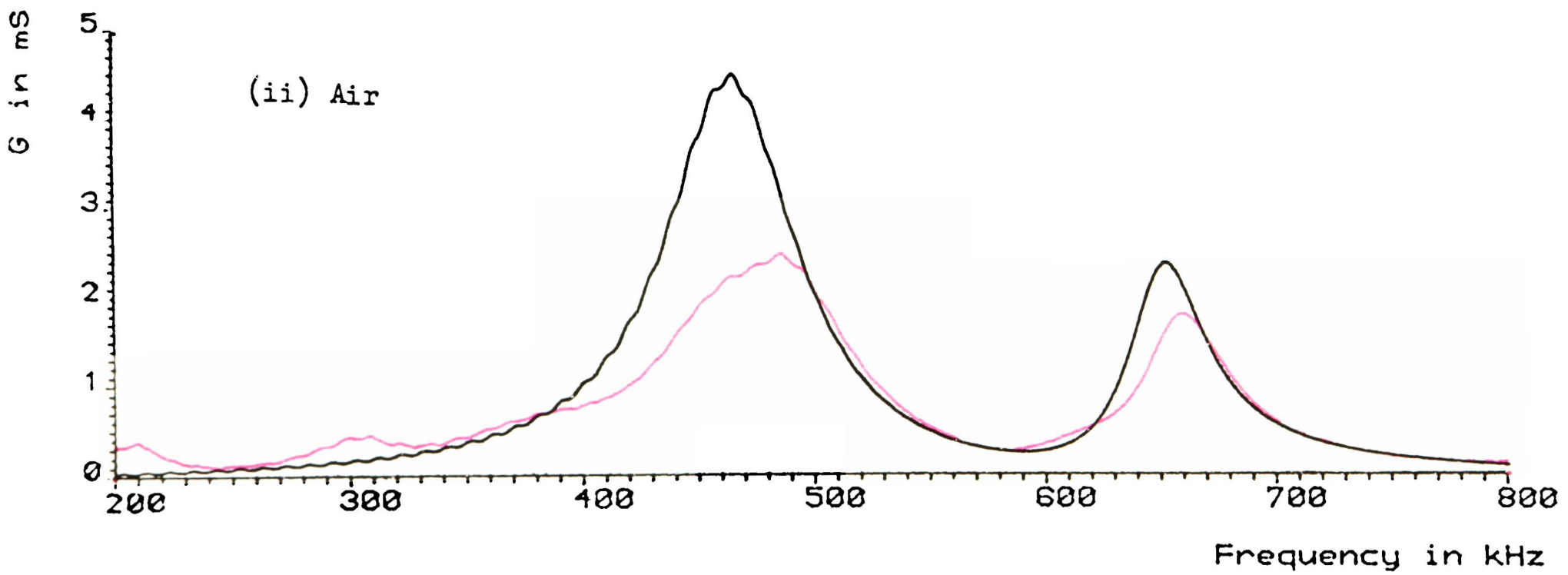

3.3.1 Results for TB1

Figure 3d(i) shows the predicted and measured conductance of TB1 when loaded by a 60cm perspex rod. The absorption of perspex is 0.5 dB/cm at 500 kHz so signals reflected from the end of the rod are attenuated by 60dB which is large enough to assume an infinite perspex load. Some key parameters are given in the following table. The resonant frequency f_o is identified at maximum conductance g_o, and the bandwidth is measured between $g_o/2$ points. The ratio of f_o to bandwidth is the magnification factor Q.

	Predicted	Measured
f_o (kHz)	505	525
g_o (mS)	3.7	2.6
Q	4.6	3.9

TABLE 3.1 Results for TB1 with perspex load

The measured values of g_o and Q are lower than predicted and there are two possible causes. The backing impedance was assumed in the program to be 7.1 MRayls as this figure was measured by Pelmore (26) for an epoxy/iron composite. However particle size and packing factor strongly influence the properties of such materials and TB1 may have considerably higher backing impedance than assumed.

A second and more important source of error is the loss of energy through the sides of the ceramic. The one-dimensional transmission line analysis can only deal with thickness mode vibrations and assumes that the ceramic has infinite area or is laterally clamped. In practice thickness vibrations are accompanied by lateral displacement which radiates energy from the sides of the ceramic. The

acoustic load is thus increased giving wider bandwidth and lower conductance. At 500 kHz the wavelength in PZT-4 is 8mm so the 25mm square ceramic of TB1 is only three wavelengths across. The assumption of infinite area is therefore not valid and is the most likely cause of discrepancy between predicted and measured results.

At frequencies below 600 kHz both predicted and measured curves show ripples of small amplitude. These are caused by standing waves in the backing. The epoxy/iron composite has an absorption of 2.2 dB/cm at 500 kHz and is proportional to frequency (29) so the ripples are more pronounced at low frequencies. At 200 kHz and 310 kHz small additional resonances occur in the measured results. These are overtones of the ceramic width resonance, the fundamental being at 76 kHz.

Figure 3d(ii) shows the predicted and measured conductance of the same transducer when loaded by air. The thin Stycast 1264 layer in front of the ceramic causes the resonance to split into two separate peaks. Again the conductance is lower than predicted. Ripples due to standing waves and overtones of the width resonance can still be seen in the measured results.

3.3.2 Results for TB2

Figure 3e shows the performance of TB2 for perspex and air loads. The low impedance backing causes narrower bandwidth and higher conductance than TB1. Again the measured values for g_o and Q are lower than predicted showing that lateral displacement is significant.

The backing of TB2 is 11.3 cm long and shows no standing

Figure 3e

Predicted and measured conductance for TB2 with perspex and air loads.

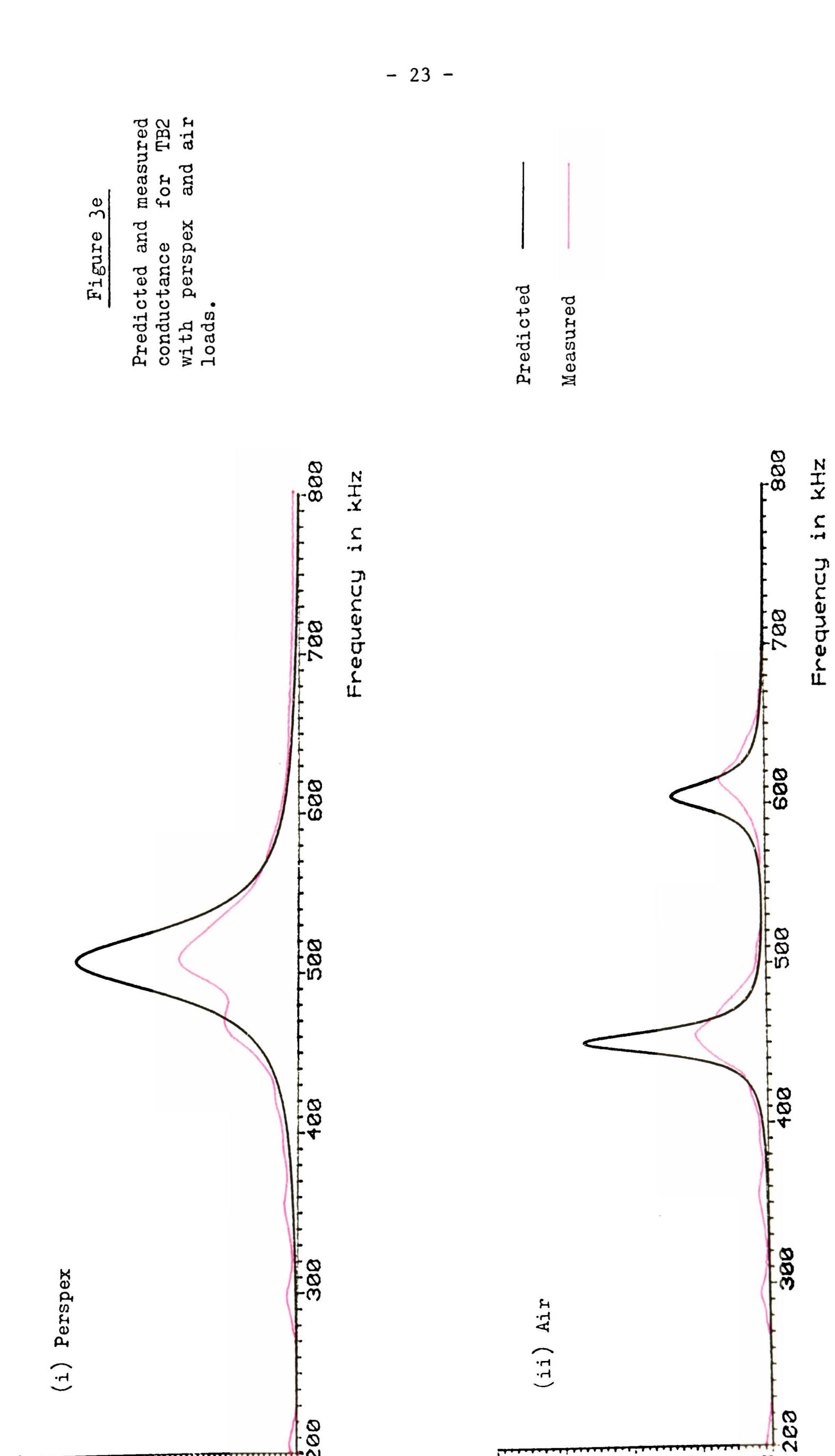

waves. This is because the backing material has an absorption of 5.5 dB/cm at 500 kHz (29) which is more than double the value for TB1 and sufficient to absorb all energy radiated into it.

A very strong overtone of the ceramic width resonance occurs at 470 kHz. When TB2 is loaded by perspex this overtone causes distortion of the thickness resonance due to intermodal coupling. In air the main resonance is closer to 470 kHz so intermodal coupling is less apparent. It is interesting to note that there is no distortion in the corresponding curves for TB1. Ceramic conductance measurements taken in air, before building the transducers, (figure 3f) show a large peak at 470 kHz for TB2 but only a group of smaller peaks for TB1. Ceramics with the latter condition are more suitable for building transducers as several small peaks are more easily damped than a single large one.

3.3.3 Standing Waves

Figure 3g(i) shows the predicted effect of a 100mm perspex rod on the front of TB1, this time plotted as a circle diagram. Large standing waves produce loops superimposed on the main resonant circle. These loops are separated by 13.4 kHz which is the frequency where 100mm=$\lambda/2$ for perspex. Figure 3g(ii) shows the corresponding measurement. Again the conductance is smaller than predicted so the circle has a smaller diameter. Loops due to standing waves in the perspex can be seen at intervals of 13.4 kHz but their amplitude is smaller than predicted. Again this is the result of energy loss in lateral displacement.

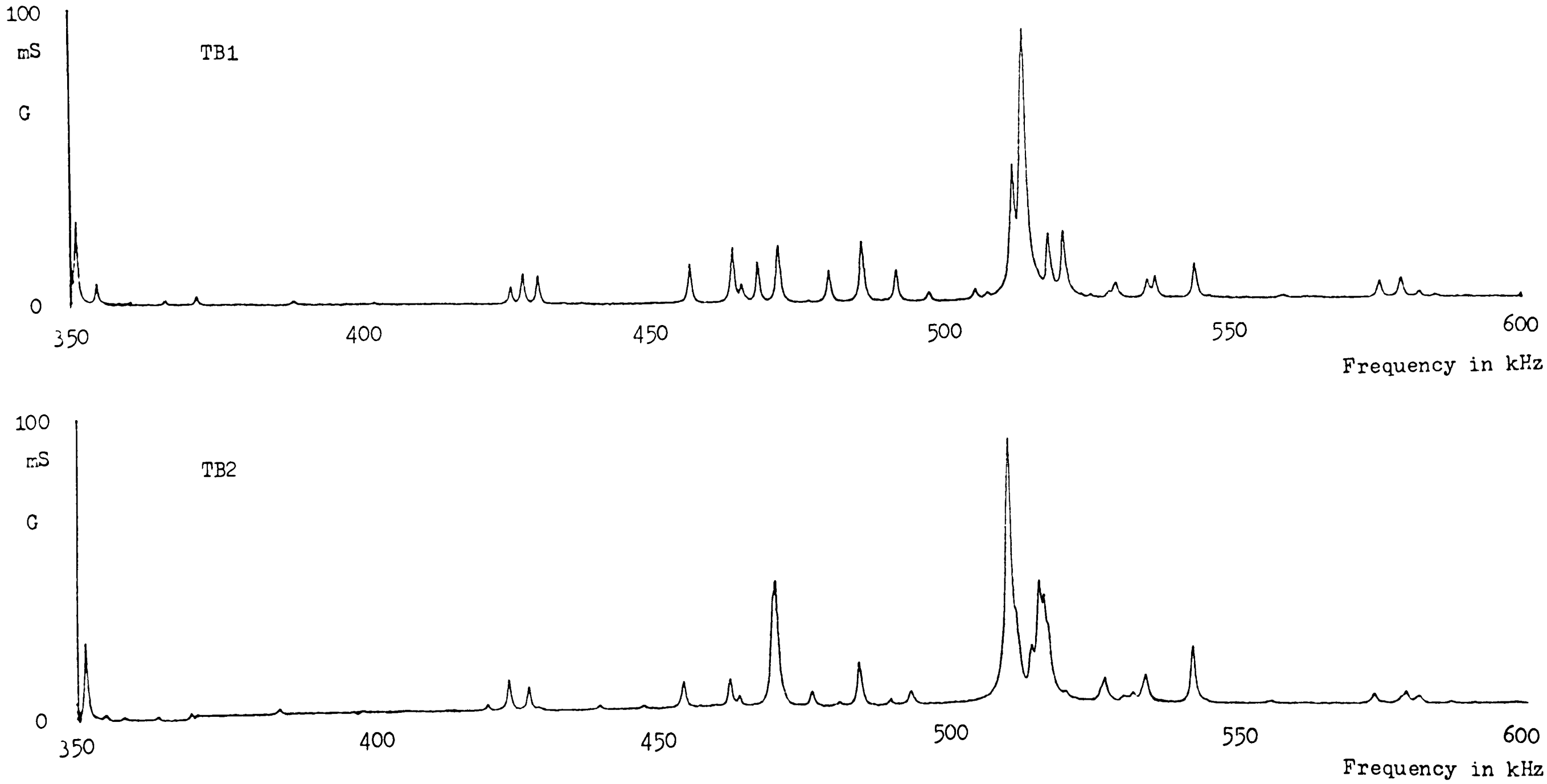

Figure 3f Ceramic conductance measurements before building transducers.

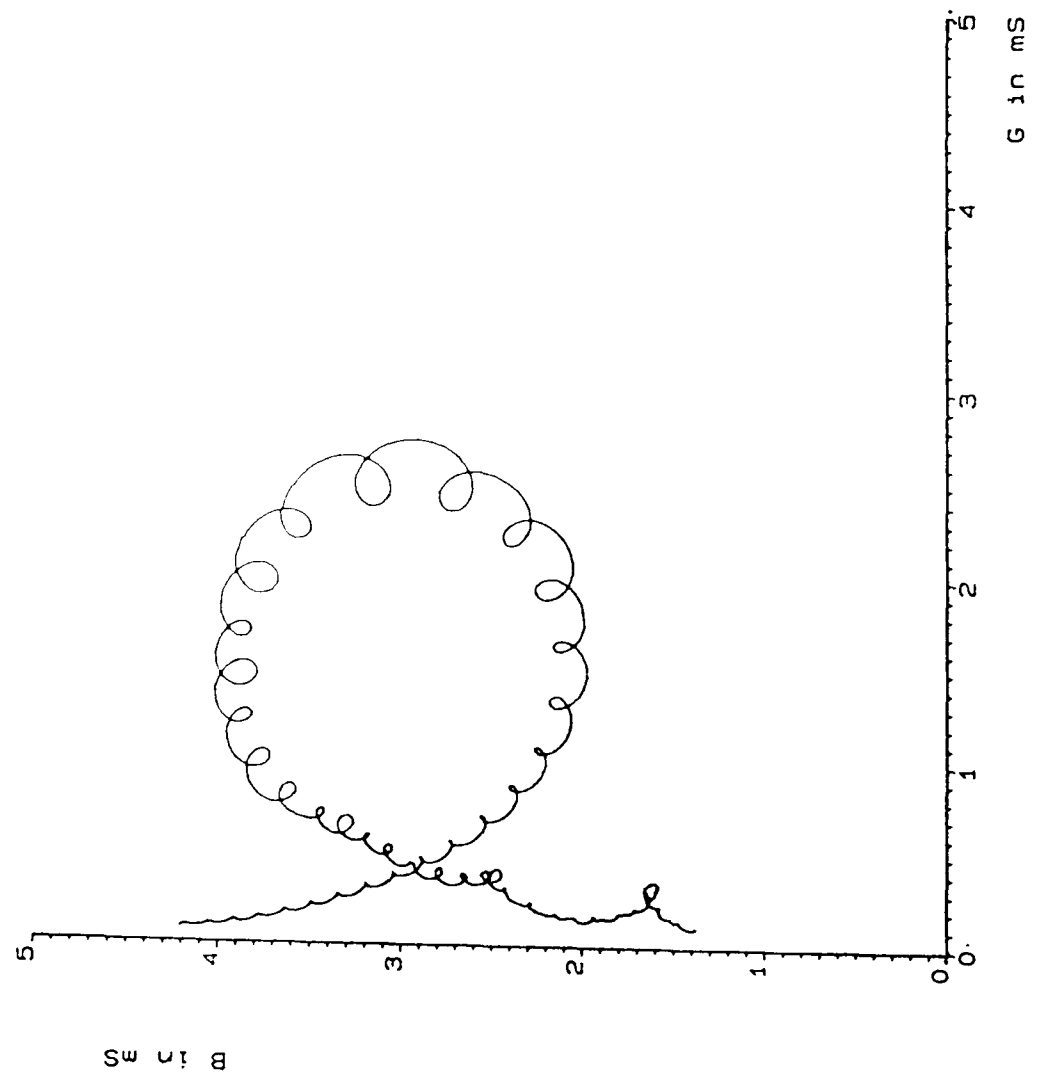

(ii) Measured

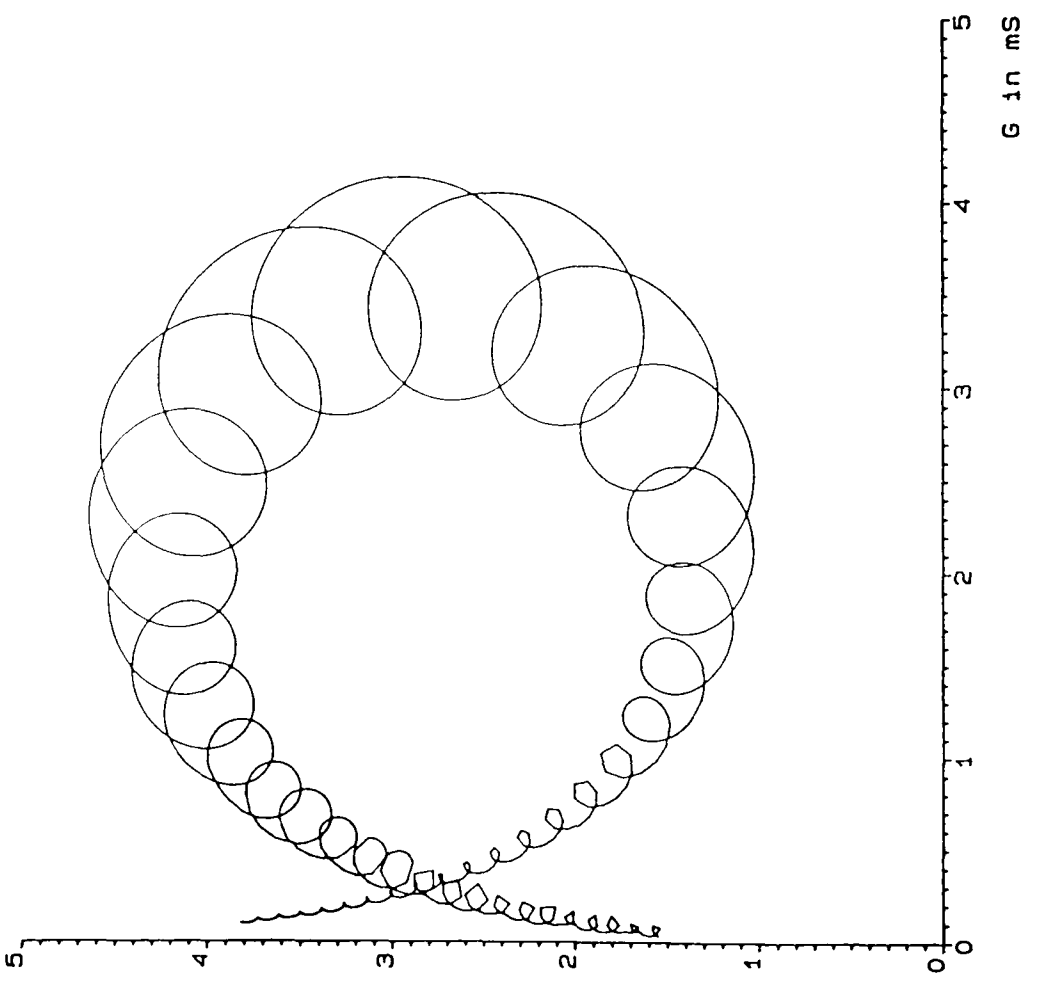

(i) Predicted

Figure 3g Conductance of TB1 when loaded by a 10cm perspex rod.
Loops are caused by standing waves in the perspex.

3.3.4 Radiation Balance Measurements

The program PASSIVE_LOAD can predict the pressure at any boundary between materials. The boundary of greatest interest is the front face of the transducer, i.e. the interface between Stycast and water. A radiation balance, described in appendix 6, was used to measure this output pressure as a function of frequency, hence giving a further check on program accuracy. Having found output pressure the efficiency is derived as the output/input power ratio.

Figure 3h shows the performance of TB1 when operating into a water load. It has already been shown that in TB1 there is significant energy loss through the sides of the ceramic. Therefore it is not surprising that measured front face pressure is lower than predicted. At low frequencies the predicted efficiency is around 25% but measured values are around 15%. As frequency increases the ceramic becomes larger in wavelengths so efficiency approaches the predicted value, the one-dimensional analysis becoming progressively more accurate.

In figure 3i similar measurements are shown for TB2. As expected its low impedance backing gives greater output pressure and higher efficiency than were observed for TB1 but the penalty is a narrower bandwidth. Measurements with the perspex load showed strong intermodal coupling at around 470 kHz. It is interesting to note the significant drop in efficiency at this frequency, showing that the coupled planar resonance delivers a large amount of power to the sides of the ceramic. Again efficiency approaches predicted values as frequency increases, although there is a drop at 650 kHz which remains puzzling.

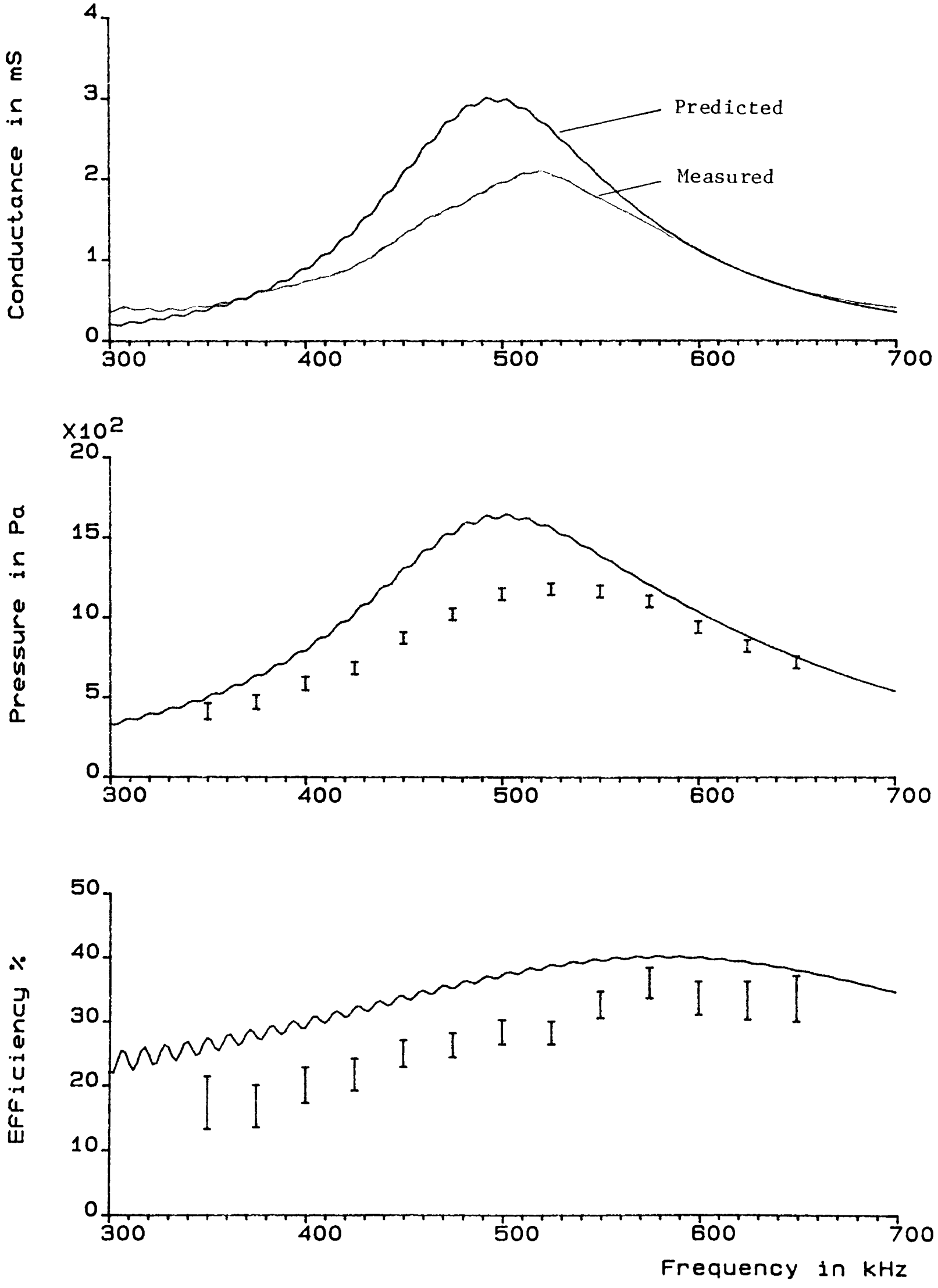

Figure 3h Performance of TB1 in water. Error bars show values measured by radiation balence.

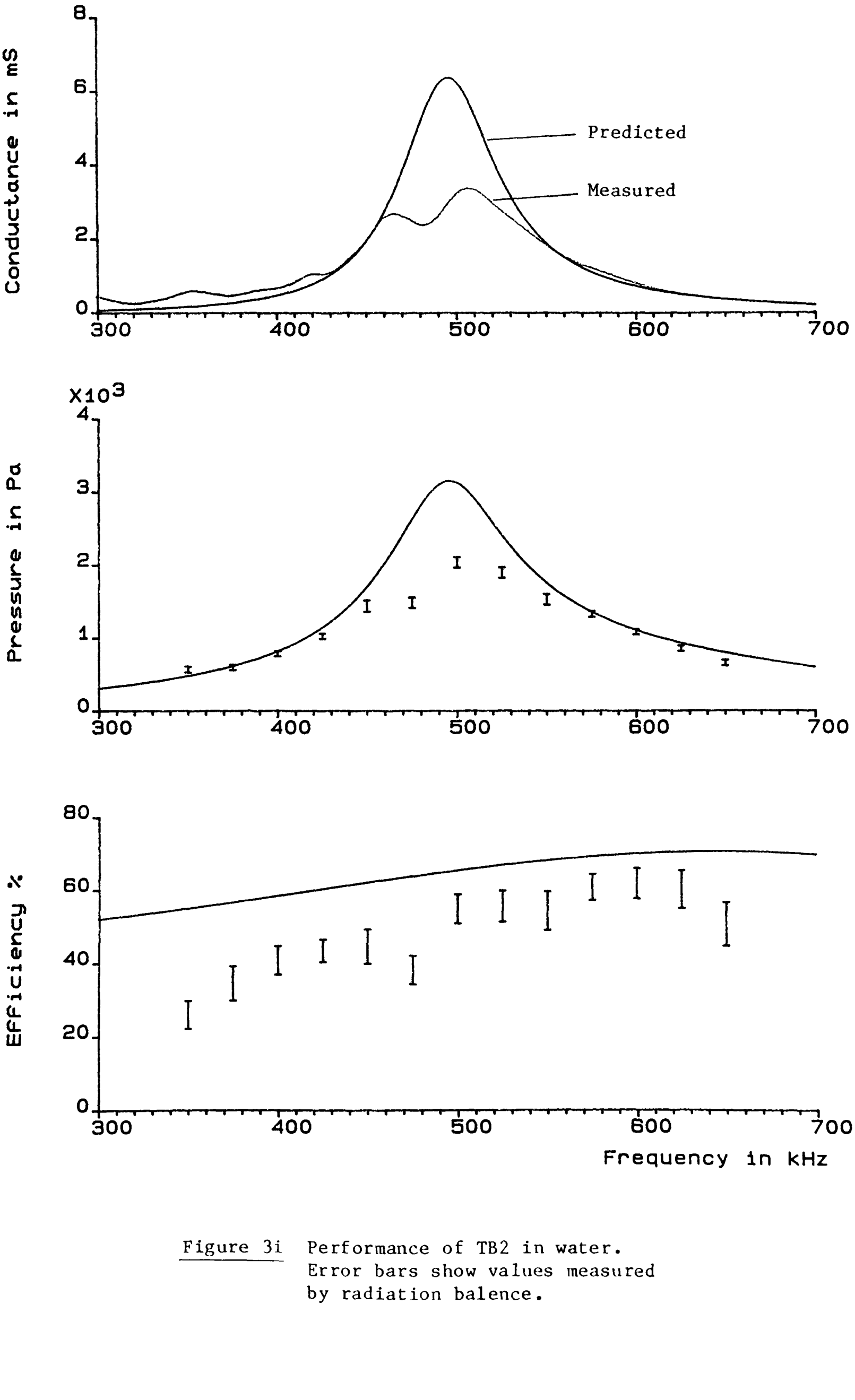

Figure 3i Performance of TB2 in water. Error bars show values measured by radiation balence.

3.4 Discussion of Program Limitations

Both Mason's equivalent circuit and the transmission line equations are one-dimensional models. Therefore they can only deal with thickness mode vibrations of the ceramic and longitudinal plane waves in the surrounding structure. In practice ceramics also have planar resonances such as radial modes for discs, or length and width modes for rectangular plates. Fundamental planar resonances occur at frequencies which are too low to be of interest, but higher overtones may couple with thickness resonances. Koymen (10) has shown that these effects become very significant for thickness/width ratios above 0.13. A further problem is that energy loss through the sides of the ceramic causes greater acoustic loading, and therefore lower conductances, than predicted.

This series of experiments has shown that the program PASSIVE_LOAD gives a satisfactory description of transducer performance and is a useful tool for further studies. However the above limitations should always be taken into account and as a general rule the larger the ceramic the more accurate will be the predictions.

CHAPTER 4

Measurement of Material Properties

4.1 Relevant Data for Transducer Design

In chapter 2 many high frequency sonar transducer designs were discussed. Most of these require an accurate knowledge of material properties, especially for construction of backing and matching layers. Often a material with the required properties is not readily available so one has to be synthesized, usually in the form of a composite. Published data for such materials does not normally exist so a rapid, convenient measuring technique is required.

The mechanical properties which are relevent to acoustics are density, sound velocity and absorption. The method employed for measurement of these parameters depends on the frequency range of interest and the physical state of the sample i.e. solid, liquid or gas.

For the purpose of the present investigation a technique is required for studying solids in the frequency range 100 kHz to 1 MHz. Sound travels through solids both by shear waves and longitudinal waves; however only the latter propagate through water (11). Therefore in this chapter attention is confined to longitudinal waves as these are of greatest importance for the design of sonar transducers.

4.2 Useful Measurement Techniques

In the frequency range 100 kHz to 1 MHz wavelengths are typically a few mm in the materials of interest. Therefore it is convenient to measure the properties of a sample immersed in a small tank of water or other low-loss fluid. Figure 4a shows the arrangement used by McSkimin (reference 9, chapter 4) and Pelmore (26). The sample has flat surfaces and is placed perpendicular to a line between transmitter and receiver.

A simple time delay measurement with and without the sample gives its velocity of sound. Absorption can be calculated from the change in amplitude of the received signal when the sample is included, proper account being taken of the transmission coefficients at the two boundaries. Another method for absorption measurement is to observe the decay of signals reflected back and forth within the sample.

An alternative technique for velocity measurement is to set up standing waves in the sample by transmitting long pulses. After several internal reflections steady state conditions are reached. Signals reflected from the sample have amplitudes which are frequency dependent. Deep minima occur at frequencies where the sample thickness is a whole number of half wavelengths, allowing accurate determination of sound velocity. This is an example of a common situation involving plane waves in three media and has been analysed by Kinsler and Frey (27). It is important that steady state conditions are reached before echoes from the sides of the tank arrive at the transducer, so this method is limited to samples with a thickness of only a few wavelengths.

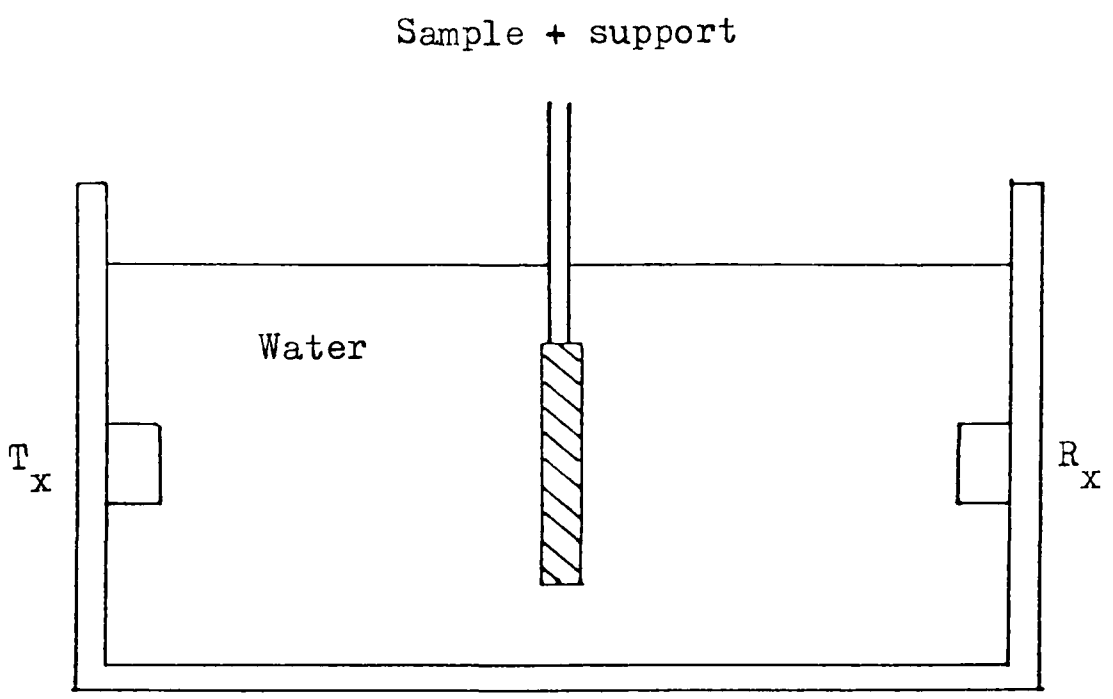

Figure 4a Typical arrangement for water tank measurements.

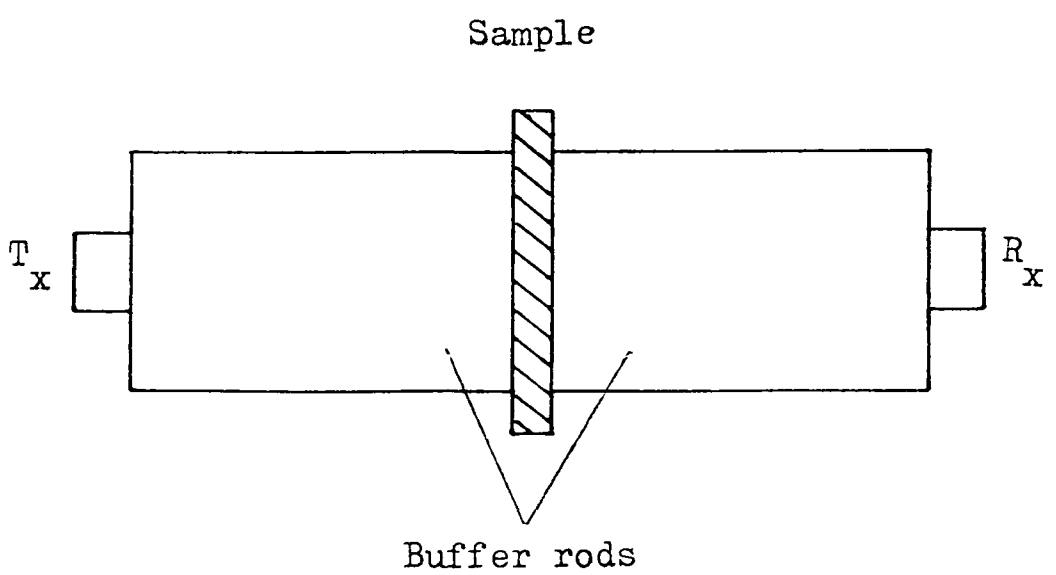

Figure 4b Replacement of water by buffer rod.

All the methods described above require accurate alignment between transducer and sample and in water this may be hard to achieve. A solution is to use a solid buffer rod in place of the fluid medium. The purpose of the buffer rod is to provide a delay between transmitted and received pulses so that ringing after transmission has time to die away. The ends of the rod are machined flat and parallel to give accurate alignment and figure 4b shows a typical arrangement (9) which is suitable for all the above techniques. A similar arrangement was used by Felix (28) to measure dispersion and attenuation in various plastics at frequencies between 1 MHz and 10 MHz.

Pelmore (29) and Koymen (10) developed a buffer rod technique which uses a single transducer to measure reflection coefficients at the rod-sample boundary. Details of this method are given in section 4.3 and the following sections describe further experiments with the same apparatus (30).

4.3 Principle of Buffer Rod Measurements

Figure 4c shows a diagram of the measuring apparatus used by Pelmore (29), and figure 4d shows a block diagram of the associated electronics. A continuous-wave signal at the desired frequency is produced by an oscillator. From this signal a pulse of six to ten cycles is derived. The pulse is amplified and transmitted into the perspex buffer rod using a wide bandwidth transducer. The reflection from the end of the rod is received by the same transducer then amplified, sampled, and entered into a phase sensitive detector. A phase reference is provided by the oscillator output. At some

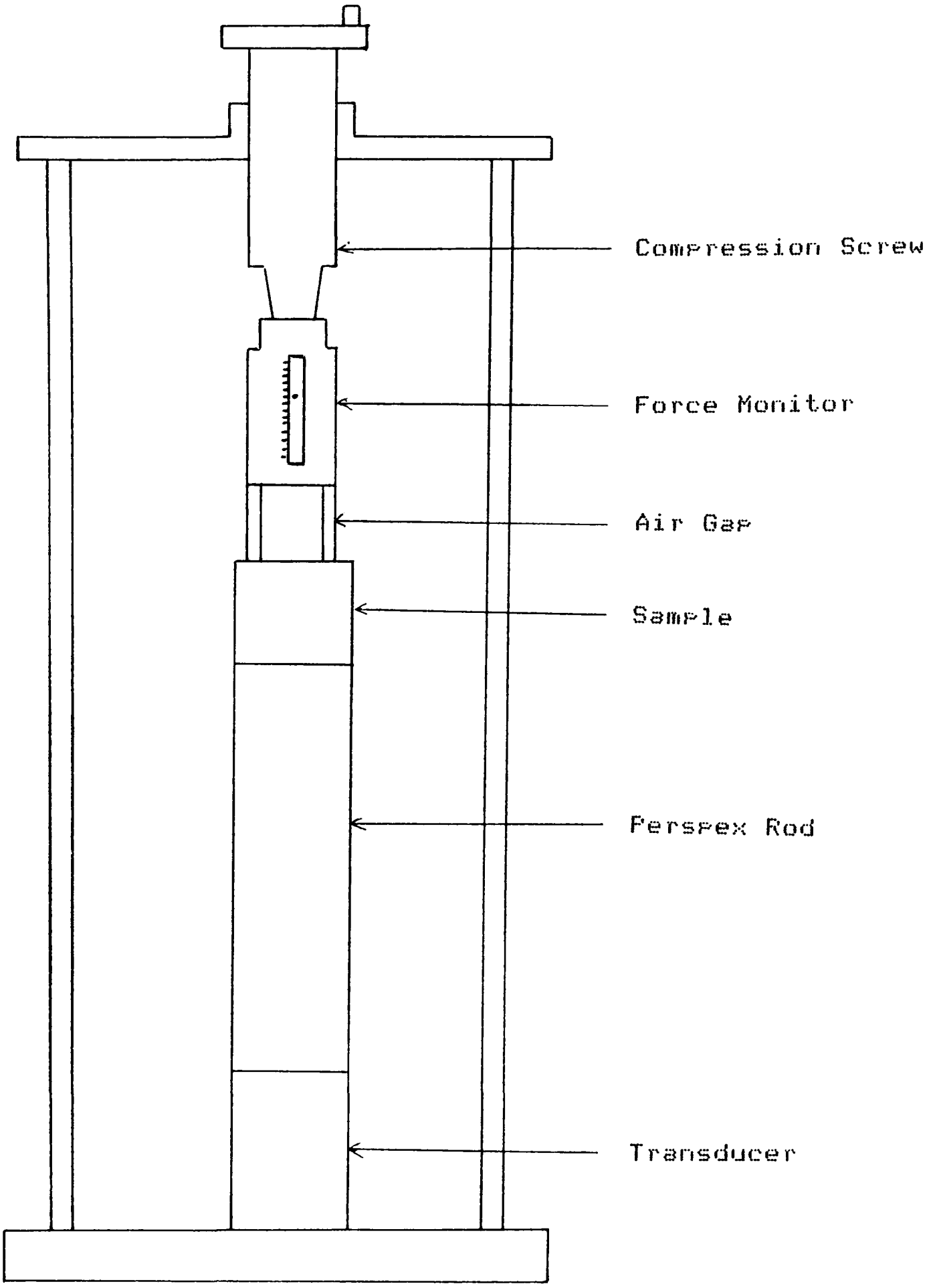

Figure 4c Diagram of buffer rod apparatus.

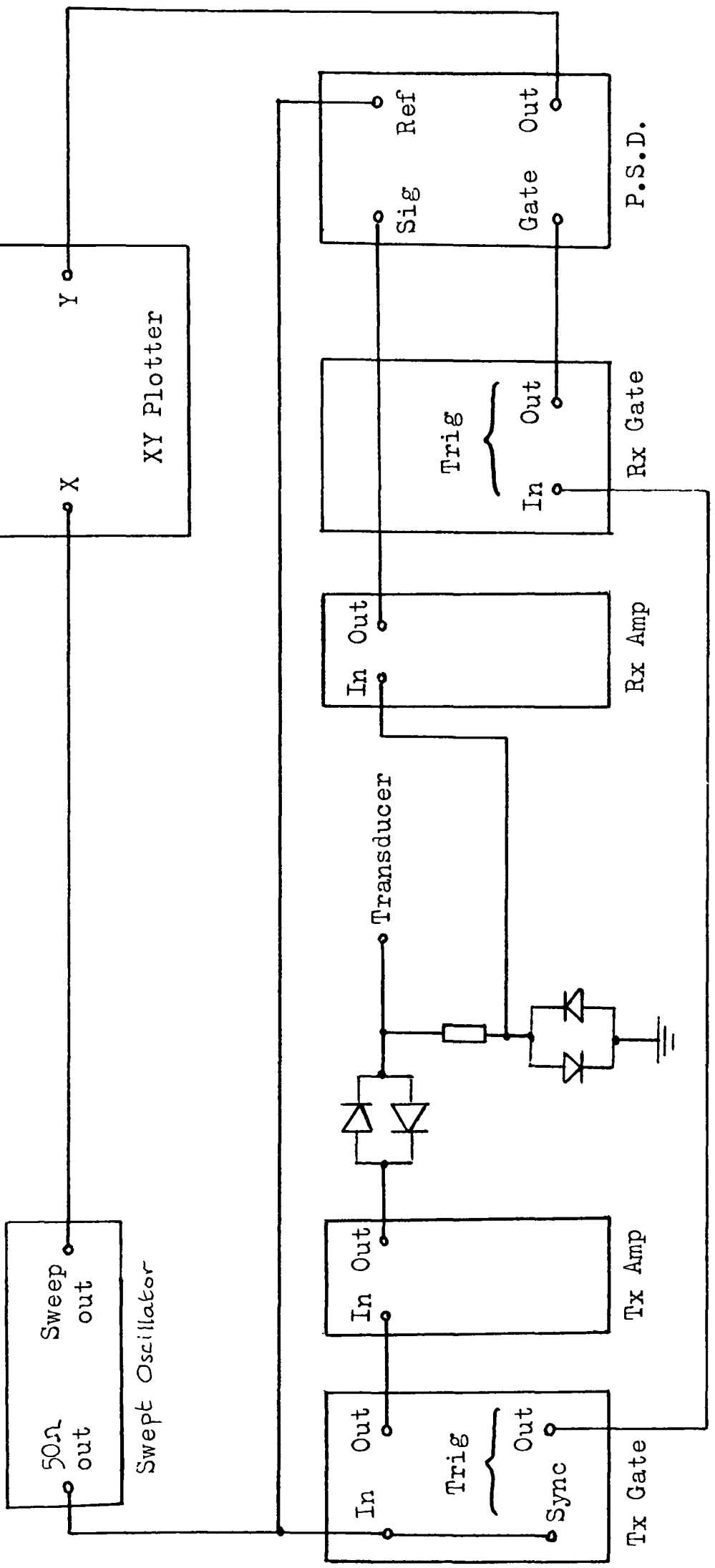

Figure 4d Circuit diagram for buffer rod experiments.

frequencies a small continuous-wave signal was observed at the transmit gate output due to carrier breakthrough, so diodes were added as shown. Each pair of diodes acts as a short circuit for large signals (>0.6 Volts) but open circuit for small signals, thus separating carrier breakthrough from the small received pulse. The returned pressure measured by the transducer is related to the transmitted pressure by:

$$Pr = P_t e^{-2a_p l_p} |R| e^{j(-2k_p l_p + \phi)} \qquad \text{Equation 4.1}$$

where

Pt = transmitted pressure

a_p = absorption of perspex in nepers/m

l_p = length of perspex buffer rod

k_p = wavenumber in perspex

$|R|$ = modulus of rod-sample reflection coefficient

ϕ = phase shift introduced on reflection

Thus the electrical phase shift relative to the reference is $\psi = -2k_p l_p + \phi$ and the output of the detector is $V\cos\psi$ where V is the maximum output voltage.

Figure 4e shows the detector output as the frequency is swept from 500 kHz to 550 kHz. With an air termination $|R|=1$, $\phi = 180^\circ$ and k_p changes with frequency giving a cosine wave. This curve can be used as a reference against which other terminating materials are compared. A comparison technique has the advantage that electrical phase shifts within the transducer are the same for any buffer rod termination. Therefore no knowledge is required of transducer phase response.

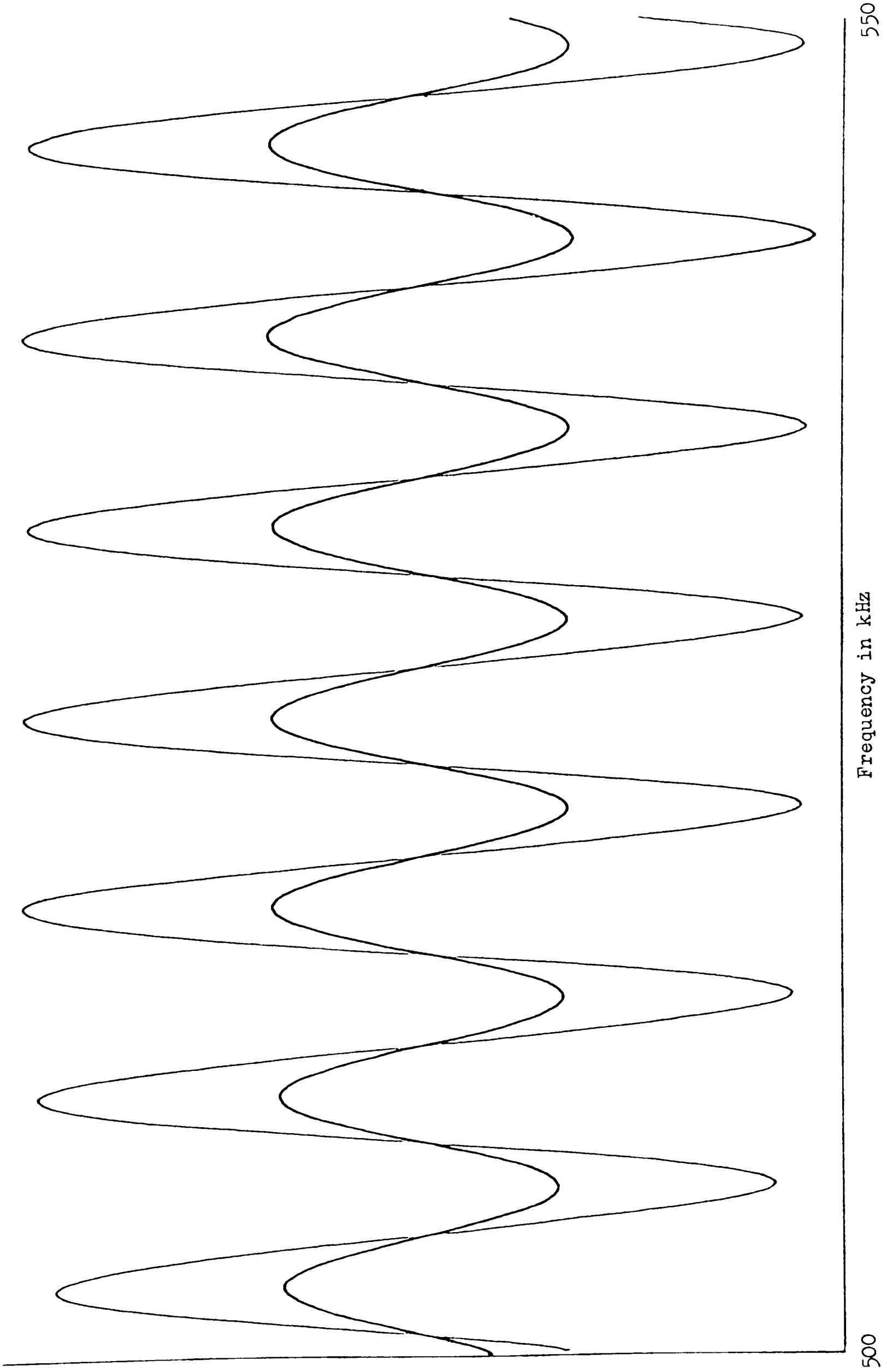

Figure 4e Phase sensitive detector output for air and water terminations.

Figure 4e also shows the effect of a water termination. The resulting cosine wave has an amplitude 0.37 times that of air so $|R|=0.37$ at the perspex-water interface. There is no relative phase shift between the air and water signals showing that $\phi = 180^{\circ}$ for water.

The terminating impedance can be expressed in terms of $|R|$ and ϕ by the equation:

$$Z_T = Z_P \left[\frac{1-|R|^2+2j|R|\sin\phi}{1+|R|^2-2|R|\cos\phi} \right] \qquad \text{Equation 4.2}$$

Substituting the measured values for water gives $Z_T=1.47+j0$ Mrayls which is close to the expected result. Using this technique the impedance of any sample can be found and since density is easily measured sound velocity can be calculated. Equation 4.2 is derived in appendix 1.

4.4 Effect of Coupling Layers

The sample being tested is usually a solid and for good acoustic contact has to be bonded to the buffer rod. To examine the effect of such bonds a perspex sample was used which for an ideal bond would give $|R|=0$. Figure 4f shows the effect of water and grease bonds. In both cases $\phi = -90^{\circ}$ and $|R|$ is small but measurable. This indicates a complex terminating impedance as predicted by transmission line theory. It is interesting to note that if ρ and c are known for the bond material then its thickness can be found from the following equation, which is derived in appendix 2.

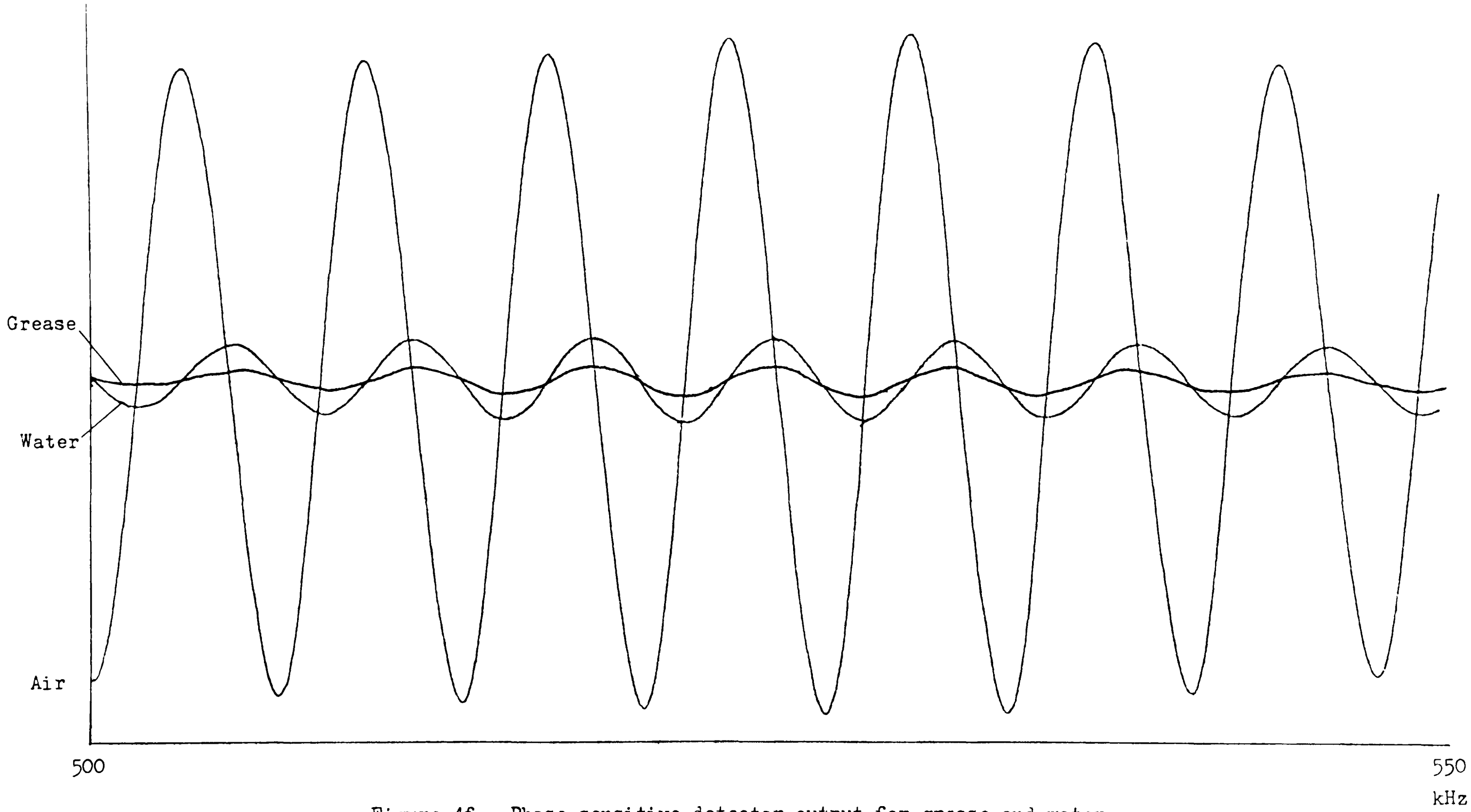

Figure 4f Phase sensitive detector output for grease and water bonds with perspex termination. An ideal bond would give a straight line.

$$l_b = \frac{Z_b Z_T}{k_b(Z_b^2 - Z_T^2)} \cdot \frac{2|R|\sin\phi}{1-|R|^2} \qquad \text{Equation 4.3}$$

where

l_b = bond thickness

k_b = wavenumber in bond

Z_b = impedance of bond

Z_T = terminating impedance

Applying equation 4.3 to water and grease bonds at 525 kHz gives the following results:

	ρ Kg/m^3	c m/s	$\lvert R\rvert$	ϕ	l_b μm
Water	1000	1500	0.129	-90	71
Grease	1140	1920	0.044	-90	67

TABLE 4.2

For the purpose of buffer rod measurements grease gives a more suitable bond than water because its impedance is closer to that of perspex. It is also an easier bond to use in practice. In all cases the grease used was "Nonaq Stopcock Grease" supplied by Fisher Scientific Co. Its sound velocity was measured by the technique described in section 4.5.

4.5 Accurate Velocity and Absorption Measurement

The measurement of $|R|$ and ϕ as described above gives good results provided $|R| > 0.2$. For smaller values of $|R|$ the data becomes

progressively harder to read and results are less accurate. For situations where $|R|$ is small, i.e. the acoustic impedance of the sample is close to that of perspex, a more accurate determination of velocity is possible by observing the reflection from the sample-air boundary (30). This signal has traversed the sample length twice and has an additional phase shift given by:

$$\phi = \phi_t - 2k_s l_s = \phi_t - 4\pi f l_s / c_s \qquad \text{Equation 4.4}$$

Where k_s, c_s and l_s are the wavenumber, sound velocity and length of the sample respectively. ϕ_t is a small phase shift introduced during transmission from the buffer rod into the sample. ϕ_t depends on the a/k ratio for the sample and can be shown to be typically small and independent of frequency. Its effect is to offset the output from the phase sensitive detector.

The sound velocity in the sample can therefore be found from the rate of change of phase with frequency:

$$\frac{d\phi}{df} = \frac{-4\pi l_s}{c_s} \qquad \therefore \; c_s = \frac{-4\pi l_s}{d\phi/df} \qquad \text{Equation 4.5}$$

In practice a small correction has to be made to allow for the grease

bond as shown in appendix 3. The result is:

$$c_s = \frac{-4\pi l_s}{d\phi/df + 4\pi F l_b/c_b} \qquad \text{Equation 4.6}$$

where

l_b = bond thickness

c_b = velocity of sound in bond

$F = \frac{Z_b^2 + Z_p Z_s}{Z_b(Z_p + Z_s)}$

Z_b = impedance of bond

Z_p = impedance of perspex

Z_s = impedance of sample

For the particular mode of operation under discussion the values of Z_b, Z_p and Z_s are all of the same magnitude so the impedance ratio F is close to unity. Substitution of practical values for the bond thickness shows that the factor $4\pi F l_b/c_b$ is only about 1% of $d\phi/df$ and therefore may be ignored in most cases.

The reflected signal from the sample-air interface has traversed the sample twice so can be used to find absorption in the sample:

$$a_s = \frac{-1}{2l_s} \ln \left[\frac{(Z_p + Z_s)^2}{4 Z_p Z_s} . |A| \right] \qquad \text{Equation 4.7}$$

The factor $|A|$ is the amplitude ratio of signals reflected with and without the sample present. See appendix 4 for the derivation of this equation.

4.6 Some Experimental Results

Figure 4g shows the expected appearance of returned signals after a ten cycle pulse is transmitted towards thick and thin air backed samples. For simple impedance calculations, of the kind described in section 4.3, a thick sample is used and the measuring gate is set to the GATE 1 position. Figures 4e and 4f were plotted in this way. The accurate velocity and absorption calculations described in section 4.5 also use a thick sample but this time measured at the GATE 2 position.

In practice it was found that all reflections from the end of the perspex rod were followed after 34μs by an unexpected signal. The cause of this signal is not known but it may be associated with edge wave effects as described by Low and Jones (19). To avoid errors due to this signal measurements were restricted to samples of thickness 4λ or less. Figure 4g shows that for thin samples there is interference between reflections from the perspex-sample and sample-air boundaries so that measurement in the GATE 2 position is not possible. However the method described in section 4.5 is only applicable to samples with impedance close to that of perspex. Therefore reflections from the perspex-sample boundary are very small and measurements taken at the GATE 3 position suffer little interference.

Figure 4h shows the output of the phase sensitive detector for a 16.3mm Stycast 1264 sample compared, as always, with an air termination. Limited transducer bandwidth gives both cosine waves a curved envelope. The amplitude and phase of reflections from the sample-air boundary are frequency dependent and are plotted in figure

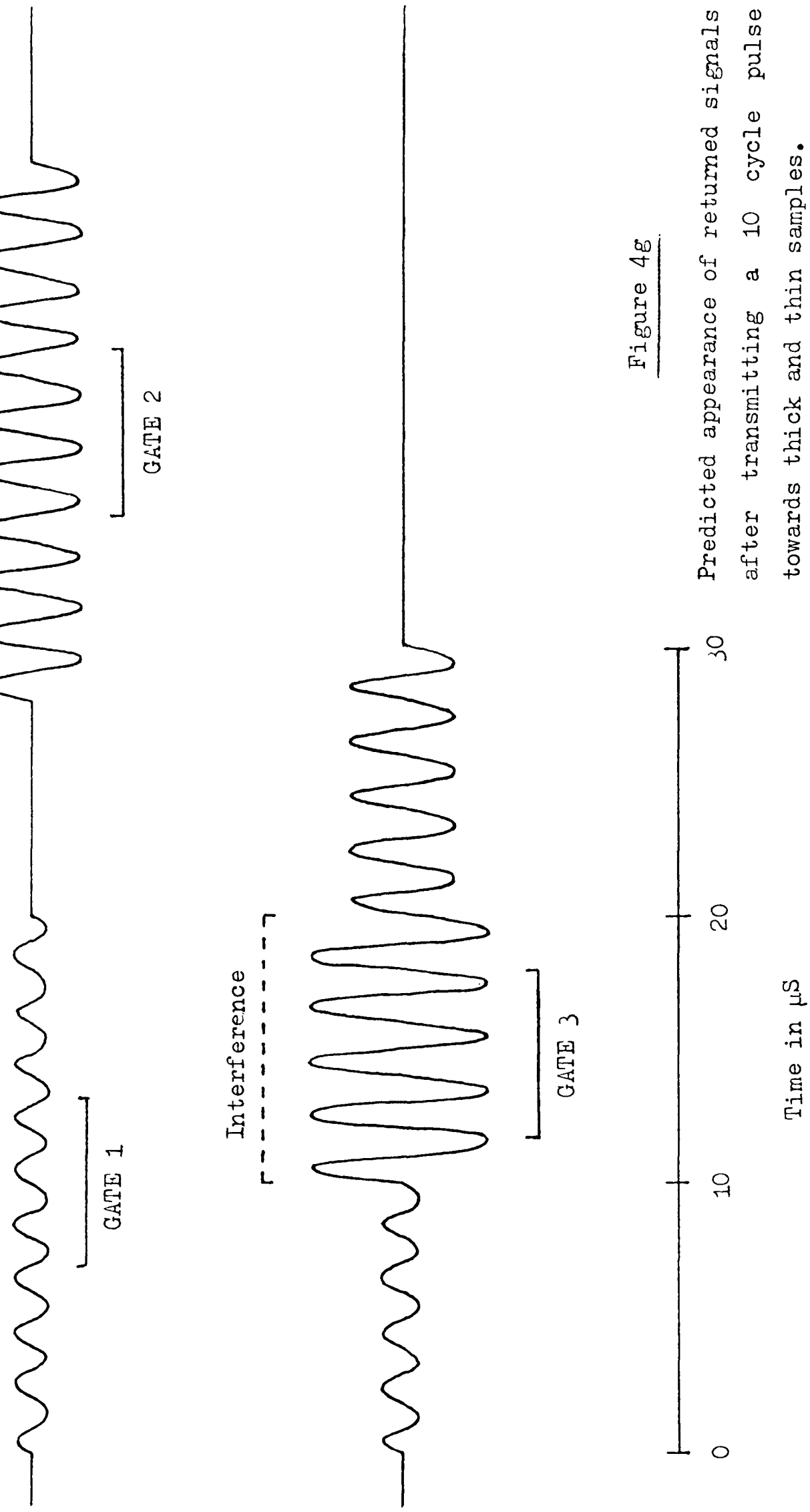

Figure 4g

Predicted appearance of returned signals after transmitting a 10 cycle pulse towards thick and thin samples.

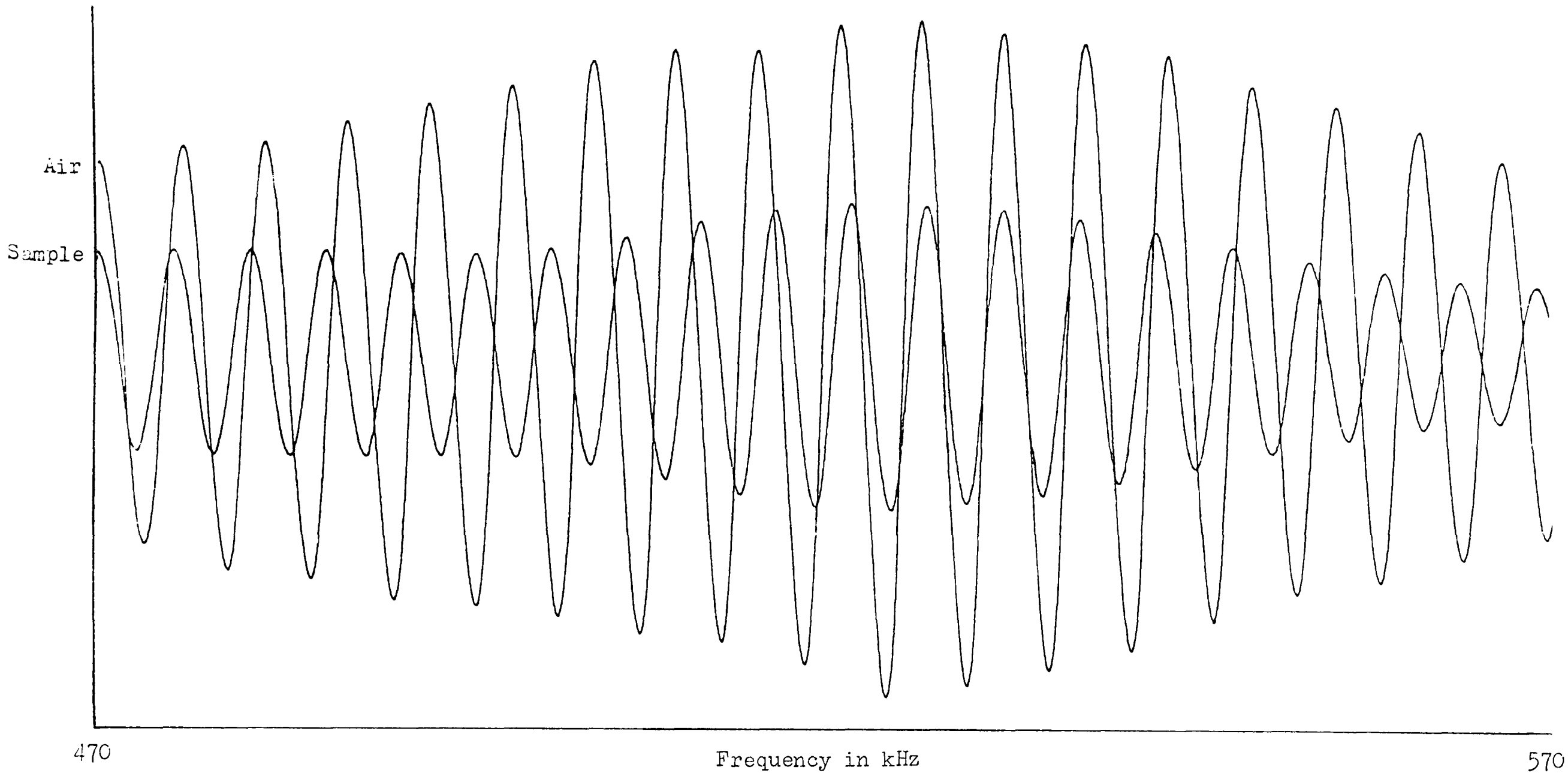

Figure 4h Phase sensitive detector output for 16.3mm Stycast sample measured at GATE 3 position.

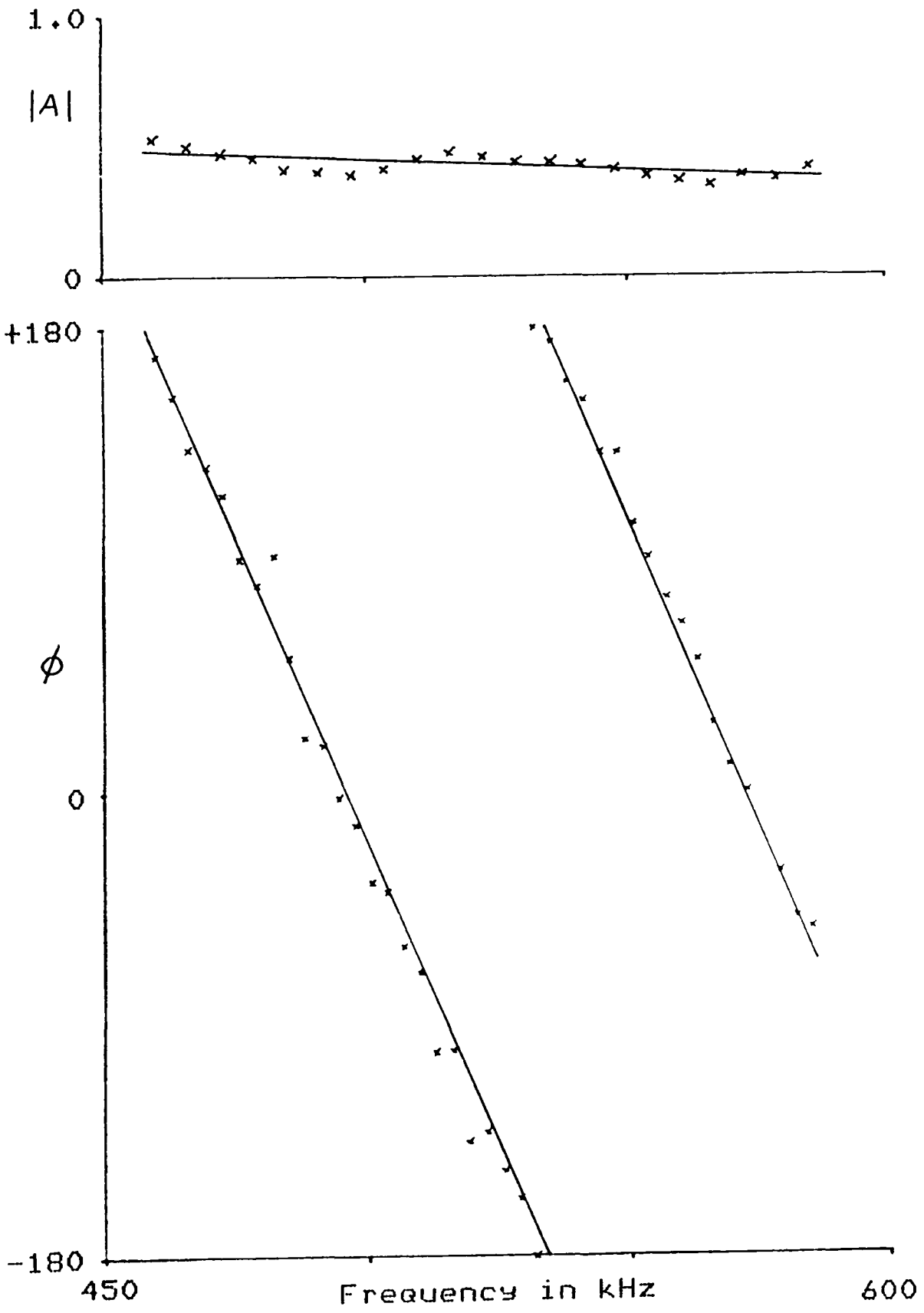

Figure 4i Amplitude and phase as functions of frequency derived from figure 4h. Straight lines are "least squares fit" approximations.

4i. Measurements were taken at the GATE 3 position so interference causes the measured points to deviate from straight lines in a sinusoidal way which is particularly noticeable in the graph for |A|. A least squares fit program was used to draw a straight line through the phase data. Its gradient is $-(8.11\pm0.26)*10^{-5}$ radians/Hz which on substitution into equation 4.5 gives a velocity of 2523±79 m/s for the Stycast 1264 sample. The tolerance is about 3% which is large enough to ignore grease bond effects.

Many materials show a decrease in sound velocity as the frequency increases (9,28). This is called dispersion. The variation of phase with frequency in a dispersive medium does not give a linear relationship, however all materials tested were found to produce straight line graphs indicating that they are not dispersive over the frequency range used.

The amplitude data in figure 4i shows that Stycast 1264 has an absorption which varies with frequency. Applying equation 4.7 at two discrete points gives:

Frequency	|A|	a
460 kHz	0.48	1.9 dB/cm
580 kHz	0.39	2.5 dB/cm

TABLE 4.2

These results suggest that absorption is proportional to frequency although measurements over a greater frequency range would be needed for confirmation.

4.7 Interference Techniques

If the sample impedance is very different from that of perspex then measurements at the GATE 3 position show strong interference effects. Figure 4j shows the phase sensitive detector output for a 14.4mm sample of epoxy/tungsten compared with an air reference. Amplitude minima occur when the sample is a whole number of half-wavelengths thick so the velocity of sound can be derived as follows:

1st minimum at 511±2 kHz
2nd minimum at 565±2 kHz
} Difference of 54±4 kHz

$\therefore \quad \lambda/2 = 14.4\text{mm at } 54\pm4 \text{ kHz}$

$c = f\lambda = 1555\pm115 \text{ m/s}$

The tolerance here is 7% which shows that this technique is not as accurate as the $d\phi/df$ measurement of section 4.5. The same calculation could be done using the positions of maxima although in general minima are more clearly defined.

Again the sound has traversed the sample twice so absorption can be calculated as shown in appendix 5. Let Λ be the amplitude ratio of maximum/minimum in the interference pattern. Interference measurements are most suitable for samples of greater impedance than perspex and for this case:

$$a_s = \frac{-1}{2l_s} \ln\left[\frac{Z_s^2 - Z_p^2}{4Z_s Z_p} \cdot \frac{(\Lambda-1)}{(\Lambda+1)}\right] \qquad \text{Equation 4.8}$$

where Λ can be either +ve or -ve depending on phase. For $Z_s > Z_p$

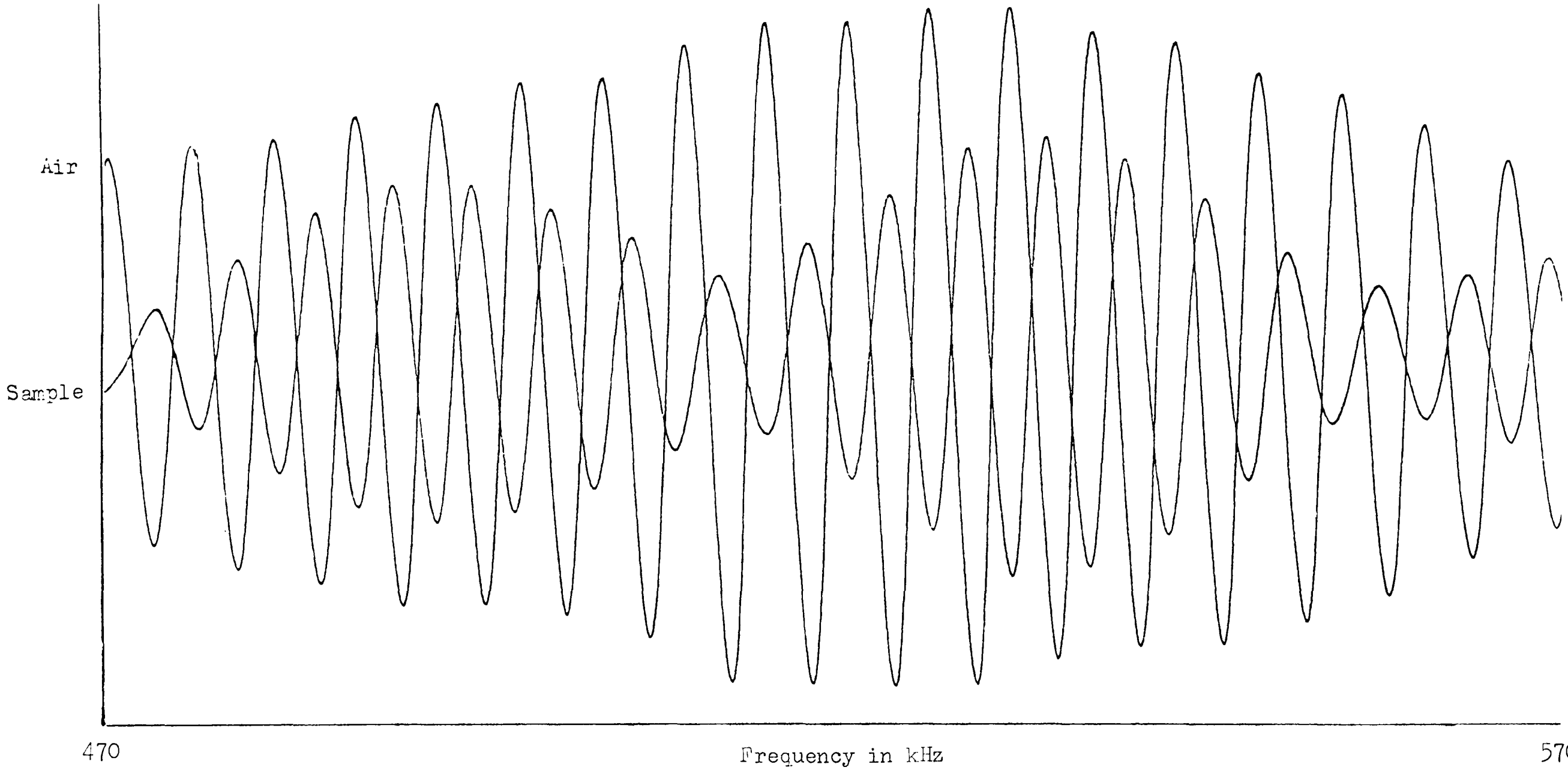

Figure 4j Phase sensitive detector output for 14.4mm epoxy/tungsten sample measured at GATE 3 position.

maxima always occur in antiphase with the air reference, but minima can be in phase or antiphase. The rule is; if minima occur in phase with the air reference then Λ is negative.

The epoxy/tungsten sample has a density of 6210 kg/m^3 and a velocity, which has already been derived above, of 1555 m/s. Therefore the characteristic impedance Z_S becomes:

$$Z_S = \rho c = 6210*1555 = 9.65*10^6 \text{ Rayls}$$

Figure 4j shows an amplitude ratio of Λ =+2.50. This is calculated taking into account the variation in amplitude of the air reference. Λ is positive because maxima and minima are both in antiphase with the air reference. Substitution into equation 4.8 gives a=43.3 nepers/m or 3.8 dB/cm at 500 kHz.

Unfortunately 14.4mm is nearly five wavelengths at 500 kHz. Sound takes 20μs to travel through the sample and back again leaving only 14μs before the arrival of the unexplained reflection. Due to limited transducer bandwidth there is insufficient time for the output to reach a steady value and measurements taken at the GATE 3 position do not have the correct amplitude. Therefore although figure 4j provides a useful demonstration of interference techniques it should not be used to derive accurate information with the existing equipment. For the same epoxy/tungsten sample Pelmore (29) measured an absorption of 1.1 dB/cm at 500 kHz which is likely to be a more accurate value although no tolerance is quoted.

4.8 Improvements to Measuring Techniques

The buffer rod apparatus has proved useful for simple impedance measurements, of the kind described in section 4.3, and these usually give results which are accurate enough for transducer design. Interference and $d\phi/df$ measurements offer greater accuracy but are limited by an unexpected transmission and subsequent reflection at the end of the perspex rod. In future work it is clear that the buffer rod should be changed, probably to a different material and perhaps also to different dimensions. If unwanted reflections prove hard to overcome with a solid buffer rod then a possible alternative is to use a water column, to which all the above equations equally apply. This arrangement is currently being investigated (43).

CHAPTER 5

The Piezoelectric-Tunable Transducer

5.1 Harmonics of the Thickness Resonance in Ceramic Discs

In previous chapters only the fundamental thickness resonance has been studied. It would be interesting to investigate the suitability of higher harmonics for sonar applications. Strictly speaking the word "harmonic" implies an exact multiple of the fundamental frequency. Ceramics with high coupling do not give simple integer relationships so in this work the terms "second harmonic" and "third harmonic" will be used to describe those resonances which occur at approximately two and three times the fundamental frequency respectively.

Consider the behavior of an 8.5mm thick PZT-4 disc which is available from Vernitron (34). Figure 5a(i) shows an air-backed ceramic of this kind radiating into water through a thin protective layer of Stycast 1264. A symbolic representation of conductance is also given. The fundamental thickness resonance occurs at 236 kHz and there is a third harmonic at 807 kHz. Both radiate power into the water and are within the frequency range of interest. An alternative design for a 236 kHz resonator is to use two 4.25mm plates bonded together, as shown in figure 5a(ii), which gives the same behavior as the single ceramic design.

A different way of driving the two ceramic structure is shown in figure 5a(iii) where the voltage is applied across only one ceramic, the other remaining open-circuit. This design gives a fundamental

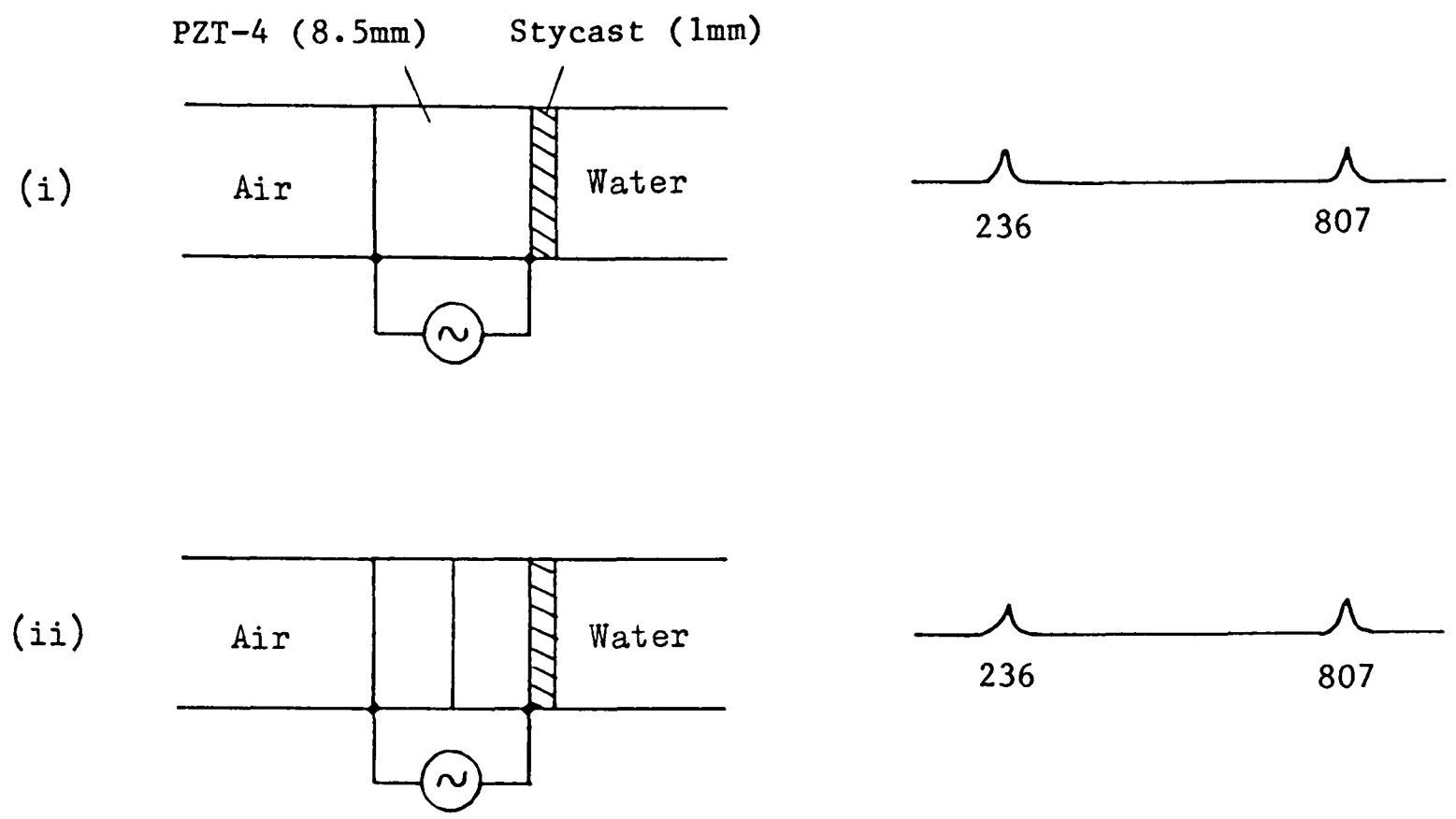

Figure 5a Natural resonances available with a total ceramic thickness of 8.5mm.

resonance at 249 kHz and a third harmonic at 812 kHz. However an additional resonance now appears at 507 kHz which can be regarded as the second harmonic of the ceramic pair. This resonance radiates power into the water and is therefore potentially useable.

Another way to connect the same structure is to replace the open-circuit by a short-circuit as shown in figure 5a(iv). This causes the second harmonic to reduce in frequency to 473 kHz, a change of about 7%. The fundamental and third harmonic frequencies also reduce but by a smaller amount.

In this way the total ceramic thickness has a resonance at around 500 kHz which is excited by one element but controlled by the other. The elements can be considered as the "drive ceramic" and "control ceramic" respectively. A transducer with an externally controlled resonant frequency may have useful practical applications and the purpose of this chapter is to investigate the behaviour of such a device.

5.2 Control of Resonances Using Passive Electrical Components

It has been shown that the transducers of figures 5a(iii) and 5a(iv) have different resonances according to the electrical load. The obvious question to ask is can the resonant frequency be changed continually between its open-circuit and short-circuit values using a variable resistance or reactance?

To answer this question the program PASSIVE_LOAD, described in Chapter 3, was modified to include analysis of the circuit in figure

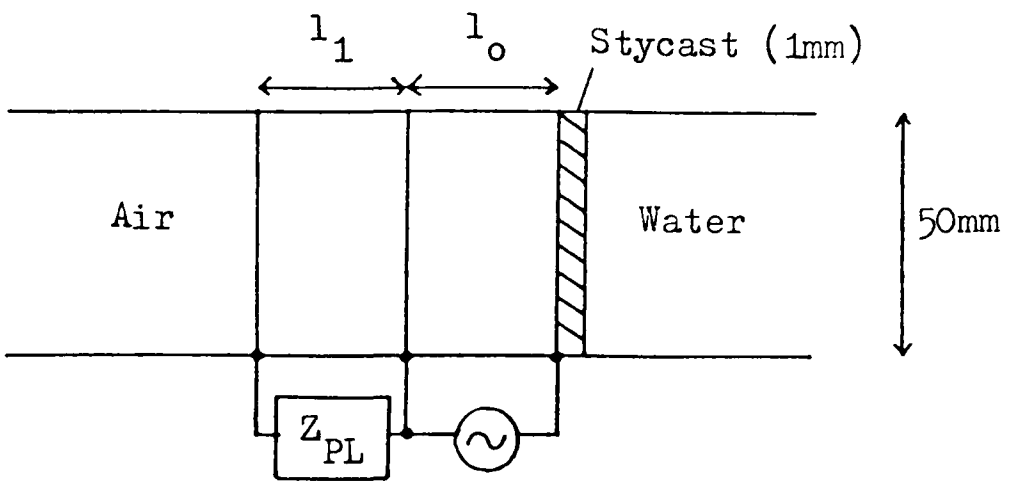

Figure 5b Active ceramic with passively loaded ceramic backing.

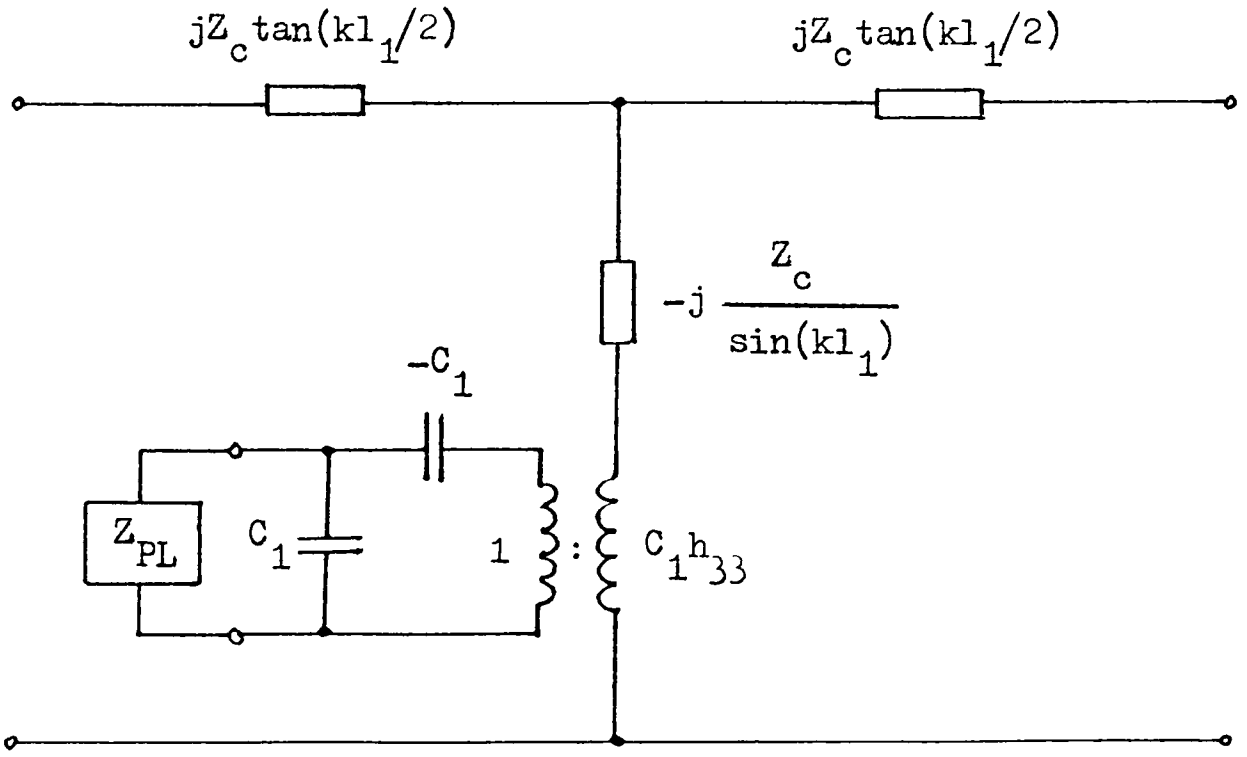

Figure 5c Equivalent circuit for a passively loaded ceramic. In general $Z_{PL} = R_{PL} + jX_{PL}$.

5c. This is Mason's equivalent circuit for a ceramic with a passive electrical load Z_{PL}, which in general can have both resistive and reactive components. Any structure containing one or more passively loaded ceramics can be represented by adding figure 5c to the general circuit of figure 2d at the relevant position(s). The program PASSIVE_LOAD is then used to calculate the admittance seen looking into the active ceramic.

Figure 5b shows the transducer design used for computer simulation. The drive ceramic has thickness l_o and is protected from the water load by a thin epoxy layer. The control ceramic has thickness l_l and is air backed. Computer simulation was run for different resistive loads and the results are shown in figure 5d(i). Resonance can indeed be varied continually between 473 kHz and 507 kHz. However dissipation of energy in the resistance causes increased acoustic loading, so the conductance and Q factor decrease as the resonance is moved away from its open-circuit or short-circuit frequencies.

A different way of changing the passive electrical load is to use a variable capacitor which has the advantage that no energy is dissipated. The predicted effect is shown in figure 5d(ii). This time the conductance at resonance is maintained at around 25mS with a Q of 20. The control ceramic is 4.25mm thick, 50mm diameter, and has a clamped capacitance of 2.6nF. It is interesting to note that if the electrical load is a capacitor of this same value then resonance occurs half way between the short-circuit and open-circuit frequencies. Furthermore the reactance of a 2.6nF capacitor at 490 kHz is 125Ω which is the value of resistance already found to produce a resonance

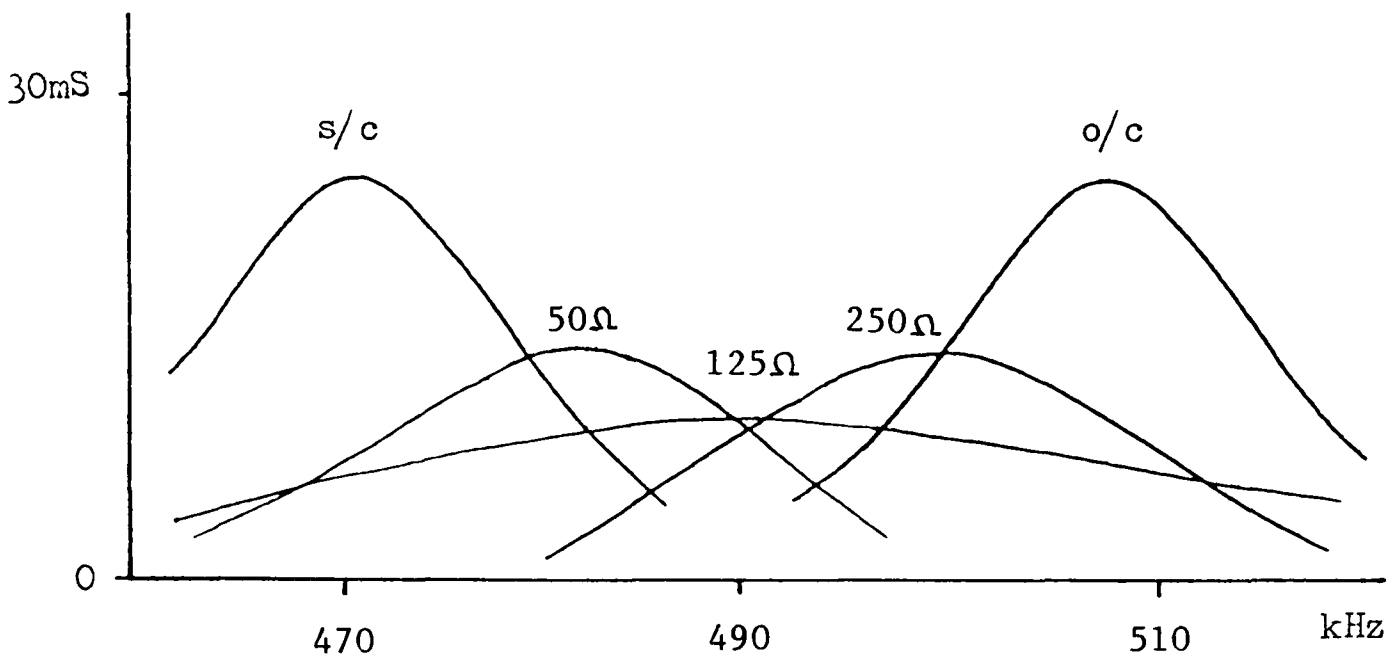

(i) Resistance variation

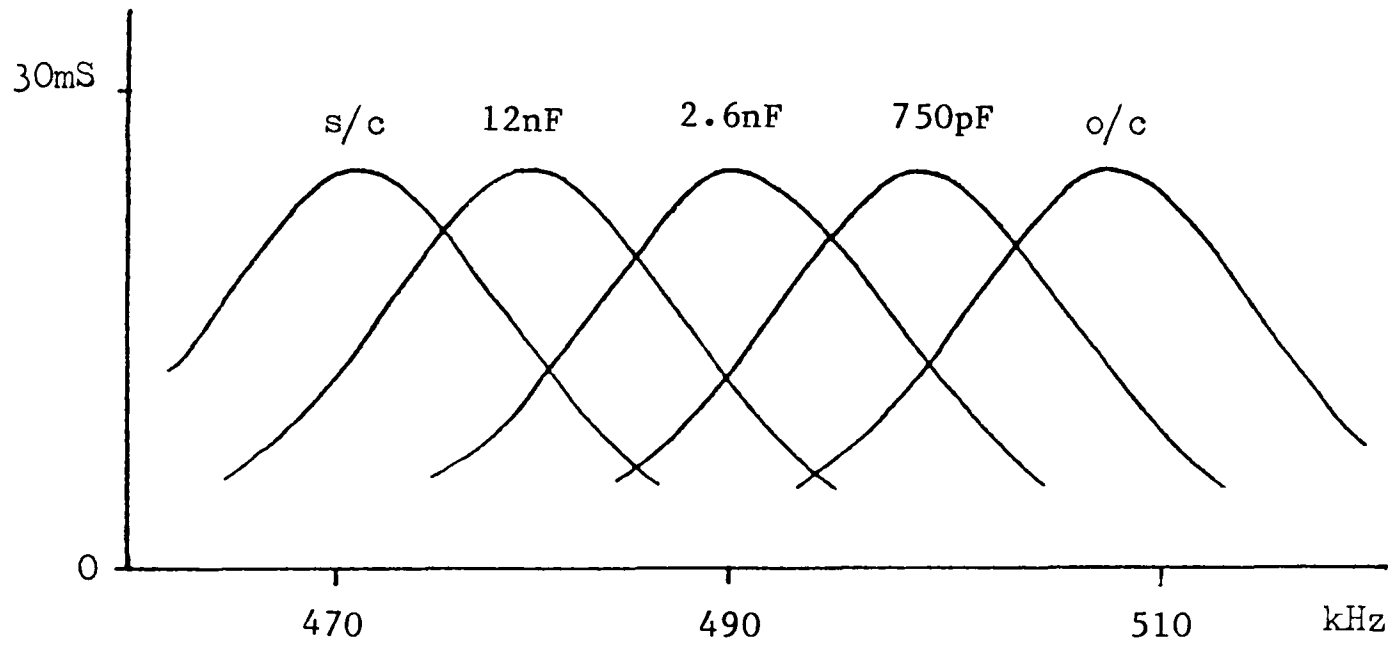

(ii) Capacitance variation

Figure 5d Predicted conductance for the transducer of figure 5b with $l_o = l_1 = 4.25$mm.

at this frequency.

Resistive or capacitive loads also affect the fundamental and third harmonic resonances but frequency variations are less than for the second harmonic. The difference in behavior of the harmonics can be explained qualitatively by considering loading effects. At around 500 kHz the active element is backed by a half wavelength thick ceramic with an air termination. At 249 kHz and 812 kHz the backing forms a $\lambda/4$ or $3\lambda/4$ layer respectively and these are less sensitive to parameter variations than the half wavelength case.

The structure described above is an example of a piezoelectric-tunable transducer. Chenghao and Zheying (31) have carried out a detailed theoretical analysis of a similar structure operating in air at around 30 kHz. They describe the region between open-circuit and short-circuit resonances as the "domain of capacitance adjustment" and they show that resonance can be moved outside this range by an inductive load. Following their example the program PASSIVE_LOAD was used to examine the effects of inductive loading on the structure of figure 5b.

A very small inductance is approximately a short circuit so produces a resonance at 473 kHz. Increasing the inductance causes the resonant frequency to decrease, tending towards 249 kHz. At the same time the fundamental resonance reduces in frequency, tending towards zero, and the third harmonic reduces towards 507 kHz. These effects are summarised in figure 5e which shows that in theory a resonance can be produced at any required frequency.

Inductance in an electrical resonant circuit is analagous to mass in a mechanical oscillator. Therefore inductive loading of a

piezoelectric-tunable transducer can be interpreted as the addition of extra mass, causing a decrease in resonant frequency.

5.3 Effects of Parameter Variation

For a piezoelectric-tunable transducer to be of general use in sonar systems it should be easily constructed, easy to control and have reliable performance. For most applications low Q and high efficiency are also important as described in Chapter 2.

The program PASSIVE_LOAD was used to investigate conductance variations of the transducer in figure 5b as a result of parameter changes in the passive electrical load.

5.3.1 Electrical Impedance and Backing Impedance Variation

Figure 5e shows that inductive loading of a piezoelectric-tunable transducer produces greater changes in resonant frequency than capacitive loading. The inductance required for resonance at a particular frequency is approximately that which tunes out the clamped capacitance. For example at 350 kHz the clamped capacitance of 2.6nF is tuned out by an inductance of 79μH. The actual inductance which causes resonance at this frequency is shown on figure 5e to be 68μH, so tuning out can be used as an indication of the order of magnitude required.

Variable capacitors are more readily available than variable inductors. The above discussion suggests that resonance could be

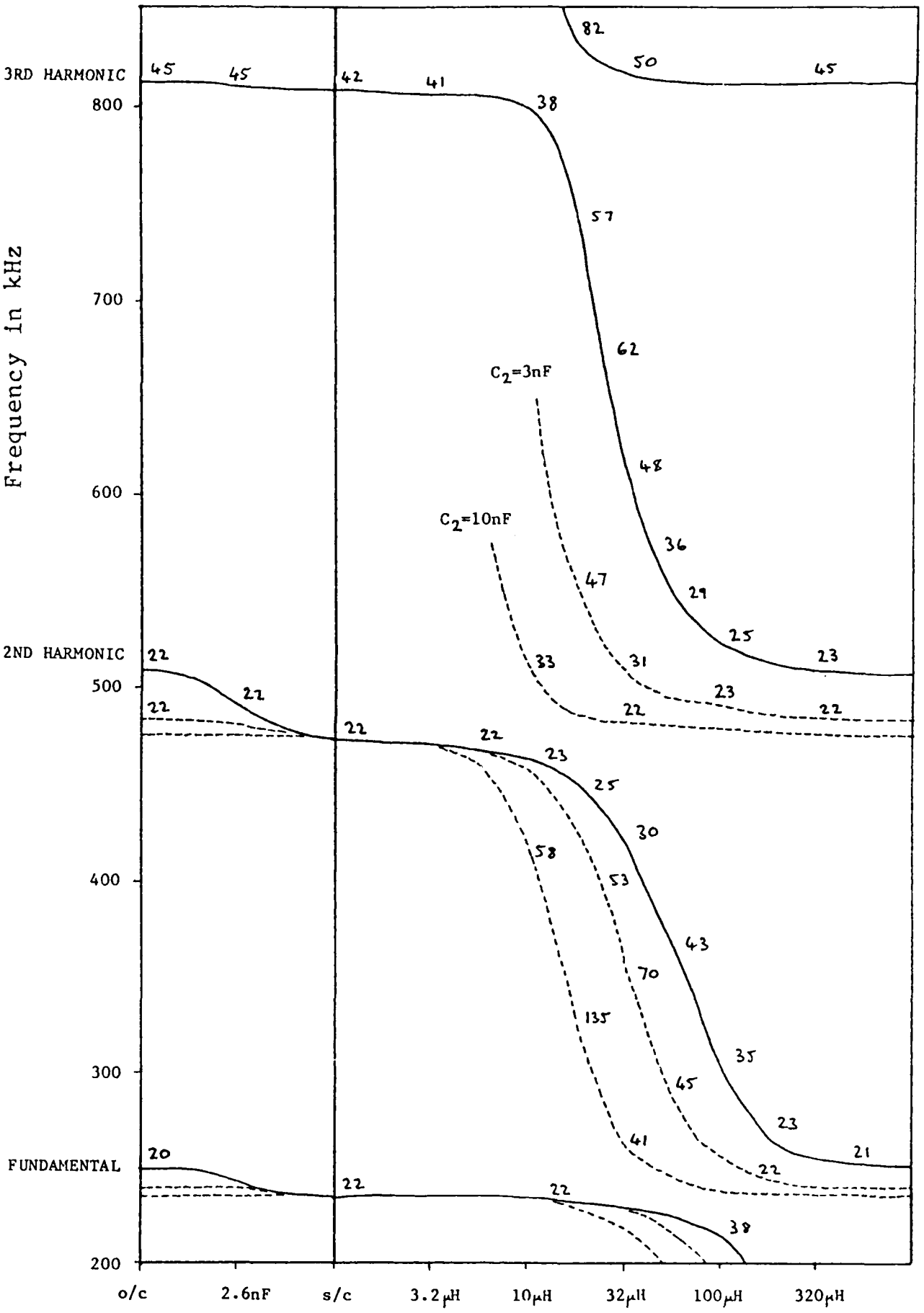

Passive electrical load

Figure 5e

Resonances for the transducer of figure 5b with $l_o = l_1 = 4.25$mm. Figures beside curves are Q values for the air backed case with $R_{PL} = 0$. Dotted lines show resonances with C_2 in parallel with clamped capacitance.

controlled using a fixed inductor in parallel with a variable capacitor, so that the clamped capacitance is effectively variable. The dotted lines on figure 5e show that this does indeed work, for example a 32μH inductor can cause resonance anywhere between 260 kHz and 420 kHz by varying a parallel capacitance from 10nF to zero. Unfortunately this technique produces very high Q resonances. These are of little use in practice so variable inductance must still be used and the dotted lines on figure 5e are not a useful operational mode.

All inductors have losses which can be represented by series resistance, and it has already been shown in figure 5d(i) that resonances are strongly influenced by resistance. For an inductive electrical load it was found that a small series resistance (less than 10Ω) causes a decrease in Q but has no effect on resonant frequency. Therefore increasing the resistive load of an air backed piezoelectric-tunable transducer has a similar effect to increasing the backing impedance of a single ceramic.

The influence of backing impedance on piezoelectric-tunable transducer performance was then investigated. It was found that resonant frequency is unchanged by backings of small impedance compared with that of ceramic (most practical cases) but the bandwidth is strongly affected. The relationship between resonant frequency and inductance on figure 5e therefore applies for all backing impedances, but the Q values only apply for the air backed case with no series resistance.

The effect of variations in backing impedance and passive electrical load are summarised in figure 5f which can be interpreted as follows:

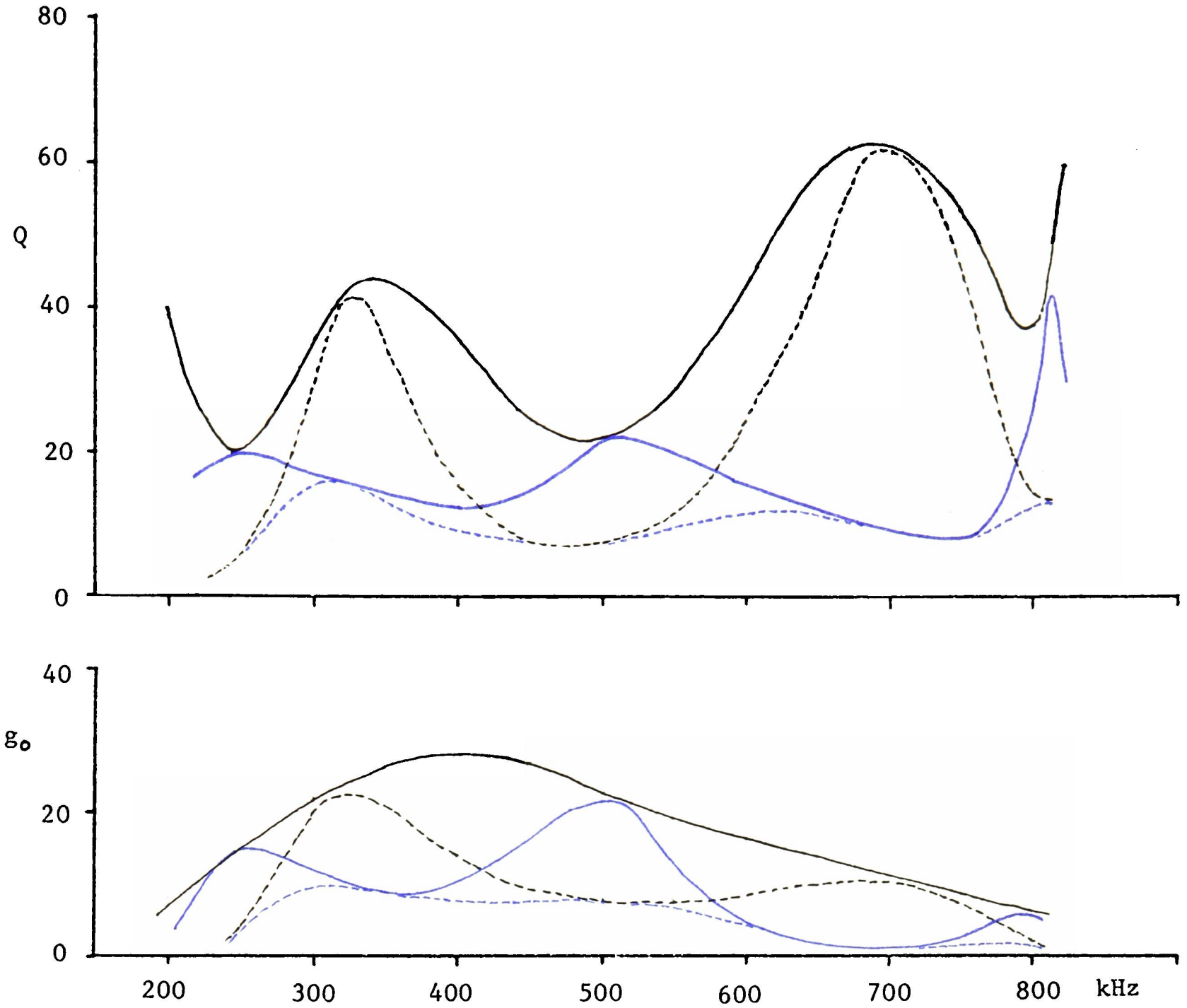

Figure 5f

Backing impedance and series resistance variations. Each curve shows the Q and g_o which would be obtained if passive electrical loading was used to cause resonance at a particular frequency. ($l_o = l_1 = 4.25$mm)

1. The natural positions of the fundamental and second harmonic are 249 kHz and 507 kHz respectively. At these frequencies Q is determined only by backing impedance. At 507 kHz this would be expected since the control ceramic is half a wavelength thick and therefore acoustically transparent.

2. When resonances are shifted away from natural positions Q is determined by series resistance. When there is no series resistance the resonances furthest from natural positions have the highest Q.

3. Higher Q resonances are more strongly damped by the addition of resistance. Heavily damped resonances have such low conductances that little power is radiated into the water. This is a further reason for not using the conditions applicable to the dotted lines on figure 5e as these very high Q resonances disappear for inductors with realistic losses.

For most sonar applications low Q transducers are of greatest use, so when resonances are far from natural positions a small series resistance may be an advantage, although it causes lower efficiency. Away from natural resonance a small change in inductance produces a large change in resonant frequency. In this region high Q operation would require complicated control electronics to ensure accurate inductance values. Therefore an extra advantage of series resistance is that the resulting low Q operation allows greater inductance errors.

Figure 5f shows that passive electrical loading can give useful resonances anywhere between 230 kHz and 750 kHz, assuming that series resistance can be kept below 10Ω. Outside this frequency range

the conductance becomes very low showing that little power can be radiated into the water.

5.3.2 Position of the Active Ceramic

Figure 5b shows the drive ceramic radiating into a water load through a thin protective epoxy layer, while the control ceramic is in contact with the backing. It would be interesting to see if the transducer would work with the ceramics the other way round i.e. the drive ceramic radiating into water through the control ceramic.

The program PASSIVE_LOAD was run for the air backed transducer of figure 5b except with the ceramics interchanged. Close to the natural resonances at 249 kHz and 507 kHz there was no change in performance but when inductive loading was used to change the resonant frequency it was found to give a very high Q. Replacing the air backing with a higher impedance caused the Q to drop. This shows that away from natural resonance very little sound travels through the control ceramic, so that the air backed drive ceramic sees almost no acoustic load. Increasing the backing impedance causes a decrease in Q because sound is radiated into the backing, which is not very useful.

This investigation shows that a piezoelectric-tunable transducer of the kind shown in figure 5b must have the drive ceramic in contact with the load.

5.3.3 Ceramic Thickness ratio

The drive ceramic has a thickness l_o and the control ceramic has a thickness l_1. All designs discussed so far have used $l_o = l_1 = 4.25$mm which gives a fundamental resonance at 249 kHz, a second harmonic at 507 kHz and a third harmonic at 812 kHz. The program PASSIVE_LOAD was used to investigate the effect of varying the ratio l_1/l_o while keeping a total ceramic thickness of $l_o + l_1 = 8.5$mm. Results showed that natural resonant frequencies are dependent only on total ceramic thickness. Hence the figures above apply for all l_1/l_o ratios. However it was found that g_o and Q are strongly dependent on the l_1/l_o ratio, especially when inductive loading is used.

Figure 5g shows the effects of ceramic thickness variations and can be summarised as follows:

1. The rule of tuning out clamped capacitance still applies so larger l_1 designs require greater inductance for resonance at a given frequency.

2. For $l_o > l_1$ passive electrical loading has little effect. The natural resonance at 249 kHz has low Q, but at higher frequencies Q increases so much that realistic inductor losses would cause resonances to disappear.

3. For $l_o < l_1$ resonances between 200 kHz and 540 kHz have similar Q but lower conductance than for $l_o = l_1$. A drop in conductance with no change in Q indicates a weakening of the resonance and should be avoided. Above 540 kHz the Q becomes too high to be of practical significance.

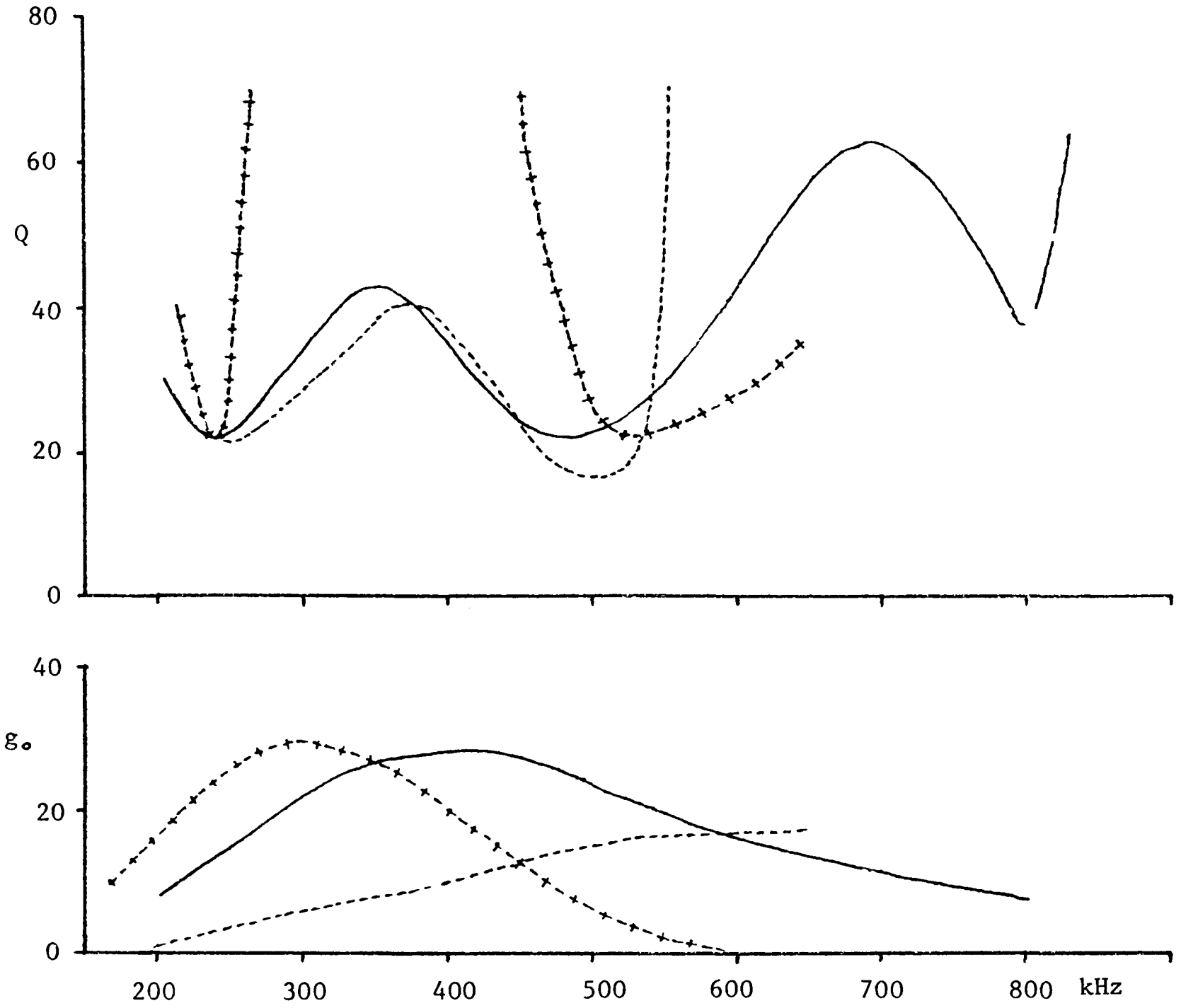

-------- l_o = 2.125mm l_1 = 6.375mm

———— l_o = 4.250mm l_1 = 4.250mm

-+-+-+-+ l_o = 6.375mm l_1 = 2.125mm

} Series resistance 0Ω

Figure 5g

The effect of varying the ceramic thickness ratio. Each curve shows the Q and g_o which would be obtained if passive electrical loading was used to cause resonance at a particular frequency. The solid black line is the same as on figure 5f.

Operation between 249 kHz and 812 kHz involves control of the second and third harmonics by inductive loading. The conclusion from figure 5g is that best performance in this frequency range is given by a transducer with $l_o=l_1=4.25$mm.

5.3.4 Effect of Bond Thickness

So far it has been assumed that the two ceramics have good acoustic contact, the bond between them being ignored. For bonding ceramics it is common practice to use epoxy resins, such as Araldite, which have very low impedance compared with ceramic. Therefore if the bond is insufficiently thin there will be an impedance mismatch at the ceramic interface, causing degradation of transducer performance.

The air backed transducer of figure 5b was studied for different bond thicknesses and passive electrical loads. It was found that resonances away from natural positions are very strongly influenced by bond thickness. Figures 5h and 5i are interesting examples. A 56μH inductor, with no series resistance, places the second harmonic resonance at 363 kHz, roughly half way between the natural positions of 249 kHz and 507 kHz. Figure 5h(i) shows that zero bond thickness gives a strong resonance at this frequency. As the bond thickness increases Q becomes progressively higher with no change in g_o, indicating a weakening of the resonance. The fundamental and fourth harmonic decrease in frequency as the total thickness of ceramic + bond increases. It is interesting to note that the third harmonic actually becomes stronger with increasing bond thickness. This is because the drive ceramic ceases to be constrained by the

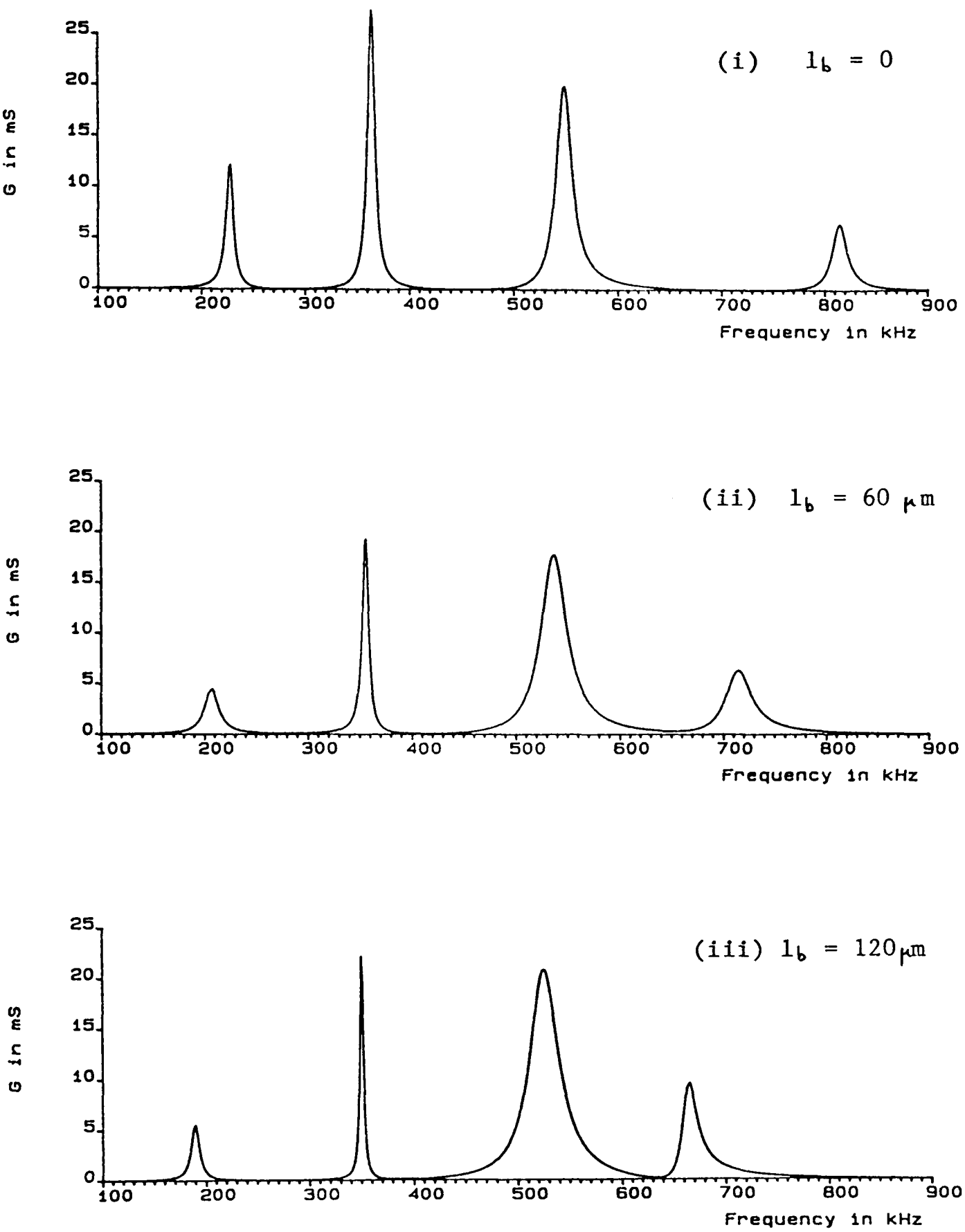

Figure 5h Predicted conductance as a function of bond thickness, l_b. In all cases the passive electrical load is a 56 μH inductor with zero series resistance.

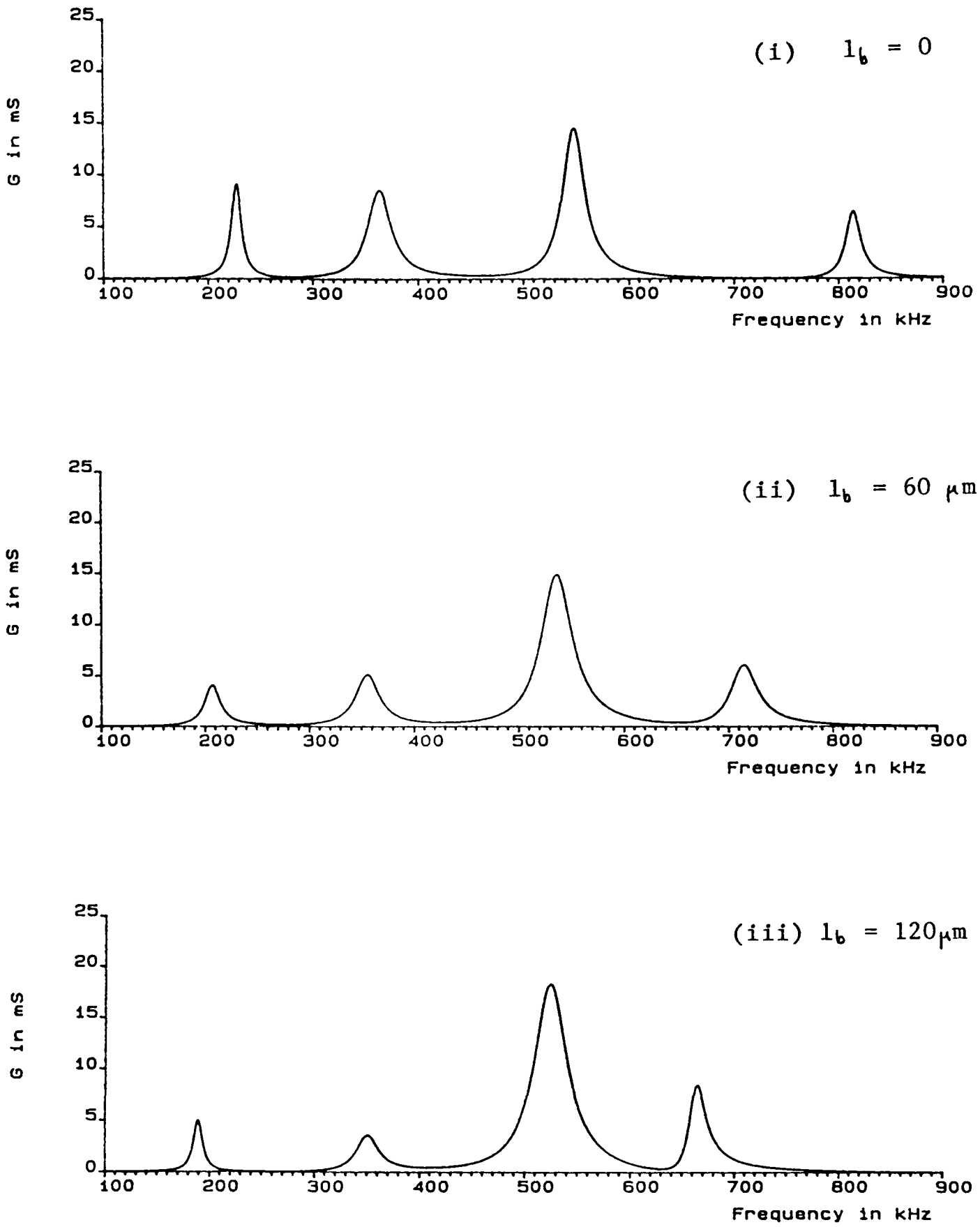

Figure 5i The effect of adding a 10Ω series resisitance to the 56 μH inductor.

passively loaded backing and so resonates at its own fundamental frequency of 500 kHz.

In practice all inductors have resistive losses. Figure 5i shows the predicted effect of adding a 10Ω resistor in series with the 56μH inductor. For zero bond thickness the Q associated with the second harmonic decreases but the other resonances show comparatively little change because they are closer to natural positions. The extra acoustic loading provided by the 10Ω resistor is therefore a useful effect as has already been shown. However increasing the bond thickness has a disastrous effect. It has been shown that high Q resonances are most strongly influenced by resistance and this is clearly demonstrated by comparing figures 5h and 5i. A bond thickness of only 120μm causes almost complete disappearance of the second harmonic for a 10Ω series resistance. Therefore the device ceases to behave as a piezoelectric-tunable transducer!

This investigation shows that bond thickness is the most important aspect of piezoelectric-tunable transducer design. Silk (6) has shown that an Araldite bond between ceramic and a high impedance backing must have a thickness of less than $\lambda/200$ to avoid adverse effects. At 500 kHz this corresponds to 20μm which can be used as an indication of the bond thickness required.

5.4 Design and Construction of TC4

A transducer was required for simple demonstration of passive control. Figure 5f shows the key design parameters to be considered.

Low Q operation is most easily achieved using an epoxy/iron backing which has a high impedance of 7.1 Mrayls. For a series resistance of 10Ω this is predicted to give acceptable performance between 250 kHz and 600 kHz, a frequency range of more than one octave. However it should be remembered that figure 5f was calculated assuming zero bond thickness between the ceramics.

As a preliminary investigation a transducer, TC4, was constructed using a pair of 50mm diameter PZT-4 discs. A piezoelectric-tunable transducer always requires a centre electrical connection. For this purpose many transducer designs include a sheet of copper gauze between the ceramics, extending beyond their edges. However piezoelectric-tunable operation can only be achieved using an extremely thin bond so copper gauze is unsuitable. Instead a small section of one ceramic was cut away to make room for a direct solder connection to the other, as shown in figure 5j. The pair were then heated to 60°C and bonded with Araldite LY558/HY992 which has suitably low viscosity at that temperature. It was assumed that the ceramics were in electrical contact over part of their area, or that the bond would be so thin as to have a large capacitance compared with the drive ceramic, therefore approximating to a short-circuit.

Conductance measurements taken at various stages during construction showed two interesting effects:

1. An open-circuit on the control ceramic was found to produce a third harmonic resonance at 760 kHz, compared with 812 kHz predicted in figure 5a. This change in frequency is caused by the Araldite bond, an effect which has already been noted in figures 5h and 5i. Reduction of

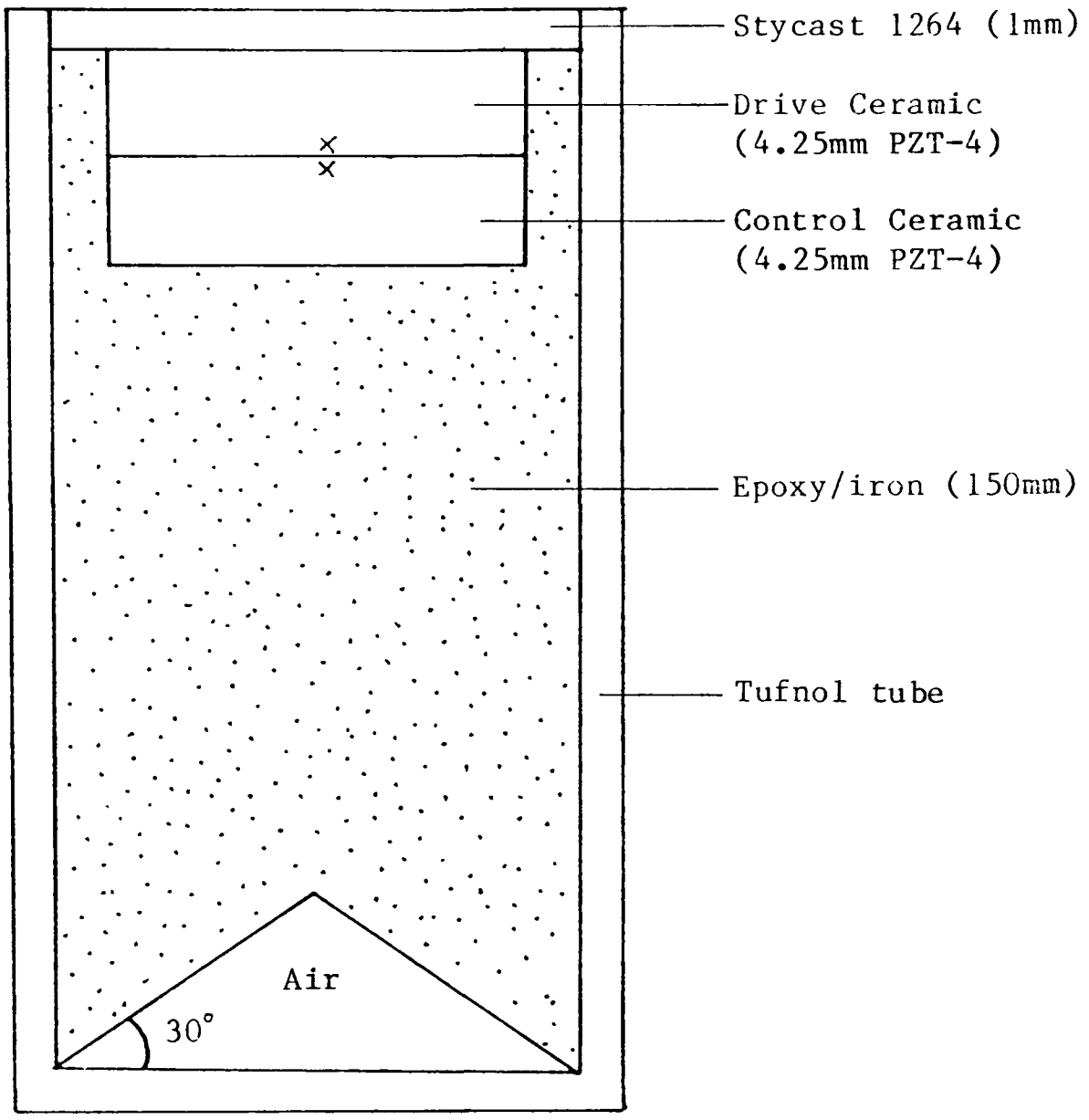

(i) Cross section

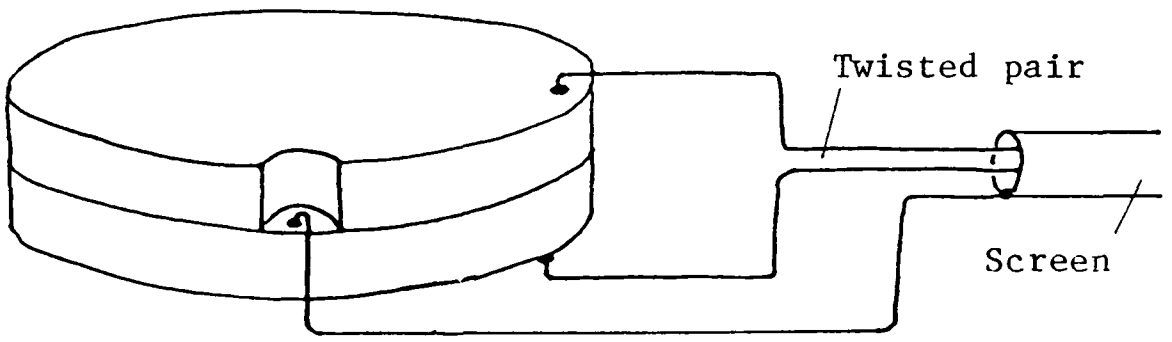

(ii) Details of ceramic connections

Figure 5j Construction of TC4

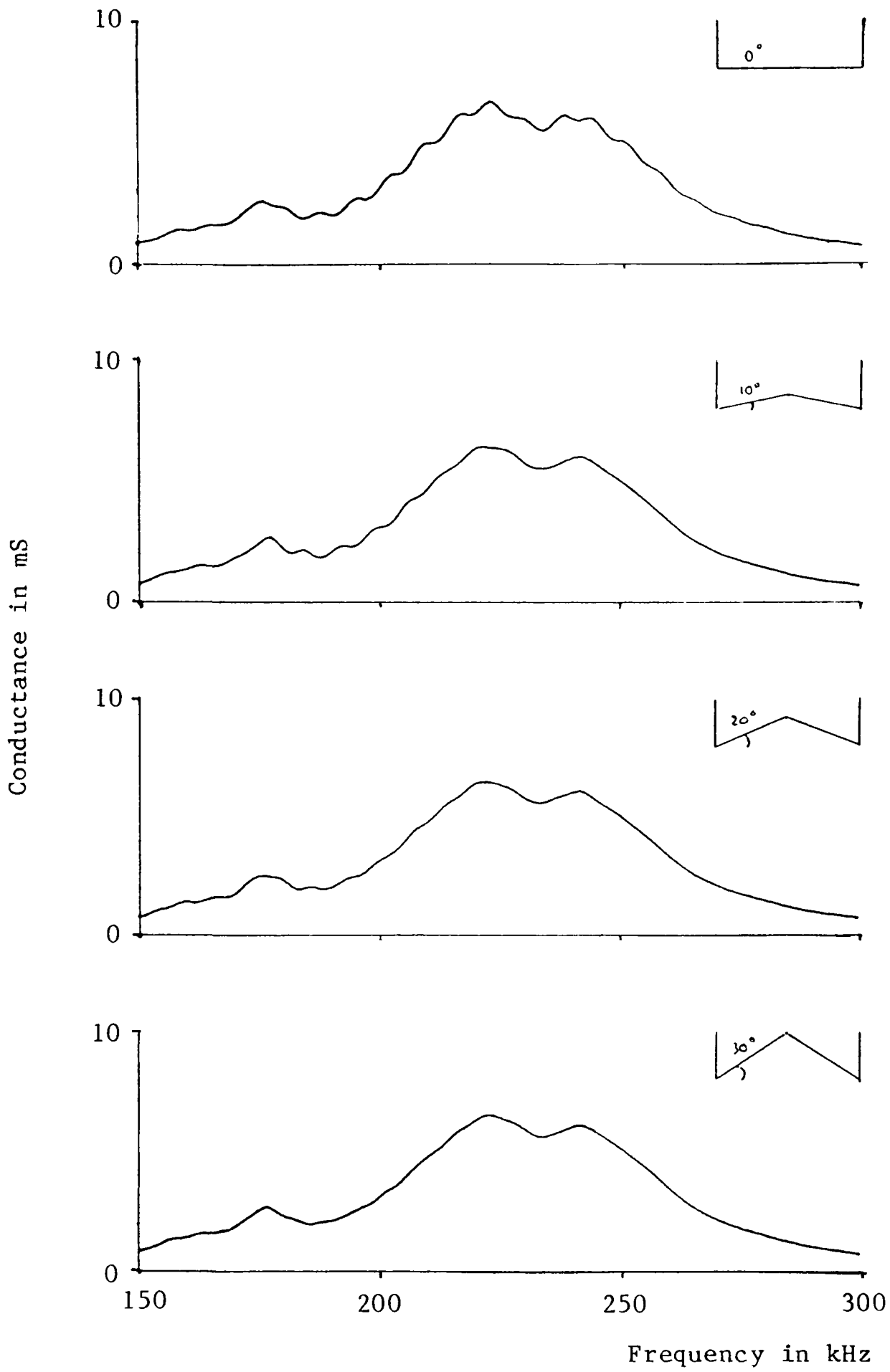

Figure 5k Elimination of standing waves by a cone in the back of TC4.

the third harmonic from 812 kHz to 760 kHz is consistant with a bond thickness of 25μm. This is approximately $\lambda/100$.

2. At frequencies below 300 kHz conductance measurements showed ripples similar to those observed for TB1 in figure 3d. Again these were caused by standing waves in the backing. A cone was cut into the back of TC4 in an attempt to break up the reflected signals. It was found that a base angle of 30° was suitable as shown in figure 5K.

The drive ceramic was protected by an epoxy layer machined to a thickness of 1mm. Connections were made to the ceramics via a screened twisted-pair cable of length 0.9m and capacitance 140pF. It was shown on figure 5e that extra capacitance in parallel with the control ceramic causes problems of high Q and decreased resonant frequency. However 140pF is small compared with the 2.6nF clamped capacitance so no adverse effects were observed.

5.5 Performance of TC4 with Passive Control

Predictions from computer simulation were compared with measured results in the following series of tests.

5.5.1 Conductance Measurements

Figure 51 shows the drive ceramic conductance as a function of frequency for different passive electrical loads on the control ceramic. An open-circuit produces natural resonant frequencies at

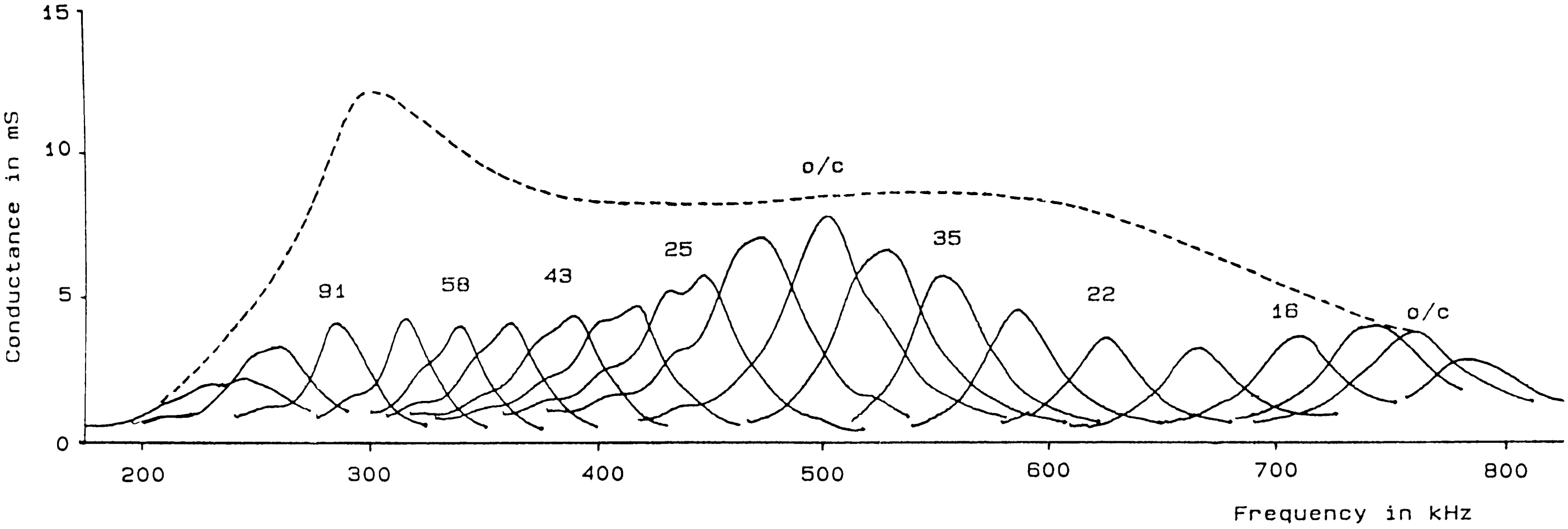

Figure 51 Conductance of TC4 for different passive loads. Figures above curves are inductance values in μH. Dotted line shows the predicted envelope for 4Ω series resistance.

240 kHz (fundamental), 503 kHz (second harmonic) and 760 kHz (third harmonic). A short-circuit reduces the second harmonic to 476 kHz but causes little change in the other two resonances. For clarity short-circuit and capacitive loads have been omitted from figure 51. Of greater interest is the effect of inductive loading, which is shown to give continuous variation in resonant frequency from 240 - 476 kHz for the second harmonic and 503 - 760 kHz for the third harmonic. Resonant frequencies are in general agreement with figure 5e but cannot be compared directly because the latter was calculated for zero bond thickness. Note that the approximate rule of tuning out clamped capacitance applies to figure 51 so that control of the third harmonic requires smaller inductors than for the second harmonic.

Also shown in figure 51 is the predicted envelope for 4Ω series resistance, calculated for 25μm bond thickness. Measured conductance maxima are significantly lower than this curve. All inductors used to plot figure 51 had series resistance of less than 4Ω so there must be an important extra loading effect which is not predicted by the one-dimensional analysis.

At 410 kHz and 440 kHz there are distortions in the resonant peaks. These are planar resonances. When the second harmonic is moved near to a planar resonant frequency intermodal coupling affects the conductance. The presence of planar modes of vibration indicates significant lateral displacement. It was shown in Chapter 3 that this causes additional acoustic loading due to energy loss through the sides of the ceramic and this accounts for the disagreement between predicted and measured results. In the case of TC4 the effect is seen most clearly at frequencies away from natural resonance, where the addition

of series resistance has also been shown to cause greatest changes in acoustic load.

Figure 5f showed that operation above 600 kHz would involve resonances with either high Q or low conductance. Therefore it was not intended to use TC4 in this range. However measured resonances have a Q of only 15, low enough to be of practical interest. This shows that for inductive control of the third harmonic the extra acoustic loading caused by lateral displacement can be helpful as it allows low Q operation up to 760 kHz.

5.5.2 Output Voltage

When a continuous wave signal is applied to the drive ceramic of TC4 a voltage appears across the control ceramic. This output voltage depends on the passive electrical load. Figure 5m(i) shows its measured amplitude, as a function of frequency, relative to the drive ceramic voltage. For inductive loads the output at resonance can be greater than the input voltage. It is interesting to note that the phase at resonance was always found to be $\pm 90^{\circ}$.

Measured results are compared with predictions on figure 5m(ii) which shows the calculated envelope for 4Ω series resistance and $25\mu m$ bond. The output is lower than predicted at frequencies away from natural resonance. Again this can be interpreted as the effect of lateral displacement.

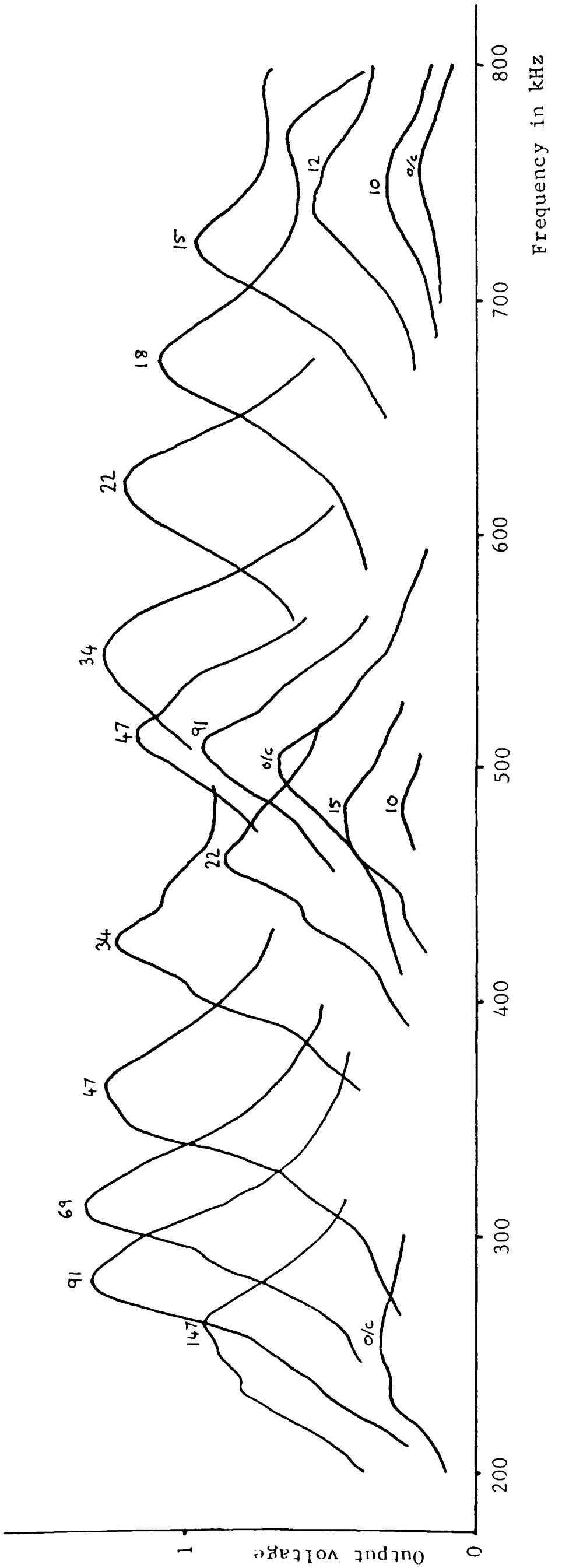

Figure 5m(i) Output voltage of TC4 for different passive loads.
Figures above curves are inductance values in μH.

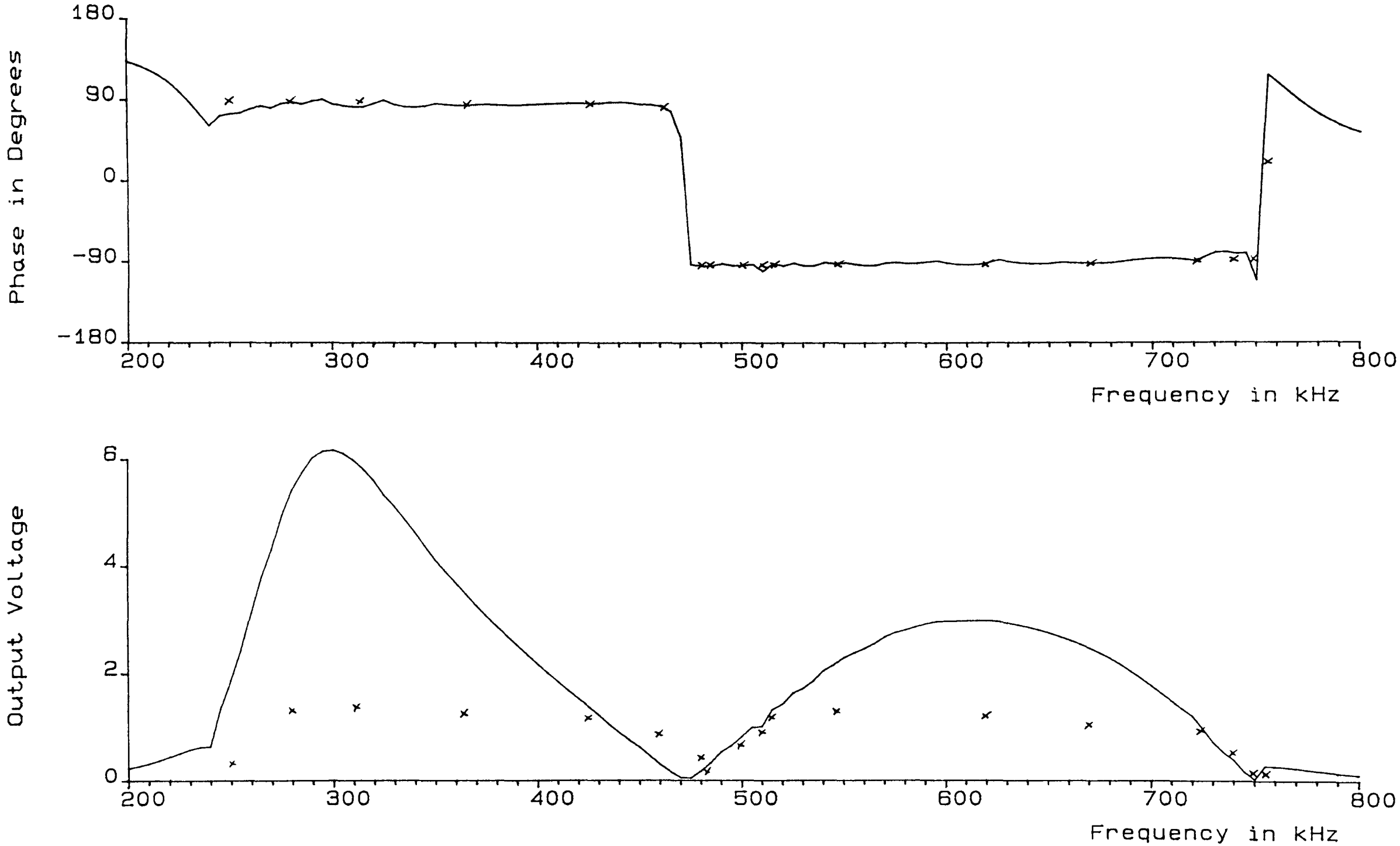

Figure 5m(ii) Predicted envelope for the output voltage of TC4 with 4Ω series resistance. Crosses show measured points fron figure 5m(i).

5.5.3 Power Output and Efficiency

The radiation balance was used to measure output power for TC4 with passive control at frequencies from 230 kHz to 760 kHz. After the test conductance measurements were not the same as those in figure 51. The transducer had clearly been damaged.

A disadvantage of the radiation balance is that high acoustic power is required for appreciable deflection. For example in appendix 6 a calibration of 91 mW/mm is derived. Suppose it is intended to produce a deflection of 10mm with TC4. The output power would be 0.91 Watts which for an efficiency of 20% (about the expected value for TC4) corresponds to an input power of 4.5 Watts. The conductance is shown on figure 51 to be around 4mS at most frequencies so a drive voltage of 100V pk-pk is required. This would produce up to 150V across the control ceramic.

In practice the maximum drive voltage applied to TC4 was 70V pk-pk. This was determined by the specified current-handling capability of the control inductors. The transparent Stycast layer on the front of TC4 allowed visual inspection of the drive ceramic. There was no sign of damage, and none would be expected for only 70V pk-pk. Although the control ceramic was not visible it is unlikely to have been damaged by the 100V pk-pk which was measured across it. Therefore it was concluded that the most likely cause of failure was the bond between the ceramics.

5.6 Stress Analysis for TC4

In Chapter 3 the program PASSIVE_LOAD was used to examine the pressure on the front faces of TB1 and TB2, and measured results confirmed the accuracy of these calculations. The same program can predict the pressure at any other boundary between materials, hence allowing analysis of the Araldite bond in TC4. (There are actually two boundaries here - the two sides of the bond - but the pressure difference is negligeable.) Figure 5n shows the predicted bond stress as a function of frequency for two passive electrical loads, both curves being plotted relative to 1V on the drive ceramic. An open-circuit load gives maximum stress at the fundamental and third harmonic frequencies, with a smaller peak at the second harmonic. Inductive loading causes a significant increase in stress at frequencies away from natural resonance, the maximum being at 290 kHz. It was not possible to obtain practical measurements but figure 51 suggests that at 290 kHz the true bond stress would be about one-third of the predicted value. A second maximum occurs at 700 khz where the true stress may be close to the predicted figure of 17 kPa/V. It is probably at this frequency that TC4 experienced its greatest bond stress. The peak drive voltage of 35V gives 595 kPa or 86 psi.

Comparison of these figures with manufacturers specified bond strengths is difficult because data is usually published only for shear stress. There is a further complication that Araldite LY558/HY992 is a non-standard mixture, chosen because of its low viscosity and long curing time. However Ciba-Geigy publish a data sheet (36) for AV138M/HV998 which is useful for comparison. Results are given for

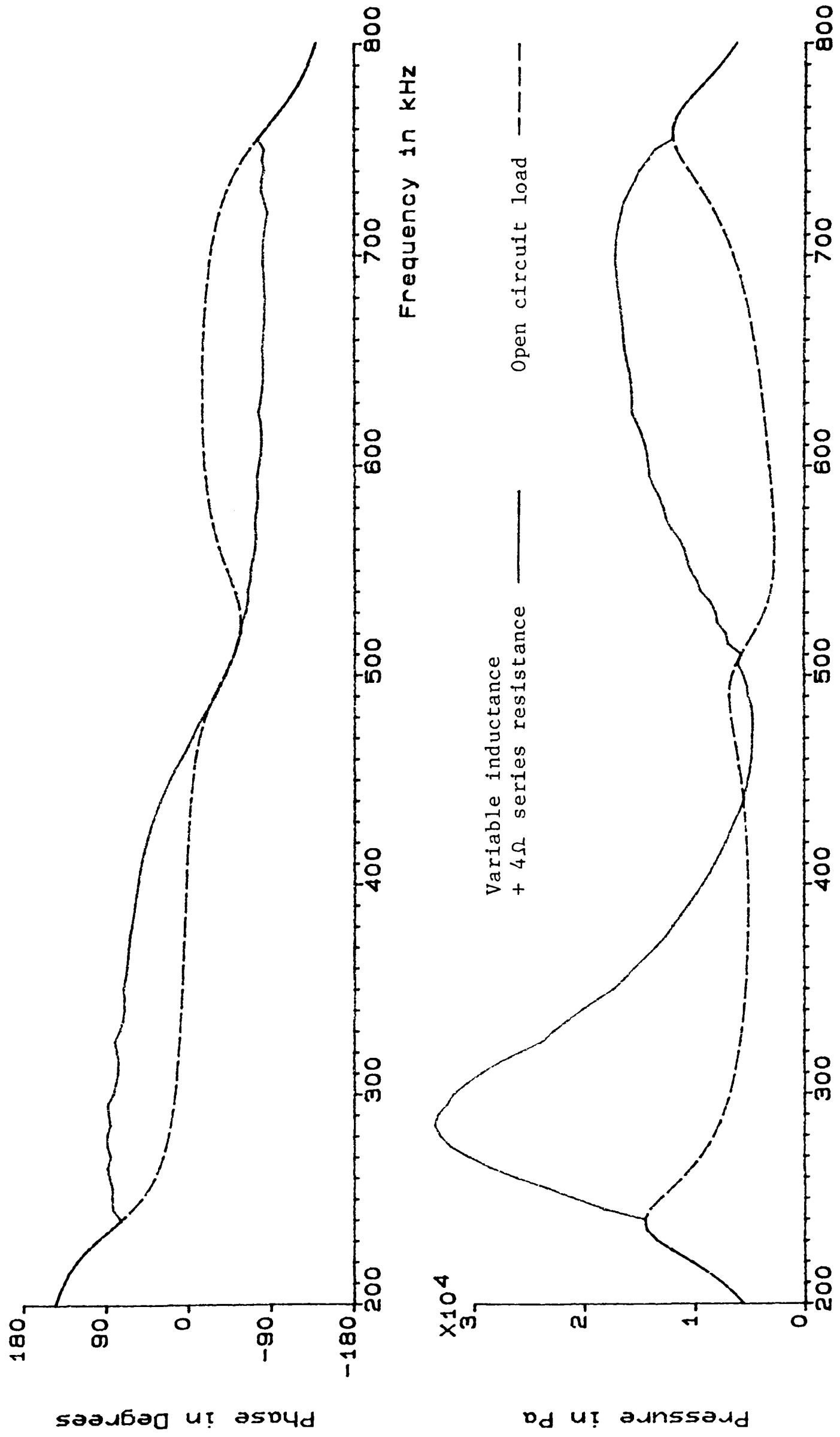

Figure 5n Predicted bond stress for TC4 as a function of frequency.

failure under cyclic tensile stress of bonds between strips of aluminium alloy. The actual stress which causes failure depends on the number of cycles but tends towards a lower limit of 4000 kPa or 580 psi. This is an order of magnitude higher than experienced by the bond of TC4, which suggests that improved performance should be possible with careful construction.

It is also of interest to examine the stresses which occur in other parts of the structure. For non-piezoelectric materials the program PASSIVE_LOAD can predict the stress at any point by introducing an extra boundary at that position. For example to find the stress half way through the 1mm Stycast layer simply enter this as two 0.5mm layers. However the same approach cannot be used for ceramic as the equivalent circuit does not divide conveniently. Therefore an alternative analysis was used, by which stress at any point in the ceramic can be calculated from the amplitude and phase of the pressure on its faces. See appendix 11 for details.

The curves in figure 5o were derived using this technique and show stress as a function of distance through TC4. As expected the greatest stress occurs within the ceramic, the bond representing a discontinuity at most frequencies. For PZT-4 Vernitron (12) quote a dynamic tensile stress of 3500 psi (peak) which can be used to define the maximum drive voltage. For example at 510 kHz figure 5o shows that the drive ceramic experiences a stress of 76 kPa/V or 11 psi/V. Therefore the maximum drive voltage which can be applied is 318V peak. This figure is considerably higher than the 35V found to cause damage, showing that operating conditions are limited by bond stress rather than ceramic deformation.

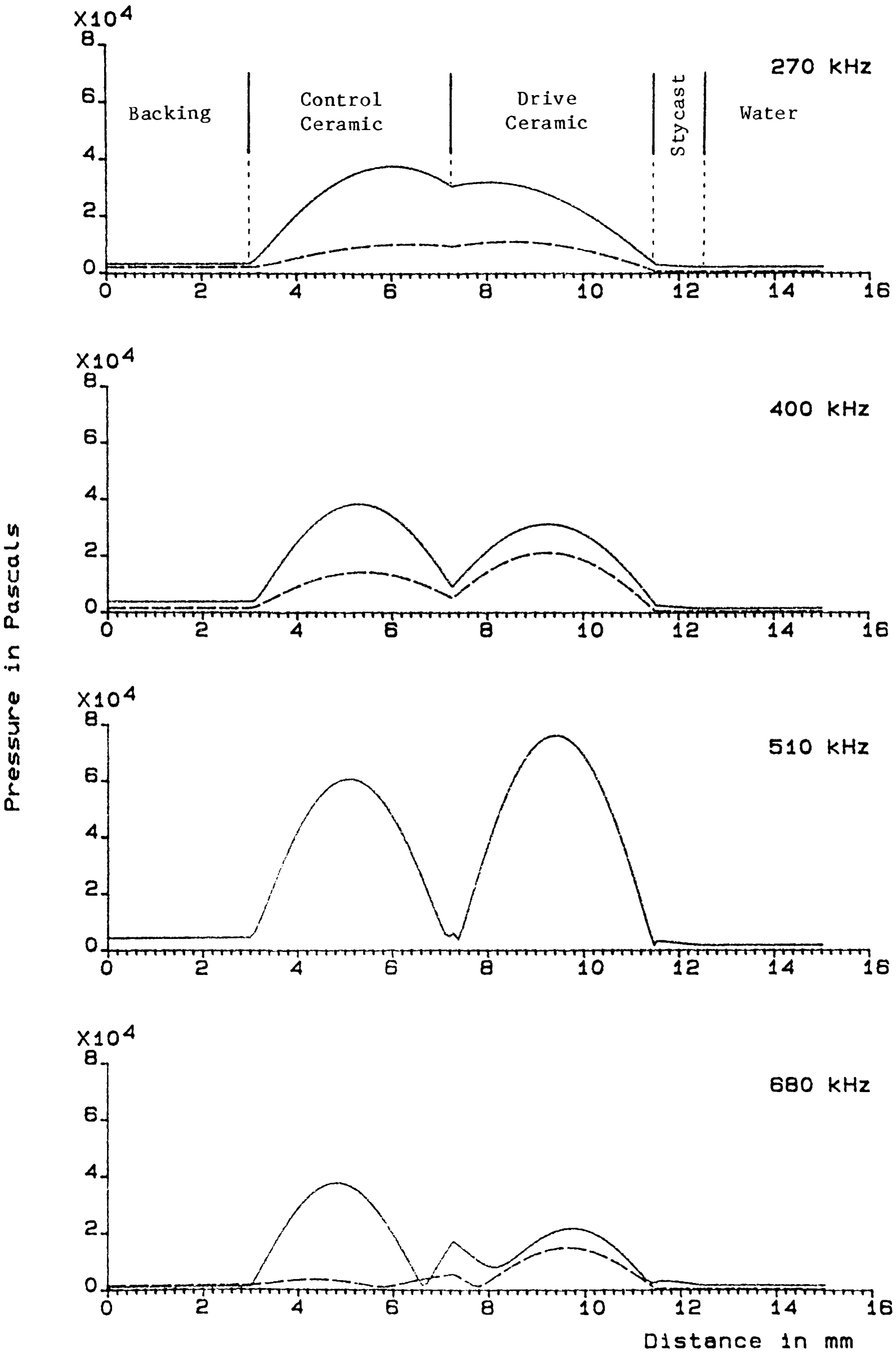

Figure 5o Stress analysis for TC4

5.7 Improvements to Transducer Design

Figure 5p summarises the predicted performance of TC4, each curve showing an envelope calculated for variable inductance with fixed series resistance. A small region of capacitive control, from 472 - 505 kHz, is also included. Measured points from figures 51 and 5m(i) have been added to conductance and voltage plots respectively. The graph for pressure refers to the front face i.e. the output pressure. A new transducer was required to replace TC4, incorporating improvements where possible.

The design of TC4 gives a problem of low efficiency at around 500 kHz. At this frequency the control ceramic is $\lambda/2$ thick, and therefore acoustically transparent, so power from the drive ceramic is delivered mainly to the epoxy/iron backing. It is clear that the backing impedance should be reduced and a composite of Stycast/fillite offers a suitable alternative.

A further improvement in efficiency at 500 kHz could be obtained by adding a $\lambda/4$ matching layer in front of the drive ceramic, as described in Chapter 2. However the effect of this layer at other frequencies is not obvious. The program PASSIVE_LOAD was used to investigate this idea. It was found that a $\lambda/4$ matching layer produces very wide bandwidth resonances at around 500 kHz with the required increase in efficiency, but at other resonant frequencies the layer has almost no effect. In figure 51 a higher conductance was measured for TC4 at 500 kHz than for inductive control. A lower backing impedance would give an even greater difference. Therefore a further advantage of a $\lambda/4$ layer is that it reduces the conductance at

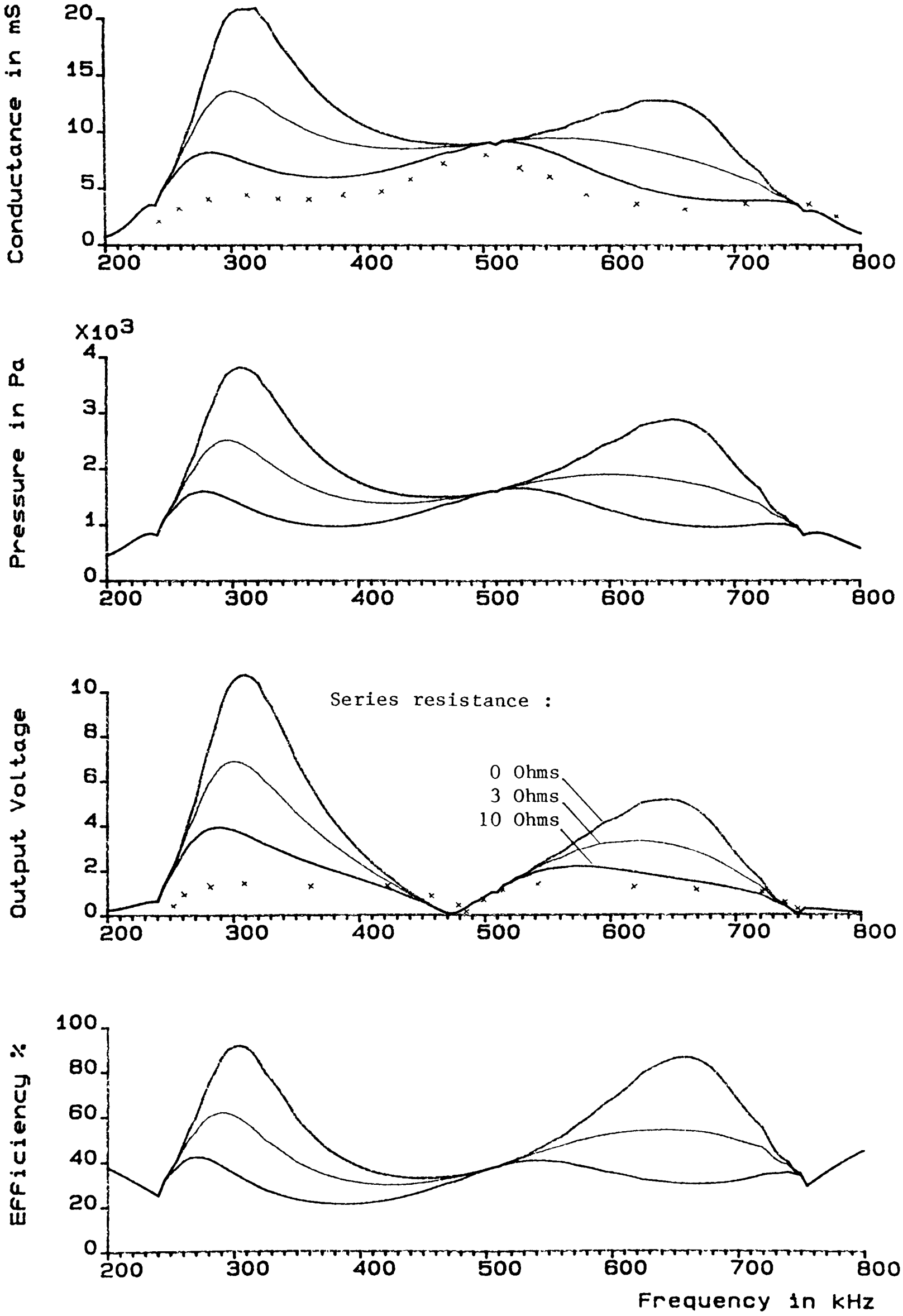

Figure 5p Summary of predicted performance for TC4. Crosses show measured values.

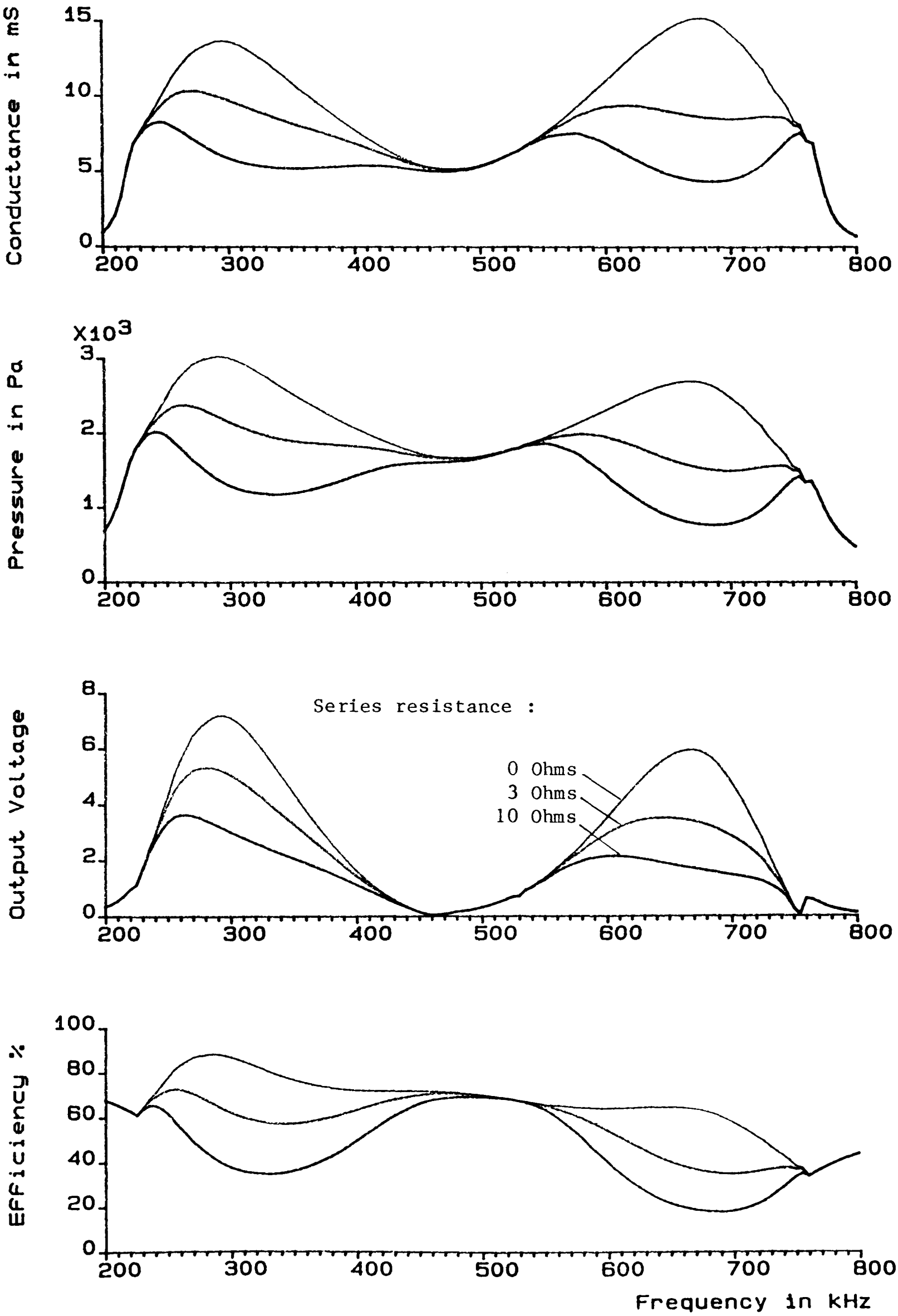

Figure 5q Summary of predicted performance for TC5.

500 kHz to give a more uniform value throughout the operating range of 240 - 760 kHz.

The actual amount by which conductance and efficiency are changed depends on the impedance of the matching layer. Koymen (10) has shown that filter theory can be used to derive an optimum matching layer impedance of 4.14 Mrayls. However a piezoelectric-tunable transducer is not operated as a filter so this theory does not apply. By computer simulation it was found that an impedance of around 5 Mrayls gives satisfactory performance so a composite of Stycast/magnesium was chosen as a suitable material. A sample was made and tested as follows:

Stycast 1264	:	44% by volume
Magnesium powder (0.15mm)	:	56% " "
Density	:	1510 ± 25 Kg/m^3
Velocity	:	3767 ± 70 m/s
Absorption	:	6.0 ± 1.0 dB/cm/MHz
Impedance	:	5.7 ± 0.2 Mrayls

TABLE 5.1 Stycast/Magnesium sample

A 2.0mm layer of this material is required to match the drive ceramic to water at the short-circuit resonant frequency.

These changes in backing impedance and front layer properties give the predicted performance shown in figure 5q. The improvements were investigated in practice by building a new transducer, TC5.

5.8 Construction of TC5

An important design aspect for piezoelectric-tunable operation is the arrangement of the centre connection. In TC4 a small part of one ceramic was removed to allow a direct solder connection to the other. There was assumed to be electrical contact or high capacitance across the Araldite bond. A possible cause of failure for TC4, which has not yet been discussed, is the breakdown of this electrical contact. This may occur either as damage to the silver on the ceramic faces, or alteration of the Araldite bond properties. The latter could be caused by local heating effects combined with high electric field.

To avoid the possibility of similar failure in TC5 small sections of both ceramics were removed, as shown in figure 5r, to allow direct solder connections to both their faces. The ceramics were then bonded in the same way as for TC4 and fixed to the Stycast/fillite backing using Quick-Set Araldite. An epoxy/iron composite of impedance 7.1 Mrayls was added at the sides of the ceramics to reduce the amplitude of planar vibrations. The front matching layer was then added, cured, and machined to a thickness of 2.0mm.

Magnesium powder reacts with water and a sample of Stycast/Mg showed corrosion after a few hours of immersion. To prevent this a thin protective layer of varnish was sprayed onto the front of TC5. It had no measurable effect on performance. Connections to the ceramics were made via a screened twisted-pair cable of length 0.9m and capacitance 140pF. As for TC4 this capacitance is small compared with the 2.6nF clamped capacitance so does not degrade the performance.

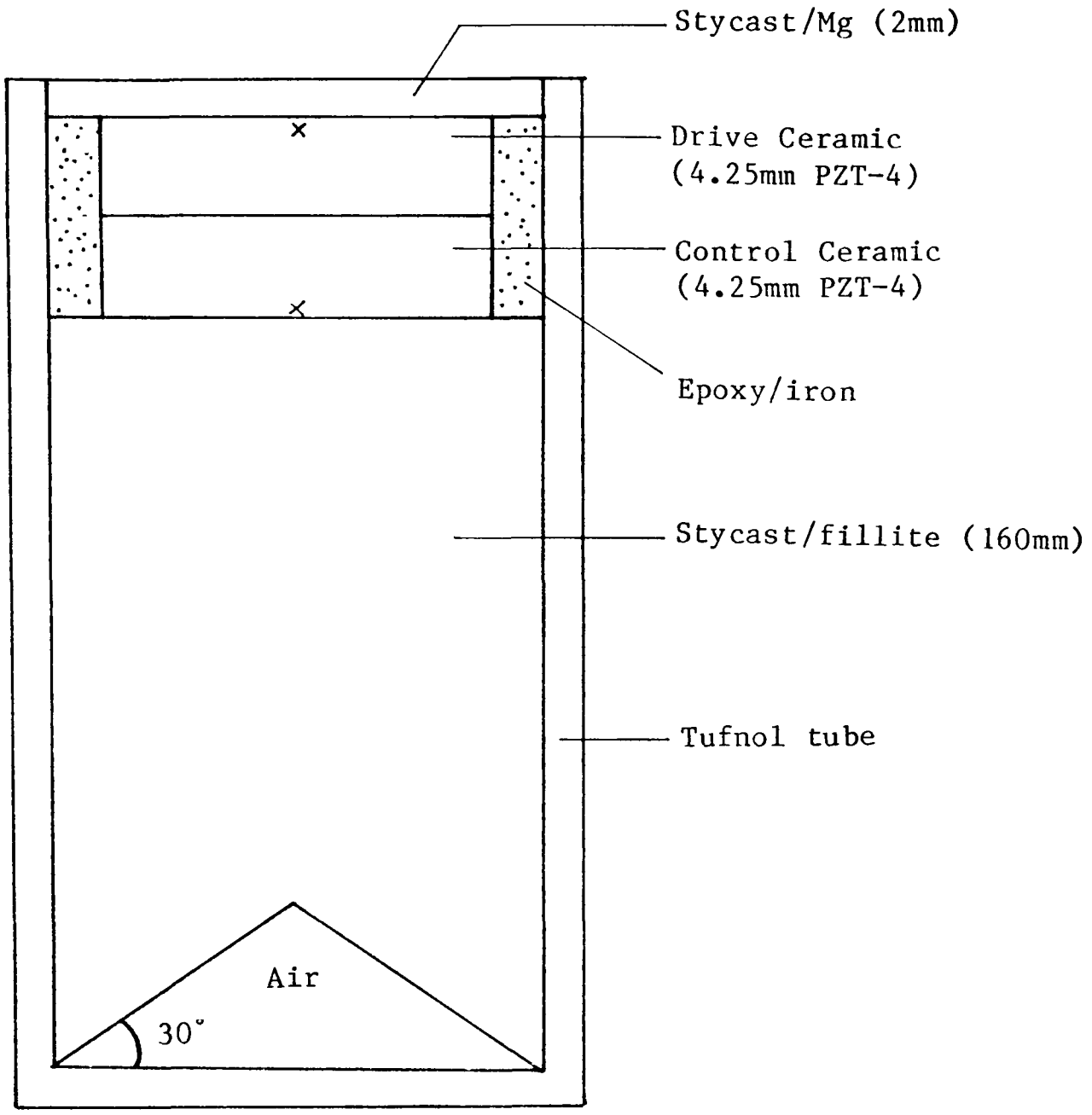

(i) Cross section

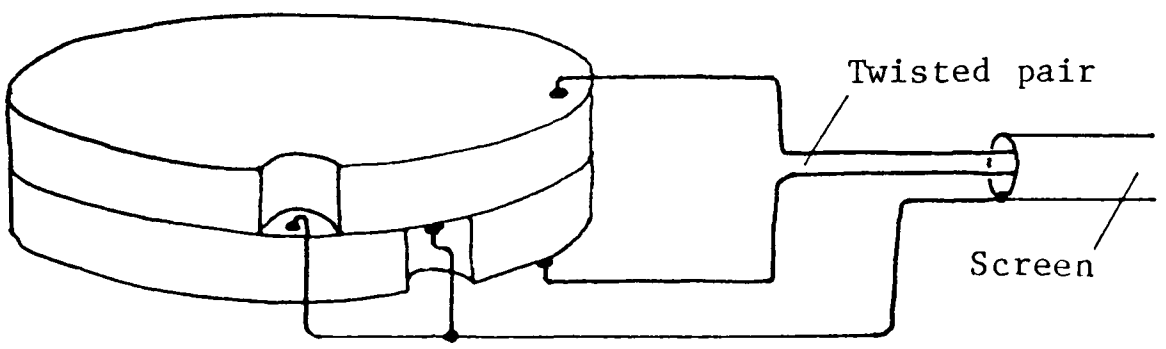

(ii) Details of ceramic connections

Figure 5r Construction of TC5

Detailed conductance measurements were taken at each stage of construction and are given in appendix 7. The third harmonic resonance occurs at 755 kHz indicating a bond thickness of 26μm. This figure was used to calculate the predicted performance curves in figure 5q.

5.9 Performance of TC5 with Passive Control

Predictions from computer simulation were compared with measured results in the following series of tests.

5.9.1 Conductance Measurements

Figure 5s shows the conductance of TC5 for different passive loads. The $\lambda/4$ matching layer causes very wide bandwidth for the short-circuit resonance while inductive control produces resonances with higher Q and slightly higher conductance. The matching layer impedance of 5.7 Mrayls is too high for optimum performance. An impedance of around 5.0 Mrayls would give higher conductance in the region 420 - 520 kHz without affecting the other resonances, hence giving more uniform conductance throughout the operating range.

The effects of intermodal coupling can be seen at low frequencies, especially around 300 kHz where strong planar resonances occur. For greater detail see appendix 7. The dotted line on figure 5s shows the predicted envelope for 4Ω series resistance and 26μm bond. In practice all inductors had series resistance of less than 4Ω. Measured resonances have lower conductance than predicted,

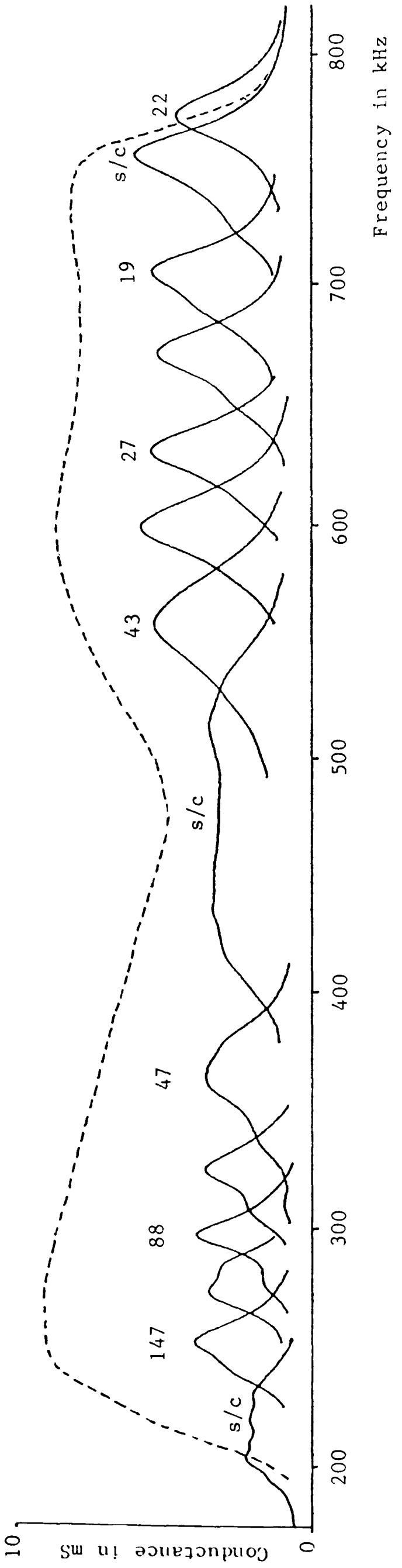

Figure 5s Conductance of TC5 for different passive loads.
Figures above curves are inductance values in μH.
Dotted line shows the predicted envelope for
4Ω series resistance.

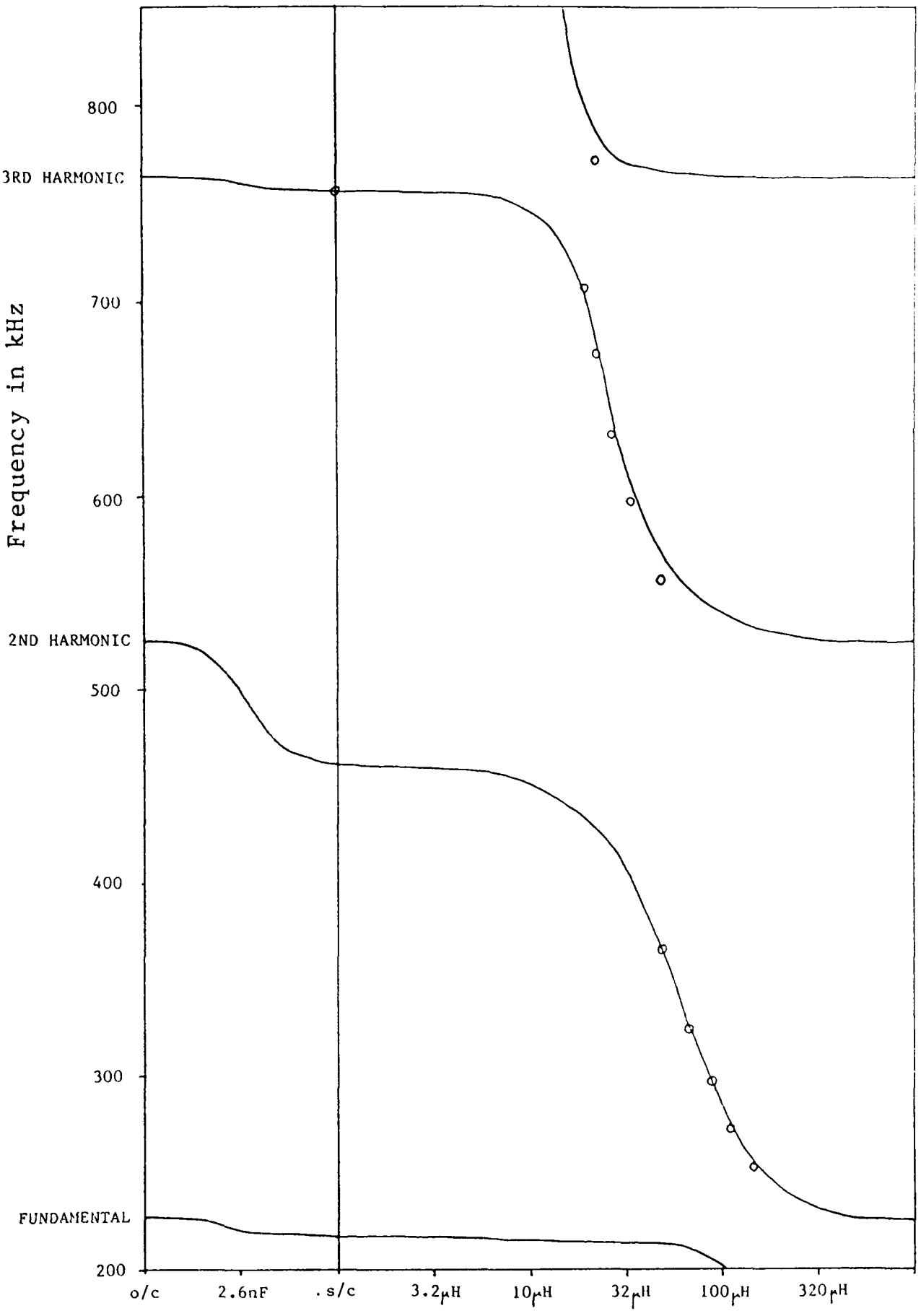

Passive electrical load

Figure 5t Resonances for TC5. Circles show measured points from figure 5s.

showing that for TC5 there is significant energy loss through the sides of the ceramic. This is to be expected since the epoxy/iron composite does not have infinite impedance so does not provide perfect lateral clamping.

In figure 5t there is shown to be close agreement between predicted and measured resonant frequencies. The greatest error occurs for 47μH which causes a third harmonic resonance at 557 kHz compared with a predicted position of 572 khz, a difference of only 3%.

Capacitive control gives resonances between 462 kHz (short-circuit) and 524 kHz (open-circuit). In this frequency range resonances have such wide bandwidth that the passive load can be switched directly from short-circuit to open-circuit without a drop in conductance. Therefore in practice capacitive control is not needed for TC5.

5.9.2 The Effects of Series Resistance

It has been shown that series resistance associated with passive components dissipates power and hence increases the acoustic load on the drive ceramic. The effect is seen most clearly when inductive control causes resonances far from natural positions. These are the resonances which have highest Q. If reduced efficiency can be tolerated then the addition of series resistance gives the advantage of increased bandwidth and allows less accurate inductive control.

For TC5 series resistance has greatest effect in the frequency range 250 - 400 kHz (second harmonic) and 600 - 700 kHz (third harmonic). As an example figure 5u shows the third harmonic at

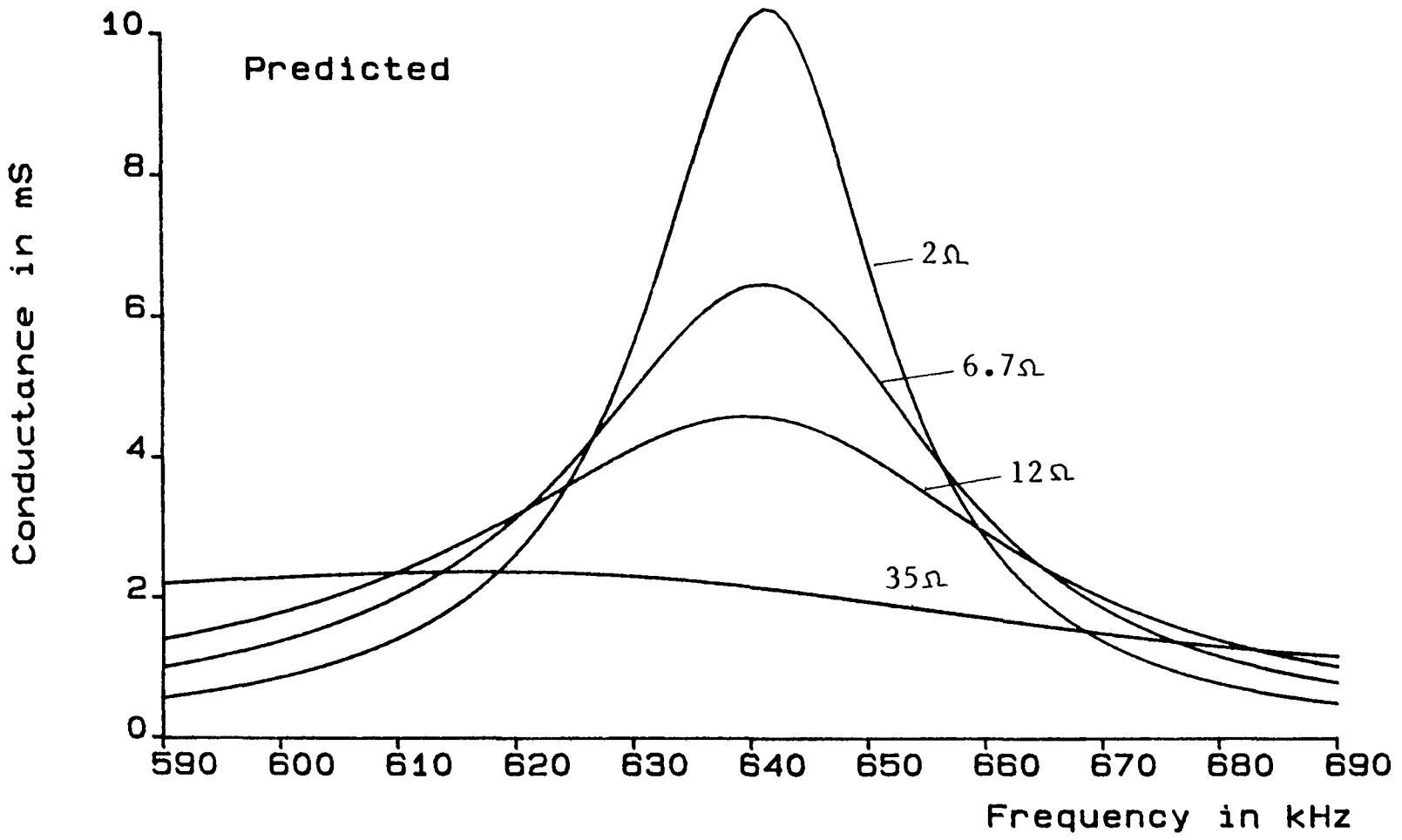

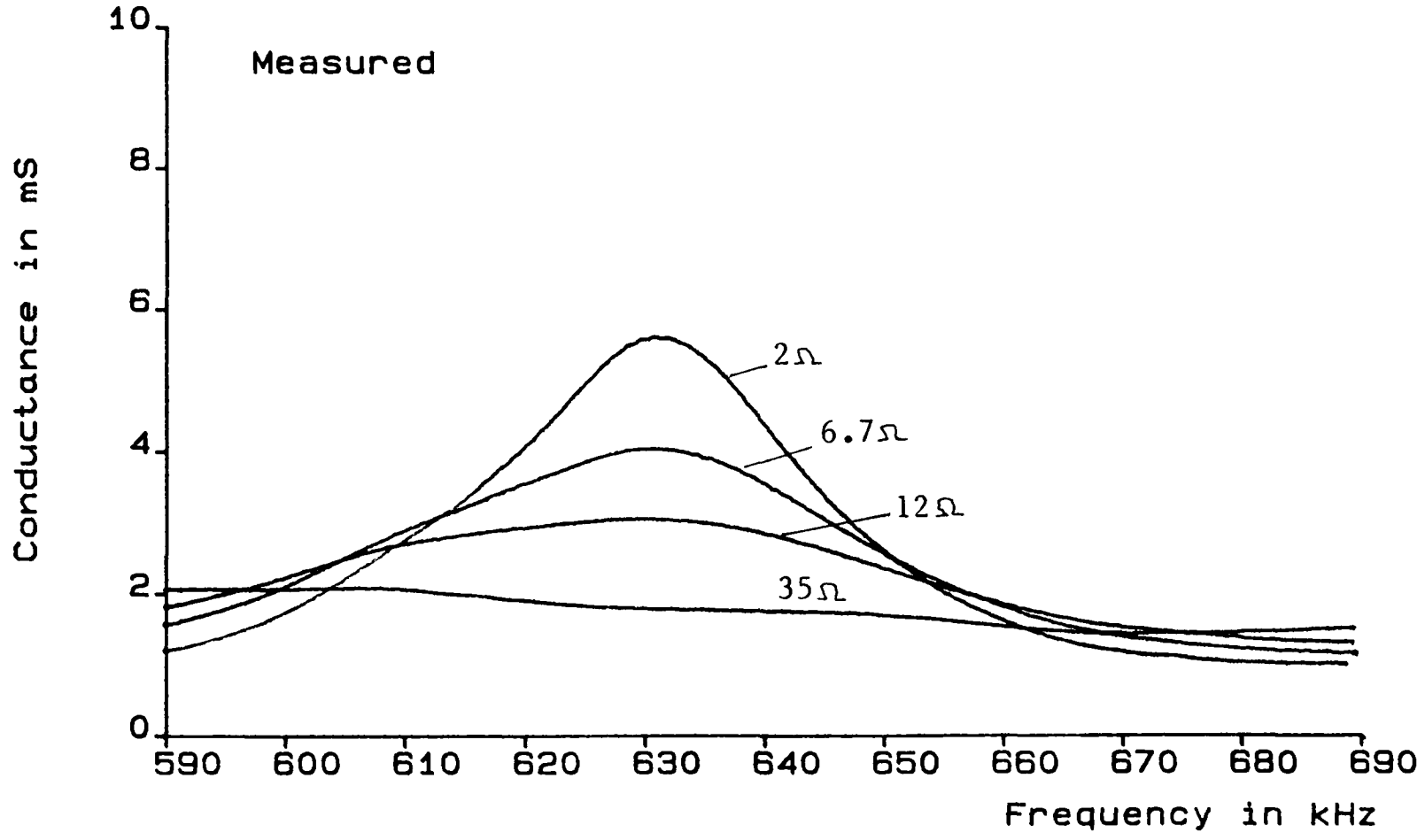

Figure 5u Effect of seies resistance on the third harmonic for 27μH passive load.

640 kHz. The 27μH inductor used to produce this resonance had a series resistance of 2Ω, and further resistors were added to give the following results:

	Predicted			Measured		
Resistance	fo	go	Q	fo	go	Q
Ohms	kHz	mS		kHz	mS	
2.0	642	10.4	25.7	631	5.6	17.0
6.7	642	6.5	16.5	631	4.1	11.5
12	640	4.6	10.7	630	3.1	7.0
35	610	2.4	-	-	-	-

TABLE 5.2 Resistance effects at 640 kHz

Acoustic loading due to lateral displacement causes lower conductance and wider bandwidth than predicted. However the addition of series resistance still allows contol of these parameters without significant change in resonant frequency.

5.9.3 Output Voltage

As for TC4 the voltage measured across passive loads is often greater than that applied to the drive ceramic. The phase at resonance is always close to $\pm 90^{\circ}$. As an example figure 5v(i) shows the output voltage across a passive load of 32μH + 4Ω. Phase follows the predicted curve at all frequencies but amplitude is less than half the

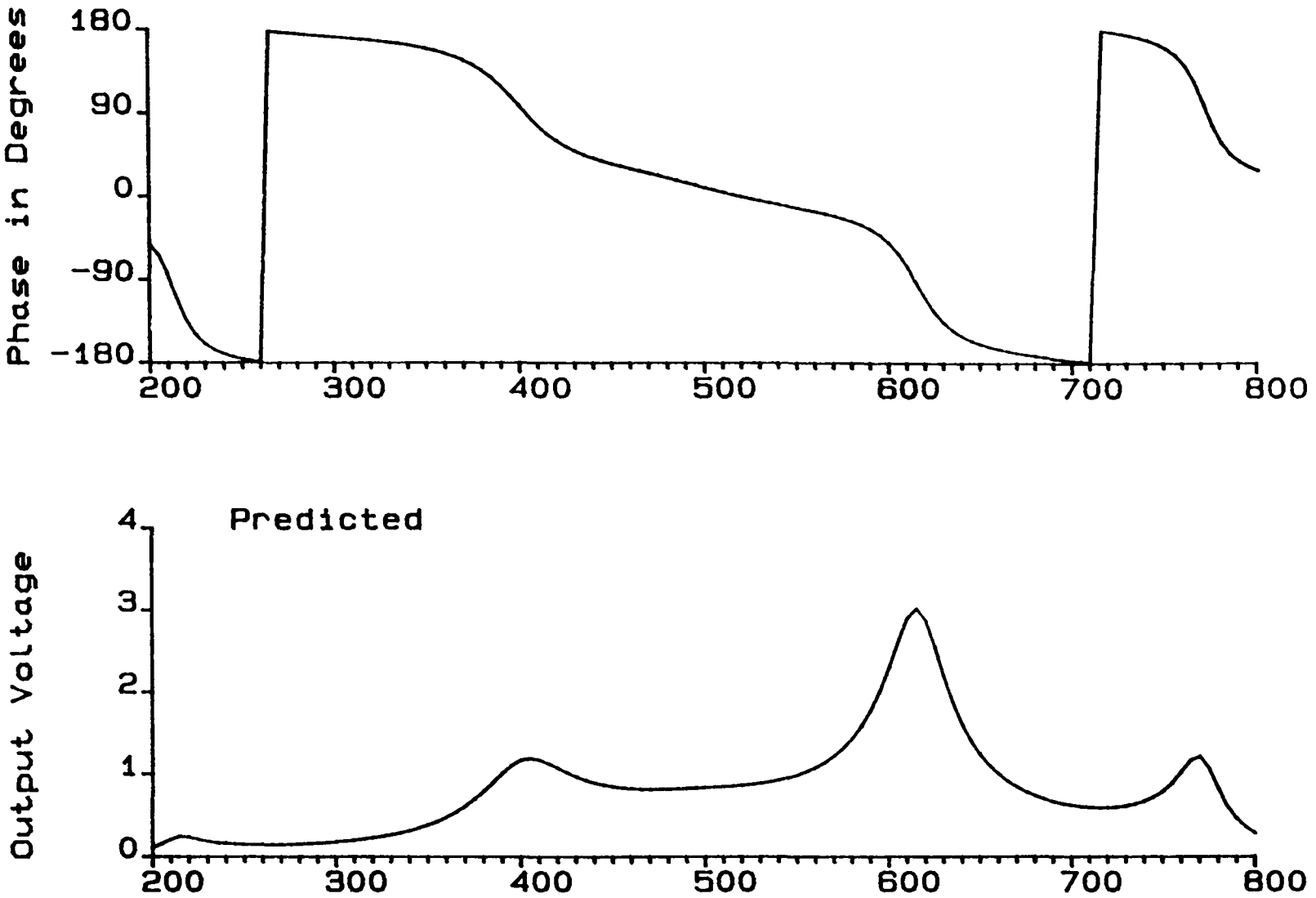

Figure 5v(i) Output voltage of TC5 for 32μH + 4Ω load.

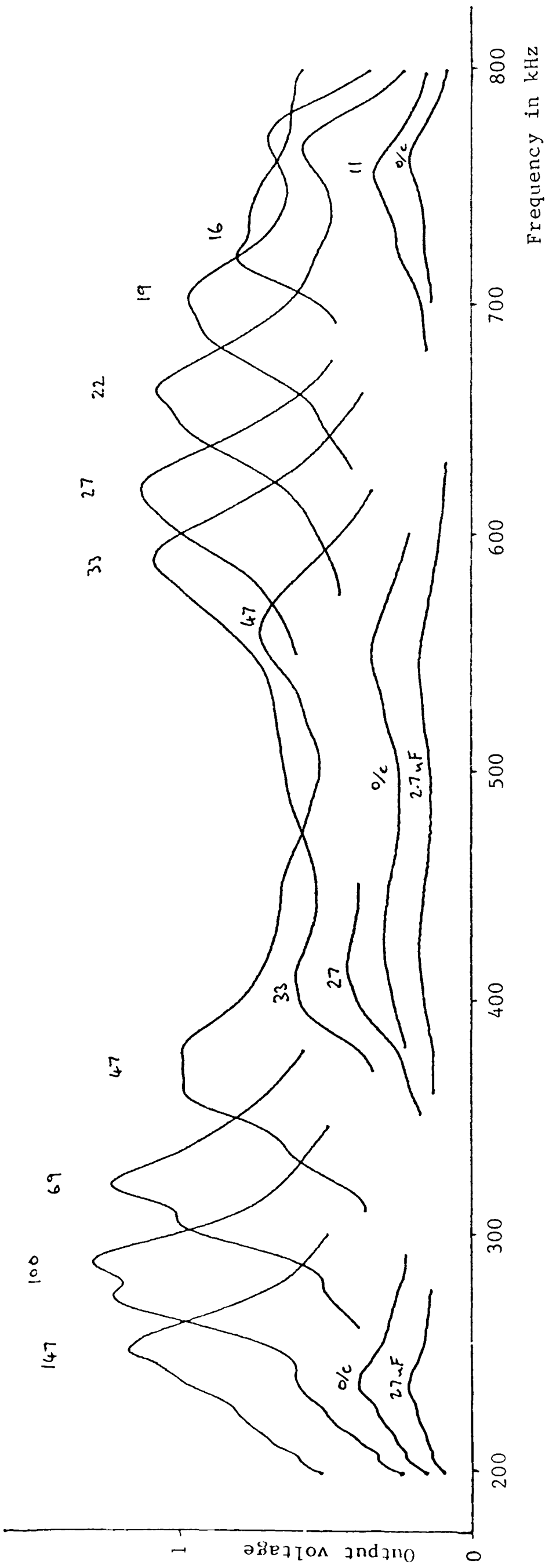

Figure 5v(ii) Output voltage of TC5 for different passive loads.
Figures above curves are inductance values in μH.

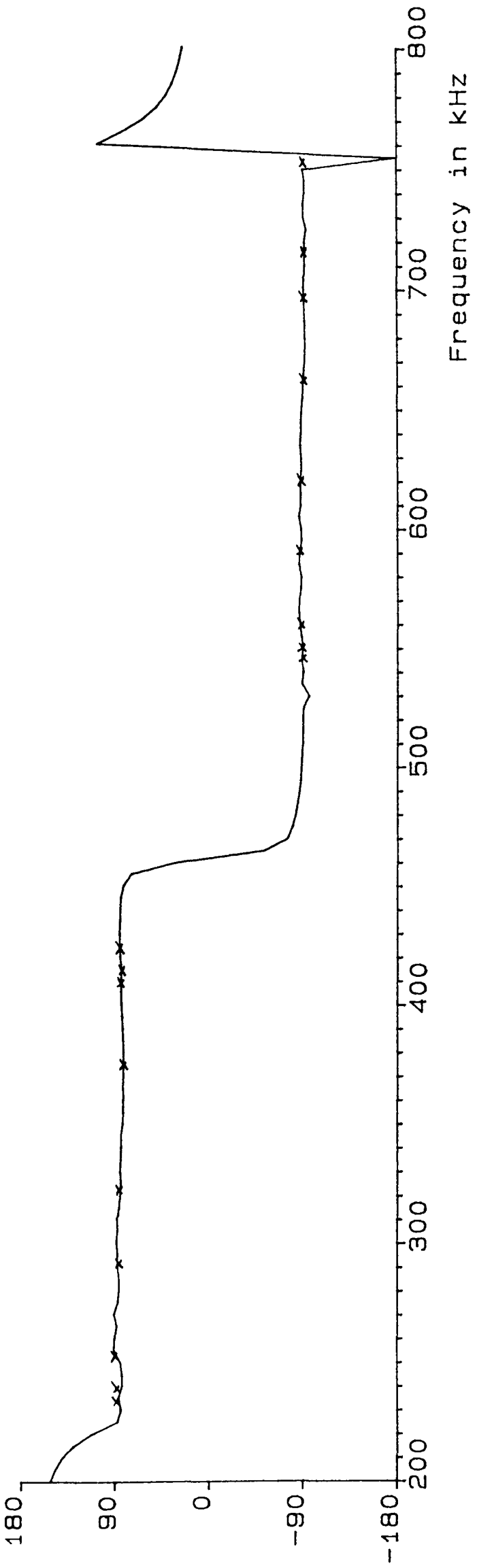

Figure 5v(iii) Predicted envelope for the output voltage of TC5 with 4Ω series resistance. Crosses show measured points from figure 5v(ii).

predicted value at resonance. Figure 5v(ii) shows amplitude measurements for a set of inductive loads and these are compared with the predicted envelope in figure 5v(iii).

5.9.4 Pressure and Efficiency Measurements

The program PASSIVE_LOAD was used to predict the front face pressure and efficiency of TC5 as functions of frequency. In figure 5w envelope curves are given for 4Ω series resistance. These are compared with measured values, shown by error bars, which were obtained using the radiation balance.

At around 500 kHz the second harmonic gives 0.75 times the predicted front face pressure. Hence the output power is lower than predicted but conductance (figure 5s) and therefore input power are also lower than predictions, giving an efficiency close to the predicted value of 70%. This high value confirms that the front matching layer is operating correctly.

Resonances below 500 kHz, produced by inductive loads, have efficiency and front face pressure which fall to less than half the predicted values. In this region figure 5s showed strong intermodal coupling, with associated energy loss through the sides of the ceramic. This accounts for the loss of efficiency.

Above 500 kHz the ceramics are large in wavelengths and conductance measurements showed closer agreement with predictions than at low frequencies. The same can be seen for pressure and efficiency measurements. The lowest efficiency occurs at 670 kHz where the third harmonic is moved furthest from its natural position. Efficiency

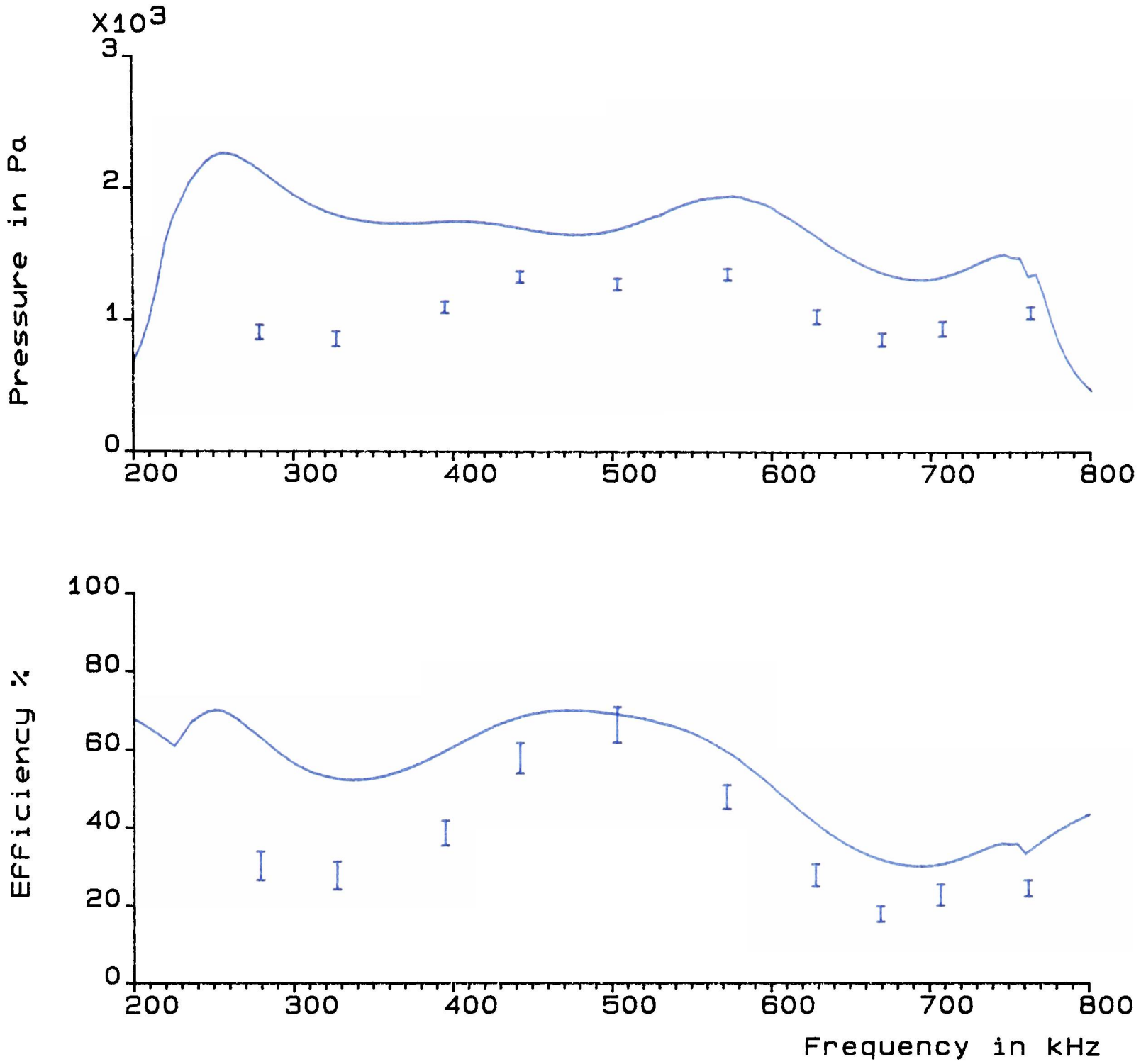

Figure 5w Pressure output and efficiency of TC5.

depends on series resistance (see figure 5q) and for 4Ω the predicted value is 32% at 670 kHz. The actual inductor used for this test had a series resistance of only 2Ω so efficiency should be higher than 32%. However the measured value is only 18% showing that even at high frequencies there is significant lateral displacement causing disagreement between predicted and measured performance.

Throughout this test power levels were kept as low as possible to avoid damaging the transducer. A drive voltage of 40V pk-pk was used and produced a deflection of around 4mm at most frequencies. This corresponds to an output power of 0.36 Watts. Conductance measurements taken after the test were identical to figure 5s showing that TC5 suffered no damage.

5.10 Stress analysis for TC5

Figure 5x shows the predicted bond stress for TC5 as a function of frequency. This graph was calculated by the program PASSIVE_LOAD in the same way as figure 5n for TC4. Comparison of figures 5n and 5x shows that bond stresses are similar for the two transducer designs although TC5 has higher bond stress when the third harmonic is close to its natural position of 755 kHz. It was not possible to obtain direct measurements of bond stress but figure 5w provides a reliable indication of the difference between predicted and measured pressures. The highest bond stress experienced by TC5 was at 760 kHz where figure 5x predicts a value of 28 kPa/V. At this frequency figure 5w shows the true pressure to be about 0.78 times the

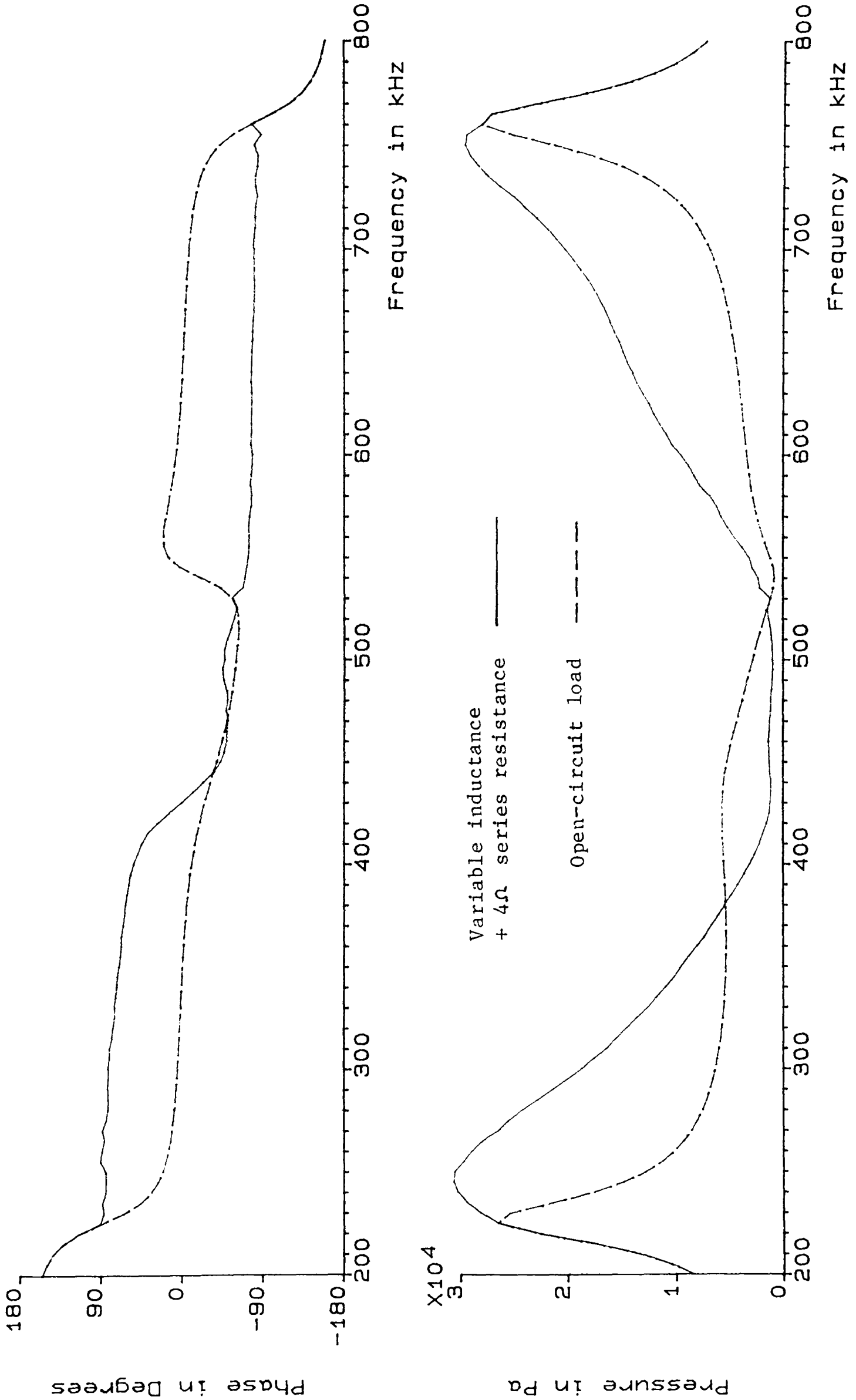

Figure 5x Predicted bond stress for TC5 as a function of frequency.

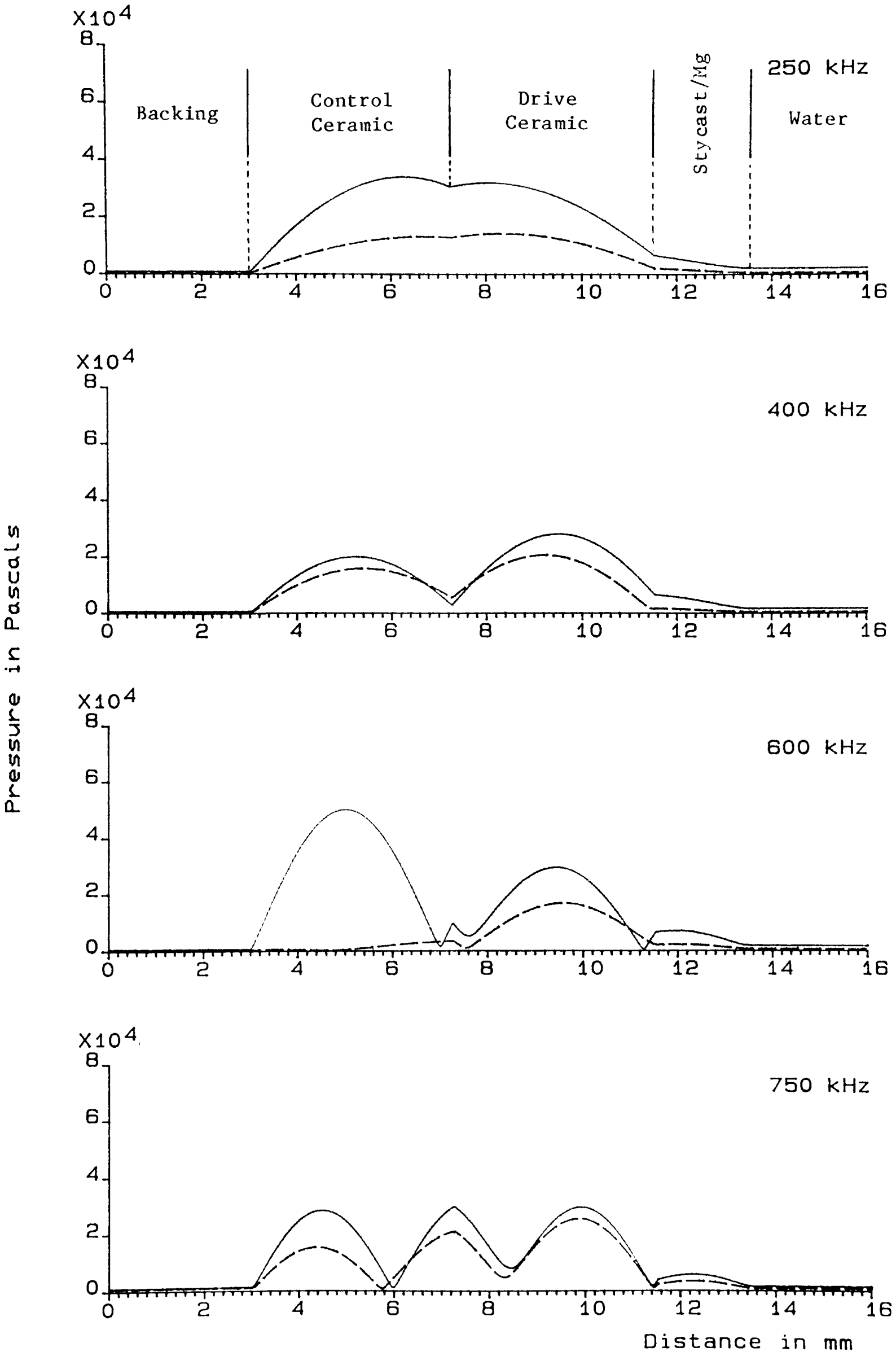

Figure 5y Stress analysis for TC5

predicted value, which for a 20V peak (40V pk-pk) drive voltage gives a peak stress of 437 kPa or 63 psi. This compares with an estimated bond stress of 595 kPa which caused damage to TC4.

Figure 5y shows stress as a function of distance through TC5 for a few selected frequencies. This graph is similar to figure 5o for TC4 and was calculated in the same way using the equations in appendix 11. Again maximum stress occurs within the ceramics, the bond representing a discontinuity at most frequencies. At 600 kHz the predicted stress reaches 50 kPa/V for the control ceramic. Figure 5w shows that the actual stress was probably around 0.65 times this value, giving 650 kPa or 94 psi for the 20V peak drive voltage. This is very small compared with the rated dynamic tensile stress of 3500 psi quoted for PZT-4 by Vernitron (12).

5.11 Discussion of Passive Control

In theory the piezoelectric-tunable transducer can be made to have a resonance at any frequency. However in practice useful resonances only occur in the range between natural frequencies of the fundamental and third harmonic. The lower limit of this range is about 200 kHz for ceramics of reasonable thickness, so piezoelectric-tunable operation does not appear to offer a solution to the difficulty in designing transducers resonant at around 100 kHz.

For a total ceramic thickness of 8.5mm passive control allows operation from 240 kHz to 760 kHz, a range of more than 1.5 octaves. This is considerably more than available with conventional transducer

designs. However some of the resonances in this range have Q>10 which is too high for transmission of short acoustic pulses. Therefore the piezoelectric-tunable transducer is most suitable for continuous-wave or long pulse applications, where frequency sweeping is gradual but extends over a wide range.

CHAPTER 6

Active Control

6.1 Low Frequency Transducer Tests

At frequencies below 100 kHz it is common practice to produce required beam patterns using arrays of sandwich transducers. At high power levels inter-element coupling causes the load on each transducer to differ according to its position in the array. Therefore prior to constructing the array it is necessary to examine the transducer performance under conditions of widely varying resistive and reactive loads.

A convenient method for carrying out such tests has been described by Auyer and Miller (37). Loading is provided by a second transducer which is connected to the first by a length of coupling material. Passive electrical loads are connected to the terminals of the second transducer and used to vary the impedance seen by the first. The arrangement is shown diagrammatically in figure 6a(i). Power handling capability of up to 1000 Watts is reported for the frequency range 3 - 4 kHz.

An alternative test procedure, for which the same apparatus can be used, is described by Bobber (32) and shown in figure 6a(ii). The second transducer is driven actively by a voltage of different amplitude and phase to the first. By this method any acoustic impedance, including negative resistance, can be generated.

In figure 6a attention is drawn to the similarity between passive loading of a sandwich transducer and passive control of a

LOW FREQUENCY

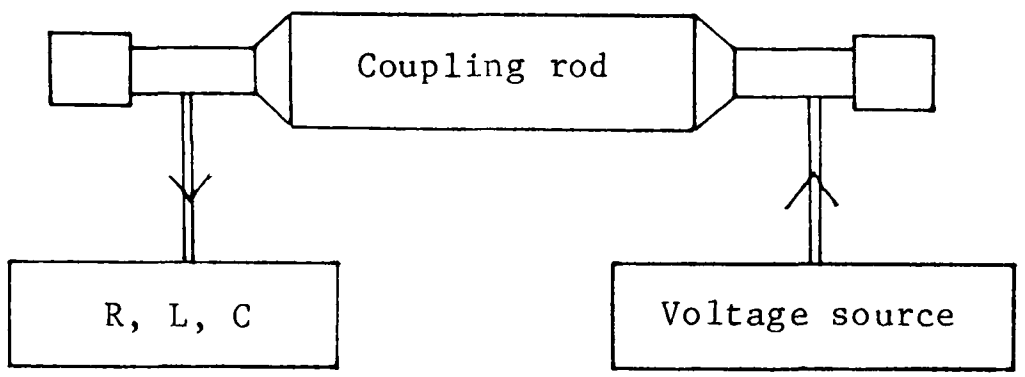

(i) Passive dumiload, Auyer and Miller

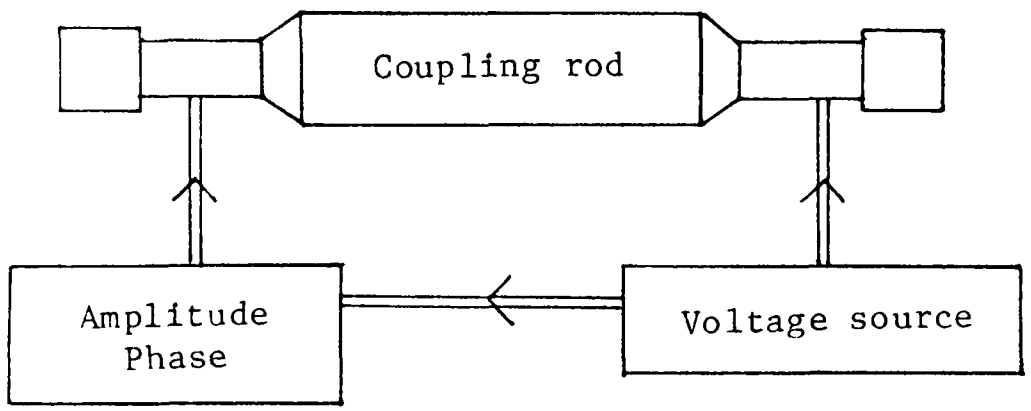

(ii) Active load, Bobber

HIGH FREQUENCY

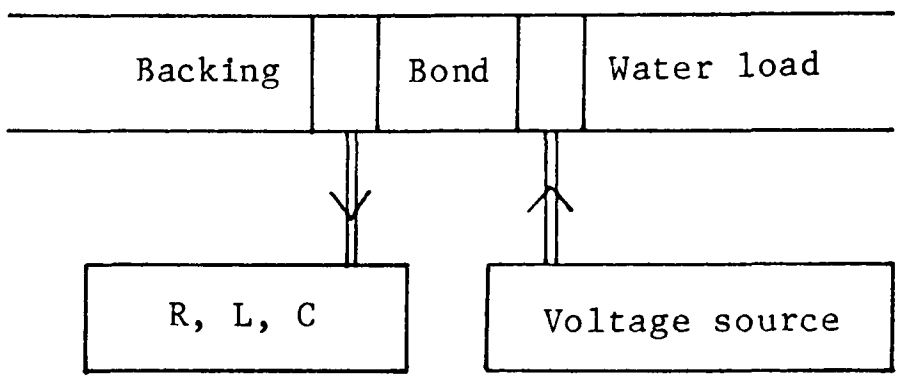

(iii) Passive control of backing impedance

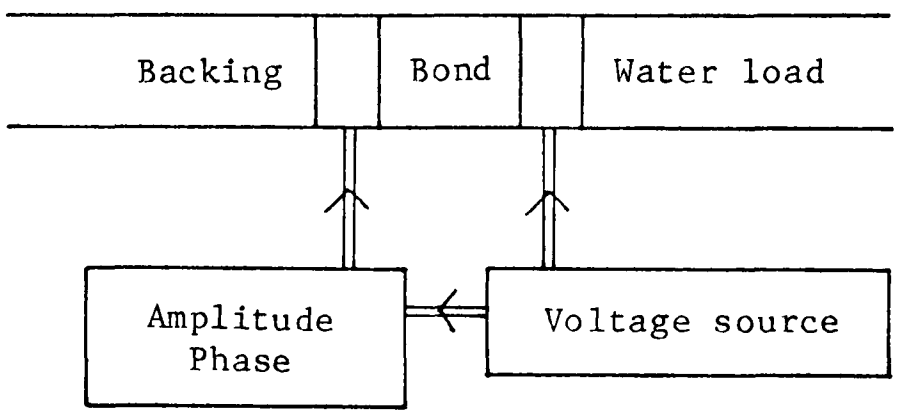

(iv) Active control of backing impedance

Figure 6a

piezoelectric-tunable transducer. If active loading can be extended to high frequencies in a similar way then it may provide a useful technique for controlling transducer characteristics. There are a number of ways in which active control could be implemented, one of which is investigated in this chapter.

6.2 Active Backing Impedance at High Frequency

Many of the transducers described in Chapter 2 have their bandwidth and efficiency determined by real (i.e. resistive) backing impedances. In Chapter 5 it was shown that reactive backings can also be used and these provide a means of controlling the resonant frequency, hence allowing tunable transducers to be constructed. The synthesis of resisitive or reactive backings by active control offers an alternative possibility for transducer design and the purpose of Chapter 6 is to investigate this technique.

The one-dimensional transmission line analysis described in Chapters 2, 3 and 5 can be applied to active control in the following way. Consider the general situation shown in figure 6b(i). The diagram represents a pair of ceramics separated by a coupling layer. The drive ceramic radiates power into a load Z_F and has an applied voltage E_o, while the control ceramic is backed by an impedance Z_B and has an applied voltage E_1. The problem to be solved is "What value of E_1 will produce a specified impedance Z_S on the back of the drive ceramic ?"

The following symbols will be used in the analysis:

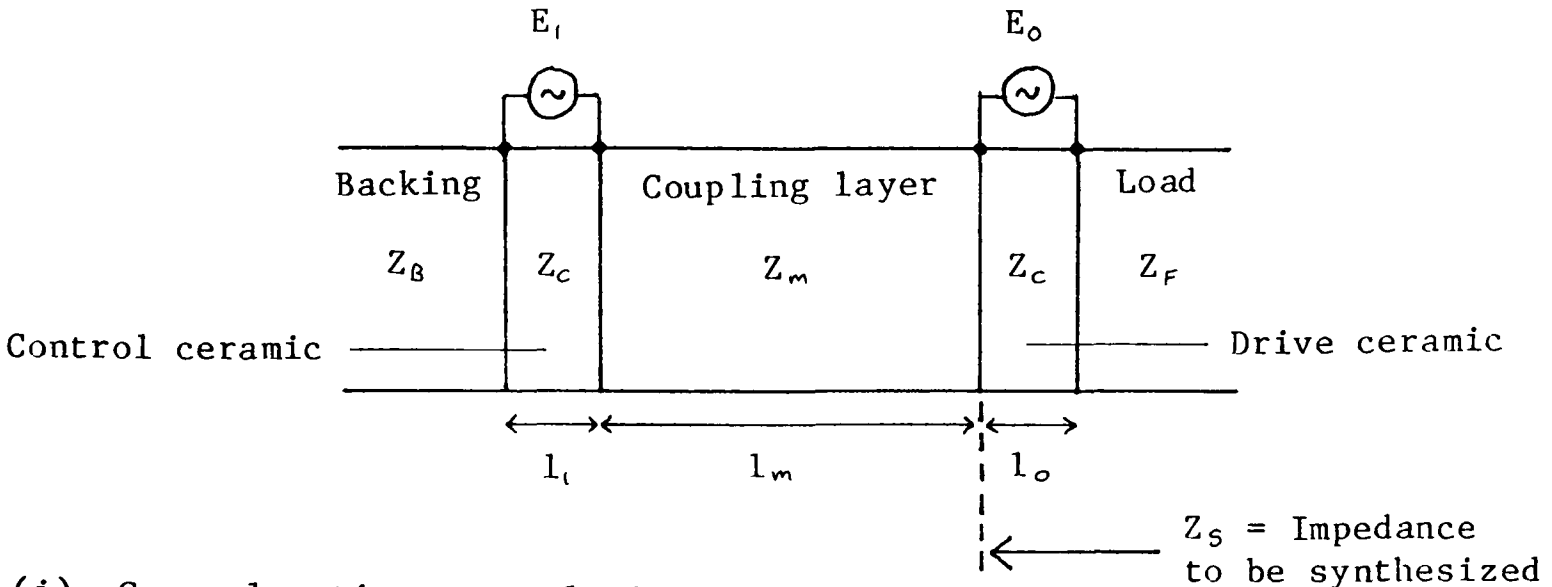

(i) General active control situation

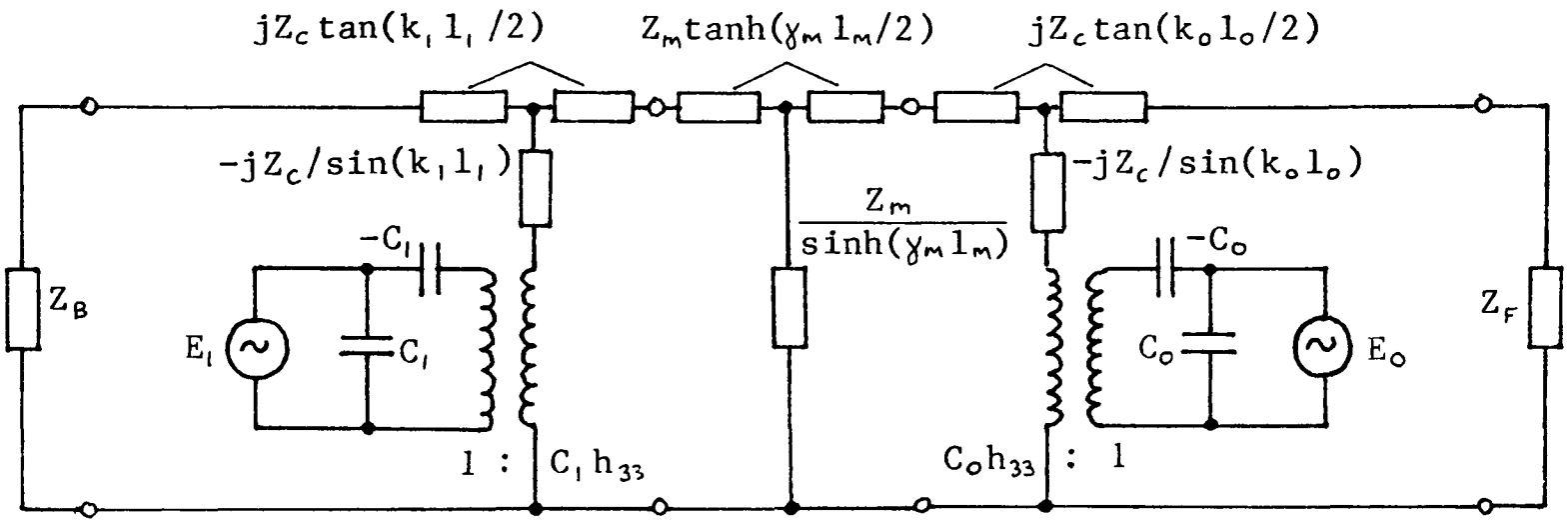

(ii) Equivalent circuit for active control analysis

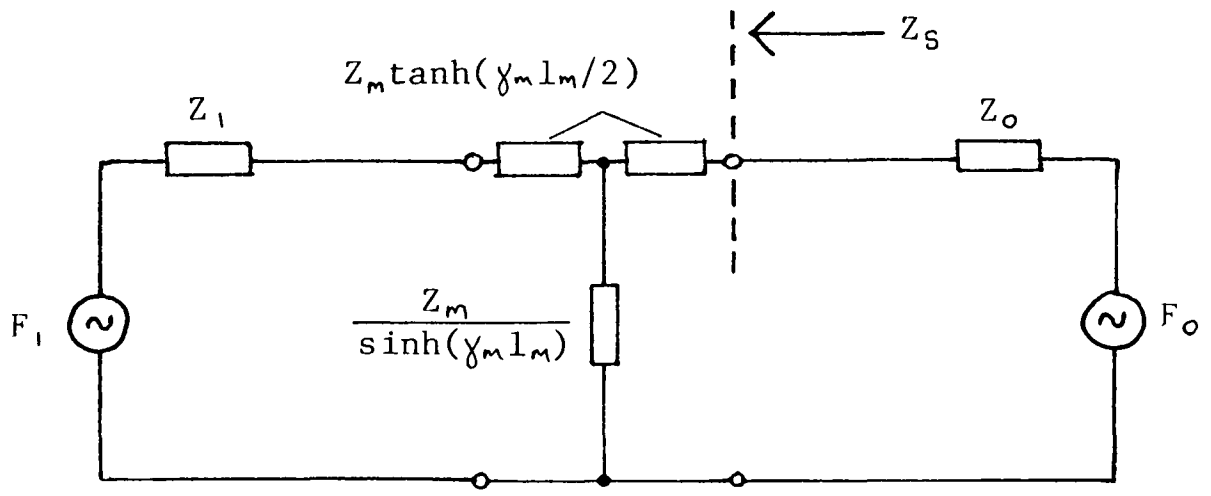

(iii) Simplified equivalent circuit

Figure 6b

	Drive ceramic	Control ceramic	Coupling layer	Units
Voltage	E_o	E_1	-	Volts
Capacitance	C_o	C_1	-	Farads
Impedance	Zc	Zc	Zm	Kg/s
Thickness	l_o	l_1	l_m	meters
Wavenumber	k_o	k_1	k_m	$meters^{-1}$

TABLE 6.1 Symbols used for active control analysis

It is assumed that the two ceramics have large diameter in wavelengths, or are laterally clamped, so that only thickness mode vibrations occur. For convenience it is also assumed that the two ceramics are made of the same material.

In figure 6b(ii) the two ceramics are represented by Mason's equivalent circuit (1). They are separated by a transmission line equivalent of the coupling layer, which has a propogation constant $\gamma_m = a_m + jk_m$ where a_m is the absorption in nepers/meter and k_m is the wavenumber. The impedances Z_F and Z_B are complex since in general the transducer may have several layers on the front of the drive ceramic and on the back of the control ceramic.

In appendix 8 it is shown that the circuit for a ceramic can be reduced to its Thevenin equivalent of a source in series with an impedance. This allows figure 6b(ii) to be redrawn as the simpler circuit of figure 6b(iii). The resulting circuit components are:

$$F_o = 2C_o h_{33} \cdot \frac{Z_{Qo}}{Z_{Po}+Z_{Qo}} \cdot E_o \qquad Z_o = Z_{Po} // Z_{Qo} - Z_F$$

$$F_1 = 2C_1 h_{33} \cdot \frac{Z_{Q1}}{Z_{P1}+Z_{Q1}} \cdot E_1 \qquad Z_1 = Z_{P1} // Z_{Q1} - Z_B$$

Where the impedance terms depend on the angular frequency ω :

$$Z_{Po} = 2Z_F + j\frac{4C_o h_{33}^2}{\omega} - 2jZ_c\cot(k_o l_o/2)$$

$$Z_{Pl} = 2Z_B + j\frac{4C_l h_{33}^2}{\omega} - 2jZ_c\cot(k_l l_l/2)$$

$$Z_{ao} = 2Z_F + 2jZ_c\tan(k_o l_o/2)$$

$$Z_{al} = 2Z_B + 2jZ_c\tan(k_l l_l/2)$$

The units of F_o and F_l are Newtons and the mechanical impedances Z_o and Z_l have units of Kg/s. The piezoelectric constant h_{33} has units of Volts/meter, for PZT-4 its value is $26.8*10^8$ V/m (12).

Analysis of figure 6b(iii) in appendix 9 shows that the required impedance Z_S is related to F_l by:

$$F_l = F_o\left[\frac{(B+C)(Z_S+Z_o) - (B+C)(A+B) + B^2}{B(Z_S+Z_o)}\right] \quad \text{Equation 6.1}$$

$$= F_o\ (\nu + j\sigma)$$

Where the impedances A,B and C refer to the coupling layer as follows:

$$A = Z_o + Z_m\tanh(\gamma_m l_m/2)$$

$$B = Z_m/\sinh(\gamma_m l_m)$$

$$C = Z_l + Z_m\tanh(\gamma_m l_m/2)$$

Note that in equation 6.1 the term in square brackets is an impedance ratio, which for convenience can be written as the complex quantity $\nu + j\sigma$. Substitution for F_o and F_l in terms of E_o and E_l gives the required solution:

$$E_1 = \frac{C_o}{C_1} \cdot \frac{Z_{Qo}}{Z_{Q1}} \cdot \frac{Z_{P1}+Z_{Q1}}{Z_{Po}+Z_{Qo}} \cdot (\nu + j\sigma) \cdot E_o \qquad \text{Equation 6.2}$$

This equation gives the amplitude and phase of E_1 required to generate an impedance Z_S on the back of the drive ceramic.

6.3 Calculation of Active Loads by Computer

An interactive FORTRAN program called ACTIVE_LOAD was written for application of equation 6.2 to any transducer represented by figure 6b(i), i.e. any transducer with two ceramics separated by a single coupling layer. The program has five sections, of which the first three are similar to PASSIVE_LOAD described in Chapter 3.

1. Density, speed of sound and absorption of a number of materials are read from data files.

2. A description of the transducer is entered. This defines the number of layers, thickness and composition of each layer, cross-sectional area and frequency range of interest.

3. The impedances Z_F, on the front of the drive ceramic, and Z_B, on the back of the control ceramic, are calculated by repeated use of equation 3.1 at specified frequency intervals.

4. The required impedance Z_S $(=R_S+jX_S)$ on the back of the drive ceramic is entered. It may be frequency dependent.

5. Equation 6.2 is used to calculate the required control voltage E_1 at each frequency.

6.4 Basic Design Requirements

Before using equation 6.2 for detailed transducer design it is worth considering the general requirements which will be relevant to practical application of active control.

The electronic circuits required for active control are more complicated than for other transducer designs because two amplifiers and a phase shift network are involved. For clarity the amplifiers will be termed the "drive amplifier" and "control amplifier" to be connected to the drive ceramic and control ceramic respectively. Unless otherwise stated the drive voltage (E_o) will be kept constant while the control voltage (E_i) will have amplitude and phase which are functions of frequency. The transducer structure should be chosen to keep the electronics as simple as possible. There are two factors to consider:

1. A frequency dependent phase shift is required. For reliable performance the rate of change of phase with frequency ($d\phi/df$) should be small, allowing slight frequency errors to be tolerated.

2. The control voltage must not have large amplitudes compared with the drive voltage. This is to allow similar designs for the drive amplifier and control amplifier, hence reducing the complexity of the system. A more important reason for avoiding excessive control voltage is that the resulting high stress in the control ceramic would define the upper limit of power handling capability. A satisfactory structure would have similar stresses in both ceramics.

For any system containing more than one source there is a possibility of negative resistance. In an actively controlled transducer negative resistance arises if power is transferred from one ceramic to the other. This situation should clearly be avoided as unnecessary power is being delivered by one amplifier while the other may be damaged by current flowing into its output terminals. Therefore the transducer should be designed to give positive conductance seen looking into both ceramics.

As with conventional transducers the requirements for wide bandwidth, high efficiency and ease of construction remain of greatest importance for most applications.

6.5 Effects of Parameter Variation

The following investigations were carried out with the aim of finding a transducer structure in which the drive ceramic can have its backing impedance varied without using excessive control voltage.

6.5.1 Ceramic Thickness Ratio

The first term in equation 6.2 is C_o/C_1, the clamped capacitance ratio. This term suggests that to achieve small values of E_1 it is necessary to use a control ceramic which is thin compared with the drive ceramic (i.e. $l_1 < l_o$). However on closer inspection the numerator of equation 6.2 contains the term Z_{p1} which depends on $\cot(k_1 l_1/2)$. As l_1 decreases the impedance Z_{p1} tends to infinity,

overriding the benefit of the capacitance ratio.

The term Z_{P1} again becomes infinite for $l_1 = \lambda$, showing that if the control ceramic has a thickness of one wavelength then active control is not possible. The transducer should be designed for $l_1 = \lambda$ to occur above the frequency range of interest.

Now consider the drive ceramic. In conventional transducers the greatest transfer of power to the load occurs for $l_o = \lambda/2$, and there is zero power output at $l_o = \lambda$. Therefore it is necessary to avoid $l_o = \lambda$, while $l_o = \lambda/2$ should be included in the frequency range of interest.

The above considerations indicate that optimum conditions for active control occur when the drive ceramic and control ceramic have the same thickness. Frequencies of interest extend up to 1 MHz so the condition $l_o = l_1 = \lambda/2$ is required to occur at around 500 kHz. For practical applications it is convenient to use the standard 500 kHz PZT-4 discs, supplied by Vernitron, which were used in Chapter 5. These discs have a thickness of 4.25mm so in Chapter 6 the values $l_o = l_1 = 4.25$mm will be used.

6.5.2 Backing Impedance and Coupling Layer Thickness

Having determined the optimum ceramic charecteristics it is now necessary to examine the coupling layer between them. It is convenient to study the effects of backing impedance during the same calculations. The program ACTIVE_LOAD was run for the structure of figure 6b with the drive ceramic radiating directly into water. There are three variable parameters:

1. Coupling layer impedance (Z_m). The following values do not correspond to any true material but give a wide impedance range for the same velocity.

Impedance Mrayls	ρ Kg/m^3	c m/s	a dB/cm/MHz
0.3	150	2000	0
3	1500	2000	0
30	15000	2000	0

2. Coupling layer thickness (l_m). Three values were chosen to include multiples of $\lambda/4$ and $\lambda/2$ and also a very thin layer corresponding to a bond.

	Thickness in wavelengths		
l_m in mm	200 KHz	500 kHz	800 kHz
0.01	~0	~0	~0
1.0	0.1	0.25	0.4
10	1.0	2.5	4.0

3. Backing impedance (Z_g). Three true materials were studied to cover the impedance range of easily constructed backings.

Material	ρ Kg/m^3	c m/s	a dB/cm/MHz
Air	1.2	343	0
Stycast/fillite	700	2500	11
Stycast/iron	3370	2120	4.4

Combinations of these parameters give 27 sets of results which are summarised in figure 6c. Each graph shows the maximum control voltage which would be required to synthesise a real acoustic impedance R_s on the back of the drive ceramic in the frequency range 200 - 800 kHz. (The frequency at which maximum voltage occurs is not

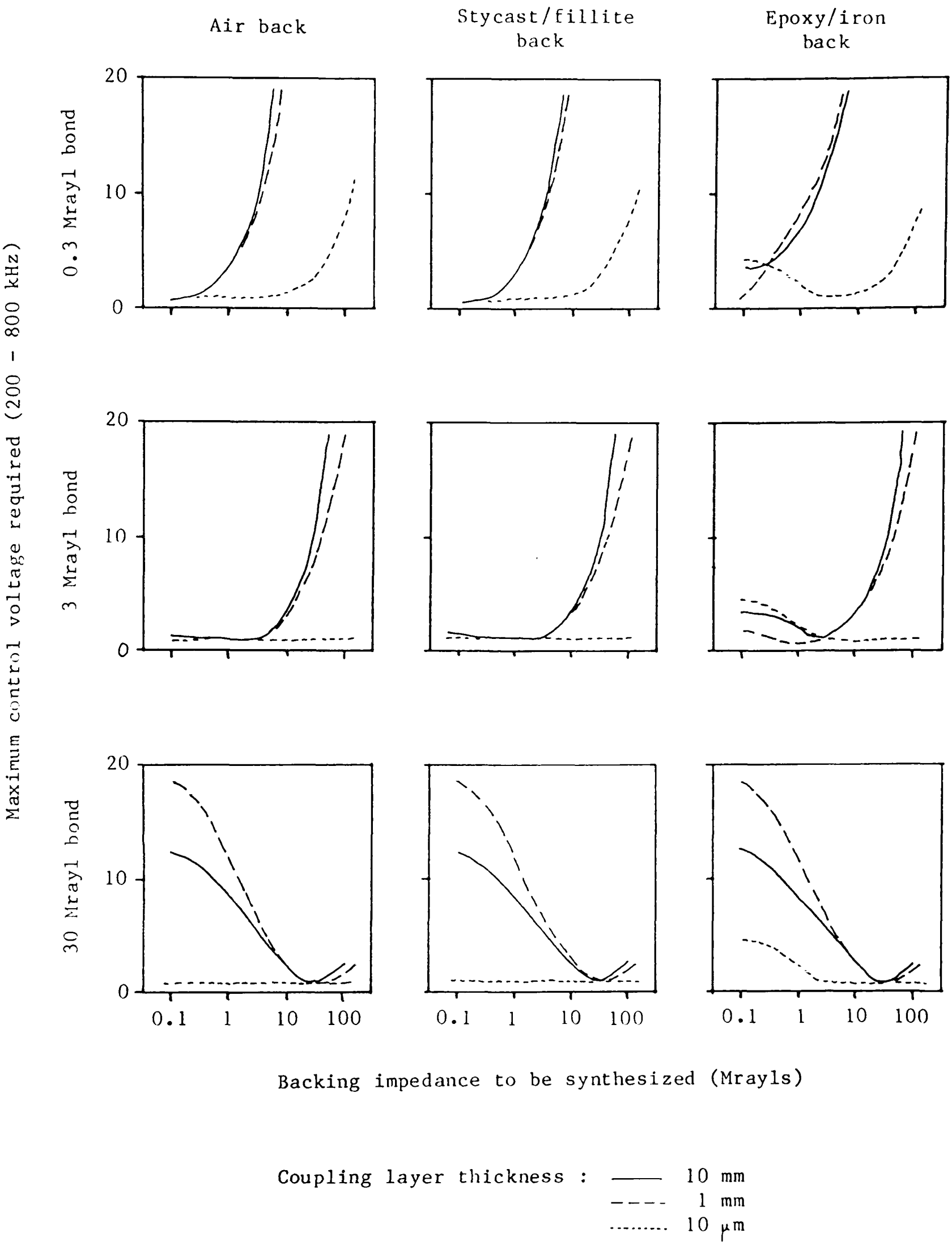

Figure 6c The effects of backing impedance and coupling layer thickness.

shown.)

The most important conclusion from figure 6c is that for optimum performance the coupling layer must be thin in wavelengths. A 10μm bond allows any impedance in the range 0.1 Mrayls to 100 Mrayls to be synthesised by a control voltage of less than ten times the drive voltage. If the bond is thin then its impedance has little effect, as would be expected from transmission line theory. Backing impedance is seen to be almost irrelevant to amplitude considerations but was found to have noticeable effects on phase (not shown on figure 6c).

6.6 Synthesis of Real Backing Impedances for TC4

It has been shown that the most suitable transducer design for active control contains two ceramics of equal thickness separated by a thin bond. Both TC4 and TC5 satisfy these requirements.

The synthesis of real backing impedances was investigated, using computer simulation, for the structure of TC4 which was shown in figure 5j. The parameters of interest are conductance, control voltage and efficiency. The program ACTIVE_LOAD was used to find the control voltage required for synthesis of four backing impedances in the range 0 - 100 Mrayls. Results are shown in figure 6d. Amplitude (solid line) and phase (dashed line) of the control voltage are shown relative to the drive voltage, and all graphs are plotted for the frequency range 200 - 800 kHz.

To synthesise a 0 Mrayl backing requires a control voltage of up to double the drive voltage. The phase is close to $\pm 180^{\circ}$ for all

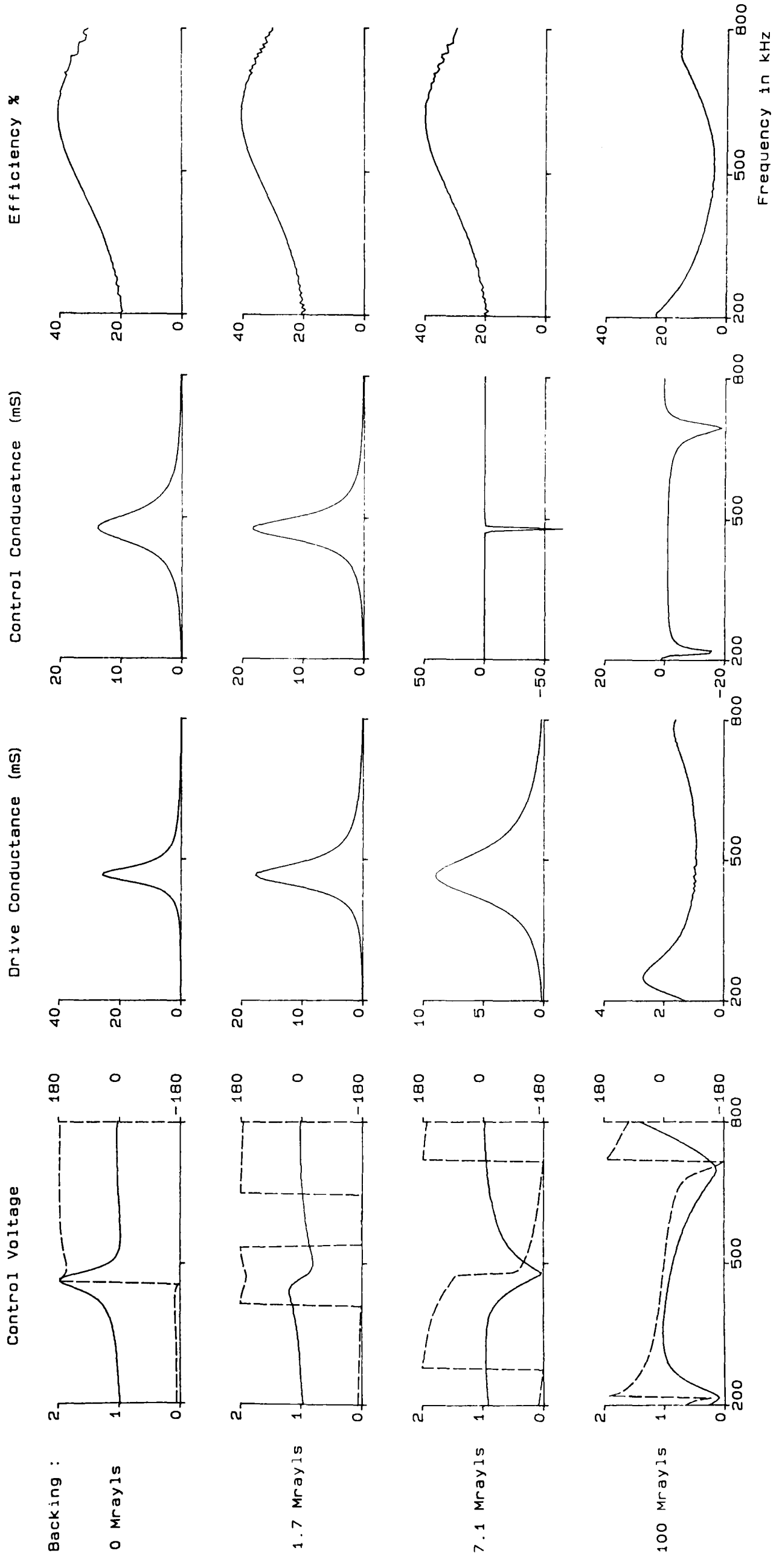

Figure 6d Synthesis of real backing impedances for TC4

frequencies so there is no problem of large $d\phi/df$. A single ceramic backed by 0 Mrayls has a theoretical efficiency of 100% since no power is lost to the backing. Similarly when a 0 Mrayl backing is actively synthesised for TC4 all electrical power delivered to the drive ceramic is converted to acoustic power in the water load, giving 100% efficiency if only the drive ceramic is considered. However electrical power is also delivered to the control ceramic. Calculation of pressure at the material boundaries reveals that all this power enters the backing. Therefore the overall efficiency is less than 100% and is defined as:

$$\eta = \frac{\text{Acoustic power delivered to water}}{\text{Power into drive ceramic + Power into control ceramic}}$$

Synthesis of a 1.7 Mrayl backing requires a control voltage of similar amplitude to the drive voltage. The relative phase is close to $\pm 180^{\circ}$. Both ceramics have similar conductance showing that roughly equal electrical power is delivered to them. In this case power from the drive ceramic is shared between the load and the backing in the same proportions as would be the case for a single ceramic backed by 1.7 Mrayls. Again power delivered to the control ceramic goes entirely to the backing.

The epoxy/iron backing of TC4 has an impedance of 7.1 Mrayls. At 470 kHz the control ceramic is acoustically transparent so requires no control voltage to synthesise 7.1 Mrayls. Above and below this frequency the control voltage rises to become comparable with the drive voltage. There is large $d\phi/df$ at 470 kHz but this causes no problem as the amplitude is zero. No electrical power is delivered to the control

ceramic, which has zero conductance, so efficiency is the same as for a single ceramic backed by 7.1 Mrayls. A peak in efficiency occurs at 650 kHz because the 1mm protective Stycast layer is $\lambda/4$ thick at this frequency.

A 100 Mrayl backing produces a $\lambda/4$ resonance at 250 kHz, and a $3\lambda/4$ resonance at 780 kHz, for the drive ceramic. The control ceramic has negative conductance. Electrical power delivered to the drive ceramic is mostly lost via the control ceramic, with only a small proportion converted to acoustic power in the water. In this situation efficiency has to be defined carefully. It is assumed that power leaving the control ceramic cannot usefully be returned to the electrical supply, therefore when the control ceramic has negative conductance efficiency is defined as:

$$\eta = \frac{\text{Acoustic power delivered to water}}{\text{Power into drive ceramic}}$$

It is clear from this definition that synthesis of a 100 Mrayl backing gives the same efficiency as would occur for a true 100 Mrayl backing.

The conclusion from figure 6d is that all real backing impedances can be actively synthesised with no problem of excessive control voltage or $d\phi/df$.

For impedances up to 7.1 Mrayls electrical power is delivered to both ceramics. Power from the drive ceramic is divided between the water and the backing, but power from the control ceramic goes only into the backing. The overall efficiency is the same as for a single ceramic backed by 7.1 Mrayls.

Synthesis of backing impedances above 7.1 Mrayls causes

negative conductance for the control ceramic. In this case electrical power is delivered only to the drive ceramic, giving the same overall efficiency as for a true backing of the impedance being synthesised. The significance of 7.1 Mrayls is that it represents the impedance of epoxy/iron, the backing material used for TC4.

Does this kind of active control have any practical use? The answer is no. For values up to 7.1 Mrayls it is easier, cheaper, and gives higher efficiency to use a single ceramic backed by the required impedance. High impedance backings, above 7.1 Mrayls, are required for production of very short acoustic pulses, the optimum backing having the same impedance as ceramic. However all the above calculations refer only to continuous waves so the solutions are not valid for short pulses.

A very high backing impedance, greater than that of ceramic, is required to produce a $\lambda/4$ resonance. This is useful as it halves the volume of ceramic compared with the conventional $\lambda/2$ resonance. But active control requires a second ceramic to do this, so gives no advantage in terms of ceramic volume. The additional problem of negative conductance is a further reason to avoid synthesis of impedances above 7.1 Mrayls.

The above discussion indicates that in general active control is of no significant use when applied to the synthesis of real backing impedances. Therefore no practical experiments were carried out.

6.7 Synthesis of Reactive Backing Impedances

So far only the synthesis of real backing impedances has been considered i.e. $Z_S = R_S + j0$. Equation 6.2 can also be used to investigate active synthesis of reactive backings, but it is not obvious what values of acoustic reactance to choose. Chapter 5 provides the answer.

In Chapter 5 it was shown that passive electrical loading of the control ceramic causes variations in resonant frequency by adjusting the acoustic reactance seen by the drive ceramic. Active control can be applied in a similar way. As an example consider the transducer TC5 with a passive load of $32\mu H + 4\Omega$. Figure 5t shows that resonances occur at 213 kHz, 405 kHz, 610 kHz, and 770 kHz. In Chapter 5 these were regarded as the first four harmonics of the ceramic pair, but now consider only the drive ceramic. The program PASSIVE_LOAD was used to calculate the backing impedance seen by the drive ceramic as a function of frequency. This is shown in figure 6e(i). The program ACTIVE_LOAD was then used to derive the control voltage which would be needed for active synthesis of the same acoustic impedance. Figure 6e(ii) shows the result.

The passive load of $32\mu H + 4\Omega$ was chosen to illustrate an interesting point. In section 5.9.3 the output voltage was measured across this same passive load and is shown in figure 5v(i). Compare this with figure 6e(ii). The predicted curves are identical!

Further computer simulation led the author to the following important conclusion: Any passive electrical load can be simulated actively by applying a voltage of the same amplitude and phase as would

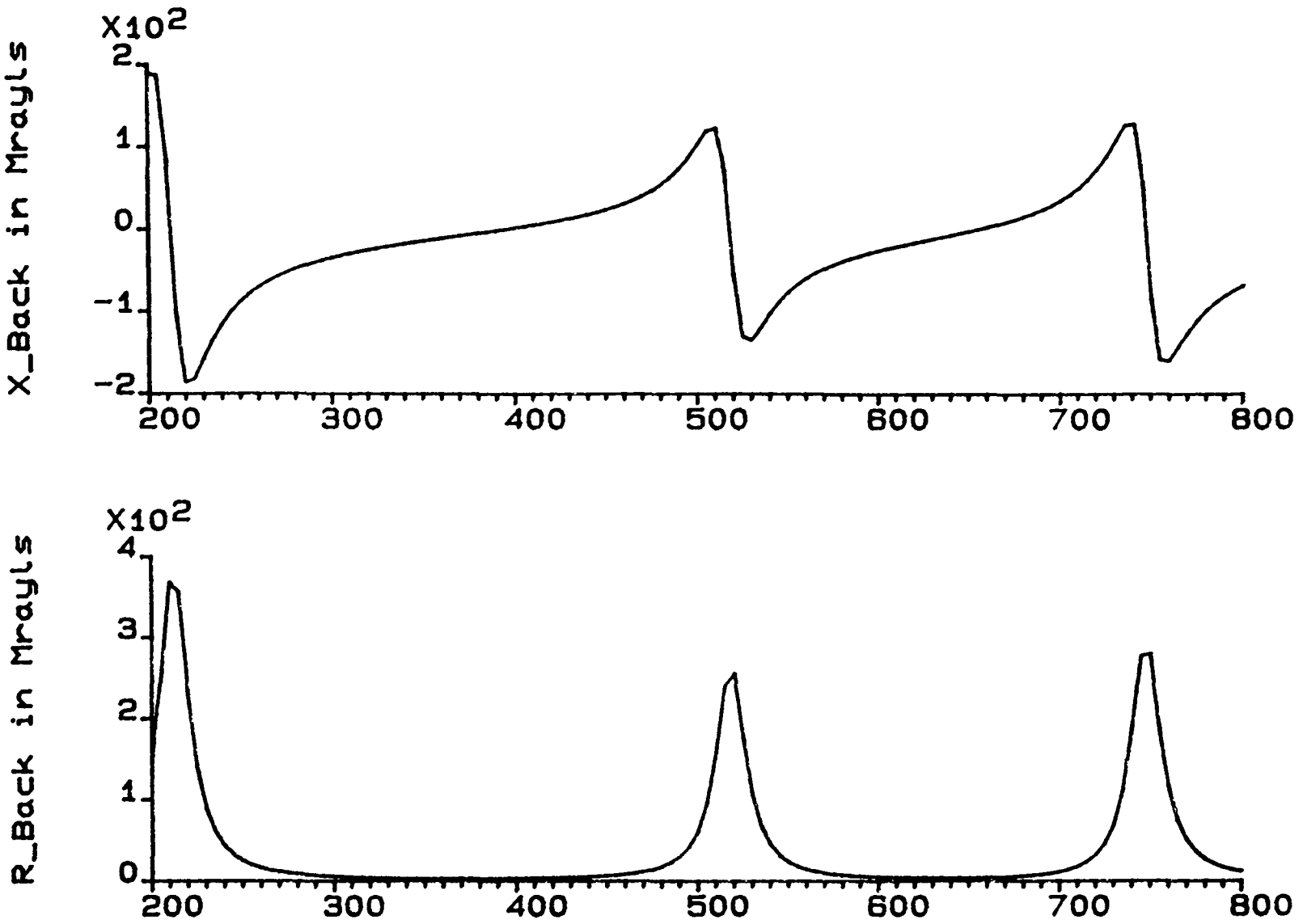

(i) Backing impedance seen by TC5 drive ceramic for a passive load of 32μH + 4Ω.

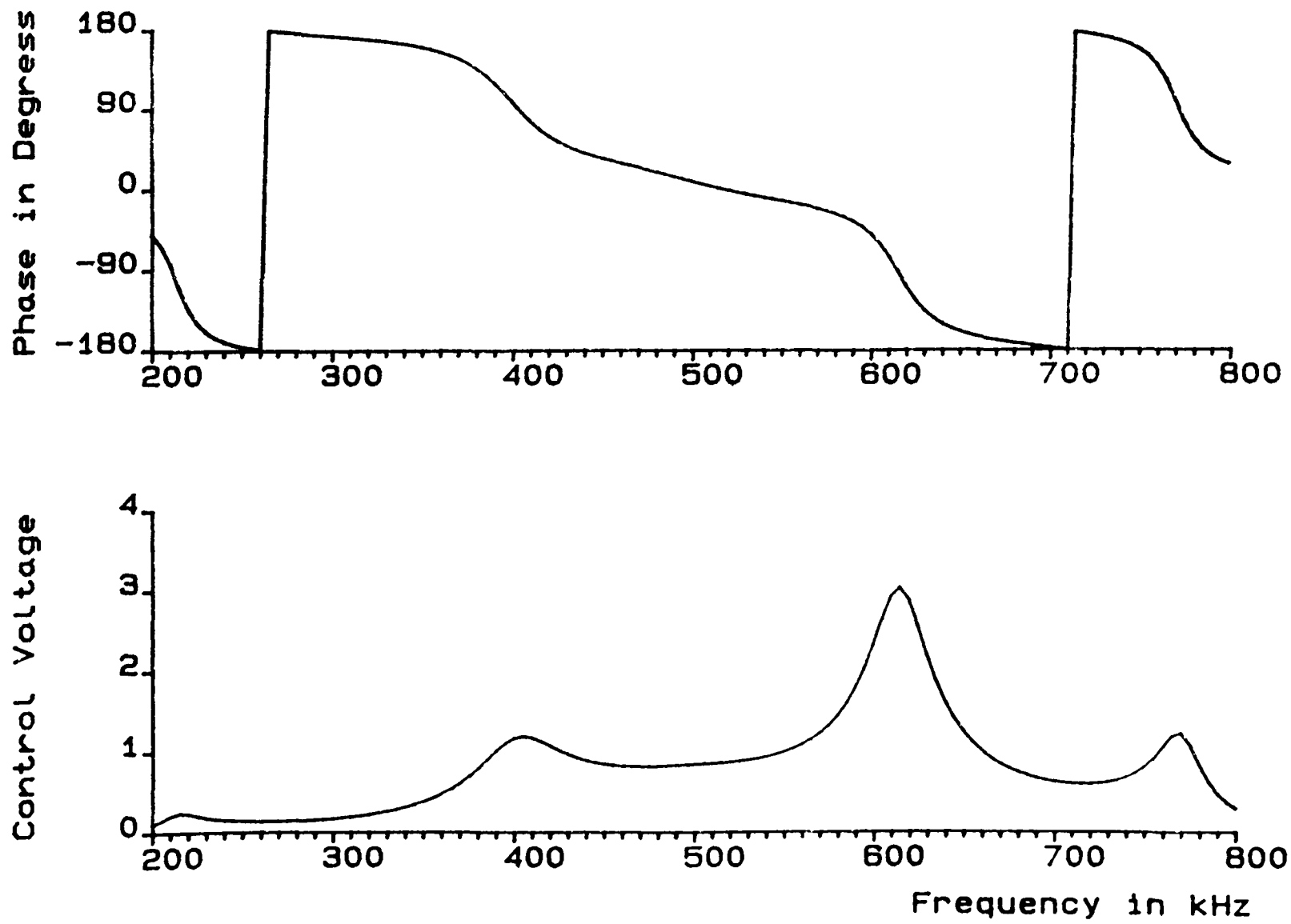

(ii) Voltage required to generate the above impedance by active control.

Figure 6e

be measured across that load. In fact this is simply a demonstration of the substitution theorem, which states that "A known voltage in a circuit can be replaced by an ideal voltage source and a known current can be replaced by an ideal current source." For proof of this theorem see Scott (44) pages 131-132. It follows that all voltages and currents in the equivalent circuit, and therefore all predicted forces and particle velocities in the transducer structure, are identical for the active and passive cases.

6.8 Active Control of Resonant Frequency for TC5

The above discussion indicates that active control can be used to vary the resonant frequency of TC5 by simulation of passive electrical loads. Simulation of a fixed inductive or capacitive load produces a set of resonances which correspond to the predicted harmonics in figure 5t. However it is of greater interest to simulate a variable passive load. In figure 5q a set of predicted curves are given for TC5. Each curve represents the envelope of the resonant peaks produced by passive control, and the height of each curve is determined by series resistance. To produce the same results by active control simply apply a voltage equal to that shown as "Output Voltage". (Phase is not shown on figure 5q but has a value of $+90^{\circ}$ below 462 kHz and -90° above this frequency.)

The curves in figure 5q are calculated for variable inductors in series with fixed resistors. This gives drive ceramic conductance and output pressure which vary slightly over the frequency range of

operation. For some applications it may be more convenient to have constant conductance or constant front face pressure. Either can be achieved. In table 6.2 small series resistance values are given as a function of frequency to produce either constant drive ceramic conductance or constant output pressure. The two do not occur simultaneously. Figure 6f shows the resulting performance calculated by the program PASSIVE_LOAD.

The acoustic impedance seen on the back of the drive ceramic is shown in figure 6g(i) for the constant conductance case. In the frequency range 240 - 760 kHz the reactive component varies from +j100 Mrayls to -j100 Mrayls while the resistive component is always less than 30 Mrayls. This impedance data was used in the program ACTIVE_LOAD to derive the control voltage required for constant drive ceramic conductance. The result, shown in figure 6g(ii), is again identical to the output voltage for the passive case (figure 6f). Note that phase remains close to $\pm 90^{\circ}$.

6.9 Performance of TC5 with Active Control

A digital circuit was constructed to generate the frequency dependent amplitude and phase shifts required for active control. Details of this circuit are given in appendix 10. The circuit includes Read Only Memories which store six separate programs (binary numbers 000 - 101) for active control of TC5 in the frequency range 200 - 800 kHz. Each program actively simulates a passive load as shown in table 6.3. Data was generated by ACTIVE_LOAD. Fixed inductance

Frequency kHz	Inductance μH	Resistance in Ohms Constant G	Constant P
229	500	55	30
236	250	40	30
247	175	23	15
270	120	11	7.5
292	95	8	5.5
309	81	7	4.5
331	67	6	3.5
365	50	5	3
388	40	4	3
415	28	1	2
438	16	0	0
461	0	0	0
534	150	15	10
544	88	20	10
567	50	20	8
586	40	13	6
618	31	8	3.5
647	26	6	2.5
687	21	5	2
726	16	7	1
739	13	9	0
746	10	15	0
755	0	30	0

TABLE 6.2 Resistance values added to passive loads to give constant conductance or constant front face pressure for TC5.

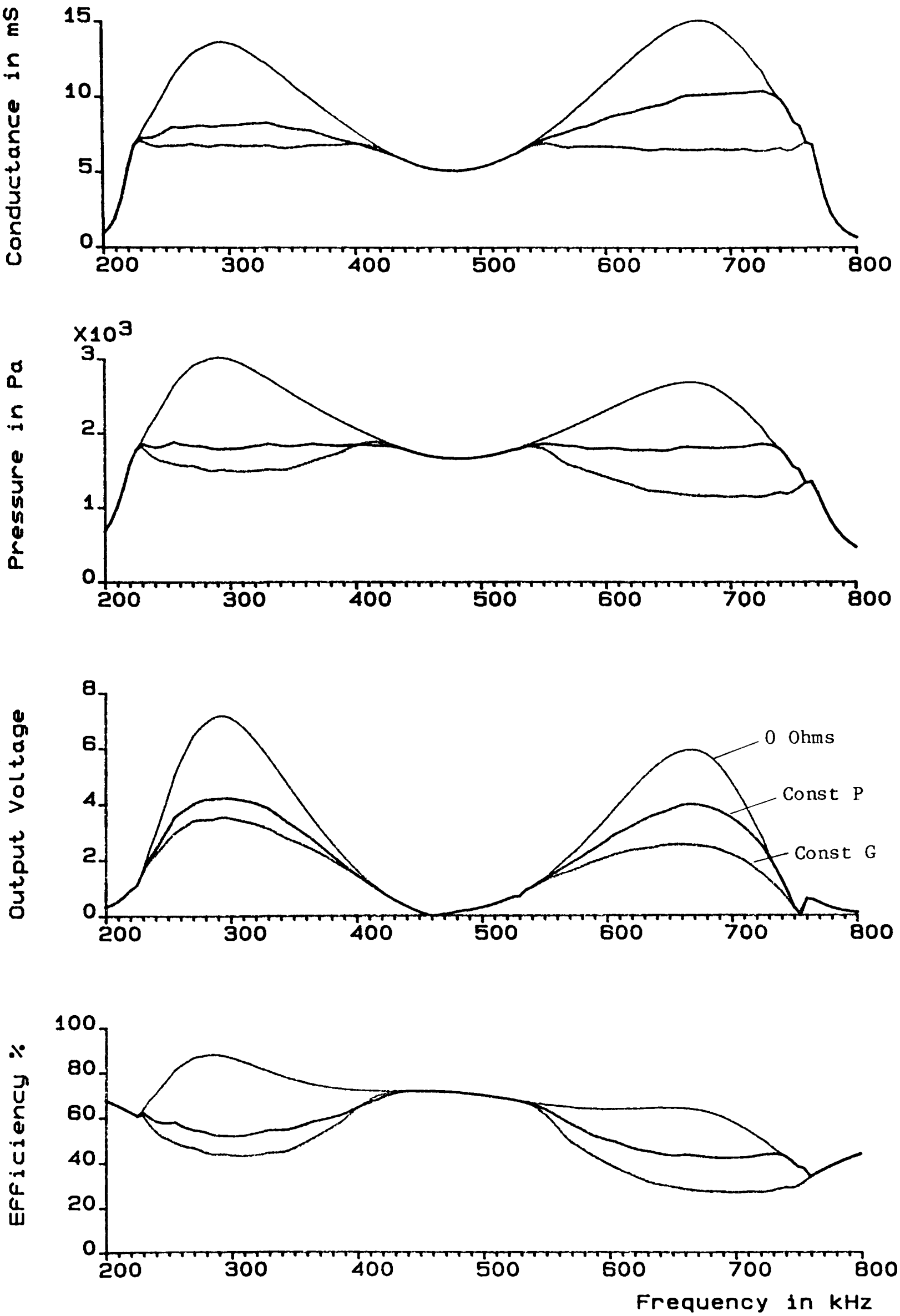

Figure 6f Predicted performance of TC5 with series resistance added to passive loads to give constant conductance or constant front face pressure.

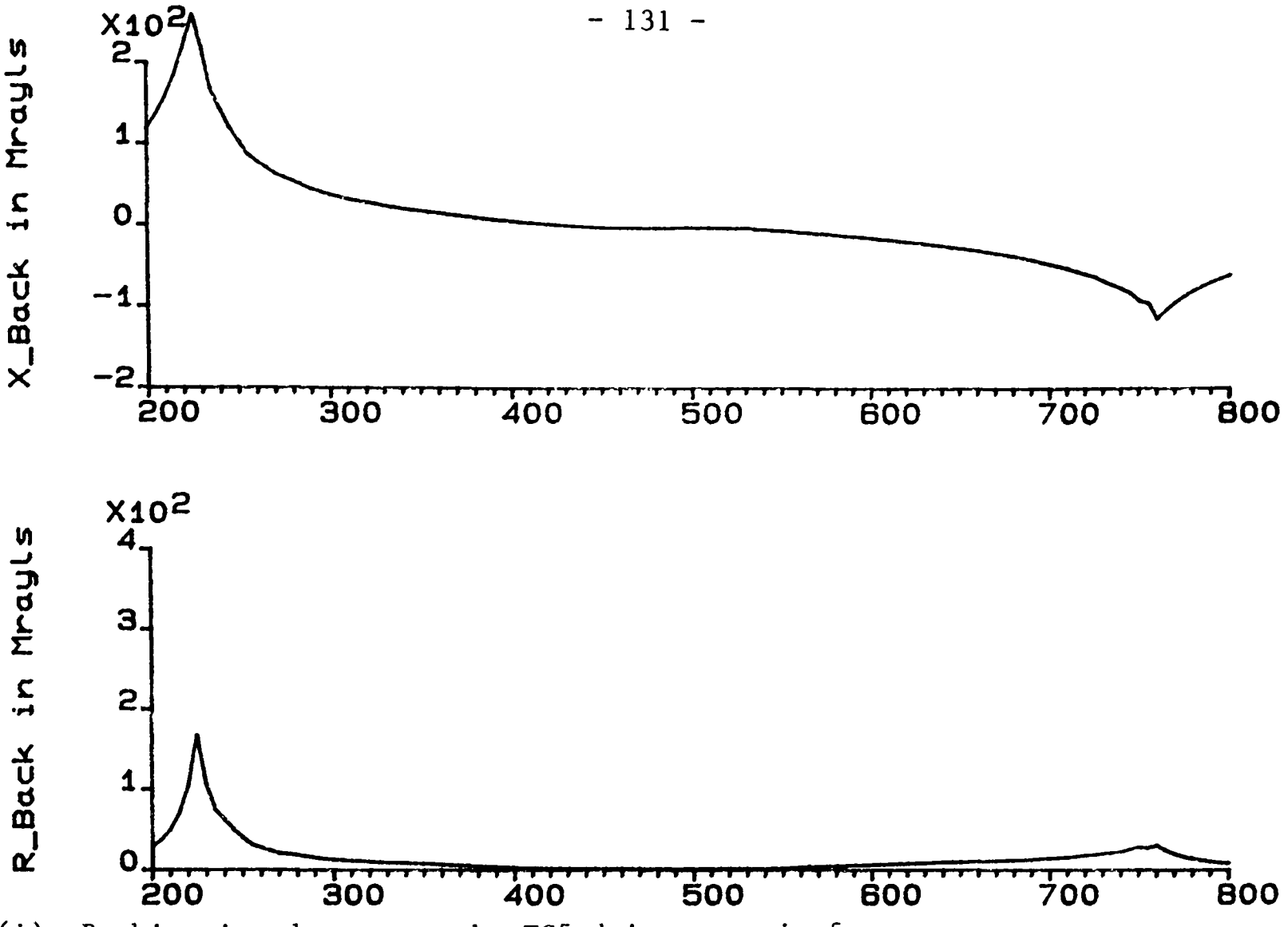

(i) Backing impedance seen by TC5 drive ceramic for variable inductive load with series resistance added to give constant conductance.

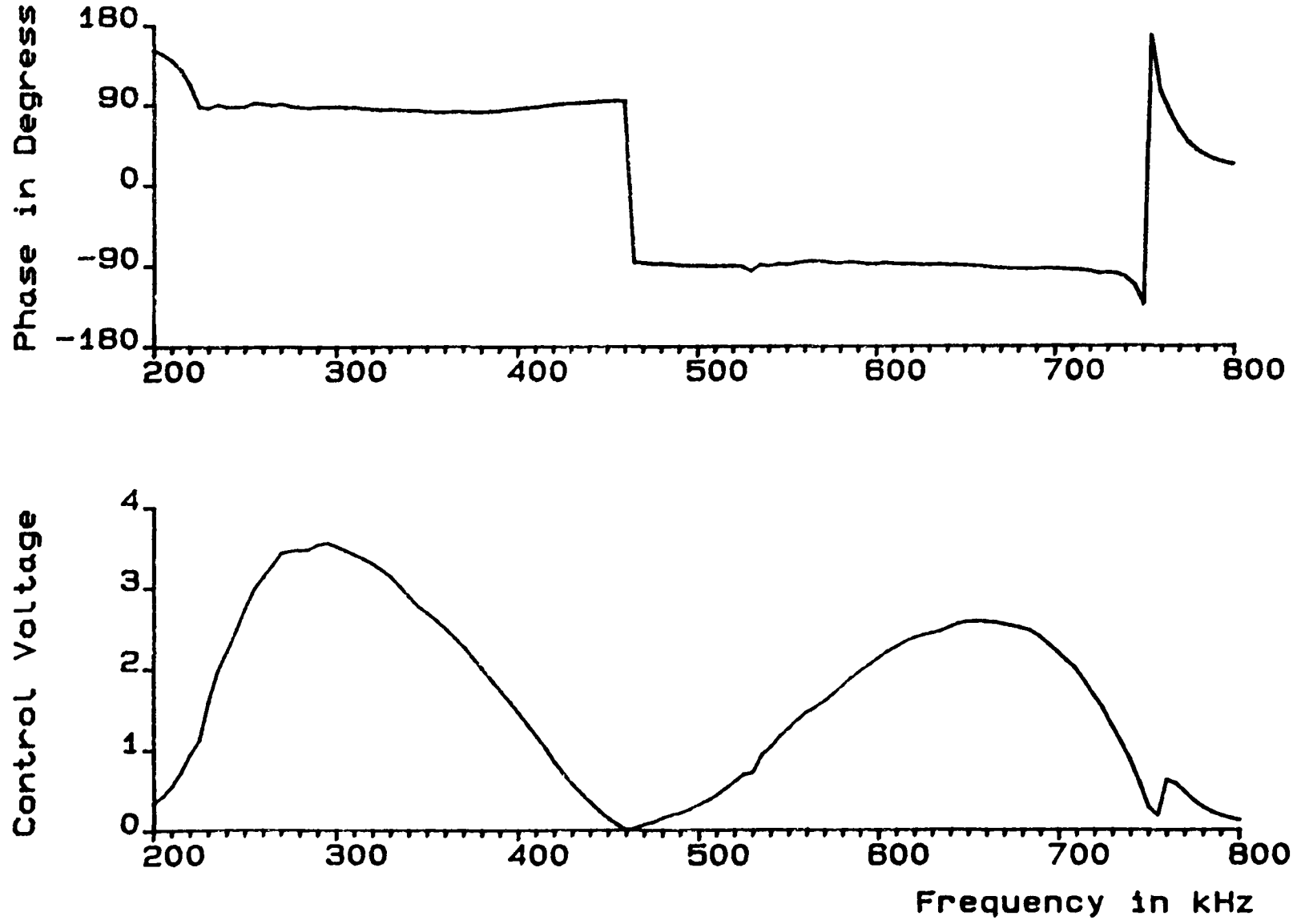

(ii) Voltage required to generate the above impedance by active control.

Figure 6g

values do not produce regularly spaced resonances so for convenience the first four programs contain break frequencies where the passive loads change. Resistance values, where quoted, have been added to give conductance maxima of around 7mS.

Program No. (binary)	Passive load simulation						
	L μH	R Ω	break kHz	L μH	R Ω	break kHz	
000	110	10	440	43	15	-	
001	68	6	485	27	6.5	-	
010	43	4.5	530	19.5	5.2	-	
011	o/c		320	10nF		650	o/c
100	Variable L and R for constant G					See table	
101	"	"	"	"	P	6.2	

TABLE 6.3 ROM Contents

6.9.1 Drive Ceramic Admittance

The passive electrical loads in table 6.3 give the predicted drive ceramic admittance in figure 6h. Simulation of these loads by active control is predicted to give identical performance. Therefore figure 6h applies equally to active or passive control.

Individual resonances are produced by fixed passive loads as shown in Chapter 5. These are simulated actively by programs 000 - 011. Discontinuities at around 500 kHz result from the sudden changes in passive loads introduced to give regularly spaced peaks. The front matching layer produces a low Q resonance at 500 kHz but Q increases above and below this frequency. It was shown in section 5.9.1 that the matching layer has an impedance slightly too

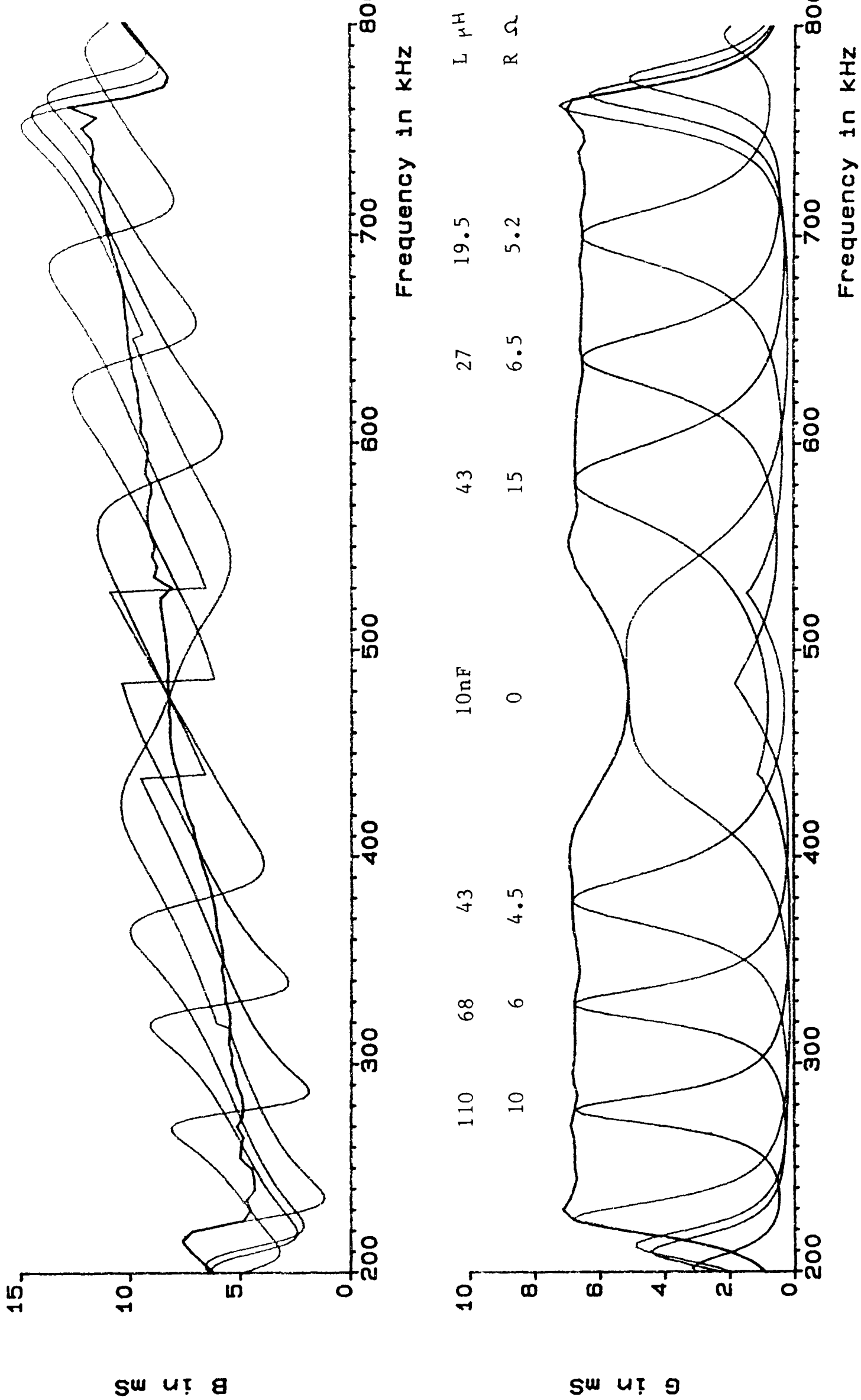

Figure 6h Predicted admittance of TC5 for the passive loads in table 6.3.

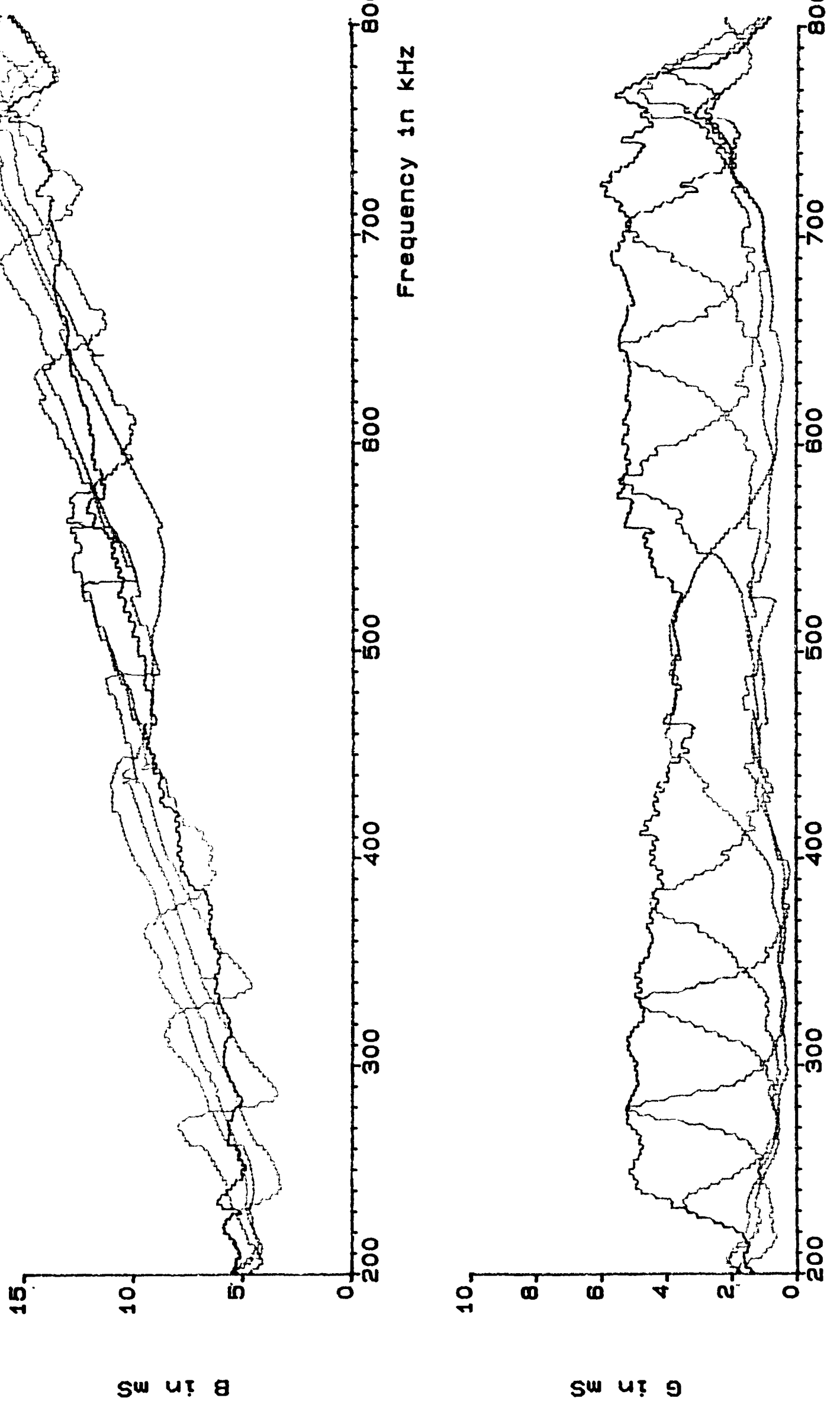

Figure 61 Measure admittance of TC5 for active simulation of the loads in table 6.3.

high for optimum performance and this explains why the central resonance (10nF) is predicted to have lower conductance than the others.

A variable passive load, simulated actively by program 100, produces a response which follows the locus of maximum conductance i.e. the envelope of the resonant peaks. The control voltage required to do this, and the synthesised acoustic backing impedance, were shown in figure 6g. Useful operation is predicted over the freqency range 230 - 760 kHz, more than 1.5 octaves.

Figure 6i shows the measured performance of TC5 with active control. The frequency range of interest was stored in 256 memory locations, hence the stepped appearance of the results.

Clearly defined resonant peaks are seen at the predicted frequencies, with conductance and susceptance close to the predicted values. Comparison of figures 5s and 6i shows that active control produces a drive ceramic conductance closer to the predicted value than was observed with passive control. This is to be expected since active control constrains both ceramics to vibrate according to the applied voltage, whereas passive loads leave the control ceramic unconstrained. For the same reason planar resonances are seen to have less effect with active control, and show up only as small ripples in conductance at around 300 kHz.

At several frequencies admittance measurements show discontinuities which are not predicted. These are caused by inaccuracies in the control electronics. As an example program 100 contains amplitude and phase data for constant drive ceramic conductance. This is plotted in figure 6j which is an enlarged version

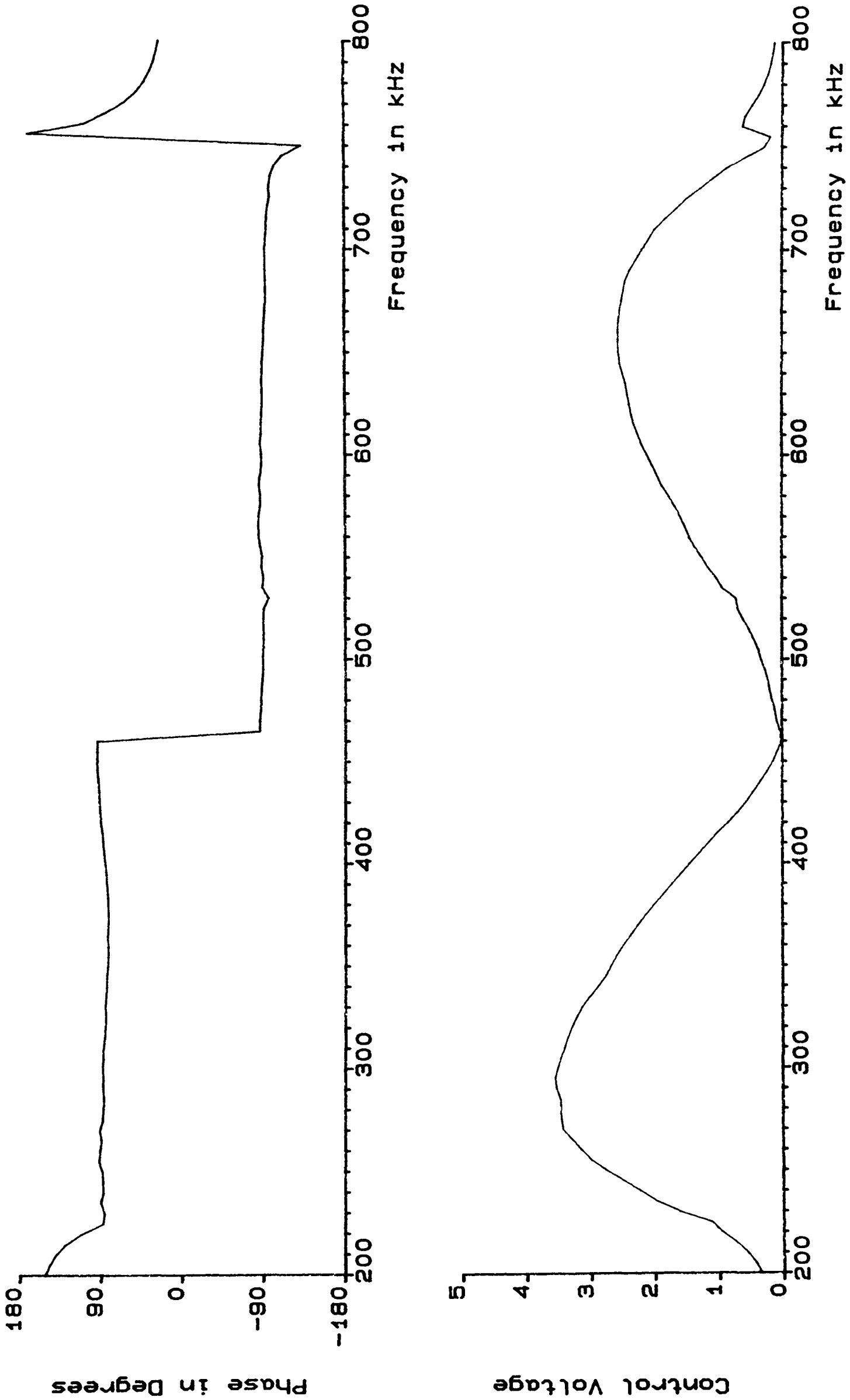

Figure 6j Control voltage required to produce constant drive ceramic conductance.

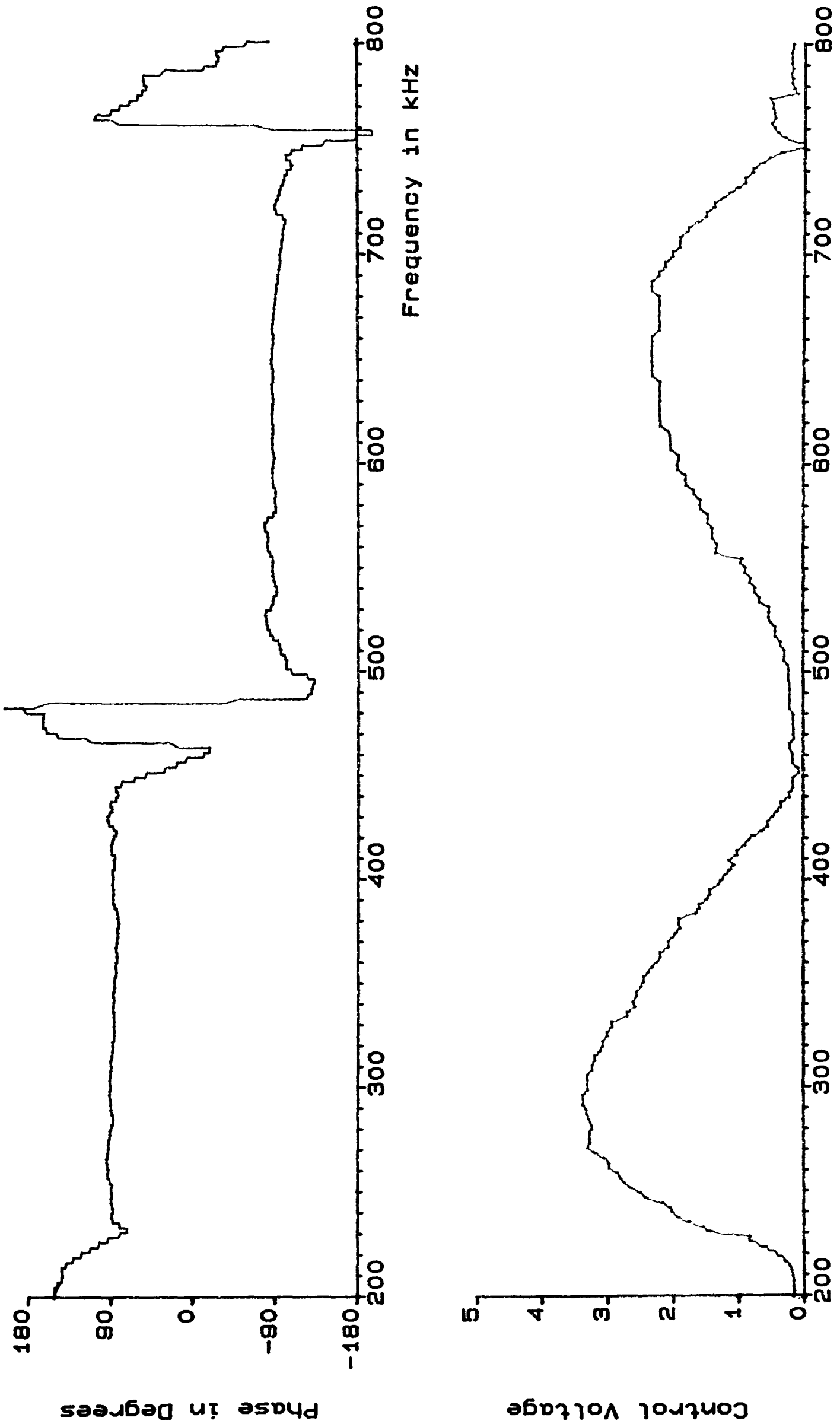

Figure 6k Actual control voltage generated by program 100.

of figure 6g(ii). On the same scale figure 6k shows the measured control voltage generated by the electronics. The amplitude curve shows large steps at 557 kHz, 640 kHz, 662 kHz and 681 kHz, all of which correspond to discontinuities in figure 6i. A large phase error is shown in the region 465 - 485 kHz but this is partly caused by inaccurate phase measurement, the phase meter being unable to operate with small amplitude signals. The step change in phase at 465 khz does however correspond to a discontinuity on figure 6i.

A similar active control test was carried out for TC4 (before it was damaged) and is reported in reference 38. Again results were found to be closer to predictions with active control than with passive control.

6.9.2 Control Ceramic Admittance

For efficiency calculations, and for control amplifier design, it is necessary to calculate the control ceramic admittance. In section 6.6 it was shown that this depends on the acoustic backing impedance being synthesised, hence it is a function of control voltage. In figure 6e the control voltage is shown for simulation of a $32\mu H + 4\Omega$ load by active control. The resulting control ceramic admittance is shown in figure 6l and graphs are also given for simulation of $32\mu H + 0\Omega$ and $32\mu H + 10\Omega$. Simulation of passive loads with a resistive component results in negative control conductance. Power is delivered from the transducer to the control amplifier and it follows from the substitution theorem that this power is the same as would be dissipated in the passive load being simulated. Power from

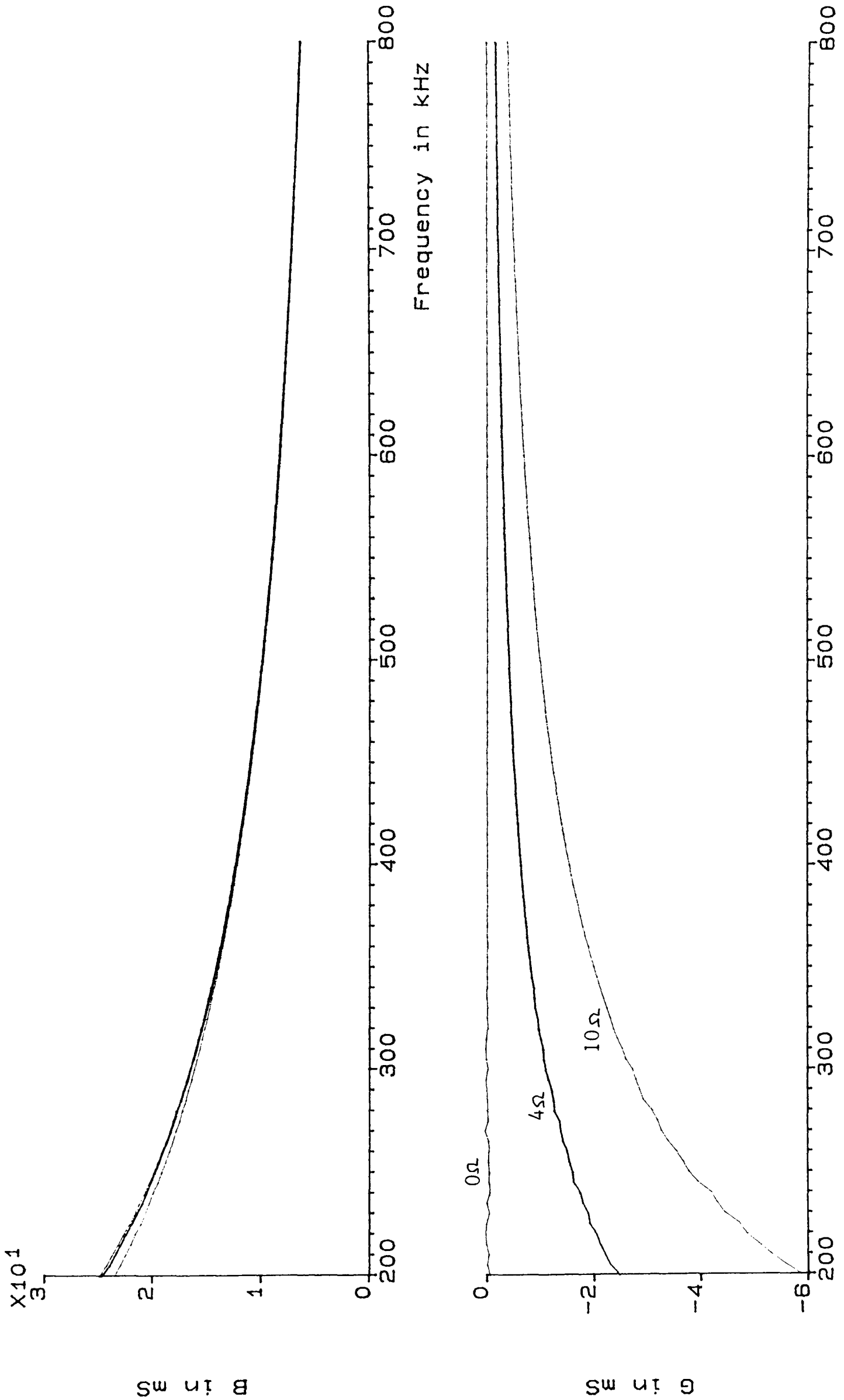

Figure 61 Predicted control admittance for active simulation of 32μH load with small series resistance.

the drive ceramic is divided between the load, the backing and the control ceramic in the same proportions for active control as for passive control, while for simulation of passive loads the control amplifier never delivers power to the system. Therefore the predicted efficiencies in figures 5p, 5q and 6f apply equally to active or passive control.

In figure 6f it was shown that constant drive ceramic conductance can be achieved by active simulation of a variable inductance in series with a frequency dependent resistance. The resulting control admittance is predicted in figure 6m. The series resistance required was given in table 6.2 and is always small, so control conductance is close to zero but slightly negative at most frequencies. At around 460 kHz and 750 kHz peaks in conductance are predicted. These are caused by rounding errors which occur near the short-circuit resonant frequencies. Figure 6n shows the corresponding measurement. Conductance remains close to zero at all frequencies showing that almost no power is delivered to the control ceramic. The effects of rounding errors can still be seen because the program ACTIVE_LOAD, which was used to predict figure 6m, was also used to calculate data for the Read Only Memory used to measure figure 6n.

6.9.3 Pressure and Efficiency Measurements

It was shown in figure 5w that passive control of TC5 produces front face pressure and efficiency values which are lower than predicted because of lateral displacement. Energy loss by this mechanism is less significant with active control so pressure and

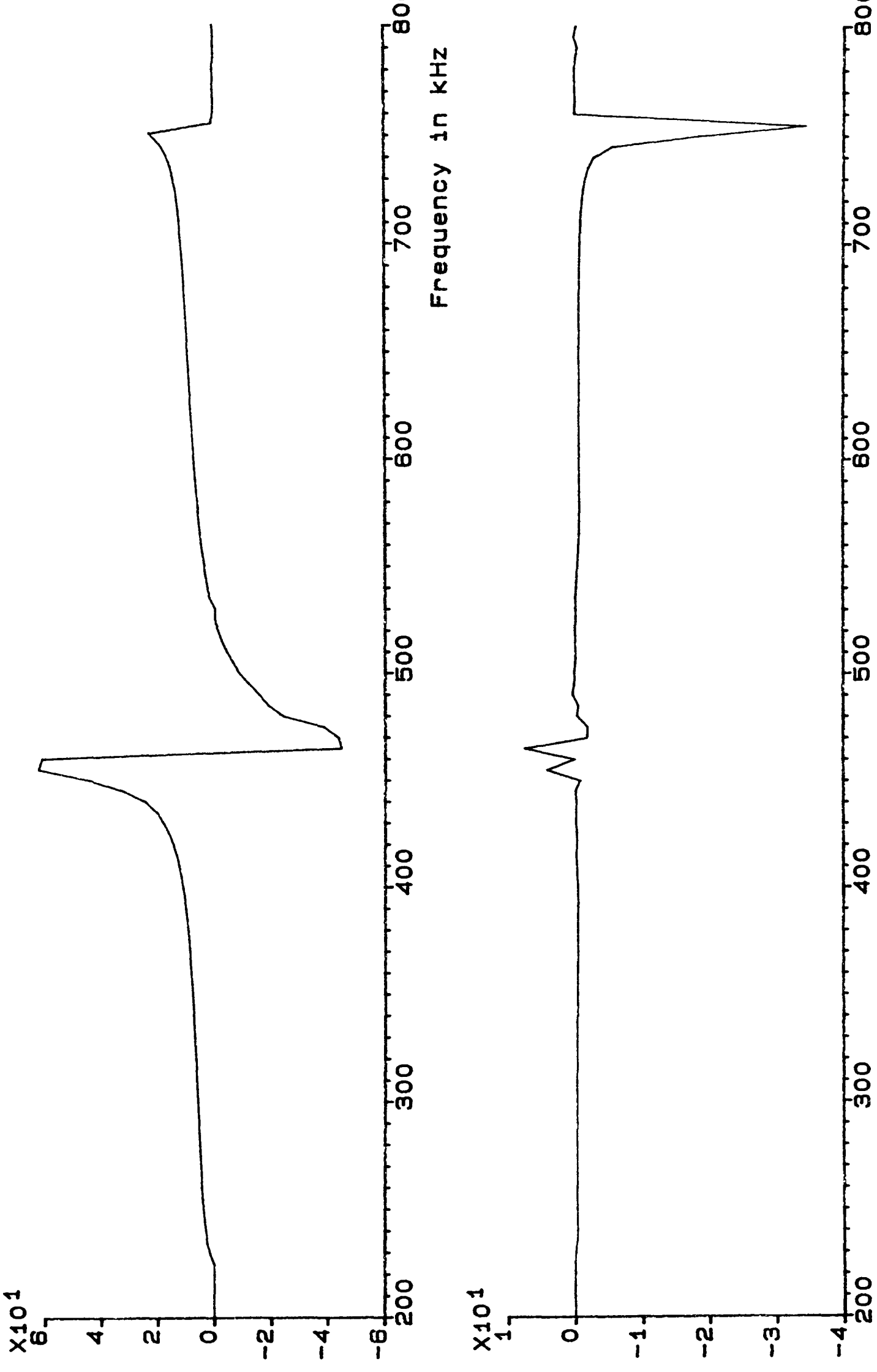

Figure 6m Predicted control admittance for program 100.

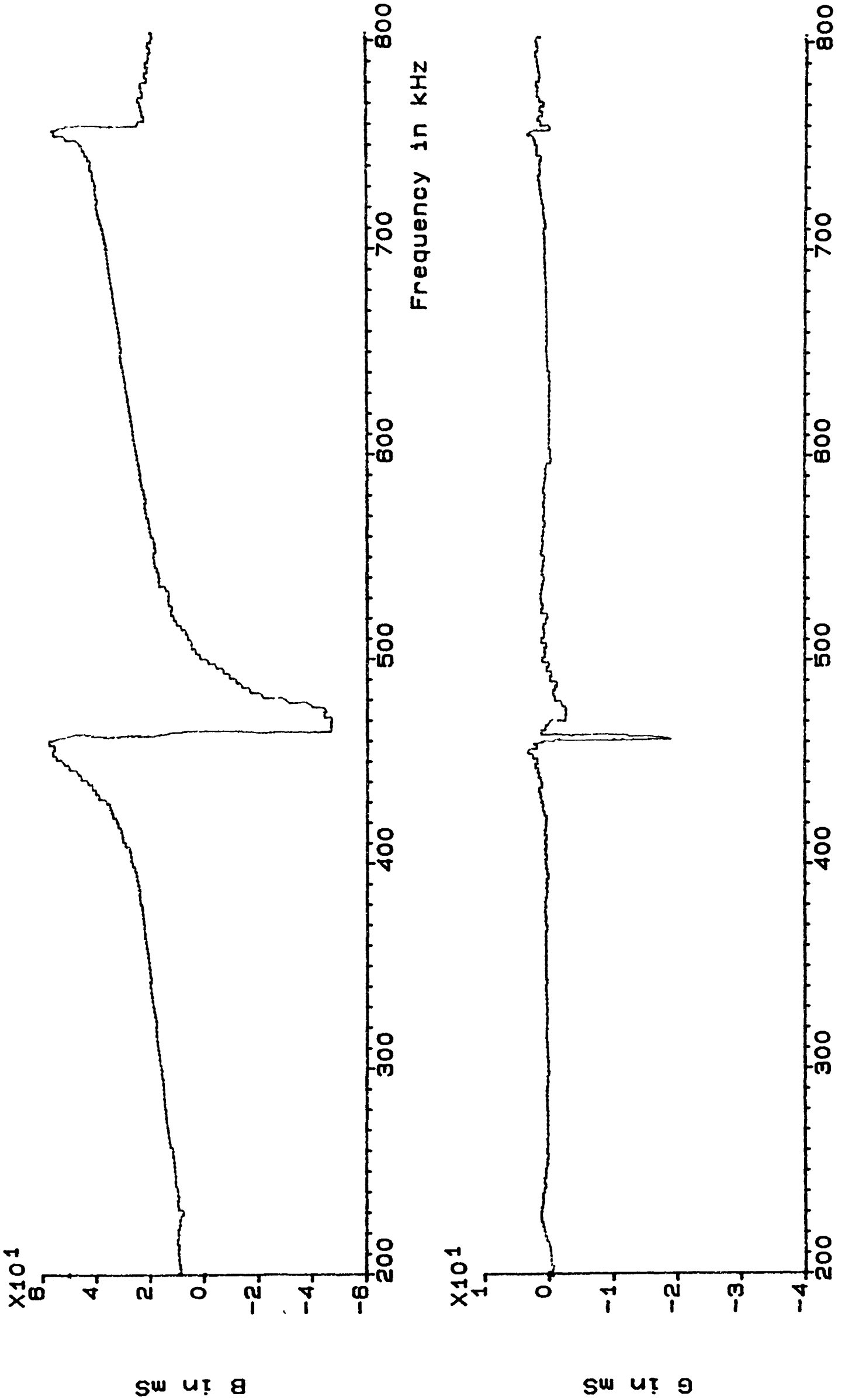

Figure 6n Measured control admittance for program 100.

efficiency measurements should be closer to predicted values. As a direct comparison with figure 5w the program ACTIVE_LOAD was used to calculate the control voltage for active simulation of passive loads with 4Ω series resistance. The required conditions are given in table 6.4.

Frequency	Applied Voltages (pk-pk)		Phase	Conductance	
kHz	Drive	Control	Degrees	Drive	Control
250	15	59	90	7.9	0.45
300	15	69	90	7.8	0.13
350	20	62	90	6.4	0.34
400	40	60	90	5.6	0.23
450	40	4	90	4.1	0.00
500	40	12	-90	3.7	-0.07
550	40	56	-90	6.3	0.82
600	20	56	-90	7.7	0.25
650	20	62	-90	7.6	0.18
700	25	62	-90	6.9	0.16

TABLE 6.4 Conditions used for radiation balance measurements.

These voltages were applied to TC5 using a pair of power amplifiers and the radiation balance was used to measure output pressure. Results are shown in figure 6o. To avoid damage to the transducer power levels were kept as low as possible, the maximum output power being 0.93 Watts at 550 kHz.

In the frequency range 462 - 524 kHz resonances are controlled by capacitance variations. Active simulation of capacitive loads requires only a small control voltage so the control ceramic remains free to vibrate in both thickness and planar modes. The resulting energy loss through the sides of the ceramic is similar for active and passive cases, causing front face pressure and efficiency measurements to be lower than predicted.

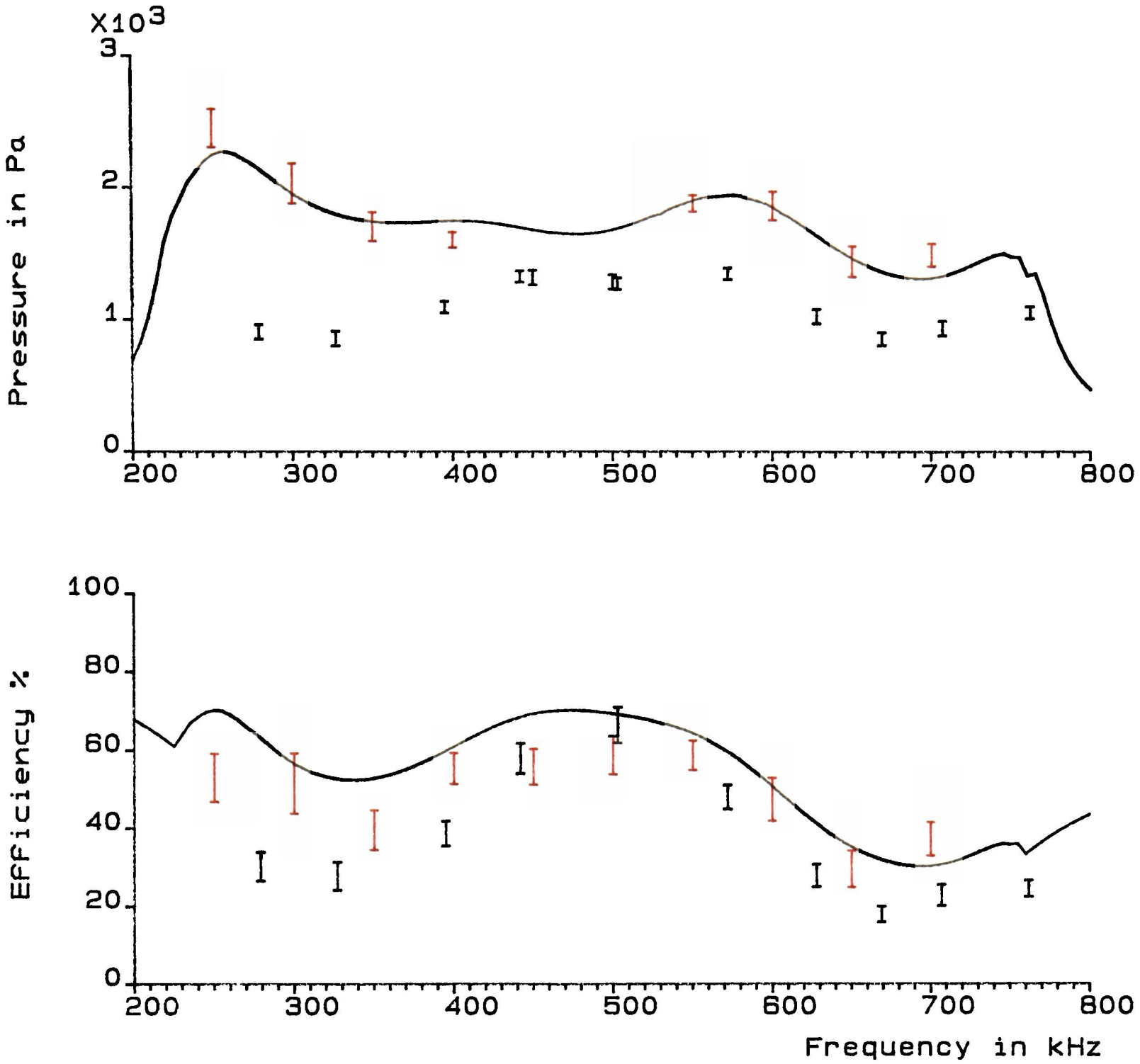

Figure 6o Pressure output and efficiency of TC5.

Active simulation of inductive loads constrains both ceramics to vibrate according to the applied voltage. Planar modes of vibration are suppressed and the structure behaves in a way which is accurately represented by the one-dimensional analysis.

Measurements of front face pressure show close agreement with predictions for both the second harmonic (250 - 400 kHz) and the third harmonic (550 - 700 kHz). Efficiency is closer to predicted values than with passive control but remains about 10% lower than predictions at most frequencies. Active simulation of loads with 4Ω series resistance is predicted to result in negative conductance for the control ceramic, hence taking no power from the control amplifier. However accurate conductance measurements, taken with an impedance analyser, showed the control conductance to be small but positive at most frequencies (see table 6.4). Therefore a small amount of power is delivered to TC5 by the control amplifier and this accounts for the reduced efficiency values. In practice this may be an advantage since the problems of negative conductance do not arise.

This test was intended as a comparison between active and passive control so a series resistance of 4Ω was included. The resulting efficiency falls to less than 40% at some frequencies. Figure 5q predicts that active simulation of loads with no series resistance gives an efficiency of around 70% at frequencies up to 700 kHz. This was not investigated in practice but figure 6o suggests that efficiencies of greater than 50% would be expected at all frequencies.

6.10 Stress Analysis with Active Control

The stress calculations in figures 5x and 5y apply equally to active or passive control and it has been shown that active control gives pressures which agree very closely with predictions. Combining the drive voltages in table 6.4 with the stress values in figure 5x shows that the maximum bond stress experienced by TC5 during active control was 253 kPa or 37 psi, which occurred at 700 kHz. This is less than the 437 kPa experienced during passive control (section 5.10) and a further set of conductance measurements again showed that there was no damage.

6.11 Discussion of Active Control

There are certain similarities between TC5 and the distributed transducer described by Greenspan and Wilmotte (45). The latter consists of a number of piezoelectric elements arranged in a stack and separated by inactive material. Each element is excited by the same electrical signal but with appropriate time delays added so that ultrasonic waves within the stack arrive at the load in phase. Trott (46) describes a development of this technique in which the transducer can be made to have low Q and high efficiency. The transducer is reversible hence suitable for transmission or reception.

The structure of TC5 resembles a distributed transducer containing two piezoelectric elements. However there are important differences in the way the electrical signals are applied. In a

distributed transducer the phase shift from one element to the next is proportional to frequency but for active control of TC5 the phase shift has more complicated frequency dependence and is chosen according to the required response. A further difference between the two designs is that all elements in a distributed transducer deliver power to the load but for TC5 output power originates only from the drive ceramic.

Conductance measurements for TC5 in figure 6i show a flat response from 240 kHz to 760 kHz. It is tempting to regard this as a wide band system with $Q \approx 1$, hence allowing operation with very short acoustic pulses. Unfortunately this is not the case. Active control adjusts the acoustic reactance of the backing so that the transducer is resonant at the particular frequency of operation. It was shown in chapter5 that some of these resonances have $Q>10$ which is too high for good transient response. Therefore active control, in the form described here, is only suitable for use with continuous-waves or long pulses. These limitations are the same as were observed for passive control.

CHAPTER 7

Conclusion

This investigation has shown that Mason's model of a piezoelectric ceramic can be used along with transmission line theory to give reliable predictions of transducer performance. The one-dimensional analysis can only represent thickness mode vibrations of the ceramic and longitudinal plane waves in the surrounding structure. Therefore ceramics of large width/thickness ratio give closest agreement between predicted and measured results. If ceramics of small area are used then there is significant lateral displacement. This gives the problem of intermodal coupling between planar and thickness modes of vibration, and there is increased acoustic loading due to energy loss through the sides of the ceramic.

At several stages during the work it has been important to have an accurate knowledge of the acoustic properties of materials being used. Many of these are composite materials for which data is not available. Therefore a measuring technique was required to determine velocity and absorption at frequencies between 100 kHz and 1 MHz. Several methods were investigated, all using a perspex buffer rod in place of the more common water tank measurements. A buffer rod has the advantage of accurate alignment and simple experimental set up. Results of sufficient accuracy for transducer design can often be obtained simply by measuring the reflection coefficient at the perspex-sample boundary. However more accurate results can be achieved by allowing pulses to reflect from air at the end of the sample. This

gives a linear relationship between phase shift and frequency. For samples with impedance close to that of perspex the measurement of $d\phi/df$ allows velocity to be calculated to an accuracy of better than 5%. For higher impedance samples a more convenient technique is to observe interference between reflections from the perspex-sample and sample-air boundaries. This is less accurate than $d\phi/df$ measurements but can be applied to a greater number of materials. Both techniques allow absorption to be calculated as sound travels twice through the sample.

Many sonar systems require information over a wide frequency range. Usually these systems include a transducer of fixed resonant frequency and very low Q. An alternative approach is to use a piezoelectric-tunable transducer, which has higher Q but variable resonant frequency. The transducer developed in this work consists of two ceramics, of equal thickness, which are bonded together and operated in their thickness mode. They are backed by a material with high absorption. The drive ceramic radiates power into the water through a protective layer and has its backing impedance determined by the control ceramic. Both active and passive control have been investigated.

Passive control uses inductive or capacitive loads on the control ceramic to vary the acoustic reactance on the back of the drive ceramic. By this method a resonance can be produced at any frequency. However in practice useful resonances occur only between the fundamental and third harmonic of the total ceramic thickness. Outside this range conductance becomes too low to be of practical significance, and for ceramics of reasonable thickness the lower limit

is about 200 kHz. The most important design aspect concerns the bond thickness between the ceramics. Computer simulation shows that this must be less than $\lambda/100$ for satisfactory performance. A total ceramic thickness of 8.5mm allows passive control from 240 kHz to 760 kHz, most of this range being covered by inductive loads. The inductance required at any frequency is approximately that which tunes out the clamped capacitance and it has been shown that the equivalent series resistance of the inductors must be less than 10Ω. Predicted efficiency is greater than 50% at most frequencies but depends on series resistance. Some of the measured values were found to be less than 30%, the difference resulting from significant lateral displacement especially at low frequencies. Most resonances produced by passive control have Q>10 which is too high for use with short acoustic pulses.

Any passive electrical load can be simulated actively by applying a voltage of the same amplitude and phase as would be measured across that load. Active control of this kind again allows resonance to be varied by adjusting the acoustic reactance on the back of the drive ceramic, the frequency range of useful operation being the same as for passive control. The neccessary amplitudes and phase shifts can be applied using a digital technique which allows programmable frequency response. Simulation of passive loads with a resistive component gives negative conductance seen looking into the control ceramic. In this case the power delivered from the transducer to the control amplifier is the same as the power which would be dissipated in the load being simulated. It was found that active simulation of loads with 4Ω series resistance gives more than 40% efficiency at most

frequencies compared with predicted values of around 50%. In practice the efficiency can be increased to over 50% by simulation of lossless passive loads.

It follows from the substitution theorem that all predicted forces and particle velocities in the transducer structure are identical for the active and passive cases. However in practice active control constrains both ceramics to vibrate according to the applied voltage but passive loads leave the control ceramic unconstrained. Thus in all measurements active control was found to give closer agreement with predictions than passive control. Most resonances produced by this method of active control have Q>10 so the transducer is only suitable for transmission of continuous-waves or long pulses where frequency sweeping is gradual but extends over a wide range. These are the same limitations which apply to passive control.

An alternative form of active control, for which the same transducer is suitable, is the synthesis of real (i.e. resistive) acoustic impedances on the back of the drive ceramic. This was investigated for a range of impedance values and found to give no advantage over existing transducer designs.

CHAPTER 8

Suggestions for Future Work

The use of active and passive control at low frequencies is an obvious extension of the present investigation. This was mentioned in section 6.1 with regard to dumiload testing facilities (32,37). Inclusion of extra ceramic layers in sandwich transducer designs may allow control of resonant frequency, bandwidth and impulse response, perhaps involving the use of feedback. It may also be possible to overcome the adverse effects of the reactive loads which are experienced during high power operation of large arrays.

The equations which were used in this work are only valid for continuous waves. Therefore the study of active control in situations involving transient response requires a different method of analysis. There are several possibilties. The computer model described by Low (20) predicts the behavior of multilayer structures driven by a transient waveform and has been shown to give close agreement with measured results (19). This technique could be extended to study the interaction between acoustic signals from more than one piezoelectric element. Alternatively the lattice model developed by Hayward and Jackson (40) could be employed. This allows transient responses to be calculated using z-transforms, and a further z-transform technique, based on Mason's equivalent circuit, is described by Challis and Harrison (47). By one of these methods it may be possible to design a transducer with programmable impulse response. This would be a significant improvement on the design of TC5, which has programmable

frequency response but can only be used with narrow band signals.

Finally the study of material properties is a large area in which further work would be useful. It is possible that the use of anisotropic materials may simplify the synthesis of acoustic impedances. For example an aluminium honeycomb is commercially available from Ciba-Geigy (41). This could be compressed to a required cell size then filled with epoxy resin. The resulting composite material may have well defined and easily predictable properties (dependent on cell size) which are different in orthogonal directions. It would be interesting to investigate the possibility of producing an anisotropic material with very high absorption in one direction but low absorption in the other. Such a material would be of particular interest in array design, where inter-element coupling is often a problem.

REFERENCES

1. Mason, W.P.

"Electromechanical Transducers and Wave Filters"

Van Nostrand, Princeton N.J., 1948.

2. Kossoff, G.

"The effects of backing and matching on the performance of piezoelectric ceramic transducers"

I.E.E.E. Transactions SU-13, pp 20-30, 1966.

3. Smith, B.V. and Gazey, B.K.

"High-frequency sonar transducers: a review of current practice"

I.E.E. Proceedings, Vol.131 Part F, pp 285-297, 1984.

4. Krimholtz, R., Leedom, D. and Matthaei, G.

"New equivalent circuits for elementary piezoelectric transducers"

Electronics Letters, Vol.6, pp 398-399, 1970.

5. Desilets, C.S., Fraser, J.D. and Kino, G.S.

"The design of efficient broad-band piezoelectric transducers"

I.E.E.E. Transactions SU-25, pp 115-125, 1978.

6. Silk, M.G.

"Predictions of the effect of some constructional variables on the performance of ultrasonic transducers"

Ultrasonics, Vol.21, pp 27-33, 1983.

7. Hayward, G., Macleod, C.J., and Durrani, T.S.
"A systems model of the thickness mode piezoelectric transducer"
J.A.S.A., Vol.76, pp 369-382, 1984.

8. Augustine, L.J. and Andersen, J.
"An algorithm for the design of transformerless broadband equalizers of acoustic transducers"
J.A.S.A., Vol.66, pp 629-635, 1979.

9. Mason, W.P. (Ed)
"Physical Acoustics"
Vol.1 Part A, Academic Press, 1964.

10. Koymen, H.
"Optimisation of the design of high frequency sonar transducers"
Ph.D. Thesis, University of Birmingham, 1979.

11. Tucker, D.G. and Gazey, B.K.
"Applied Underwater Acoustics"
Pergamon Press, London, 1966.

12. Vernitron Ltd.
"Five modern piezoelectric ceramics"
Data sheet, revised 1976.

13. Smith, B.V. and Gazey, B.K.
"Equivalent circuits of transducer structures embodying piezoelectric elements - a tutorial article"
Memorandum No. 426, Department of Electronic and Electrical Engineering, University of Birmingham, 1971.

14. Koymen, H., Smith, B.V. and Gazey, B.K.
"Equivalent circuits for high frequency sonar transducers"
Electronics Letters, Vol.15, pp 600-601, 1979.

15. Goll, J.H. and Auld, B.A.
"Multilayer impedance matching schemes for broadbanding of water loaded piezoelectric transducers and high Q electric resonators"
I.E.E.E. Transactions SU-22, pp 52-53, 1975.

16. Bainton, K.E. and Silk, M.G.
"Some factors which affect the preformance of ultrasonic transducers"
British Journal of NDT, Vol.22, pp 15-19, 1980.

17. Koymen, H., Gazey, B.K. and Smith, B.V.
"The use of matching layers in the design of broadband, high efficiency, high frequency transducers, capable of being operated at depth"
I.O.A. Proceedings, Transducers for Sonar Applications, 1980.

18. Sayers, C.M. and Tait, C.E.
"Ultrasonic properties of transducer backings"
Ultrasonics, Vol.22, pp 57-60, 1984.

19. Low, G.C. and Jones, R.V.
"Design and construction of short pulse ultrasonic probes for non-destructive testing"
Ultrasonics, Vol.22, pp 85-95, 1984.

20. Low, G.C.

"A simple computer method for predicting the transient response of ultrasonic NDT probes"

NDT International, Vol.13, pp 285-290, 1980.

21. Preston, R.C., Bacon, D.R., Livett, A.J. and Rajendran, K.

"PVDF membrane hydrophone performance properties and their relevance to the measurement of the acoustic output of medical ultrasonic equipment"

Journal of Physics E, Vol.16, pp 786-796, 1983.

22. Bainton, K.F., Hillier, M.J., and Silk, M.G.

"An easily constructed, broad bandwidth ultrasonic probe for research purposes"

Journal of Physics E, Vol.14, pp 1313-1319, 1981

23. Swartz, R.G. and Plummer, J.D.

"On the generation of high-frequency acoustic energy with polyvinylidene fluoride"

I.E.E.E. Transactions SU-27, pp 295-303, 1980.

24. Connor

"Wave Transmission"

Edward Arnold, London, 1972.

25. Bobber, R.J.

"Underwater Electroacoustic Measurements"

Naval Research Laboratory, Washington D.C.,1970.

26. Pelmore, J.M.

"The ultrasonic properties of some filled epoxy materials"

Proceedings, Ultrasonics International, 1977.

27. Kinsler, L. and Frey, A.

"Fundamentals of Acoustics"

John Wiley and Sons, 2nd Edition, 1962.

28. Felix, M.P.

"Attenuation and dispersion characteristics of various plastics in the frequency range 1-10 MHz"

Journal of Composite Materials, Vol.8, pp 275-287, 1974.

29. University of Birmingham Acoustics Group

"A study of optimised high frequency underwater acoustic transducer performance"

Final Report to S.R.C. on Contract B/RG/59553, GR/A 51402, 1978.

30. Steel, G.A., Gazey, B.K. and Smith, B.V.

"A technique for measuring the acoustic properties of materials using a buffer rod"

I.O.A. Proceedings, Underwater Acoustic Calibration and Measurement, 1984.

31. Chenghao, W. and Zheying, Z.

"Principle of piezoelectric-tunable transducer"

Chinese Journal of Acoustics, Vol.2, pp 16-24, 1983.

32. Bobber, R.J.

"Active load impedance"

J.A.S.A., Vol.34, pp 282-288, 1962.

33. Kervel, S.J.H. and Thijsson, J.M.

"A calculation scheme for the optimum design of ultrasonic transducers"

Ultrasonics, Vol.21, pp 134-140, 1983.

34. Vernitron Ltd

"Specific purpose transducers in PZT ceramics"

Information sheet No. 66047/A, 1975

35. Heuter, T.F. and Bolt, R.M.

"Sonics"

Wiley, New York, 1955.

36. Ciba-Geigy

"Araldite AV138M"

Instruction sheet No. A.63d, 1984.

37. Auyer, S.E. and Miller, W.A.

"Development of a high-power transducer dumiload"

J.A.S.A., Vol.34, pp 734-740, 1976.

38. Steel, G.A., Smith, B.V. and Gazey, B.K.

"Tunable sonar transducer"

Electronics letters, Vol.22, pp 758-759, 1986.

39. Thijsson, J.M., Verhof, W.A., and Cloostermans, M.J.
"Optimisation of ultrasonic transducers"
Ultrasonics, Vol.23, pp 41-46, 1985.

40. Hayward, G. and Jackson, M.N.
"A lattice model of the thickness mode piezoelectric transducer"
I.E.E.E. Transactions UFFC-33, pp 41-50, 1986.

41. Ciba-Geigy
Information Sheet No. ATA.20c, 1979.

42. Holly, A.C.
"A method for the generation of broadband acoustic transmissions"
J.A.S.A., Vol.75, pp 973-976, 1984.

43. Flowers, N.J.
Contract reference 2027/0162
Acoustics and Sonar Group, University of Birmingham, 1986.

44. Scott, R.E.
"Linear Circuits"
Addison-Wesley, U.S.A., 1960.

45. Greenspan, M. and Wilmotte, R.M.
"Distributed transducer"
J.A.S.A., Vol.30, pp 528-532, 1958.

46. Trott, W.J.
"Theory of a passive, reversible, distributed-coupling transducer"
J.A.S.A., Vol.34, pp 333-337, 1962.

47. Challis, R.E. and Harrison, J.A.

"Rapid solutions to the transient response of piezoelectric elements by z-transform techniques"

J.A.S.A., Vol.74, pp 1673-1680, 1983.

APPENDIX 1

Calculation of terminating impedance

If a perspex rod of impedance Z_ρ is terminated by an impedance Z_T then the reflection coefficient (27) at the boundary is:

$$R = \frac{Z_T - Z_\rho}{Z_T + Z_\rho}$$

In general this quantity is complex and can be split into a modulus and argument:

$$R = |R| e^{j\phi}$$

$$= |R| (\cos\phi + j\sin\phi)$$

$$\left.\begin{array}{l} \text{Let } |R|\cos\phi = U \\ \text{Let } |R|\sin\phi = V \end{array}\right\} \therefore R = U + jV$$

Rearranging the first equation gives Z_T in terms of R and Z_ρ:

$$Z_T = Z_\rho \left[\frac{1+R}{1-R}\right]$$

$$= Z_\rho \left[\frac{1+U+jV}{1-U-jV}\right]$$

$$= Z_\rho \left[\frac{1-(U^2+V^2)+j2V}{(1-U)^2+V^2}\right]$$

But $U^2+V^2 = |R|^2(\cos^2\phi + \sin^2\phi) = |R|^2$

$$(1-U)^2+V^2 = 1-2|R|\cos\phi + |R|^2\cos^2\phi + |R|^2\sin^2\phi$$

$$= 1+|R|^2-2|R|\cos\phi$$

$$\therefore\ Z_T = Z_\rho \left[\frac{1-|R|^2+2j|R|\sin\phi}{1+|R|^2-2|R|\cos\phi} \right]$$

In perspex the attenuation is 1dB/cm/MHz so Z_ρ is not purely real. When the absorption is small the complex impedance of a solid is given by:

$$Z \approx \rho c(1+ja/k)$$

The figure of 1dB/cm/MHz corresponds to a/k=0.0048 which is very small compared with 1. Therefore in all practical measurements the impedance of perspex was assumed to be real with a value of $Z_\rho = \rho c = 3.2$ MRayls.

APPENDIX 2

Calculation of bond thickness

If a terminating impedance Z_T is joined to a buffer rod by a bond of impedance Z_b then the input impedance of the combination can be found fron the transmission line equation:

$$Z_{in} = Z_b \left[\frac{Z_T + jZ_b \tan(k_b l_b)}{Z_b + jZ_T \tan(k_b l_b)} \right]$$

where

k_b = wavenumber in bond ($=\omega/c$)

l_b = thickness of bond

However the bond is always very thin in wavelengths at the frequency of interest so $\tan(k_b l_b) \approx k_b l_b$

$$\therefore \quad Z_{in} = Z_b \left[\frac{Z_T + jZ_b k_b l_b}{Z_b + jZ_T k_b l_b} \right]$$

Separating into real and imaginary parts:

$$Z_{in} = \frac{Z_b}{Z_b^2 + (Z_T k_b l_b)^2} \cdot (Z_T + jZ_b k_b l_b)(Z_b - jZ_T k_b l_b)$$

$$\approx \frac{Z_b}{Z_b^2 + (Z_T k_b l_b)^2} \cdot \left[Z_b Z_T + jk_b l_b (Z_b^2 - Z_T^2) \right]$$

Therefore the ratio of imaginary to real parts is approximately given

by:

$$\text{Ratio} = \frac{\text{Im}}{\text{Real}} = \frac{k_b l_b (Z_b^2 - Z_T^2)}{Z_b Z_T}$$

But the ratio of imaginary to real parts can be found from measurements of $|R|$ and ϕ, from appendix 1:

$$Z_{in} = Z_p \left[\frac{1 - |R|^2 + 2j|R|\sin\phi}{1 + |R|^2 - 2|R|\cos\phi} \right]$$

The ratio is given by

$$\text{Ratio} = \frac{\text{Im}}{\text{Real}} = \frac{2|R|\sin\phi}{1 - |R|^2} = \frac{k_b l_b (Z_b^2 - Z_T^2)}{Z_b Z_T}$$

Therefore if ρ and c are known for both the bond and the terminating impedance then the above equation can be rearranged to give the bond thickness:

$$l_b = \frac{Z_b Z_T}{k_b (Z_b^2 - Z_T^2)} \cdot \frac{2|R|\sin\phi}{1 - |R|^2}$$

APPENDIX 3

Effect of grease bond on reflected signals

Consider a sample of impedance Z_2 bounded on one side by the perspex rod (Z_1) and on the other side by air (Z_3).

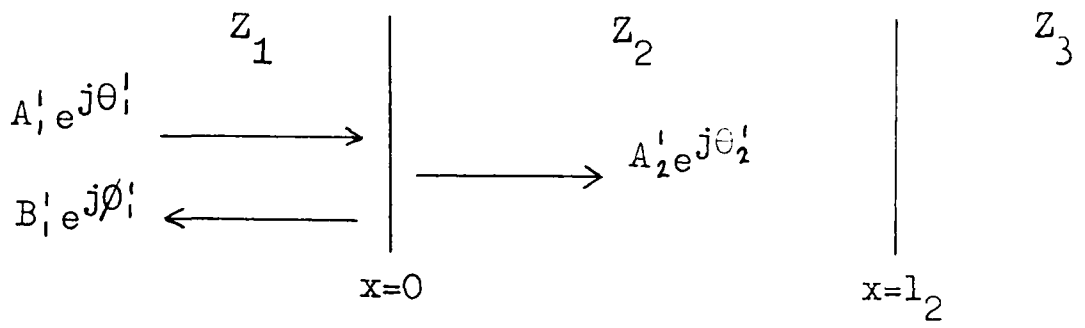

For each variable the subscript is the number of the medium and the superscript shows the order of events, e.g. B_1' is the amplitude of the first pulse to travel from right to left in medium 1. Define transmission and reflection coefficients at the boundaries as follows, for the moment ignoring the grease bond at x=0.

$$T_{12} = |T_{12}|e^{j\angle T_{12}} = 2Z_2/(Z_1+Z_2)$$

$$T_{23} = |T_{23}|e^{j\angle T_{23}} = 2Z_3/(Z_2+Z_3)$$

$$T_{21} = |T_{21}|e^{j\angle T_{21}} = 2Z_1/(Z_1+Z_2)$$

$$R_{12} = |R_{12}|e^{j\angle R_{12}} = (Z_2-Z_1)/(Z_2+Z_1)$$

$$R_{23} = |R_{23}|e^{j\angle R_{23}} = (Z_3-Z_2)/(Z_2+Z_3)$$

$$R_{21} = |R_{21}|e^{j\angle R_{21}} = (Z_1-Z_2)/(Z_1+Z_2)$$

The first signal crosses the boundary at x=0 and has its amplitude and phase affected as follows:

$$A_2^1 e^{j\theta_2^1} = A_1^1 |T_{12}| e^{j(\theta_1^1 + \angle T_{12})}$$

At some time later this signal reflects from the boundary at $x=l_2$ and returns to $x=0$.

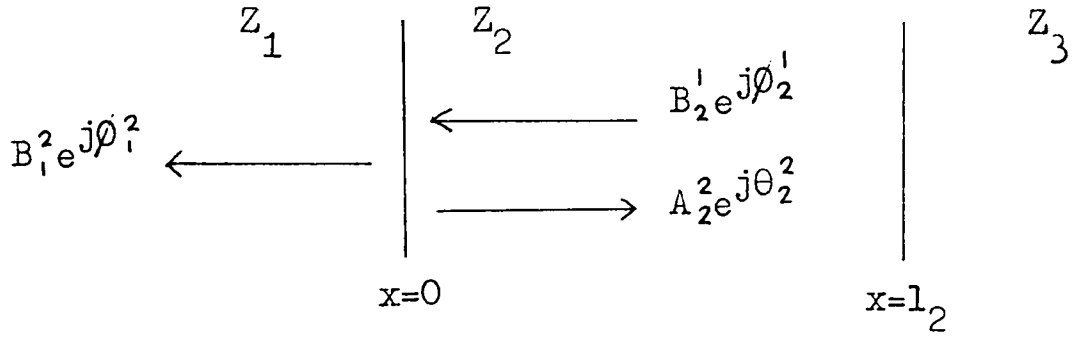

$$B_2^1 e^{j\phi_2^1} = A_2^1 e^{j\theta_2^1} e^{-2a_2 l_2} e^{-j2k_2 l_2} |R_{23}| e^{j\angle R_{23}}$$

$$= A_1^1 |T_{12}| e^{-2a_2 l_2} |R_{23}| e^{j(\theta_1^1 + \angle T_{12} - 2k_2 l_2 + \angle R_{23})}$$

This signal then crosses the boundary at $x=0$ and has a further change of amplitude and phase:

$$B_1^2 e^{j\phi_1^2} = B_2^1 e^{j\phi_2^1} |T_{21}| e^{j\angle T_{21}}$$

So the general results with no grease bond are:

$$B_1^2 = A_1^1 |T_{12}| e^{-2a_2 l_2} |R_{23}| |T_{21}|$$

$$\phi_1^2 = \theta_1^1 + \angle T_{12} - 2k_2 l_2 + \angle R_{23} + \angle T_{21}$$

It is now necessary to examine the effect of the grease bond on T_{12}, T_{21} and R_{12}. Let the grease bond have impedance Z_b, thickness l_b and wavenumber k_b. From Kinsler and Frey (27):

$$\frac{A_1^1}{A_2^1} = \frac{Z_2 + Z_1}{2Z_2} \cos(k_b l_b) + j \frac{Z_b^2 + Z_1 Z_2}{2Z_b Z_2} \sin(k_b l_b)$$

If $k_b l_b$ is small then $\cos(k_b l_b) \approx 1$ and $\sin(k_b l_b) \approx 0$

$$\therefore A_2' = A_1' \frac{2Z_2}{Z_2 + Z_1}$$

$$\theta_2' = \theta_1' - \tan^{-1}\left[\frac{Z_b^2 + Z_1 Z_2}{Z_b(Z_1 + Z_2)}\, k_b l_b\right]$$

This shows that the grease bond makes no difference to the amplitude of the signals but does have an effect on phase.

Let $$F = \frac{Z_b^2 + Z_1 Z_2}{Z_b(Z_1 + Z_2)}$$

In general F is close to 1 and $k_b l_b$ is small so:

$$\tan^{-1}(F k_b l_b) \approx F k_b l_b$$

The change in $\angle T_{12}$ is the same as $\angle T_{21}$ because F is symmetrical in Z_1 and Z_2. Therefore with the grease bond included the amplitude and phase of the reflected signals are:

$$B_1^2 = A_1' |T_{12}| e^{-2a_2 l_2} |R_{23}| |T_{21}|$$

$$\phi_1^2 = \theta_1^2 + \angle T_{12} - 2k_2 l_2 - 2F k_b l_b + \angle R_{23} + \angle T_{21}$$

The rate of change of phase with frequency is:

$$d\phi_1^2/df = -4\pi(l_2/c_2 + F l_b/c_b)$$

Solving this for c_2, the velocity in medium 2, gives:

$$c_2 = \frac{-4\pi l_2}{d\phi/df + 4\pi F l_b/c_b}$$

APPENDIX 4

Calculation of absorption without interference

Consider a buffer rod with sample and air termination. It was shown in appendix 3 that the returned signal amplitude, after passing both ways through the sample, is given by:

$$B_1^2 = A_1^1 \, |T_{12}| \, e^{-2a_2 l_2} \, |R_{23}| \, |T_{21}|$$

The amplitude ratio of signals returned with and without the sample is:

$$|A| = B_1^2 / A_1^1 = |T_{12}| \, e^{-2a_2 l_2} \, |R_{23}| \, |T_{21}|$$

where

$$|T_{12}| = 2Z_2/(Z_1+Z_2)$$

$$|T_{21}| = 2Z_1/(Z_1+Z_2)$$

For an air termination $|R_{23}|=1$ so the amplitude ratio is:

$$|A| = \frac{4Z_1 Z_2}{(Z_1+Z_2)^2} \, e^{-2a_2 l_2}$$

$$\therefore \; a_2 = \frac{-1}{2l_2} \ln \left[\frac{(Z_1+Z_2)^2}{4Z_1 Z_2} \, |A| \right]$$

The units of a_2 are Nepers/meter. To convert to dB/cm multiply by $0.02/\ln 10 = 0.08686$.

APPENDIX 5

Calculation of absorption with interference

In appendix 3 it was shown that after traversing the sample twice the returned signal is given by:

$$B_2^1 e^{j\phi_2^1} = A_1^1 |T_{12}||T_{21}| e^{-2a_2 l_2} |R_{23}| e^{j(\Theta_1^1 + \angle T_{12} + \angle T_{21} - 2k_2 l_2 + \angle R_{23})}$$

When interference occurs this adds to the reflected signal from the perspex-sample boundary giving a total of:

$$B_1^T e^{j\phi_1^T} = B_1^1 e^{j\phi_1^1} + B_1^2 e^{j\phi_1^2}$$

$$= A_1^1 |R_{12}| e^{j(\Theta_1^1 + \angle R_{12})} + B_1^2 e^{j\phi_1^2}$$

For the perspex-sample-air combination the following parameters are constant:

$$\angle T_{12} = \angle T_{21} = 0$$

$$|R_{23}| = 1, \quad \angle R_{23} = \pi$$

Also interference measurements are most suitable for the case when $Z_2 > Z_1$, so that $\angle R_{12} = 0$. Substitution of all these terms gives:

$$B_1^T e^{j\phi_1^T} = A_1^1 e^{j\Theta_1^1} \left[|R_{12}| + |T_{12}||T_{21}| e^{-2a_2 l_2} e^{j(\pi - 2k_2 l_2)} \right]$$

This can be recognised as the equation for an interference pattern. There is a maximum when $\cos(\pi - 2k_2 l_2) = 1$ and a minimum when $\cos(\pi - 2k_2 l_2) = -1$. The ratio between them is:

$$\Lambda = \frac{\text{Max. value of } B_1^T}{\text{Min. value of } B_1^T} = \frac{|R_{12}| + |T_{12}||T_{21}|e^{-2a_2 l_2}}{|R_{12}| - |T_{12}||T_{21}|e^{-2a_2 l_2}}$$

Notice that Λ can be either positive or negative depending on the relative size of the transmission and reflection coefficients. Rearranging this formula gives:

$$e^{-2a_2 l_2} = \frac{|R_{12}|}{|T_{12}||T_{21}|} \cdot \frac{\Lambda - 1}{\Lambda + 1}$$

It is convenient to substitute impedance values as follows:

$$|R_{12}| = (Z_2 - Z_1)/(Z_1 + Z_2)$$

$$|T_{12}| = 2Z_2/(Z_1 + Z_2)$$

$$|T_{21}| = 2Z_1/(Z_1 + Z_2)$$

So for $Z_2 > Z_1$ the absorption of medium 2 is:

$$a_2 = \frac{-1}{2l_2} \ln\left[\frac{Z_2^2 - Z_1^2}{4Z_1 Z_2} \cdot \frac{\Lambda - 1}{\Lambda + 1}\right]$$

The units of a_2 are Nepers/meter.

APPENDIX 6

The radiation balance

A radiation balance allows direct measurement of acoustic power output from a transducer (25,35). Figure A6.1 shows a simplified diagram of its construction. The transducer is driven by a continuous wave signal and placed so that all radiated power is collimated on the reflector. The resulting radiation pressure causes deflection of the pointer. It is important to eliminate standing waves and for this purpose the sides of the tank are lined with absorbing material. Weights placed on the reflector provide a means of calibration as follows:

Let a mass M produce a deflection D_M. The force on the reflector is Mg where $g = 9.8ms^{-2}$. If the radiation from a transducer produces a deflection D_S then the force on the reflector is:

$$F = \frac{D_S}{D_m} . Mg$$

This force is equal to radiation pressure * area:

$$F = Pr.A = \frac{D_S}{D_m} . Mg$$

From Bobber (25) the radiation pressure (Pr) is related to r.m.s. sound pressure (Ps) by:

$$Pr = \frac{Ps^2}{\rho c^2}$$

Where ρ = density of water
c = sound velocity in water

$$\therefore \quad Ps^2 = \rho c^2 . Pr = \rho c^2 \cdot \frac{D_S}{D_m} \cdot \frac{Mg}{A}$$

The acoustic power output of the transducer is given by:

$$W = \text{Intensity} * \text{Area}$$

$$= \frac{ps^2}{\rho c} \cdot A$$

Substituting for Ps^2 gives:

$$W = cg \frac{M}{D_m} D_S$$

This shows that deflection of the pointer is proportional to output power from the transducer.

Small aluminium weights were placed on the reflector and produced deflections shown in figure A6.2. All points lie on a straight line confirming linear response over the range of interest. In the above equations buoyancy must be taken into account. For aluminium a 50mg weight corresponds to M = 31.5mg in water and produces a deflection of D_m = 5.1mm.

$$\therefore \quad W = cg * \frac{31.5*10^{-6}}{5.1} D_S$$

$$= 91*10^{-3} \; D_S$$

where D_S is in mm. This provides the required calibration of 91 mW/mm. In practice deflection could be read to an accuracy of ±0.2mm which gives a calibration of 91±4 mW/mm.

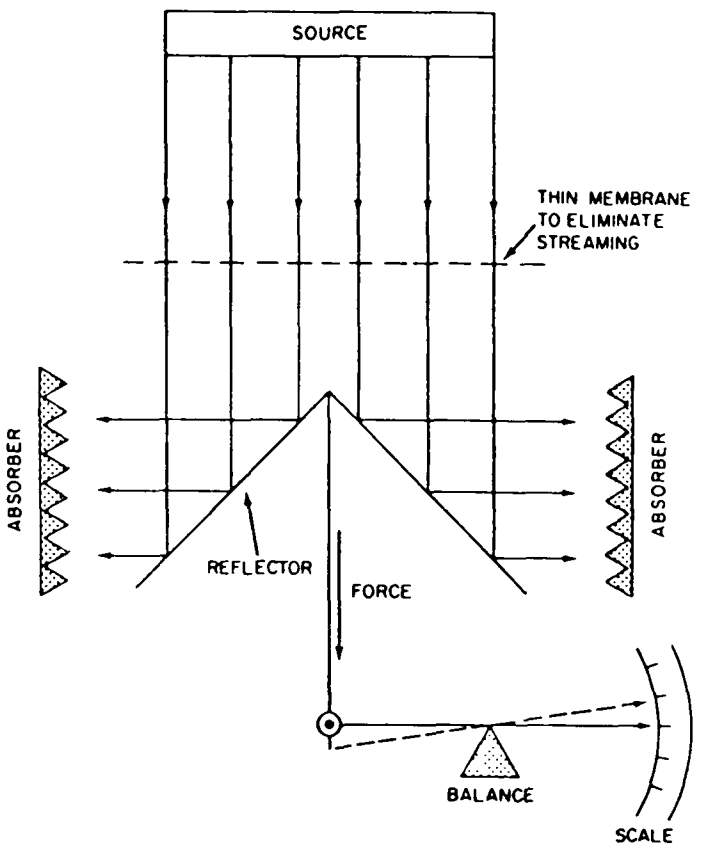

Figure A6.1 Simplified diagram of radiation balance. From Bobber (25).

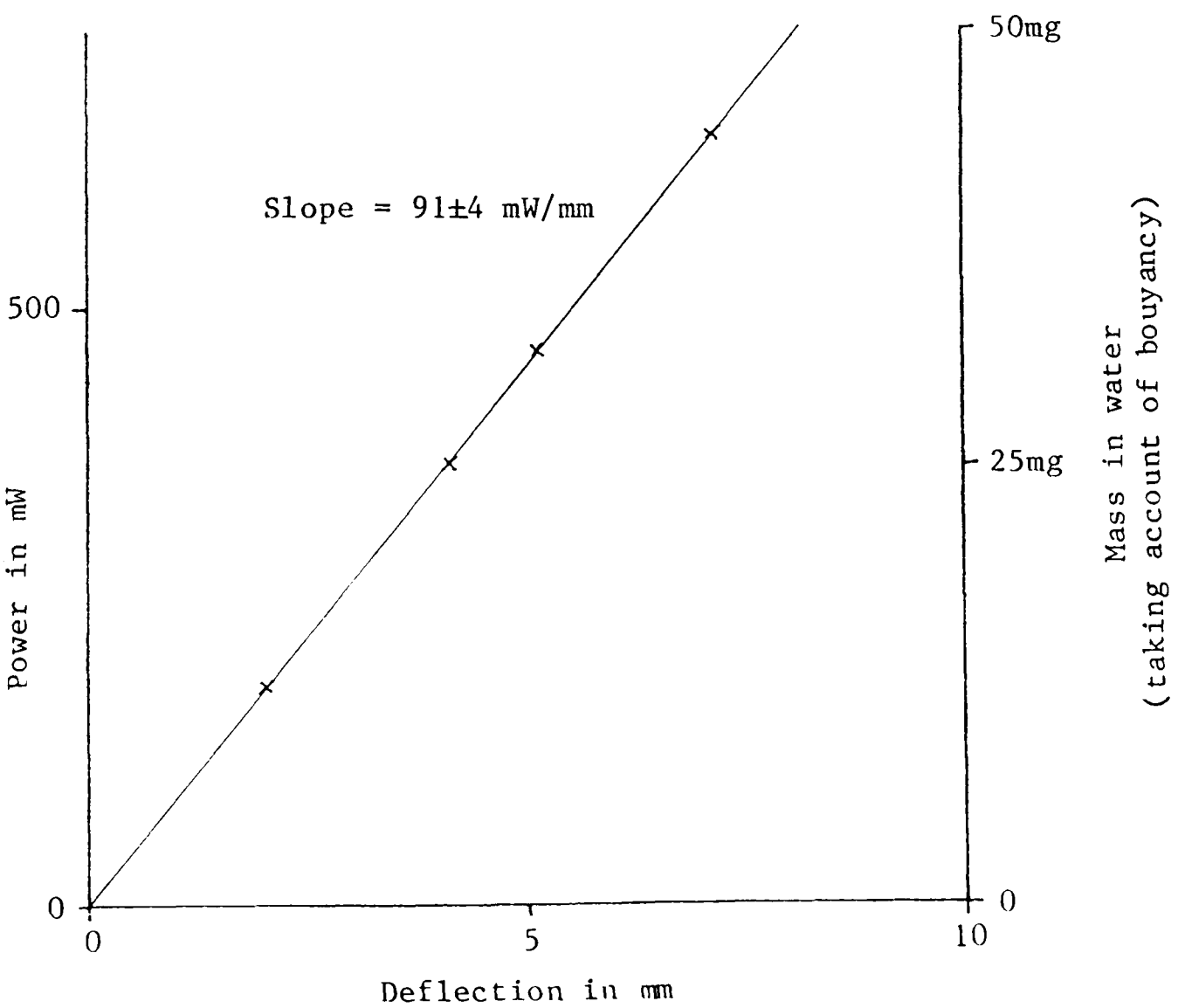

Figure A6.2 Calibration of radiation balance.

APPENDIX 7

Detailed conductance measurements for TC5

Conductance measurements were taken for TC5 at each stage of construction to monitor the loading effects of succesive layers.

The first stage involves bonding of the two ceramics to produce a simple piezoelectric-tunable transducer operating in air. The structure is symmetrical so either element can be used as the drive ceramic. Figure A7.1 shows the performance of this structure for a number of passive electrical loads. An open-circuit produces a fundamental thickness resonance at approximately 250 kHz and a second harmonic at 500 kHz. Between these frequencies planar resonances occur at regular intervals of 30 kHz. Inductive loads cause a rapid reduction in conductance as the second harmonic reduces in frequency. When the thickness mode is moved close to a planar resonant frequency intermodal coupling produces distortions in the resonant peaks. This is seen most clearly at 380 kHz where two separate peaks occur for a 47 μH load. The third harmonic is less influenced by intermodal coupling because at high frequencies the ceramics have large diameter in wavelengths. For an open-circuit load the third harmonic occurs at 755 kHz indicating a bond thickness of 26 μm.

The ceramics were then bonded to the stycast/fillite backing and the result is shown in figure A7.2. The increased acoustic loading causes all resonant peaks to have lower Q and lower conductance than in air. At around 500 kHz thickness mode vibrations are damped more strongly than planar modes because a large amount of power is delivered to the backing. At other frequencies both modes show roughly equal

damping.

An epoxy/iron composite was then added at the sides of the ceramic to reduce the amplitude of planar vibrations. The result is shown in figure A7.3. Most resonant peaks have smooth outlines showing that intermodal coupling has been largely eliminated. However there remains a problem at 380 kHz where the double resonance can still be seen.

The final stage of construction is the addition of the front matching layer. Figure A7.4 shows the result, with the transducer operating into a water load. Significant power is delivered to the water at all frequencies so all resonances have lower conductance than in figure A7.3. As predicted the matching layer produces very wide bandwidth resonances (Q=3.5) at around 500 kHz but has less effect above and below this frequency. The matching layer constrains lateral displacement sufficiently to produce a single resonance at 380 kHz, but planar resonances still occur at around 300 kHz where they show up as ripples in the conductance curves.

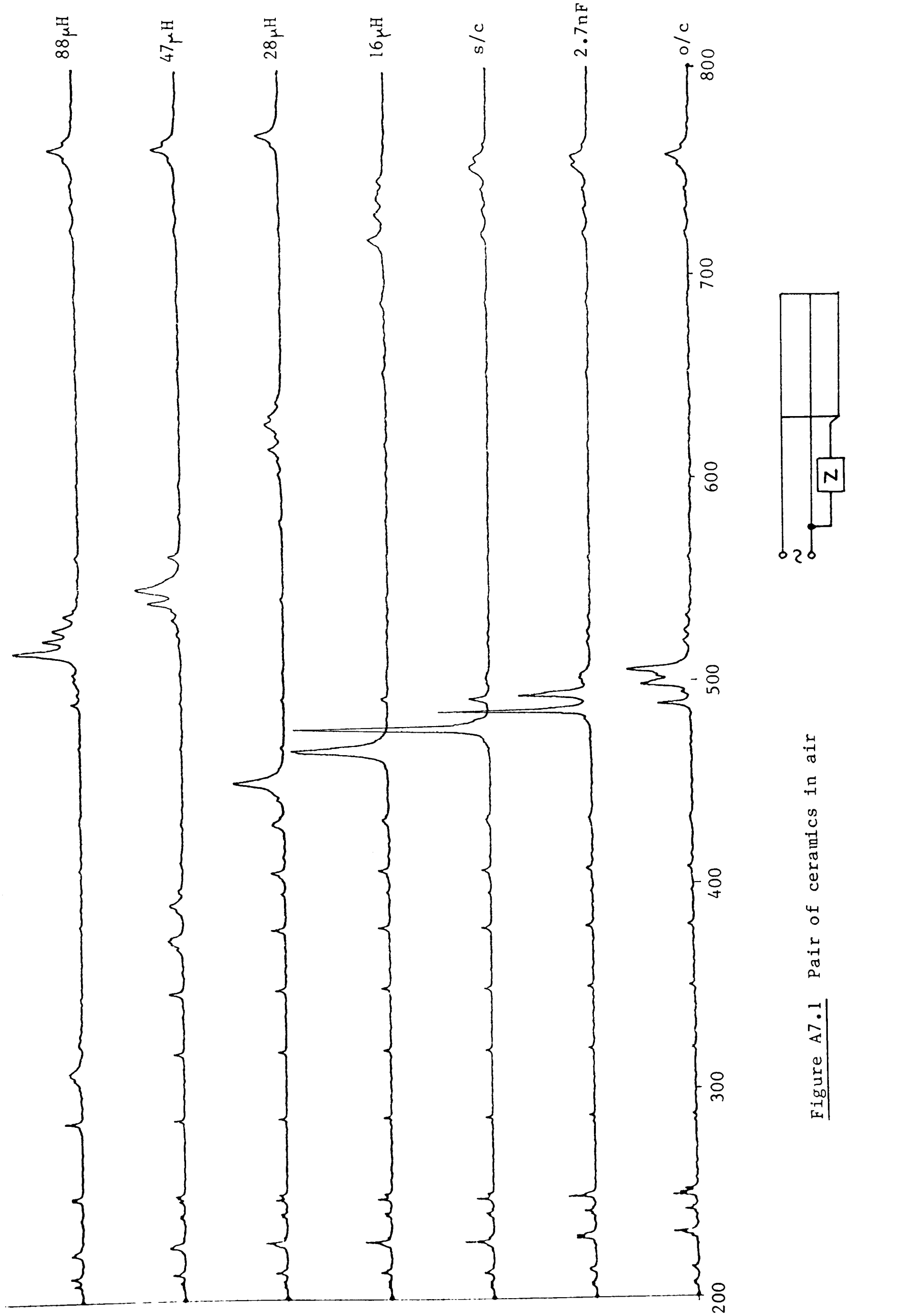

Figure A7.1 Pair of ceramics in air

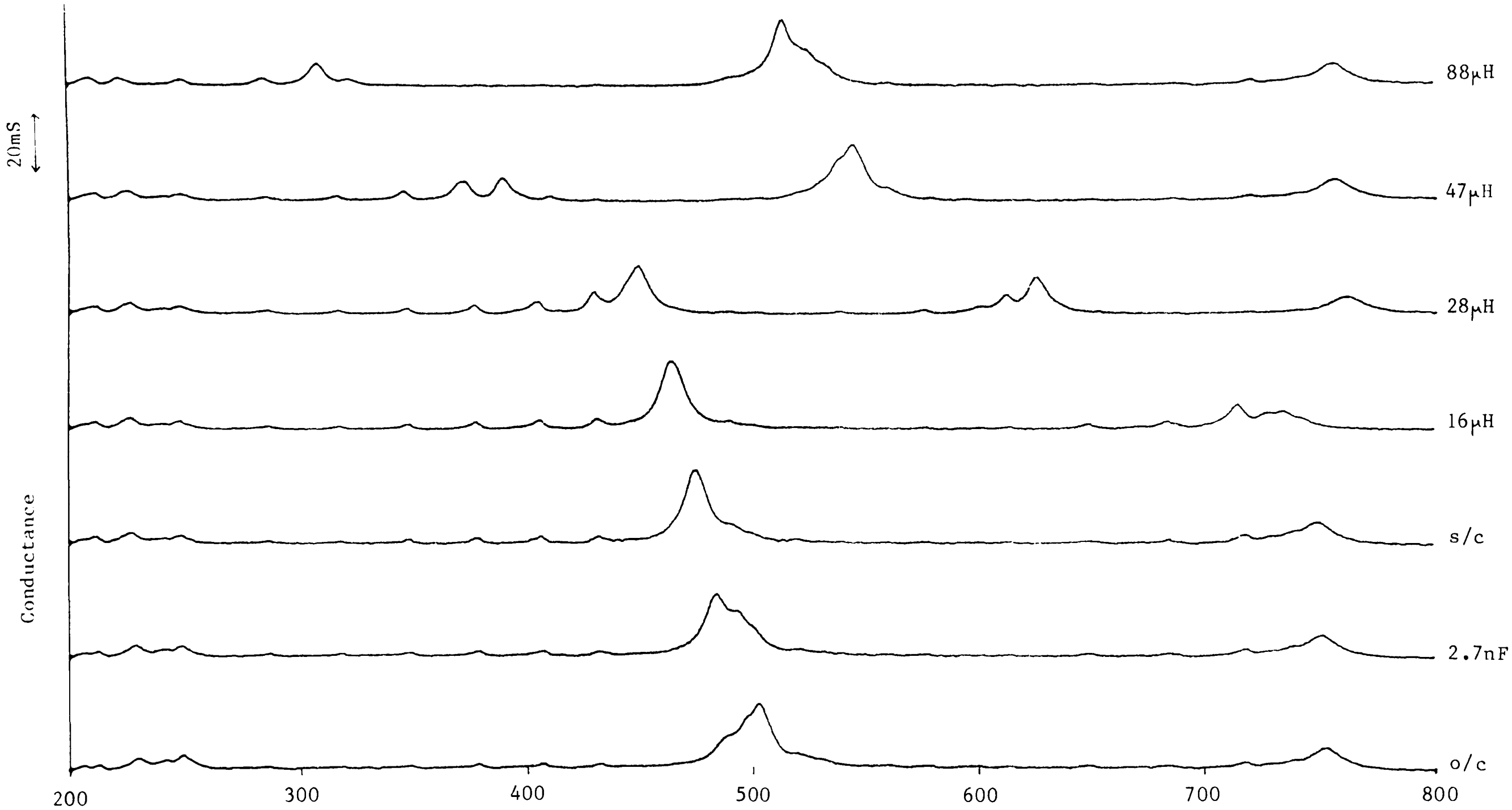

Figure A7.2 Pair of ceramics in air on stycast/fillite backing

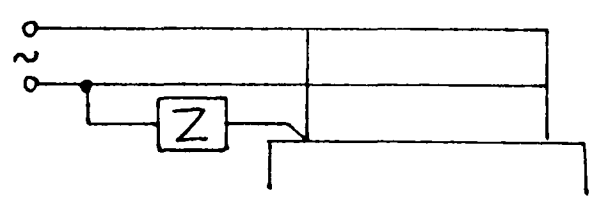

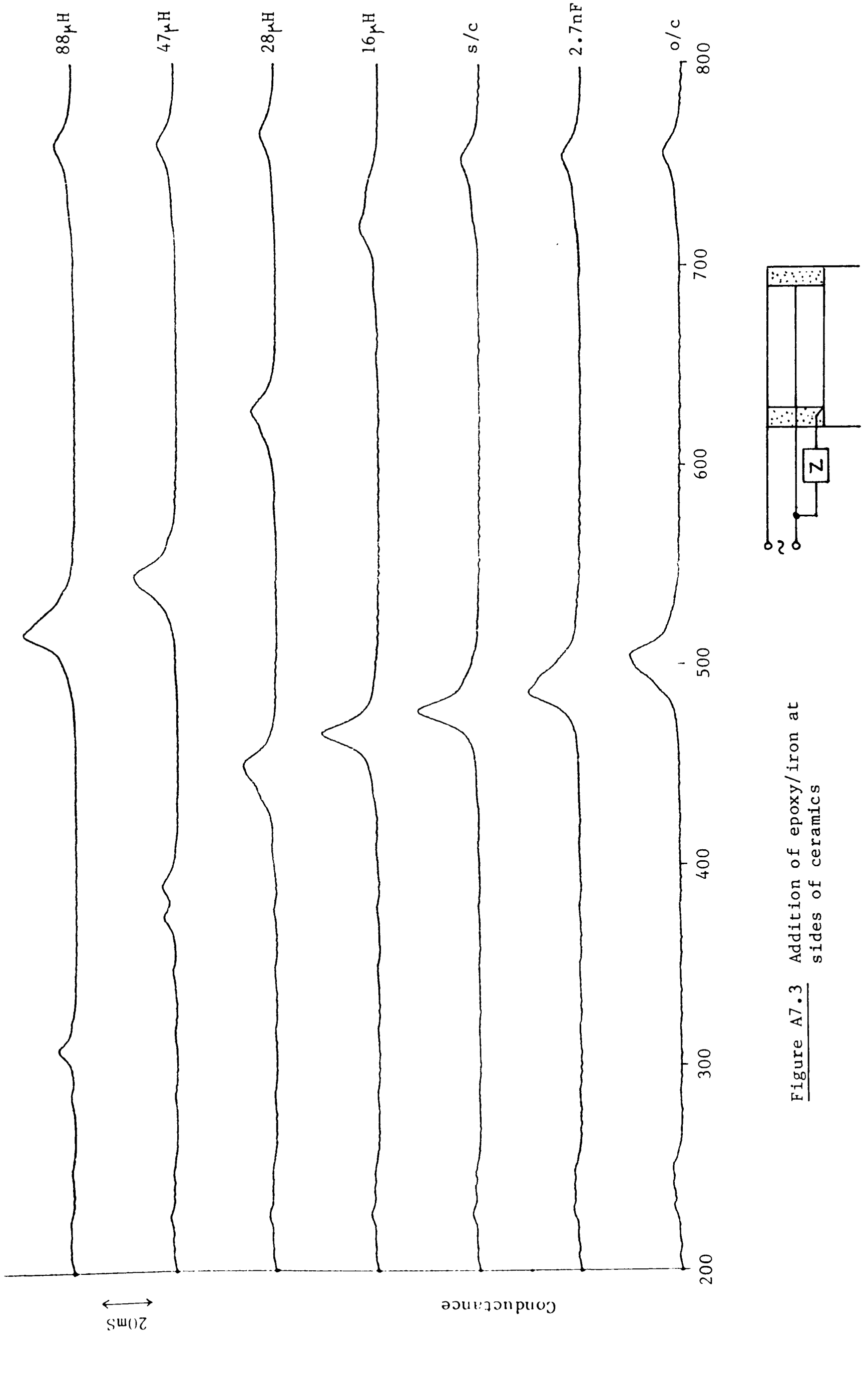

Figure A7.3 Addition of epoxy/iron at sides of ceramics

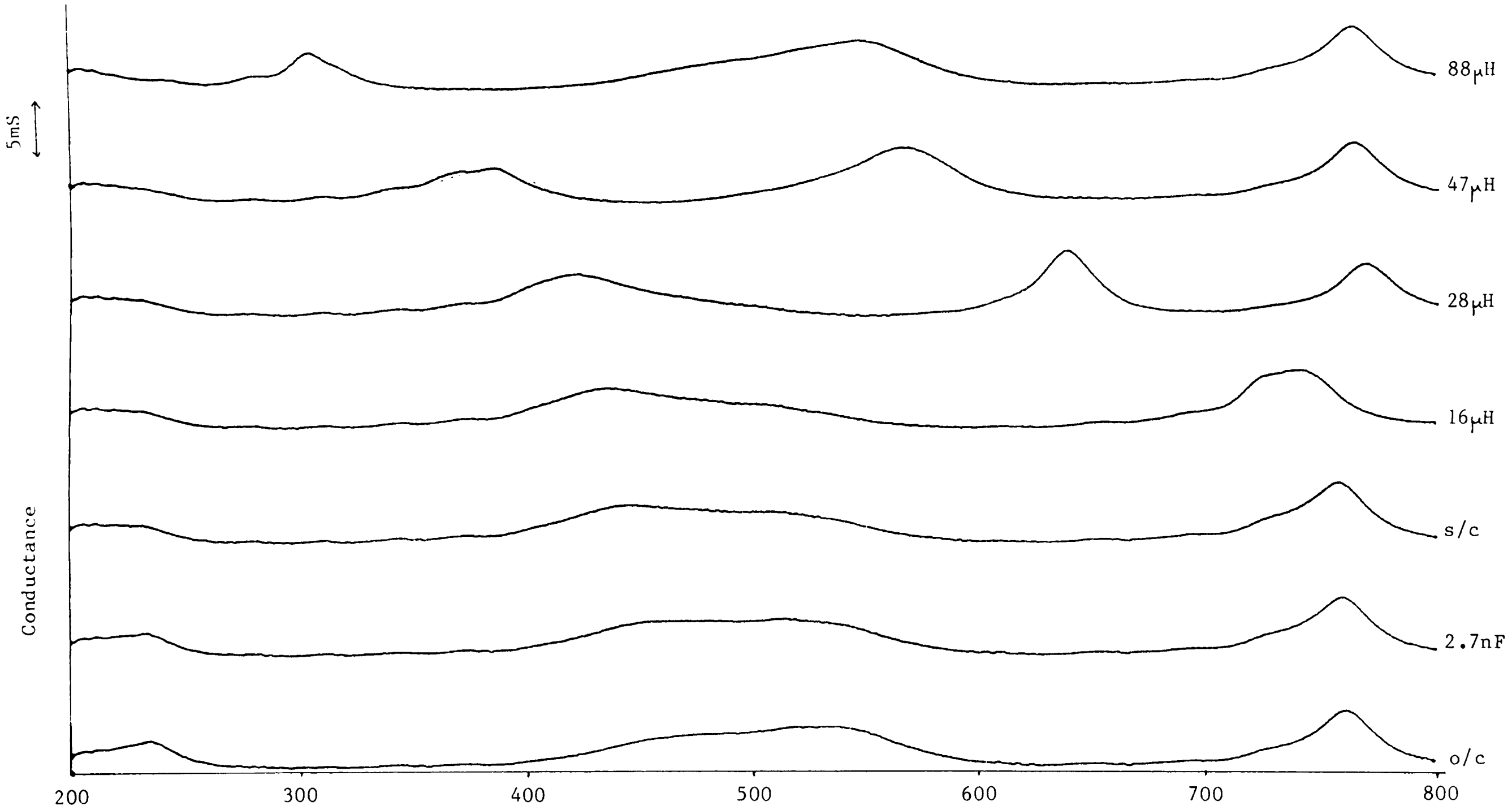

Figure A7.4 Finished transducer in water

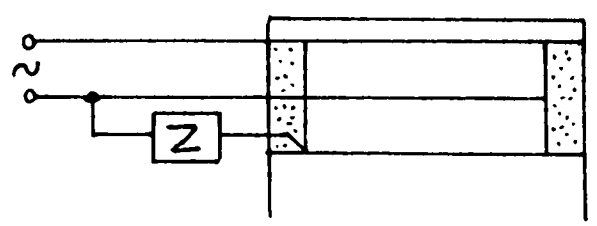

APPENDIX 8

Source simplification

Mason's equivalent circuit (1) for a ceramic vibrating in thickness mode is too complicated for direct analysis related to active control. Therefore it is necessary to reduce the circuit to its Thevenin equivalent of a source in series with an impedance. In figure A8.1 the ceramic has thickness l, wavenumber k, and impedance Z_c. The impedances Z_x and Z_y load the front and back faces respectively. It is convenient to consider the transformed version of Mason's circuit due to Kossoff (2) which is shown in figure A8.2.

On the electrical side of the transformer a voltage source E is in series with a negative capacitance $-C_o$. These can be moved to the mechanical side of the transformer as follows:

$$\frac{-1}{j\omega C_o} \Rightarrow \frac{-1}{j\omega C_o} \cdot (2C_o h_{33})^2 = j\frac{4C_o h_{33}^2}{\omega}$$

$$E \Rightarrow 2C_o h_{33} E$$

The positive clamped capacitance C_o can be ignored because it is in parallel with a voltage source. Combining these results gives the circuit of figure A8.3, which in turn reduces to the simple T network of figure A8.4, where:

$$Z_P = 2Z_y + j\left[\frac{4C_o h_{33}^2}{\omega} - 2Z_c \cot(kl/2)\right]$$

$$Z_Q = 2Z_y + 2jZ_c \tan(kl/2)$$

The pair of transformations in figure A8.5 reduce the T network to its Thevenin equivalent shown in figure A8.6. For this solution:

$$F = 2C_o h_{33} \frac{Z_Q}{Z_p + Z_Q} \cdot E$$

$$Z_o = Z_p // Z_Q - Z_y$$

The units of F are newtons and the mechanical impedance Z_o has units of Kg/s.

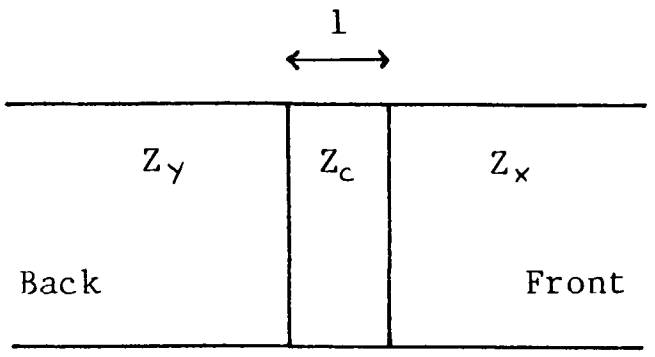

Figure A8.1 Ceramic loaded on both faces

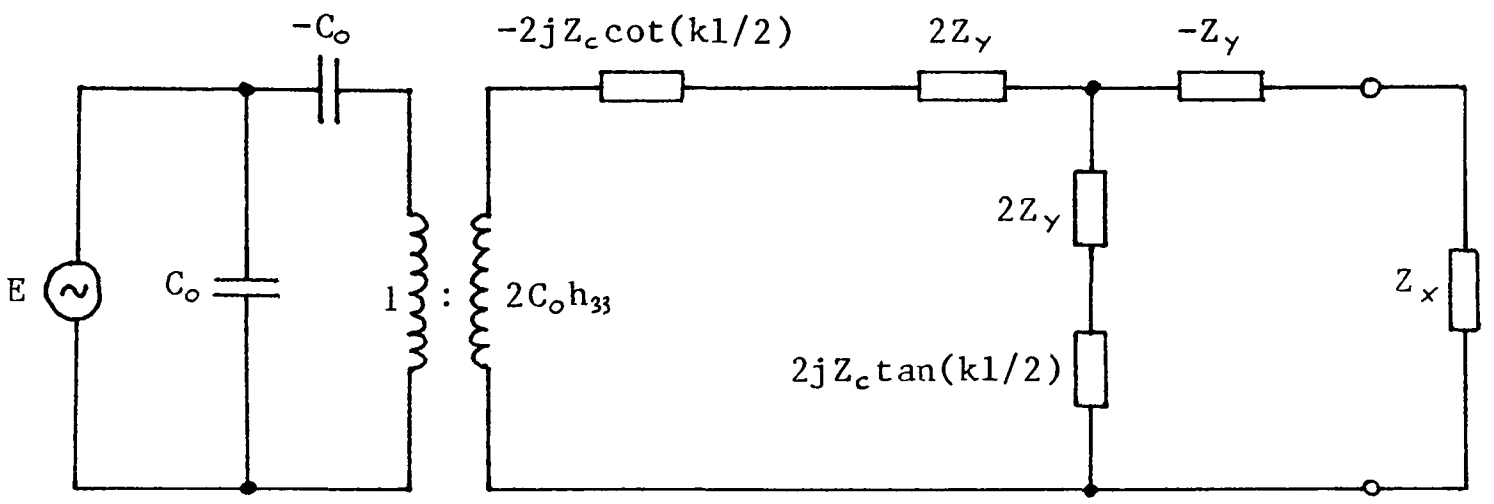

Figure A8.2 Transformed version of equivalent circuit

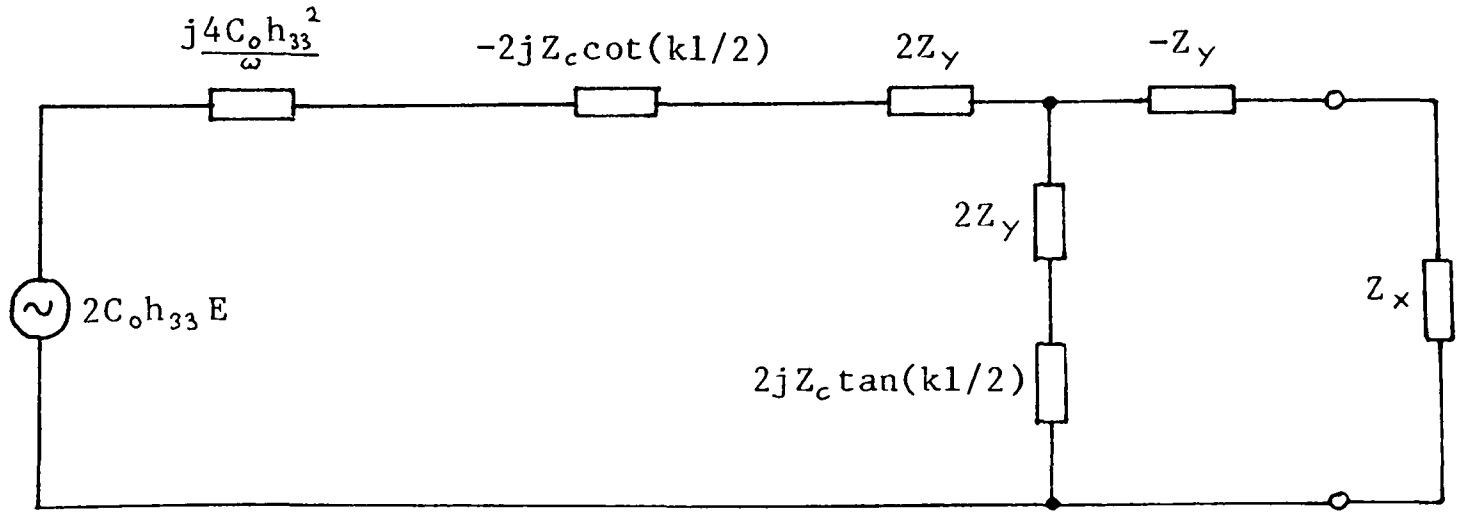

Figure A8.3 Removal of transformer

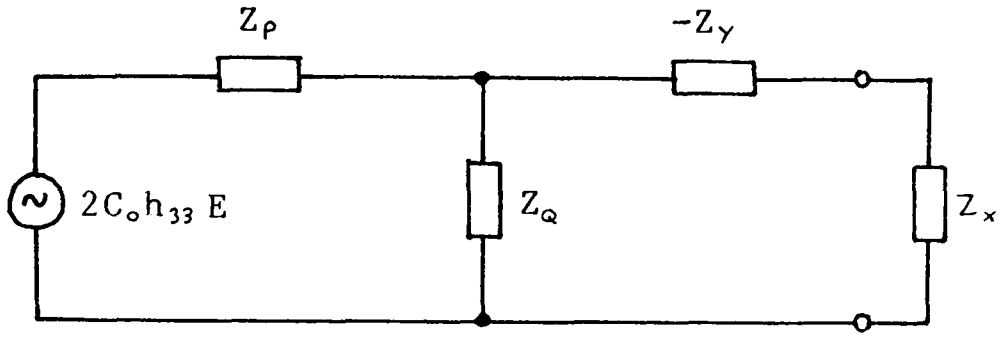

Figure A8.4 Simple T-network

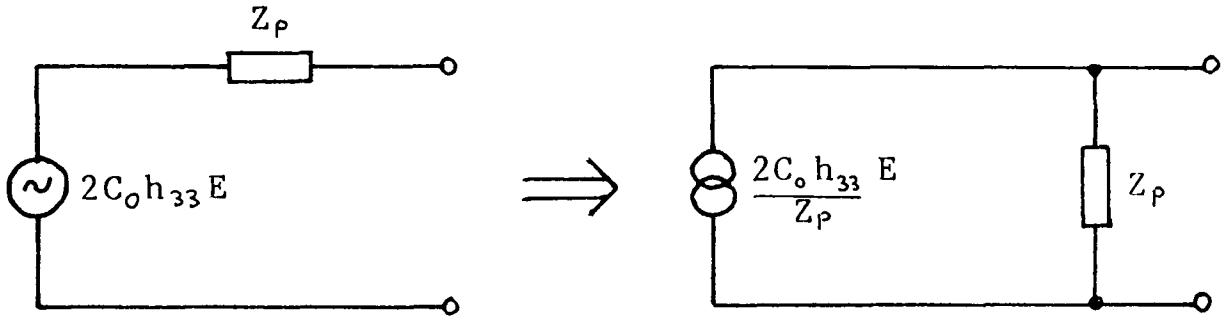

Figure A8.5 Source transformations

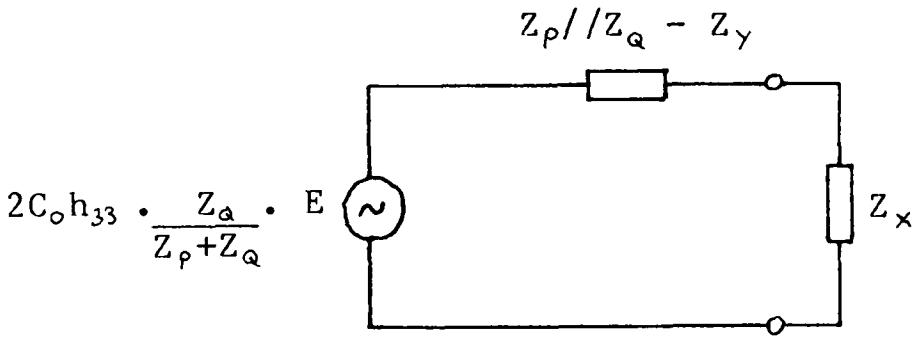

Figure A8.6 The resulting Thevenin equivalent circuit

APPENDIX 9

Derivation of active control parameters

Figure A9.1 shows the simplified circuit for a pair of ceramics separated by a coupling layer. The circuit components are defined in section 6.2. It is required to generate an impedance Z_S looking into the coupling layer by controlling the amplitude and phase of F_1 relative to F_o. The simple T network of figure A9.2 results from the following combination of impedances:

$$A = Z_o + Z_m \tanh(\gamma_m l_m/2)$$

$$B = Z_m / \sinh(\gamma_m l_m)$$

$$C = Z_1 + Z_m \tanh(\gamma_m l_m/2)$$

The total impedance seen by the source F_o is required to be $Z_S + Z_o$. Loop analyisis gives the following matrix representation of the circuit:

$$\begin{pmatrix} A+B & B \\ B & B+C \end{pmatrix} \begin{pmatrix} I_o \\ I_1 \end{pmatrix} = \begin{pmatrix} F_o \\ F_1 \end{pmatrix}$$

The unknown current I_1 can be eliminated to give:

$$\left[\frac{A+B}{B} - \frac{B}{B+C} \right] I_o = \frac{F_o}{B} - \frac{F_1}{B+C}$$

But $I_o = F_o/(Z_s+Z_o)$ so the above equation can be rearranged to give the required solution:

$$F_1 = F_o \left[\frac{(B+C)(Z_s+Z_o) - (B+C)(A+B) + B^2}{B(Z_s+Z_o)} \right]$$

The complex impedance ratio in square brackets defines the amplitude and phase of F_1 relative to F_o.

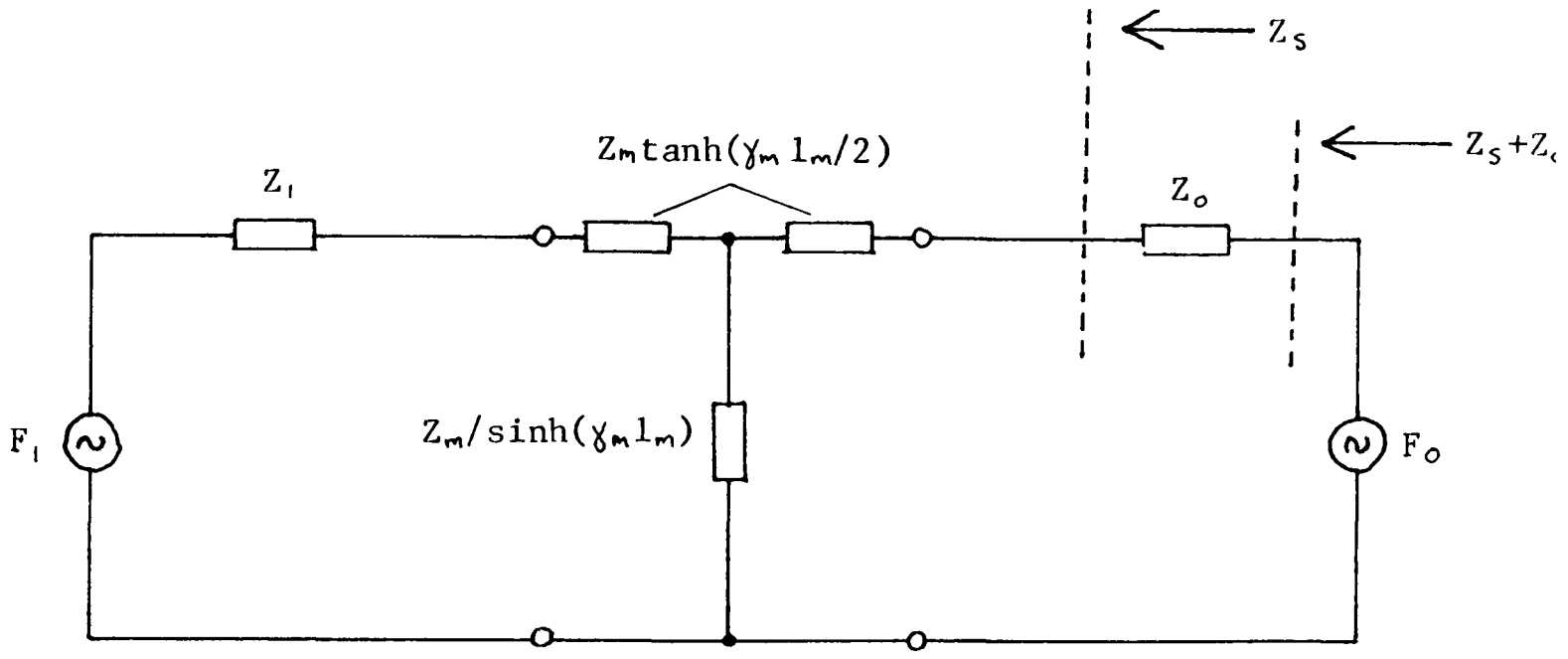

Figure A9.1 Simplified circuit for active control analysis

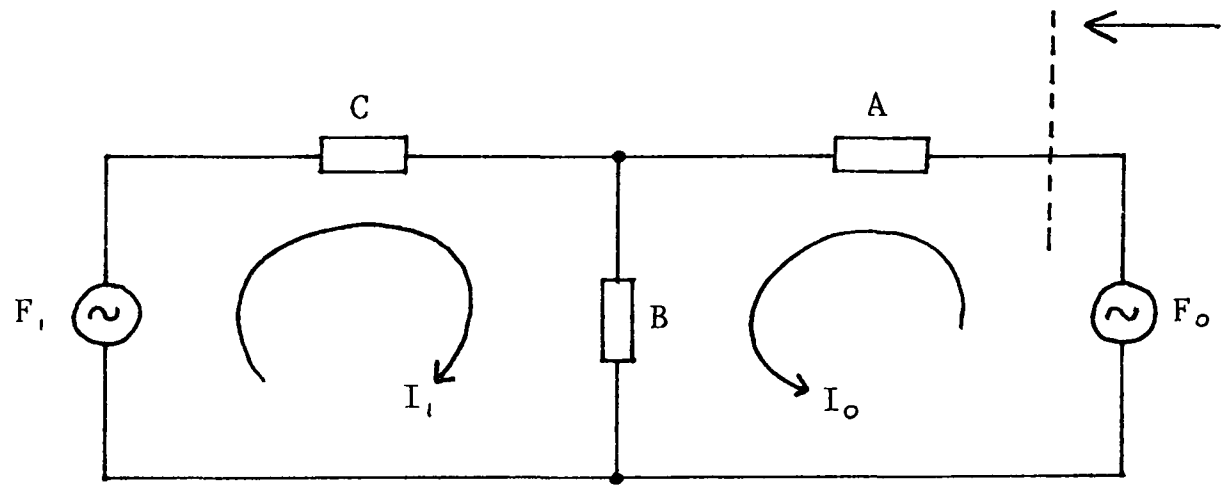

Figure A9.2 Loop analysis

APPENDIX 10

Active control electronics

Figure A10.1 shows a block diagram of the control electronics. The circuit is designed to give constant drive voltage and variable control voltage, both of which have small amplitude (<1V pk-pk).

Consider first the analogue components. A voltage controlled oscillator drives the circle plotter with a continuous wave signal at the required frequency. The circle plotter output is a 100mV pk-pk sine wave which is applied directly to the drive ceramic and used to measure its admittance. This signal also enters a ×10 amplifier which has high input impedance. The amplifier output is divided into two channels; IN PHASE and QUADRATURE. Both channels then enter multiplying digital to analogue converters (DACs) which are connected as digitally controlled potential dividers. In this way both channels have amplitudes in the range 0V to ±1V. A summing amplifier combines these signals to produce the control voltage, which therefore has digitally controlled amplitude and phase.

The operating frequency sweeps from 200 kHz to 800 kHz in 256 steps. This is done by an 8-bit binary counter whose output drives the voltage controlled oscillator via a DAC. The counter output is also connected to the address lines of two Read Only Memories, one for each analogue channel. Data lines from the memories control the amplitude of the IN PHASE and QUADRATURE channels, hence defining the amplitude and phase of the control voltage.

In practice the ×10 amplifier, the DACs, and the summing

amplifier all introduce additional phase shifts which are frequency dependent. These phase shifts were measured and compensated for by adjusting the ROM contents accordingly. The DACs also have amplitude dependent phase shifts, especially for very small signals. This effect could not be compensated and accounts for the errors shown in figure 6k.

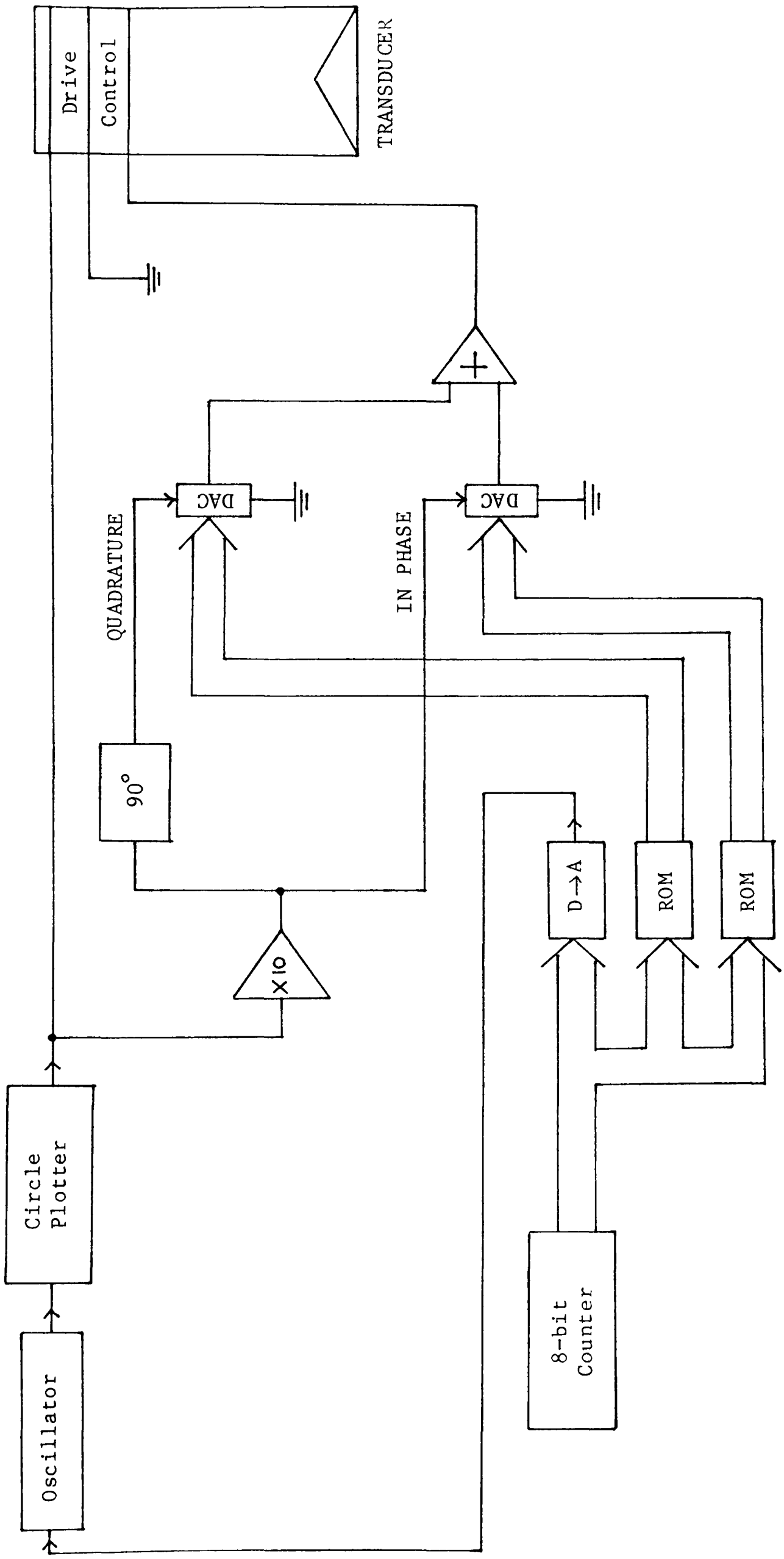

Figure A10.1 Active control electronics

APPENDIX 11

Stress Distribution in Piezoelectric Material

This calculation is based on the equations given by Berlincourt et al in reference 9 pages 229-230. Consider a ceramic plate of thickness 1 and wavenumber k, driven by a sinusoidal applied voltage $Ve^{j\omega t}$. It is required to find the stress T as a function of distance through the material. Choose the electric displacement D and strain S as independent variables, giving the following pair of piezoelectric equations:

$$T = c^D S - hD \qquad \text{Equation 11.1}$$

$$E = -hS + D/\varepsilon \qquad \text{Equation 11.2}$$

The symbols in these equation represent the following variables:

		Units:
E	= electric field	V/m
c^D	= stiffness at constant D	N/m^2
h	= piezoelectric constant	V/m
ε	= permittivity	F/m
ρ	= density	Kg/m^3
ξ	= particle displacement	m

The wave equation for this situation is

$$\frac{\partial^2 \xi}{\partial t^2} = \frac{c^D}{\rho} \cdot \frac{\partial^2 \xi}{\partial x^2}$$

And the solution is a travelling wave in the x direction:

$$\xi = \left[A\sin(kx) + B\cos(kx) \right] e^{j\omega t}$$

Therfore the strain at any point is:

$$S = \frac{\partial \xi}{\partial x} = \left[Ak\cos(kx) - Bk\sin(kx) \right] e^{j\omega t} \qquad \text{Equation 11.3}$$

Let the stress at the ceramic faces be T_o at x=0 and T_l at x=1. For sinusoidal excitation $D=D_o e^{j\omega t}$ so the constants A and B can be found from equation 11.1.

$$A = \frac{T_o + hD_o}{c^D k}$$

$$B = \frac{(T_o + hD_o)\cos(kl) - (T_l + hD_o)}{c^D k \sin(kl)}$$

Therefore equation 11.1 can be used to find T at any point in the ceramic by substitution of A and B into equation 11.3 to find S. The problem is that the electric displacement D is not known. It can be found from equation 11.2.

$$Ve^{j\omega t} = \int_o^l E dx = -h \int_o^l S dx + \int_o^l D_o e^{j\omega t} / \varepsilon \; dx$$

$$\therefore \; V = -h \left[A\sin(kl) + B(\cos(kl) - 1) \right] + D_o l/\varepsilon$$

Substituting for A and B, and using the identity $\tan(\theta/2) = (1-\cos\theta)/\sin\theta$, gives:

$$D_o = \varepsilon \left[\frac{Vc^D k + h(T_o + T_l)\tan(kl/2)}{c^D kl - 2h^2 \varepsilon \tan(kl/2)} \right]$$

For computing purposes the quantities T_o, T_l, D_o and V are all complex since they have both amplitude and phase. For analysis of the control

ceramic the quantity V is the voltage which appears across the passive electrical load, i.e. the output voltage.

Conference on Underwater Acoustic Calibration and Measurements
PROC. INST. ACOUSTICS VOL 6 PT 5 1984

A technique for measuring the acoustic properties of materials using a buffer rod.

G.A.Steel, B.K.Gazey and B.V.Smith.

Department of Electronic and Electrical Engineering,
University of Birmingham.

1.0 Introduction

The design of high-performance transducers often requires composite structures which include passive sections of materials whose acoustic properties need to be known accurately. As many of these materials are especially synthesised for a given application published data does not normally exist and a rapid, convenient technique is required for measuring the appropriate parameters, eg. sound velocity, acoustic impedance and absorption.

Generally the methods adopted involve immersing a sample of material, whose acoustic properties are to be determined, in a suitable low-loss fluid (often water). The substitution of a solid medium in the form of a buffer-rod in place of a fluid medium facilitates rapid and accurate alignment between the measurement transducers and the sample under test. Buffer-rods are frequently used, eg. (1) to provide time delays in order to separate transmitted and reflected signals and this principle was incorporated by Felix (2) into equipment to measure attenuation and dispersive characteristics of various plastics at a number of discrete frequencies. In this equipment velocity is determined by measuring the transit times of sound pulses through the various sections, with and without the test sample. Two transducers are required and accurate time measurements are essential. Absorption is measured by comparing the received amplitudes with and without the sample present, proper account being taken of the transmission coefficients at the sample boundaries.

At Birmingham Pelmore (3) and Koymen (4) developed a technique which uses a single transducer. This has since been extended by the present authors so that sound passes through an air-backed sample twice having been reflected from the air termination. The frequency of the pulse carrier is swept slowly and velocity is determined from the variations of phase with frequency. Absorption data is obtained in a similar manner to that outlined above.

The authors believe the method presented here is convenient and lends itself readily to on-line computer data processing.

2.0 Principle of the buffer rod measurement

2.1 Impedance and velocity measurement

The measuring equipment as developed by Pelmore (3) is detailed in Figure 1. It comprises a widebandwidth transducer, a perspex buffer rod, a sample of material to be tested and an air terminating section. The assembly is loaded mechanically using calibrated spring pressure, "Nonaq" high vacuum grease being used between the various components to ensure good acoustic coupling.

A pulse of six to ten cycles of carrier is launched by the transducer into the buffer rod and reflected from the end. This reflection is received by the

same transducer, amplified, sampled and entered into a phase sensitive detector. A reference signal for the detector is provided by the sweep generator. The reflected pressure, p_r, measured by the transducer during the pulse may be approximated by the guided plane wave expression :

$$p_r = p_i |R| \exp(-2\alpha_p \ell_p) \cos(2\pi ft - 2k_p \ell_p + \emptyset) \qquad (1)$$

where

p_i = incident pressure in the transmitted wave.

α_p = absorption coefficient in the perspex buffer rod.

ℓ_p = length of the buffer rod.

k_p = wavenumber for perspex.

$|R|$ = modulus of reflection coefficient at the rod-sample interface.

$\emptyset$ = phase shift introduced upon reflection.

f = frequency of both the carrier and the reference signal used in the phase detector.

Therefore the electrical phase shift relative to the detector reference becomes :-

$$\psi = -2k_p \ell_p + \emptyset = -\frac{4\pi f \ell_p}{c_p} + \emptyset \qquad (2)$$

where c_p is the sound velocity in the rod. The amplitude of the detector output voltage is thus $V\cos\psi$; V being the maximum output voltage.

As the frequency of the carrier within the pulse is varied linearly from pulse to pulse the detector output voltage will vary considerably as shown by the measured data in Figure 2, in which the frequency varies from 500 kHz to 550 kHz. Figure 2(a) shows the results for two extreme terminating conditions corresponding to an acoustically 'soft', ie. low acoustic impedance (air) termination and to an acoustically 'hard', ie. high acoustic impedance (Aluminium) terminating section. Both terminations result in an $|R|$ approaching unity but the 'soft' boundary introduces a 180^o phase shift on reflection compared with the 'hard' boundary, which is demonstrated in the results. Figure 2(b) compares the results of a water termination with that of air. Water is acoustically 'soft' as compared with the perspex, but being of intermediate impedance, leads to a smaller reflection coefficient (0.37), which can be deduced from the amplitude change, together with a 180^o phase shift.

The impedance, Z_s, of the terminating sample can be expressed in terms of $|R|$ and $\emptyset$ by the equation :-

$$Z_s = Z_p \left[\frac{1 - |R|^2 + 2j|R|\sin\emptyset}{1 + |R|^2 - 2|R|\cos\emptyset} \right] \qquad (3)$$

where Z_p is the acoustic impedance of the buffer rod. Substituting the values of $|R|$ and $\emptyset$ for water measured from the results in Figure 2(b) gives :-

$Z_s = 1.47 + j0$ M rayls, which is close to the expected result.

Using this technique the impedance of any sample can be found and since density is easily measured sound velocity can thus be derived.

The measurement of $|R|$ and ϕ as described above gives good results provided $|R| > 0.2$. For smaller values of $|R|$ the data becomes progressively less accurate because of the smaller reflected signal.

For situations where $|R|$ is small, ie. the acoustic impedance of the sample material is similar to that of perspex, a more accurate determination of velocity is possible by observing the reflection from the sample-air boundary. Also, since the reflected signal has traversed the sample length twice information on absorption in the sample may be obtained.

This additional phase shift associated with propagation through the sample is given by :-

$$\phi = -2k_s \ell_s + \phi_t = -\frac{4\pi f}{c_s}\ell_s + \phi_t \qquad (4)$$

where; ℓ_s, k_s, c_s are the sample length, the wavenumber and the sound velocity in the sample respectively, and ϕ_t is a small phase shift introduced during transmission from the buffer rod into the sample. ϕ_t depends upon the α/k ratio for the sample and can be shown to be typically small and largely independent of frequency. It has the effect of introducing a small offset in the output of the phase sensitive detector.

The rate of change of ϕ with frequency as obtained from equation (4) is approximately given by :

$$\frac{\partial\phi}{\partial f} = -\frac{4\pi\ell_s}{c_s}$$

and therefore the sound velocity in the sample becomes :-

$$c_s = -\frac{4\pi\ell_s}{\partial\phi/\partial f} \qquad (5)$$

In view of the nature of ϕ_t it does not appear in equation (5) because of the differentiation.

The variations of ϕ with frequency are determined from the phase differences between the detector outputs with and without the sample present. The ambiguity in the absolute value of ϕ is not a problem since the graph of ϕ with frequency is linear and it is its gradient which is used in determining the velocity, see equation (5). A typical practical result of ϕ plotted against frequency for a sample of Stycast 1264 epoxy resin is shown in Figure 3. The gradient can be determined using a least squares fit to the data.

According to equation (4), ignoring the small correction ϕ_t, the value of ϕ is a multiple of 2π whenever ℓ_s is a multiple of a half wavelength. Therefore a graph of equation (4) assuming only phase shifts between, $-\pi$ to $+\pi$, can be recognised, is shown in Figure 4. Having found an estimate of the velocity c_s from the gradient of this graph the absolute phase may be estimated by estimating the value of the multiple, n , of halfwavelengths that gives a zero phase in the frequency range actually measured.

Fitting a straight line estimate to the data, but now taking the absolute value of ϕ into account, enables ϕ_t to be estimated from the intercept with the $f = 0$ axis. In the absence of ϕ_t this intercept would be zero, as shown by equation (4). Evaluating ϕ_t by this method has the implicit assumption that

ϕ_t is largely independent of frequency over the frequency spread of the practical data.

2.2 Absorption measurement

The amplitude ratio $|A|$, of signals reflected with and without the sample present is given by :-

$$|T_{ps}||T_{sp}| \exp(-2\alpha_s \ell_s). \; |R_{pa}| / |R_{sa}| \quad ,$$

where $|T_{ps}|$ and $|T_{sp}|$ are the amplitudes of the pressure transmission coefficients from the rod to the sample and back again respectively, $|R_{pa}|$ and $|R_{sa}|$ are the amplitudes of the pressure reflection coefficients for the rod and sample when terminated in air respectively and $\alpha_s \ell_s$ is the absorption in the sample.

Owing to the large mismatch in impedance between both the rod and the sample and air ratio $|R_{pa}| / |R_{sa}|$ is very close to unity.

The transmission coefficients are given by :-

$$T_{ps} = \frac{2Z_s}{Z_p + Z_s} \quad \text{and} \quad T_{sp} = \frac{2Z_p}{Z_p + Z_s}$$

Therefore $|A|$ becomes :-

$$|A| \simeq \frac{4|Z_s \; Z_p|}{(|Z_p + Z_s|)^2} \exp(-2\alpha_s \ell_s)$$

The absorption coefficient in the sample is therefore :-

$$\alpha_s = - \frac{1}{2\ell_s} \; \ell n \left[\frac{(|Z_p + Z_s|)^2}{4|Z_s Z_p|} \cdot |A| \right]$$

which may be determined from measurements of Z_p, Z_s and $|A|$.

2.3 Effects of coupling layer

So far the effects of the acoustic coupling medium between the sections have been ignored. Although in practice this is a very thin layer it nevertheless introduces an additional frequency dependent phase shift in addition to that of the sample under test.

It can be shown that a thin layer introduces an additional frequency dependent phase shift, ϕ_c, given by :-

$$\phi_c = - \tan^{-1} \left(\frac{Z_c^2 + Z_p \; Z_s}{Z_c (Z_p + Z_s)} \cdot \tan k_c \ell_c \right)$$

$$= - \tan^{-1} (F . \tan k_c \ell_c)$$

where Z_c, Z_p, Z_s are the respective characteristic impedances of the grease coupling sections, the perspex buffer rod and the sample under test, ℓ_c, k_c are the thickness and wavenumber of the coupling layer respectively and F is an

impedance ratio as defined in the above expression.

Provided $k_c \ell_c \ll 1$; the usual case since the grease coupling layer is kept as thin as possible, then :-

$$\phi_c \simeq - \tan^{-1} (F\, k_c \ell_c).$$

For the particular mode of operation under discussion the impedances Z_p, Z_c & Z_s are always much of the same magnitude and so the parameter F is close to unity. Therefore ϕ_c may be further approximated :-

$$\phi_c \simeq - F k_c \ell_c \text{ radians.}$$

The total phase shift introduced by this coupling layer is $2\phi_c$ because it is traversed twice by the acoustic pulse and its reflection. When this additional correction term is introduced into equation (4) it modifies the value of c_s :-

$$c_s \simeq \frac{-4\pi \ell_s}{\frac{\partial \phi}{\partial f} + 4\pi \frac{F \ell_c}{c_c}}$$

where c_c is the sound velocity in the coupling layer.

Substitution of practical values for the coupling layer thickness, ℓ_c, show that the term $4\pi F \ell_c / c_c$ is only of the order of 1% of $\partial\phi/\partial f$ and therefore may be ignored in most cases.

3.0 Some experimental results

Figure 5 shows plots of the detector output, with and without a sample of Stycast 1264 epoxy resin, as a function of frequency. From these variations in the amplitude and phase of the ratio A as a function of frequency have been determined and are shown in Figure 3. The measured data is subject to small interference effects because the rear portion of the pulse which has been reflected from the rod-sample boundary arrives simultaneously with the front portion of the pulse which has been reflected from the sample-air boundary. This arises because the sample is not sufficiently thick to separate the two reflections in time. Obviously the use of a thicker sample would avoid this problem. However, the properties of this particular sample had been determined by other methods thereby providing useful confirmation of the validity of the present method. The straight lines fitted to the data in Figure 3 have been determined by least squares fit procedures and enable sample velocity and absorption to be evaluated. For example, for the Stycast sample the following data was obtained :-

sound velocity = 2523 m/s
absorption coefficient = 2.0 dB/cm at 500 kHz.

A number of different materials have been measured and the results obtained compare favourably with measurements made using other techniques (5).

It is worth noting that the variation of phase with frequency in a dispersive medium would not produce a linear relationship. Since the plots presented are in fact linear then the materials to which they relate are clearly non-dispersive over the frequency range used.

4.0 Conclusions

A technique based upon the use of a buffer-rod has been developed which has enabled sound velocity, impedance and absorption data to be determined for a variety of acoustic media. The results obtained to date are generally in good agreement with measurements made using alternative techniques.

The method is convenient as compared with water immersion techniques with their attendant alignment and standing wave problems. It lends itself to automation under computer control through the use of a digital frequency synthesiser to provide the signal and reference sources. With suitable precision in the analog to digital conversion process the method should be capable of giving accurate results quickly.

In many instances the dimensions of the sample measured can be those required for the passive sections in an actual composite transducer structure. The uncertainty which often exists concerning the precise values of velocity and impedance to be used and which can depend upon lateral dimension may thus be removed.

5.0 Acknowledgements

The authors wish to acknowledge the assistance of G.E.C.(Sonics) for the support of Mr.G.Steel.

6.0 References

1.0 McSkimin,H.J., 1964. "Ultrasonic methods of measurement", Chapter 4, Physical Acoustics, Vol.1, pt.A. Ed. W.P.Mason, Academic Press.

2.0 Felix,M.P., 1974. "Attenuation and dispersion characteristics of various plastics in the frequency range 1 - 10 MHz". J.Composite Materials, Vol.8, 275 - 287

3.0 Birmingham University, Acoustics Group, 1978. "A study of optimised high frequency underwater acoustic transducer performance", Final Report to S.R.C. on contract B/RG/59553, GR/A 51402.

4.0 Koymen,H., 1979. "Optimisation of the design of high frequency sonar transducers", University of Birmingham, PhD. thesis.

5.0 Pelmore,J.M., 1977. "The ultrasonic properties of some filled epoxy materials", Proceedings, Ultrasonics International.

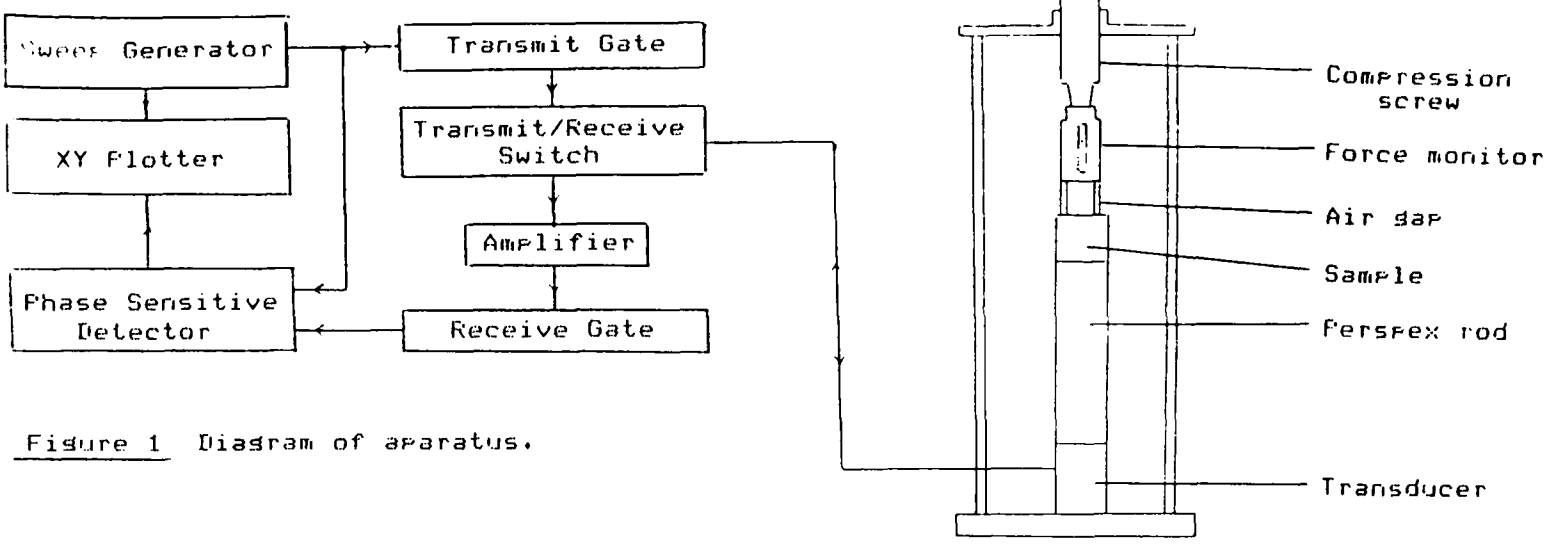

Figure 1 Diagram of apparatus.

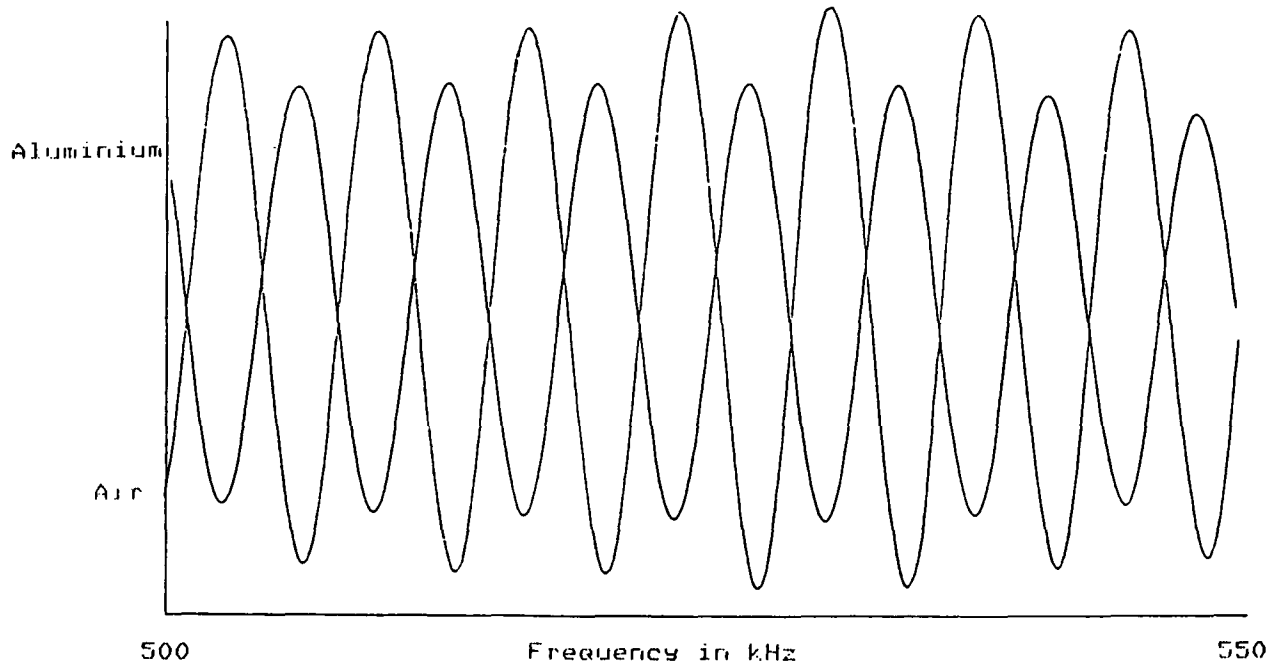

Figure 2a

Detector output for hard and soft terminating impedences.

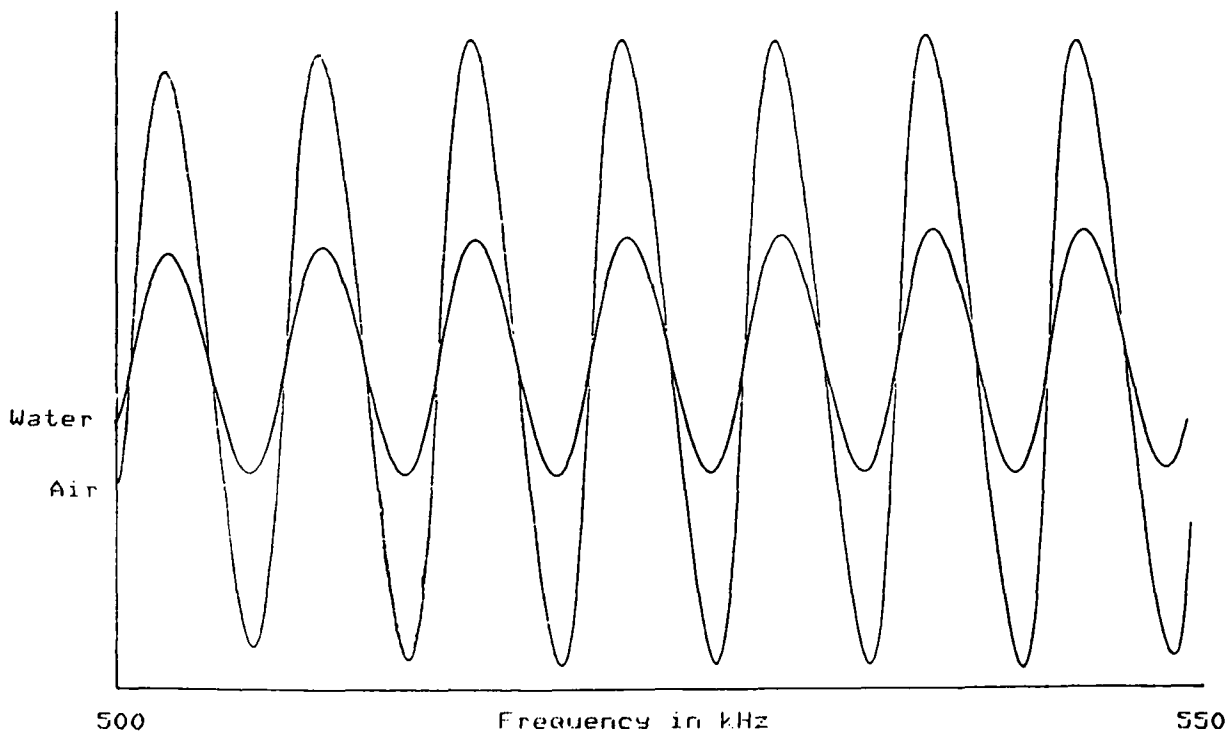

Figure 2b

Comparison of detector outputs with air and water terminatons

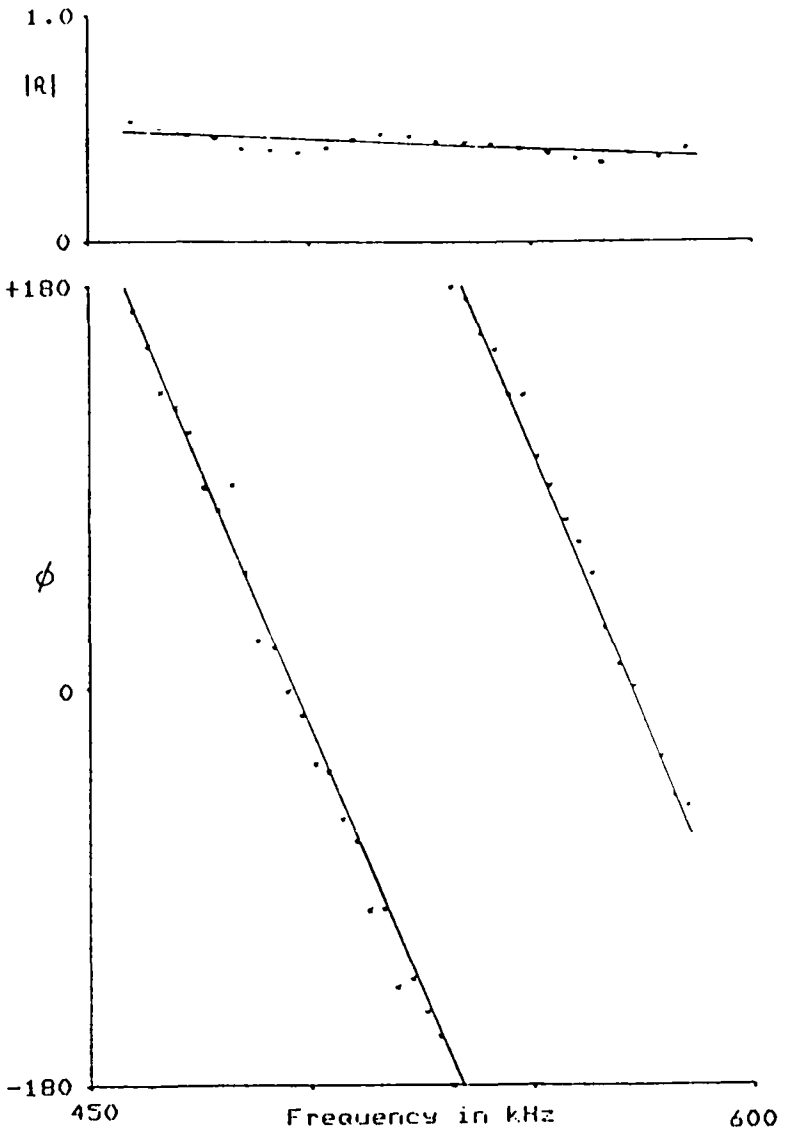

Figure 3

Experimental values of |R| and ϕ derived from figure 5. Straight lines are "least squares fit" approximations.

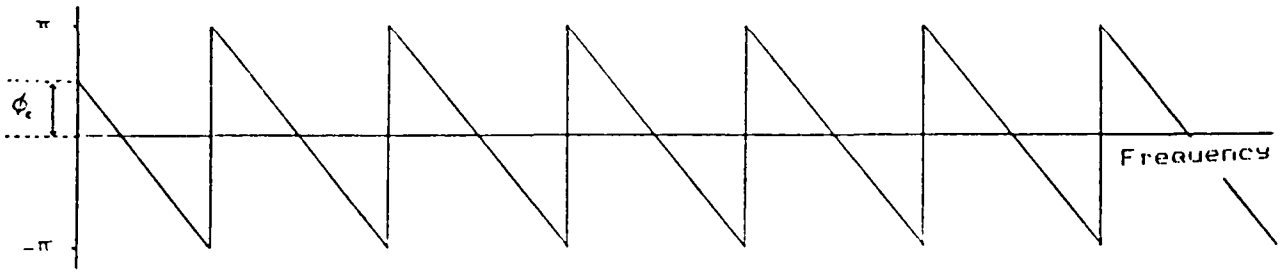

Figure 4 Graph of equation 4 for limits of ± π

Figure 5 Detector output for a 16.3 mm sample of Stycast 1264 resin.

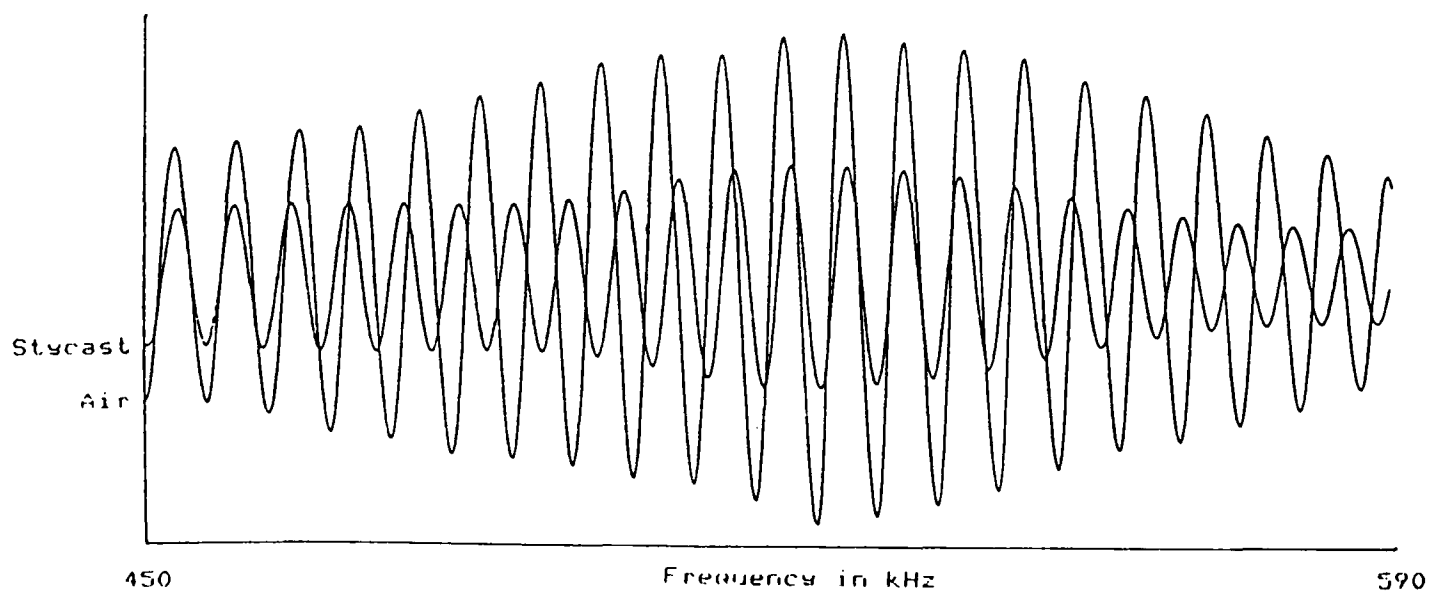

4 BUHL, L. L.: 'Optical losses in metal/SiO_2-clad Ti:$LiNbO_3$ waveguides', *Electron. Lett.*, 1983, **19**, pp. 659–660
5 ORDAL, M. A. *et al.*: 'Optical properties of the metals Al, Co, Cu, Au, Fe, Pb, Pt, Ag, Ti, and W in the infrared and far infrared', *Appl. Opt.*, 1983, **22**, pp. 1099–1119
6 ABELÈS, F.: 'La détermination de l'indice et de l'épassieur des couches minces transparentes', *J. Phys. Radium*, 1950, **11**, pp. 310–314
7 BOZHEVOL'NYI, S. I. *et al.*: 'Photogalvanic mechanism of the rotation of the light polarisation plane in optical Ti:$LiNbO_3$ waveguides', *Sov. Tech. Phys. Lett.*, 1983, **9**, pp. 690–692 (in Russian)
8 LAM, J. F., and YEN, H. W.: 'Dynamics of optical TE to TM mode conversion in $LiNbO_3$ channel waveguides', *Appl. Phys. Lett.*, 1984, **45**, pp. 1172–1174

TUNABLE SONAR TRANSDUCER

Indexing terms: Transducers, Sonic propagation, Acoustics

Details are given of an underwater transducer which is tunable over the frequency range 250 kHz to 700 kHz. The structure comprises a pair of 50 mm-diameter lead zirconate titanate ceramic plates suitably mounted. The resonant frequency of the structure is electronically controlled by varying in a predetermined manner the amplitude and phase of the voltage applied to one of the ceramics.

A transducer has been reported[1] which is tunable over $\sim 1\frac{1}{2}$ octaves in air. Lead zirconate titanate ceramic bars, which were operated in their length modes, were used. A central portion of the ceramic was driven actively and the overall structure was passively loaded using electrical reactances. The resonance of the structure was changed by varying the magnitude, and in some circumstances the type, of this passive electrical load. In the present letter this technique is extended to underwater transducers which use ceramics operated in their thickness modes. In addition, active control is employed such that the transducer can be tuned electronically.

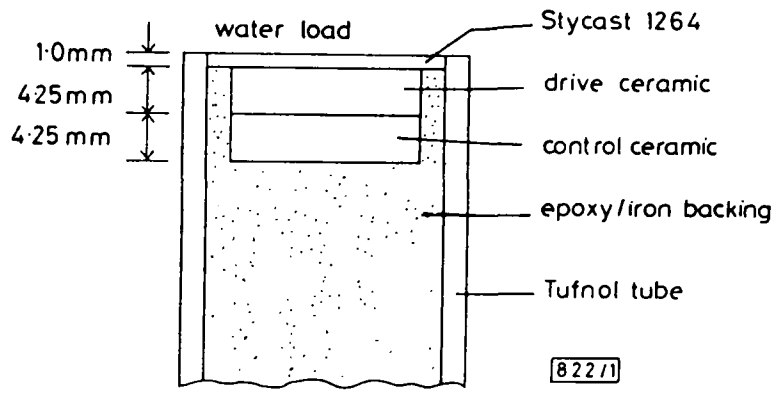

Fig. 1 *Details of transducer construction*

The transducer investigated is shown diagrammatically in Fig. 1. It comprises two 50 mm-diameter PZT-4 discs bonded together with an epoxy resin. The total ceramic thickness is 8·5 mm. The front face of the ceramic pair is protected from the water by a thin layer of epoxy resin and the rear face is loaded by a composite material of iron and epoxy, which has an acoustic impedance of 7·1 Mrayls.

A voltage source applied across both ceramics, with no connection to the centre, gives a fundamental thickness resonance at 240 kHz and a third harmonic at 750 kHz. This is the conventional method of operating such a device. However, an alternative driving arrangement is to connect the voltage source across only one ceramic, the other remaining open-circuit. The fundamental and third-harmonic resonances of the structure remain unchanged, because of the strong mechanical coupling between the ceramics, but there is an additional resonance at 500 kHz. This can be regarded as the second harmonic of the ceramic pair. If the open circuit is replaced by a short-circuit this second harmonic reduces in frequency to 475 kHz. In this way the total ceramic thickness has a resonance which is excited by one element but is controlled by the other. The elements will be designated the 'drive ceramic' and the 'control ceramic', respectively.

In Reference 1 it is shown that resonance can be varied between the open-circuit and the short-circuit frequencies by loading the control ceramic with a variable capacitor. Furthermore, the resonant frequency can be moved outside this range by inductive loading.

An analysis of the effects of passive electrical loads on the resonance of the transducer of Fig. 1 has been made using a one-dimensional transmission-line equivalent circuit based on the ceramic model of Reference 2. A very small inductance behaves approximately as a short-circuit and thus a second harmonic resonance at 475 kHz is produced. Increasing the inductance causes the second harmonic to decrease in frequency, tending towards 240 kHz, and the third harmonic decreases towards 500 kHz. The fundamental also decreases in frequency, tending towards zero, but the conductance becomes too low to be of practical significance.

A more detailed computer simulation of the transducer shows that the most important design aspects are:

(i) The bond thickness between ceramics must be less than $\lambda/100$ for acceptable performance.

(ii) The equivalent series electrical resistance of the inductances must be less than 10 Ω.

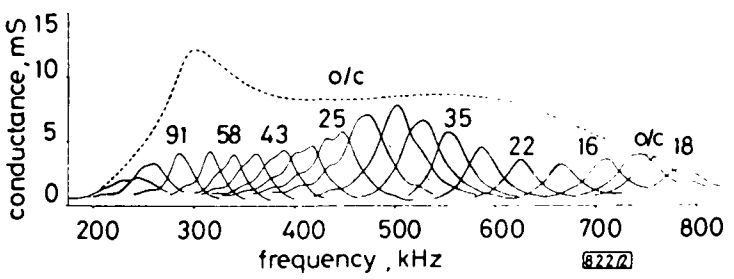

Fig. 2 *Drive ceramic conductances measured with passive control*

Quantities above curves are inductances in μH. Dotted line shows predicted envelope for a 4 Ω series resistance

Fig. 2 shows the measured conductances of the transducer of Fig. 1 when it is operated in water with different inductive loads. The epoxy bond was estimated to have a thickness of 25 μm and all the inductances had series resistances of less than 4 Ω. The observed conductances are lower than the predicted values at all frequencies. These differences are explained by the fact that the acoustic loading on the drive ceramic is invariably greater than that predicted by a simple one-dimensional analysis. This is particularly noticeable at frequencies around 350 kHz and 650 kHz where resonances are furthest removed from 'natural' positions.

Passive electrical loading of the control ceramic can be regarded as producing variations in the reactive part of the backing impedance as seen by the drive ceramic, hence causing changes in the resonant frequency. Bobber[3] has shown that any resistive or reactive acoustic load can be generated actively by using a second transducer whose drive voltage has appropriate values of amplitude and phase. The two ceramics in Fig. 1 can be regarded as such a pair of transducers which are separated by a short transmission line (the epoxy bond). Therefore it is possible to measure a similar graph to Fig. 2 by using a variable voltage source connected to the control ceramic.

A transmission-line analysis was used to investigate this active control method. At each frequency the complex backing impedance seen by the drive ceramic was calculated for

Table 1

Inductance	Resistance	Resonant frequency	Voltage amplitude at resonance
μH	Ω	kHz	V
120	8	278	4·3
69	5·5	335	4·1
43	3·3	390	2·6
19	2	444	0·8
120	8	519	1·5
35	4	590	3·0
26	2·5	639	3·5
19	0·5	700	2·5

passive electrical loads on the control ceramic. Then the voltage required to generate this same complex impedance was derived. It was found that any passive electrical load can be simulated actively by applying a voltage of the same amplitude and phase as would be measured across that load. As an example the output voltage was calculated across the passive loads in Table 1 for the frequency range 270–700 kHz. The voltage is frequency-dependent and its required amplitude at each resonant frequency is shown in Table 1. The small series resistances are included to give all resonances a peak conductance of around 9 mS.

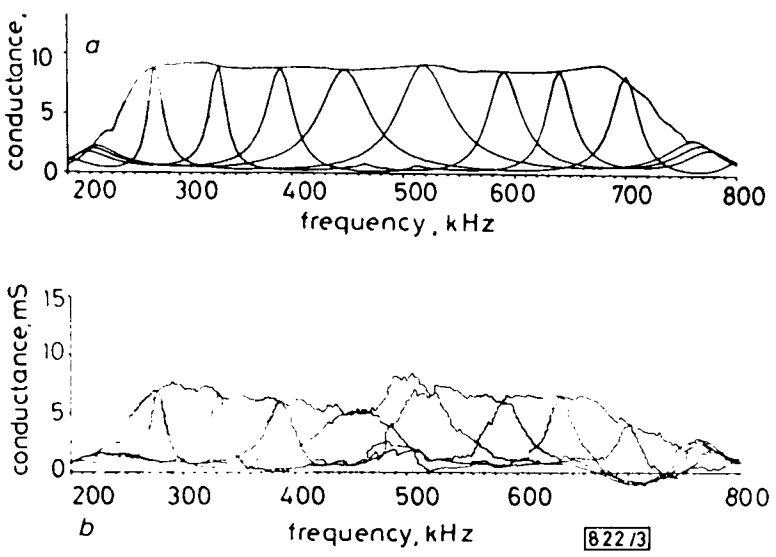

Fig. 3 *Drive-ceramic conductances with active control*

a Predicted
b Measured

A digital technique was used to apply the calculated voltages to the control ceramic, the frequency range being divided for convenience into 256 steps. Fig. 3 shows the results obtained. Active control gives well defined resonant peaks at the predicted frequencies and the measured conductances are closer to the predicted values than was observed with passive control. Also shown in Fig. 3 is the effect of an active load calculated to follow the locus of the conductance maxima, i.e. the envelope of the resonant peaks. The control voltage required to achieve this is shown in Fig. 4, where phase is defined relative to the voltage applied to the drive ceramic. At most frequencies the control ceramic requires the larger voltage, but under these conditions it has very low conductance and hence the input power is delivered mainly to the drive ceramic.

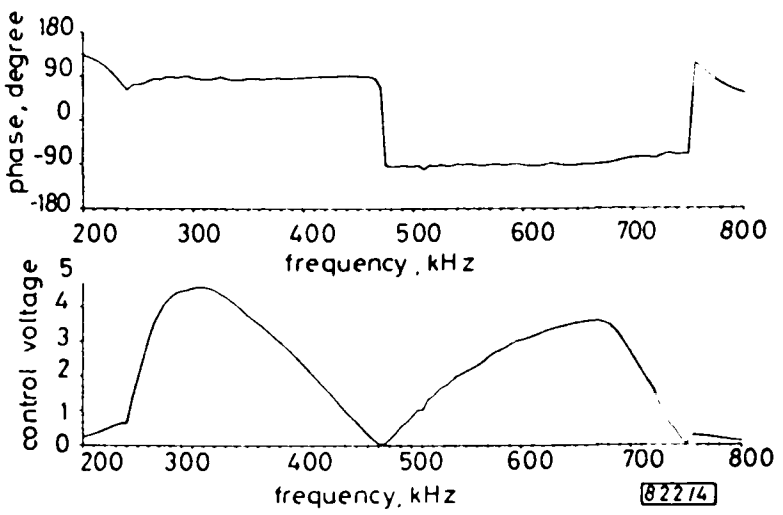

Fig. 4 *Control voltage used to generate the 'envelope' conductance curve of Fig. 3*

Predicted overall efficiency is 30% for this transducer because some acoustic power is absorbed by the backing. Alternative structures are being investigated which employ a backing material with a lower impedance aimed at increasing the overall efficiency.

Acknowledgment: The authors wish to acknowledge the support of Marconi Underwater Systems Ltd. for this investigation.

G. A. STEEL
B. V. SMITH
B. K. GAZEY

Department of Electronic & Electrical Engineering
University of Birmingham
PO Box 363
Birmingham B15 2TT, United Kingdom

14th May 1986

References

1 CHENGHAO, W., and ZHEYING, Z.: 'Principle of piezoelectric-tunable transducer', *Chinese J. Acoust.*, 1983, **2**, pp. 16–24
2 MASON, W. P.: 'Electromechanical transducers and wave filters' (Van Nostrand, Princeton, 1948)
3 BOBBER, R. J.: 'Active load impedance', *J. Acoust. Soc. Am.*, 1962, **34**, pp. 282–288

POWER-DEPENDENT ENHANCEMENT IN REPEATER SPACING FOR DISPERSION-LIMITED OPTICAL COMMUNICATION SYSTEMS

Indexing term: Optical communications

We have found numerically an intensity-dependent increase in the repeater spacing for dispersion-limited lightwave transmission systems. The enhancement is due to the combination of nonlinearity and anomalous dispersion occurring in conventional fibres at 1·55 μm. For moderate powers we find about a factor of two enhancement in the repeater distance compared to the linear case. We also investigate the effects of laser frequency chirp.

At high bit rates exceeding 1 Gbit/s, the performance of 1·55 μm optical communication systems is generally limited by dispersion rather than loss occurring inside conventional silica fibres. Using numerical computations, we have found a power-dependent increase in the repeater distance for such dispersion-limited optical communication systems. This effect is due to the nonlinear refractive index n_2 associated with silica fibres. For moderate launch powers (~3 mW), we find about a factor of two enhancement over the linear case ($n_2 = 0$) for unchirped pulses at bit rates in the range 4–8 Gbit/s. We have also investigated the effect of frequency chirp on the propagation characteristics using a simple yet realistic model.[1] This model yields results in agreement with recent experimental measurements.[2] Using this model, we find that laser chirp severely reduces the repeater distance; the nonlinear enhancement still occurs but requires relatively high powers (~20–30 mW). We compare our analysis with the recent transmission experiments[3,4] and discuss the possible improvement in performance by optimising the launched power.

A linear theory is generally used to estimate pulse broadening in dispersive fibres. However, we go beyond this and investigate the nonlinear dispersive equation[5]

$$i\frac{\partial A}{\partial z} + i\gamma A + \frac{1}{2}\frac{\lambda D}{\omega_0}\frac{\partial^2 A}{\partial \tau^2} + \frac{1}{2}\frac{n_2\omega_0}{c}|A|^2 A = 0 \qquad (1)$$

where A is the slowly varying amplitude of the electromagnetic field at the carrier frequency ω_c, γ is the loss coefficient, n_2 is the nonlinear index of refraction, and D is the group-velocity dispersion. We consider a conventional single-mode silica fibre with a dispersion of 16 ps/km nm occurring at 1·55 μm where the fibre loss is a minimum. The numerical calculations were performed using the Fourier-transformed-based beam-propagation technique[6] with $\gamma = 0{\cdot}2$ dB/km, $n_2 = 3{\cdot}2 \times 10^{-16}$ cm²/W and the fibre-mode diameter $w_0 = 8{\cdot}6$ μm.

Theoretical models have often treated the emitted pulse as Gaussian with a linear frequency chirp. However, realistic optical pulses have much sharper leading and trailing edges than a Gaussian. In addition, time-resolved measurements of the pulse spectrum have shown that the frequency chirping in directly modulated semiconductor lasers occurs mainly near the leading and trailing edges.[2] For a more realistic model[1] we assume the initial pulse to be super-Gaussian with

$$A(0, \tau) = A_0 \exp\left[-\tfrac{1}{2}(1 - i\alpha)(\tau/\sigma)^{2m}\right] \qquad (2)$$